INVESTIGATING THE ROLE OF PHD3 IN MOUSE AND HUMAN β-CELL GLUCOSE METABOLISM

by

FEDERICA CUOZZO

A thesis submitted to the University of Birmingham for the degree of

DOCTOR OF PHILOSOPHY

Institute of Metabolism and Systems Research

College of Medical and Dental Sciences

University of Birmingham

March 2022

ABSTRACT

Prolyl-4-hydroxylase 3 (PHD3) is a dioxygenase that uses oxygen and α-ketoglutarate (α-KG) to hydroxylate prolyl residues. Although historically known to hydroxylate the hypoxia-inducible factor α-subunits (HIFα), PHD3 has been associated with several other targets, involved in numerous cellular events. Given the importance of the PHD3 co-factor, α-KG, for the amplification of glucose-stimulated insulin secretion, PHD3 represents a strong candidate for the regulation of glucose homeostasis. Previous work highlight a role for PHD3 in liver insulin sensitivity and insulin secretion from immortalized INS-1 832/13 cells. Whether and how PHD3 might influence primary β-cell function, both *in vivo* and *in vitro*, remains unknown.

In this thesis, a central role for PHD3 in β-cell glucose metabolism is described, through the characterization of a β-cell specific PHD3 knockout (βPHD3KO) mouse model. In the early phase of metabolic stress, induced by high fat feeding, βPHD3KO islets rewire their metabolism to rely on the β-oxidation of fatty acids to fuel the TCA cycle for insulin secretion. At the same time, the glycolytic supply is diverted into the direct conversion of pyruvate to lactate. However, these adaptations lead to generalized β-cell failure in mice exposed to longer durations of high fat feeding. Finally, through gas chromatography-mass spectrometry (GC-MS)- and nuclear magnetic resonance (NMR)-based metabolomics, it is shown that results from the rodent model are likely to translate to human β-cells.

ACKNOWLEDGEMENTS

First and foremost, I would like to thank my first supervisor, Prof David J. Hodson for his invaluable support before and during the years of my PhD. He has welcomed me in his lab in 2017 and since then has helped me develop both professionally and personally, with his expertise and friendly mentorship. I am immensely grateful to him and hope that our collaboration will extend to future endeavors.

I also wish to thank my second supervisor, Prof. Daniel A. Tennant for inspiring me to follow my ambition and step out of my comfort zone in the first place. If I continued on this path it is also thanks to him and to his gentle guide. He has always been incredibly willing to provide me with help and support whenever I needed it.

A big thank you goes to all past and present members of the Hodson lab (the HodSquad). To Dr. Julia Ast, Dr. Katrina Viloria, Dr. Annie Hasib, Nick Fine, Anne de Bray, Dr. Fiona Ashford, Lewis Everett and Anastasia Arvaniti for their kindness, patience and continued support. Most of all, I wish to thank Dr. Daniela Nasteska, not only has she been my partner for the work described in this thesis, but she has also been an unlimited source of practical advice and the keeper of secrets and fears. She has been my absolute go-to person for any doubts and I am very thankful for her friendship.

I additionally thank Dr. Ildem Akerman of the University of Birmingham for her collaboration to the transcriptomic analyses and for sharing her supply of human islets with me. Moreover, I wish to thank Dr. James Cantley of the University of Dundee and Prof. Leanne Hodson of the University of Oxford for their contribution to the ^{14}C glucose studies and D31-palmitate incorporation and oxidation assays, respectively. I would like to acknowledge the San Raffaele Diabetes Research Institute of Milan (Italy) and Translational Research for Diabetes at the University of Lille (France) for their provision of human islets. Their

collaboration was fundamental to investigating the translation of our findings to humans. I am also extremely grateful to Dr. Alpesh Thakker, Dr. Jennie Roberts and Dr. Christian Ludwig for their help running and analyzing GC-MS and NMR samples.

I would also like to thank all members of the IMSR for providing a very welcoming and stimulating environment to work in and the Medical Research Council for funding this PhD.

My thanks go to my friends, whether longtime or recent they have always been there to offer a distraction, a piece of advice, to motivate me and listen to my vents. My love and gratitude go to my family which untiredly loves, believes and supports me and my career.

Last but certainly not least, thank you to Paolo for being my number one supporter. He believed I could do a PhD way before I even considered it. He helped me in many practical and emotional ways. Through all the highs and the lows, he shares every day with me and above all else I am grateful for our love.

TABLE OF CONTENTS

TABLE OF FIGURES

TABLE OF TABLES

LIST OF ABBREVIATIONS

1D: One-Dimensional

^{1}H-^{13}C HSQC: Proton-Carbon Heteronuclear Single Quantum Coherence Spectroscopy

^{1}H-^{1}H COSY: Proton-Proton Homonuclear Correlated Spectroscopy

^{1}H-^{1}H TOCSY: Proton-Proton Homonuclear Total Correlation Spectroscopy

2D: Two-Dimensional

$^{2}H_2O$: Deuterated Water

ACC: Acetyl-Coa Carboxylase

ACLY: ATP Citrate Lyase

ADP: Adenosine Diphosphate

ADPR: Adipose Differentiation-Related Protein

AGPAT2: Acylglycerol-3-Phosphate Acyltransferase 2

AML: Acute Myeloid Leukemia

ATF-4: Activating Transcription Factor 4

ATP: Adenosine Triphosphate

BAD: Bcl-2-Associated Death Promoter

BAT: Brown Adipose Tissue

BAX: Bcl-2-Associated X Protein

BCH: 2-Aminobicyclo-(2,2,1)-Heptane-2-Carboxylic Acid

Bcl-2: B-Cell Lymphoma 2

BNIP3: BCL2 interacting protein 3

BNIP3L: BCL2 interacting protein 3 like

BSA: Bovine Serum Albumin

Ca^{2+}: Calcium

CA9: Carbonic Anhydrase 9

cAMP: Cyclic Adenosine Monophosphate

CBP: cAMP Response Element-Binding Protein

Ccnd1: Cyclin D1

CDKs: Cyclin-Dependent Kinases

CIC: Citrate/Isocitrate Carrier

CO_2: Carbon Dioxide

COX: Cytochrome Oxidase

CPT1: Carnitine Palmitoyl Transferase 1

CREB: cAMP Response Element Binding Protein

D_2O: Deuterium Oxide

D4-TMSP: Propionic-2,2,3,3-D4 Acid Sodium Salt

DAG: Diacylglycerol

DPP-4: Dipeptidyl Peptidase-4

DRI: Diabetes Research Institute

EDHB: Ethyl-3,4-Dihydroxybenzoate

EDTA: Ethylenediaminetetraacetic acid

Egln3$^{fl/fl}$: *Egln3* flox'd

Epac2: Exchange Protein Directly Activated By cAMP

ER: Endoplasmic Reticulum

ERK1/2: Extracellular Signal-Regulated Kinases 1 And 2

ETC: Electron Transport Chain

ETX: Etomoxir

Eu^{3+}: Europium

Ex4: Exendin4

F: Fluorescence At Any Time Point

FABP3: Fatty Acid Binding Proteins 3

FABP7: Fatty Acid Binding Proteins 7

$FADH_2$: Reduced Flavin Adenine Dinucleotide

FAO: Fatty Acid Oxidation

FAS: Fatty Acid Synthase

FBS: Fetal Bovine Serum

Fe^{2+}: Iron

Fe^{3+}: Ferric Iron

FFAR1: FFA Receptor 1

FFAs: Free Fatty Acids

FID: Free Induction Decay

FIH: factor-inhibiting HIF

FKBP38: FK506 Binding Protein 38

Fmin: Minimum Fluorescence

FOXO3a Forkhead Box O3

FRET: Fluorescence Resonance Energy Transfer

G6P: Glucose-6-phosphate

GC: Gas Chromatography

GC-MS: Gas Chromatography-Mass Spectrometry

GDH: Glutamate Dehydrogenase

GIP: Insulinotropic Polypeptide

GIPR: GIP Receptor

GK: Glucokinase

GLP-1: Glucagon-Like Peptide-1

GLP-1R: GLP-1 Receptor

GLS: Glutaminase

GLUT: Glucose Transporter

GPR40: G-Protein Coupled Receptor 40

GRKs: G Protein Receptor Kinases

GRP: Gastrin-Releasing Peptide

GRX1: Glutaredoxin

GSH: Reduced Glutathione

GSIS: Glucose-Stimulated Insulin Secretion

GSR: Glutathione Reductase

GSSG: Glutathione Disulfide

GYS1: Glycogen Synthase 1

HCO_3^-: Sodium Bicarbonate

HFD: High Fat Diet

HIFs: Hypoxia-Inducible Factors

HIFα: hypoxia-inducible factor α-subunits

HK: Hexokinase

HK1: Hexokinases 1

HK3: Hexokinases 3

hPSCs: Human Pluripotent Stem Cells

HREs: Hypoxia-Responsive Elements

HTRF: Homogenous Time Resolved Fluorescence

IAPP: Islet Amyloid Polypeptide

IDH1: Cytosolic Isocitrate Dehydrogenase

IDH2: Mitochondrial Isocitrate Dehydrogenase

IFN: Interferon

IHC: Immunohistochemistry

IP3: Inositol Triphosphate

IPGTT: Intraperitoneal Glucose Tolerance Test

IRF7: Interferon Regulatory Factor 7

Irs2: Insulin Receptor Substrate-2

ITT: Insulin Tolerance Test

K^+: Positively Charged Potassium Ions

K_{ATP}: ATP-Sensitive Potassium

KCl: Potassium Chloride

KIF1B-β: Kinesin Family Member 1B

Kir6.2: Inward-Rectifier Potassium Channels

Km: Michaelis Constant

KOH: Potassium Hydroxide

LCFAs: Long-Chain FFAs

LDHA: Lactate Dehydrogenase

MAG: Monoacylglycerols

MAP4K3: Mitogen-Activated Protein Kinase Kinase Kinase Kinase 3

MAPK: Mitogen-Activated Protein Kinase

MAPK6: Mitogen-Activated Protein Kinase 6

MCT: Monocarboxylate Transporter

MDH: Malate Dehydrogenase

ME: Malic Enzyme

$MgCl_2$: Magnesium Chloride

MID: Mass Isotopologues Distribution

MS: Mass Spectrometry

MTA: Material Transfer Agreement

MTBSTFA: N-Tertbutyldimethylsilyl-N-Methyltrifluoroacetamide

mTOR: Mammalian Target Of Rapamycin

Na_2HPO_4: Disodium Phosphate

NAAD: Nicotinic Acid Adenine Dinucleotide

NAD^+: Nicotinamide Adenine Dinucleotide

NADH: Reduced Nicotinamide Adenine Dinucleotide

$NADP^+$: Nicotinamide Adenine Dinucleotide Phosphate

NADPH: Reduced Nicotinamide Adenine Dinucleotide Phosphate

NaH_2PO_4: Monosodium Phosphate

NF-κB: Nuclear Factor Kappa-Light-Chain-Enhancer Of Activated B Cells

Ngn3: Neurogenin3

NMR: Nuclear Magnetic Resonance

O_2: Molecular Oxygen

ODDD: Oxygen-Dependent Degradation Domain

OGC: 2-Oxoglutarate Carrier

OGTT: Oral Glucose Tolerance Test

Pax2: Paired Box 2

PBS: Phosphate Buffered Saline

PC: Pyruvate Carboxylase

PCNA: Proliferating Cell Nuclear Antigen

PDH: Pyruvate Dehydrogenase

PDK1: Pyruvate Dehydrogenase Kinase-1

PEP: Phosphoenolpyruvate

PHD3: Prolyl-4-Hydroxylase 3

PHD3KO: PHD3 Knockout

PHDs: Prolyl Hydroxylase Domain Proteins

PHGDH: Phosphoglycerate Dehydrogenase

PI-3K: Phospatidylinositol- 3 Kinase

PIP2: Phosphoinositide Bisphosphate

PK: Pyruvate Kinase

PKA: Protein Kinase A

PKB: Protein Kinase B

PKC: Protein Kinase C

PKD1: Protein Kinase D

PKM2: Pyruvate Kinase M2

PLC-ε: phospholipase C-ε

PP: Pancreatic Polypeptide

PPAR-γ: Peroxisome Proliferator-Activated Receptor-γ

pVHL: Von Hippel-Lindau Protein

qRT-PCR: Quantitative Real-Time PCR

R: Fluorescence At Any Time Point

R0: Fluorescence At 0 Min

Rag: Ras-Related GTPase

REST: Repressor Element 1 Silencing Transcription Factor

RF: Radiofrequency

RIM: Rab3-Interacting Molecule

RIM-BP: RIM-Binding Proteins

ROS: Reactive Oxygen Species

RP: Reserve Pools

RRP: Readily Releasable Pools

RT: Room Temperature

SAT: Subcutaneous Tissue

SC: Standard Chow

SENP1: Sentrin/SUMO-Specific Protease 1

SGLT: Sodium-Glucose Cotransporter

SM: Sec1/Munc18-Like Proteins

SNAP: N-Ethylmaleimide-Sensitive Factor Attachment Protein

SNAP-25: Synaptosomal-Associated Protein Of 25 kDa

SNAREs: N-Ethylmaleimide-Sensitive Factor Attachment Protein Receptor

SUR1: Sulfonylurea Receptor

TBDMCS: Tertbutyldimethyl-chlorosilane

TCA: Tricarboxylic Acid

TET: Ten-Eleven Translocation

UCSC: University of California Santa Cruz

VAMP: Vesicle-Associated Membrane Protein

VAT: Visceral Tissue

VDCCs: Voltage-Dependent Calcium Channels

VPS34: Vacuolar Protein Sorting 34

WB: Western Blot

WT: Wild-Type

α-KG: α-Ketoglutarate

β2-AR: β2-Adrenergic Receptor

βPHD3CON: β-cell specific PHD3 Control

βPHD3KO: β-cell specific PHD3 Knockout

Chapter 1

REVIEW OF THE LITERATURE

1.1 Pancreas and glucose metabolism

1.1.1 Pancreas and islets of Langerhans

The pancreas plays a pivotal role in the regulation of macronutrient digestion and energy homeostasis. It is a retroperitoneal organ situated in the upper abdominal cavity and is structurally divided into head, body and tail. The pancreas is both an exocrine and an endocrine organ, releasing both digestive enzymes and pancreatic hormones. The exocrine cells, representing the majority of the organ, are acinar and duct cells. The endocrine portion is composed of clusters of cells, named Islets of Langerhans, accounting for only 1-2% of the entire pancreas, corresponding to 1,000-5,000 islets in mice and 1,000,000-15,000,000 in humans (Dolensek, Rupnik, & Stozer, 2015; Leung, 2010a; Roder, Wu, Liu, & Han, 2016). The role of the pancreatic acinar cells is to produce and secrete the pancreatic juice, containing three categories of digestive enzymes, namely α-amylase, lipase and protease, responsible for carbohydrates, lipids and proteins digestion respectively (Leung, 2010b). The pancreatic duct cells are a minority of the exocrine cells, about 10%. However, they have the fundamental role of secreting sodium bicarbonate (HCO_3^-) which provides the optimal pH for digestive enzyme activity and for the protection of the duodenal mucosa (Leung, 2010b). Moreover, a recent study has identified a role for the duct cells in the neogenesis of β-cells. Although limited to mice, the work showed that duct cells expressing the transcription factor neurogenin3 (Ngn3), can replenish the β-cell pool, through the formation of a somatostatin-expressing intermediate (Gribben et al., 2021).

The islets of Langerhans are highly vascularized, endocrine, island-like cell clusters that can be found within the exocrine tissue and are responsible for the release of the pancreatic hormones. There are five types of cells within the islets: α-cells producing

glucagon, β-cells secreting amylin and insulin, γ-cells producing pancreatic polypeptide (PP), δ-cells releasing somatostatin and ε-cells secreting ghrelin **(Figure 1.1)**. These cell types are present in variable ratios among species. The α-cells make up 20-40% of the human and 10-20% of the mouse islet. Constituting the most abundant subgroup, the β-cells represent 50-70% and 60-80% of the total islet in humans and mice, respectively. The γ-cells and δ-cells are less abundant, accounting for less than 10% in humans and less than 5% in mice. Finally, the ε-cells represent less than 1% of the entire human or mouse islet (Dolensek et al., 2015). Each of the hormones produced within the islets of Langerhans has its specific function. Blood glucose levels are increased by glucagon and lowered by insulin, somatostatin inhibits both glucagon and insulin secretion and PP tunes the secretory activity of the pancreas (Roder et al., 2016; Rorsman & Huising, 2018). The pancreas is responsible for maintaining the levels of glucose between 4 and 6 mM in humans, by keeping the balance between glucagon and insulin release, known as glucose homeostasis (Roder et al., 2016). During hypoglycemia, the α-cells can increase blood glucose levels by secreting glucagon that promotes hepatic glycogenolysis and gluconeogenesis (i.e. endogenous glucose production). Conversely, in response to high glucose levels, the β-cells secrete insulin which enables glucose uptake by muscle and adipose tissue, thus lowering the glucose levels in the bloodstream. Moreover, insulin induces lipogenesis, hepatic glycogenesis and protein synthesis (Leung, 2010b; Roder et al., 2016).

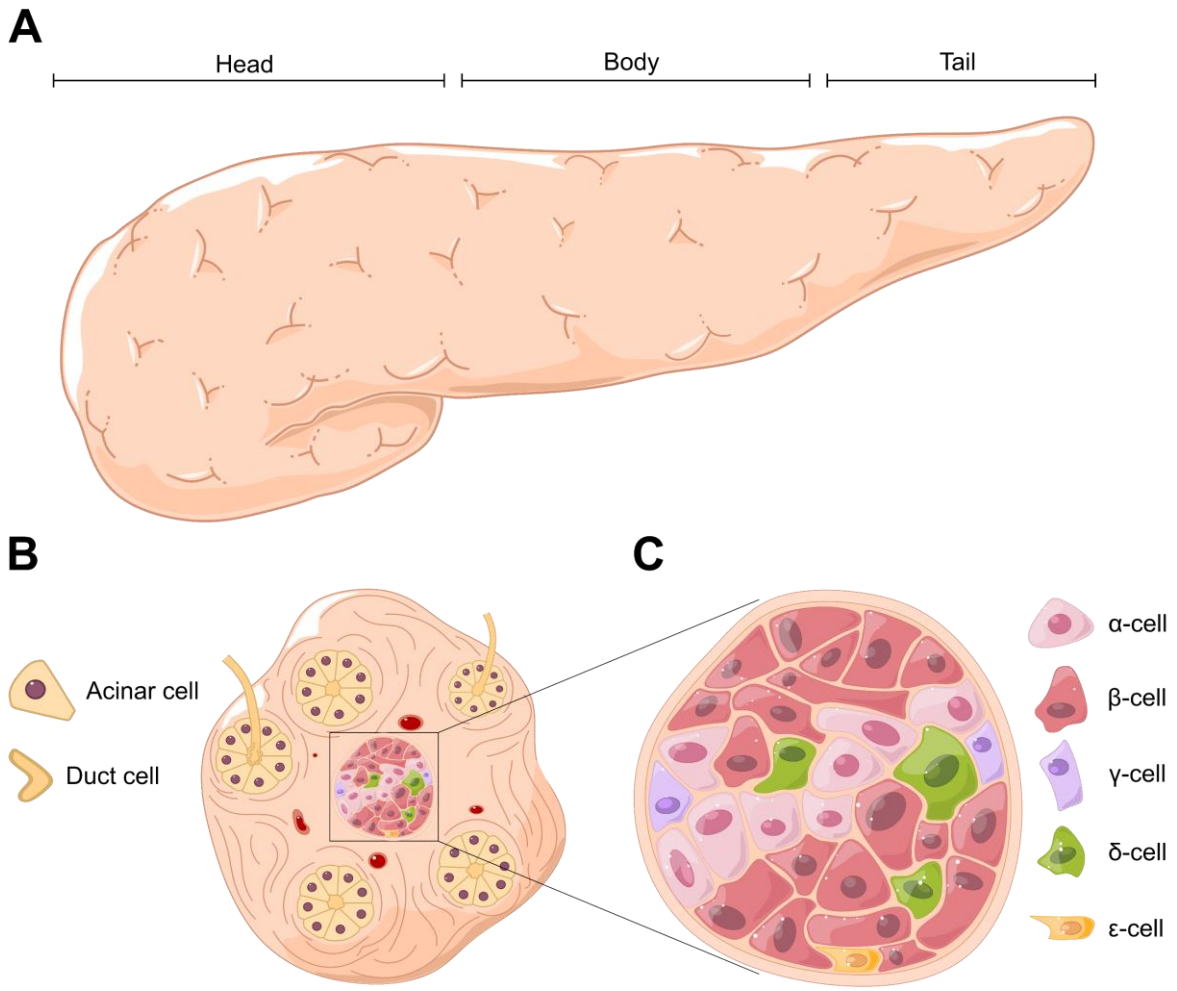

Figure 1.1 Exocrine and endocrine pancreas: (**A**) The human pancreas is a 15-25 cm long organ divided into three sections: head, body and tail. It encloses exocrine and endocrine cells secreting digestive enzymes and pancreatic hormones, respectively. (**B**) The cross-section shows the exocrine acinar and duct cells as well as the endocrine islet of Langerhans. (**C**) The magnification shows the cluster structure of the islet of Langerhans, comprising of α-cells, β-cells, γ-cells, δ-cells and ε-cells.

1.1.2 β-cells and insulin secretion

Pancreatic β-cells are the most numerous cell type within the endocrine pancreas and the sole source of circulating insulin. They are characterized by some key features, such as insulin synthesis and processing of insulin precursors, storage of secretory granules, insulin secretion and its cessation in response to hypoglycemia (Kaestner et al., 2021). The primary secretagogue for β-cells is high blood glucose. This is responsible for the direct stimulation of insulin secretion in the so-called triggering pathway, but also for the activation of amplifying pathways, involving various agents that potentiate glucose-stimulated insulin secretion (GSIS) (Campbell & Newgard, 2021; Henquin, 2000).

1.1.3 Glucose-stimulated insulin secretion: triggering pathway

The magnitude of insulin secretion is tightly linked to the β-cell glucose-sensing machinery, which guarantees the exact amount of insulin to be released to maintain blood glucose within a healthy range (Campbell & Newgard, 2021). During hyperglycemia, glucose enters the β-cells through facilitated transport, via low affinity glucose transporters (GLUT1 and GLUT2 in humans and rodents, respectively). Glucose is then phosphorylated by glucokinase (GK) to produce glucose-6-phosphate (G6P) which, subsequent to glycolysis, results in two pyruvate molecules (De Vos et al., 1995; Losada-Barragan, 2021; Rutter, Pullen, Hodson, & Martinez-Sanchez, 2015). GK is a hexokinase (HK) isozyme with a lower affinity for glucose. Indeed, it has a Michaelis constant (Km) of about 8 mM, approximately 1000-fold higher than other HKs (Campbell & Newgard, 2021; Wilson, 2003). Moreover, GK is smaller, compared to other HKs, and it lacks the N-terminal responsible for product inhibition

by G6P. Therefore, GK can change sharply in response to glucose entrance, allowing the β-cells to finely regulate glucose metabolism and insulin secretion (Campbell & Newgard, 2021; Rutter et al., 2015). Glycolitycally-derived pyruvate is metabolized to enter the tricarboxylic acid (TCA) cycle evenly via pyruvate dehydrogenase (PDH) and pyruvate carboxylase (PC). On the other hand, the direct conversion of pyruvate to lactate is reduced, due to the gene for lactate dehydrogenase (*Ldha*) being one of the disallowed genes of β-cells (Campbell & Newgard, 2021; Komatsu, Takei, Ishii, & Sato, 2013; Pullen & Rutter, 2013). Following the mitochondrial TCA cycle and oxidative phosphorylation, adenosine triphosphate (ATP) is generated, increasing the ATP/adenosine diphosphate (ADP) ratio and leading to the closure of the ATP-sensitive potassium (K_{ATP}) channels (Affourtit, Alberts, Barlow, Carre, & Wynne, 2018) **(Figure 1.2)**.

Recently, a more dynamic 2-state model by which the closure of the K_{ATP} channel is regulated upstream of the pyruvate entry into the mitochondrion was proposed. This ADP privation model is characterized by a dual function of the mitochondrion switching from a synthetic to an oxidative state in response to the availability of ATP produced by pyruvate kinase (PK). The latter is the enzyme converting phosphoenolpyruvate (PEP) to pyruvate and ADP to ATP in the cytosol, therefore augmenting the ATP/ADP ratio and leading to K_{ATP} channels closure. In this ADP-deprived phase, the oxidative phosphorylation is limited and the mitochondrion goes into a synthetic state where the anaplerotic metabolism of PC boosts PEP production via the PEP cycle (Foster et al., 2022; Lewandowski et al., 2020) **(Figure 1.2)**. The closure of K_{ATP} channels leads to membrane depolarization, associated with the hydrolysis of ATP to ADP. The latter, being available for oxidative phosphorylation, pushes the mitochondrion in the

oxidative state, increasing the ATP/ADP ratio to induce closure of the K_{ATP} channels (Lewandowski et al., 2020).

The K_{ATP} channel is an octamer, comprised of four inward-rectifier potassium channels (Kir6.2), forming a pore-structure, surrounded by four regulatory sulfonylurea receptor (SUR1) subunits. While the SUR1 subunits activate the K_{ATP} channel, by binding to magnesium nucleotides, the K_{ATP} channel closure is mediated by ATP binding to the Kir6.2 subunit (Pipatpolkai, Usher, Stansfeld, & Ashcroft, 2020). The intracellular accumulation of positively charged potassium ions (K^+) leads to an increase of the membrane potential from the hyperpolarized state (-70 mV and -80 mV in humans and mice, respectively) to the depolarized level (-60 mV in humans and approximately -50 mV in mice), firing the opening of voltage-dependent calcium channels (VDCCs) (Rorsman & Ashcroft, 2018). Noticeably, humans and mice possess different VDCCs subtypes. Humans express $Ca_V2.1$ P/Q-VDCCs (40-45%), $Ca_V1.2$ and $Ca_V1.3$ L-VDCCs (40-45%) and $Ca_V3.2$ T-VDCCs (10-20%). In mice, $Ca_V1.2$ L-VDCCs (>50%), $Ca_V2.3$ R-VDCCs (25%) and $Ca_V2.1$ P/Q-VDCCs (15%) are present (Skelin Klemen, Dolensek, Slak Rupnik, & Stozer, 2017). Consequent to the opening of VDCCs, calcium (Ca^{2+}) enters the β-cell and activates the SNARE machinery, mediating the insulin granules fusion to the plasma membrane and insulin exocytosis **(Figure 1.2)**.

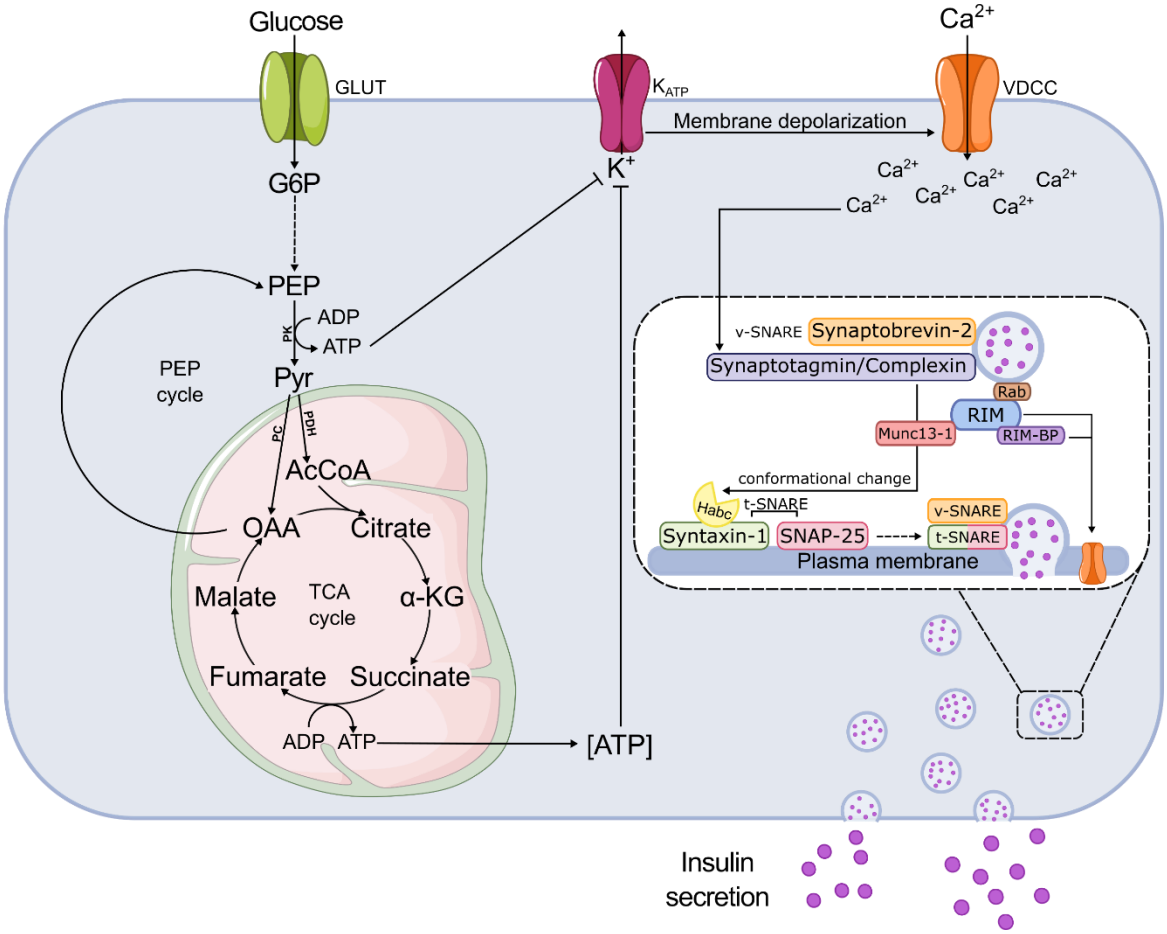

Figure 1.2 GSIS: triggering pathway and insulin exocytosis: Glucose enters the β-cells through GLUT, and is phosphorylated by GK to produce G6P which undergoes glycolysis, producing Pyr. Pyr enters the TCA cycle leading to the accumulation of ATP and consequent closure of the K_{ATP} channels. In the recently described 2-state model, the activity of PK, converting PEP into Pyr is associated with the production of ATP and consequent closure of the K_{ATP} channels. In this model the mitochondrion goes into an ADP-deprived state, during which the activity of PC boosts the PEP cycle to support the activity of PK. The accumulation of K^+ results in depolarization of the plasma membranes and opening of the VDCCs. The consequent Ca^{2+} influx activates the SNARE machinery (in the magnified insulin granule). Ca^{2+} binds to synaptotagmins or complexin on the insulin granules. This leads to Munc13-1-dependent opening of the Habc domain of syntaxin-1 on the plasma membrane. Munc13-1 is activated by binding to RIM. The latter also binds to Rab and RIM-BP, inducing vesicle docking and bringing VDCC within 100 nm of the docked vesicles, respectively. Upon Habc conformational change, v-SNARE (synaptobrevin-2) and t-SNARE (syntaxin-1 and SNAP-25) are brought in close proximity. This eventually leads to the formation of a transient pore used for insulin exocytosis.

1.1.4 Insulin exocytosis

The proteins on the surfaces of the insulin vesicles and the β-cell plasma membranes are known as N-ethylmaleimide-sensitive factor attachment protein (SNAP) receptor proteins (SNAREs). These can be distinguished into two main groups: t-SNAREs located on the plasma membrane and v-SNAREs to be found on the granules. The former group includes the synaptosomal-associated protein of 25 kDa (SNAP-25) and syntaxin-1, whereas the v-SNAREs comprises of synaptobrevin-2, of the vesicle-associated membrane protein (VAMP) family (Thurmond, 2007). The formation of the SNARE complex begins when Ca^{2+} binds to the C2 domain of synaptotagmins or complexin, leading to the opening of the Habc domain of syntaxin-1, mediated by Munc13-1. Habc is placed at the regulatory N-terminus of the syntaxin-1 and it is normally kept in a closed state by the activity of Sec1/Munc18-like proteins (SM) (Roder et al., 2016; Rorsman & Ashcroft, 2018; Vakilian, Tahamtani, & Ghaedi, 2019). Importantly, Munc13-1 together with the Rab3-interacting molecule (RIM), RIM-binding proteins (RIM-BP) and a presynaptic Ca^{2+} channel form the active zone protein complex, regulating vesicle docking and priming. RIM exerts three crucial functions: it binds to the Rab proteins on the vesicles, promoting their docking, it recruits the Ca^{2+} channel (RIM-BP-dependently or independently) to the docked vesicles for fast excitation-secretion coupling and it binds Munc13-1. It is through binding with RIM that Munc13-1 is activated and can induce the opening of the Habc domain of syntaxin-1 (Rorsman & Ashcroft, 2018; Sudhof, 2013). Once this conformational change is complete, the t-SNAREs and the v-SNAREs can bind, bringing the vesicles and plasma membranes in close proximity. This eventually causes the fusion of the two

membranes and the formation of a transient pore that is further enlarged upon *cis* to *trans* conversion of the SNARE complex itself (Vakilian et al., 2019) **(Figure 1.2)**.

The first phase of insulin exocytosis is largely due to the triggering pathway described above. It is characterized by a sharp peak of insulin secretion, from the readily releasable pools (RRP) of granules, located in the proximity of the membrane release sites, occurring in the first minutes after a glucose stimulus. The first phase is followed by a transient and then a second phase during which insulin is secreted in a sustained and prolonged manner (although at lower rates), through replenishment of the RRP from the reserve pools (RP), during the whole post-absorptive phase of a meal. The second phase involves a set of alternative stimuli known as amplifying pathways (Bratanova-Tochkova et al., 2002; Campbell & Newgard, 2021).

1.1.5 Glucose-stimulated insulin secretion: amplifying pathways

Similar to the triggering pathway, the amplifying pathway ensures the release of insulin granules from the RRP, but it also determines the recruitment, trafficking and exocytosis of insulin from a granule storage pool (Gaisano, 2017). Of note, β-cells treated with diazoxide, a K_{ATP} channel opener, displayed repolarization of the membrane and arrest of Ca^{2+} influx. However, Ca^{2+} influx could be restored through depolarization induced by extracellular potassium. In these conditions, it was proven that glucose is still capable of amplifying the secretion of insulin in a K_{ATP}-independent manner (Gembal, Detimary, Gilon, Gao, & Henquin, 1993). The amplifying phase of GSIS involves several, not fully characterized, intracellular mechanisms that occur independently of K_{ATP} channels (Campbell & Newgard, 2021; Rutter et al., 2015).

1.1.5.1 Anaplerotic metabolism

As previously mentioned, glycolitcally-derived pyruvate is metabolized equally by PDH and PC. The latter is responsible for the anaplerotic metabolism of pyruvate and therefore, for the formation and export of TCA cycle intermediates into the cytosol, via organic acid carriers, to create a signal for the amplifying phase (Campbell & Newgard, 2021; Jitrapakdee, Wutthisathapornchai, Wallace, & MacDonald, 2010). Pyruvate-cycling processes, such as the pyruvate-malate, pyruvate-citrate and pyruvate-isocitrate carriers generate reduced nicotinamide adenine dinucleotide phosphate (NADPH), from nicotinamide adenine dinucleotide phosphate ($NADP^+$). In particular, the pyruvate-isocitrate cycle is likely the most relevant NADPH-producing carrier for the amplification of GSIS (Campbell & Newgard, 2021). In this cycle, citrate and isocitrate generate α-KG through the cytosolic $NADP^+$-linked isocitrate dehydrogenase (IDH1), to subsequently regenerate citrate and isocitrate via the mitochondrial NADPH-linked isocitrate dehydrogenase (IDH2). The resulting increase in cytosolic NADPH/$NADP^+$ ratio is associated with the activity of glutathione reductase (GSR), which induces the conversion of glutathione disulfide (GSSG) to reduced glutathione (GSH). This, in turn, activates glutaredoxin (GRX1), which reduces and activates the sentrin/SUMO-specific protease 1 (SENP1). SENP1 can then enhance insulin secretion in a Ca^{2+}-dependent manner (Ferdaoussi et al., 2015) **(Figure 1.3)**.

Moreover, GSIS can be amplified by glutamine in presence of leucine and 2-aminobicyclo-(2,2,1)-heptane-2-carboxylic acid (BCH). These activate glutamate dehydrogenase (GDH) to convert glutamate to α-KG which feeds into the reductive TCA cycle flux to produce isocitrate and citrate. This reductive flux contributes to the

pyruvate-isocitrate cycle which leads to SENP1-dependent insulin exocytosis, as described above (Vetterli et al., 2012; Zhang et al., 2021) **(Figure 1.3)**.

Notably, glutamate can also induce direct insulin exocytosis, through the activity of glutamate transporters on the secretory granules, in a cyclic adenosine monophosphate (cAMP)-dependent mechanism (Campbell & Newgard, 2021; Gheni et al., 2014; Maechler & Wollheim, 1999) **(Figure 1.3)**.

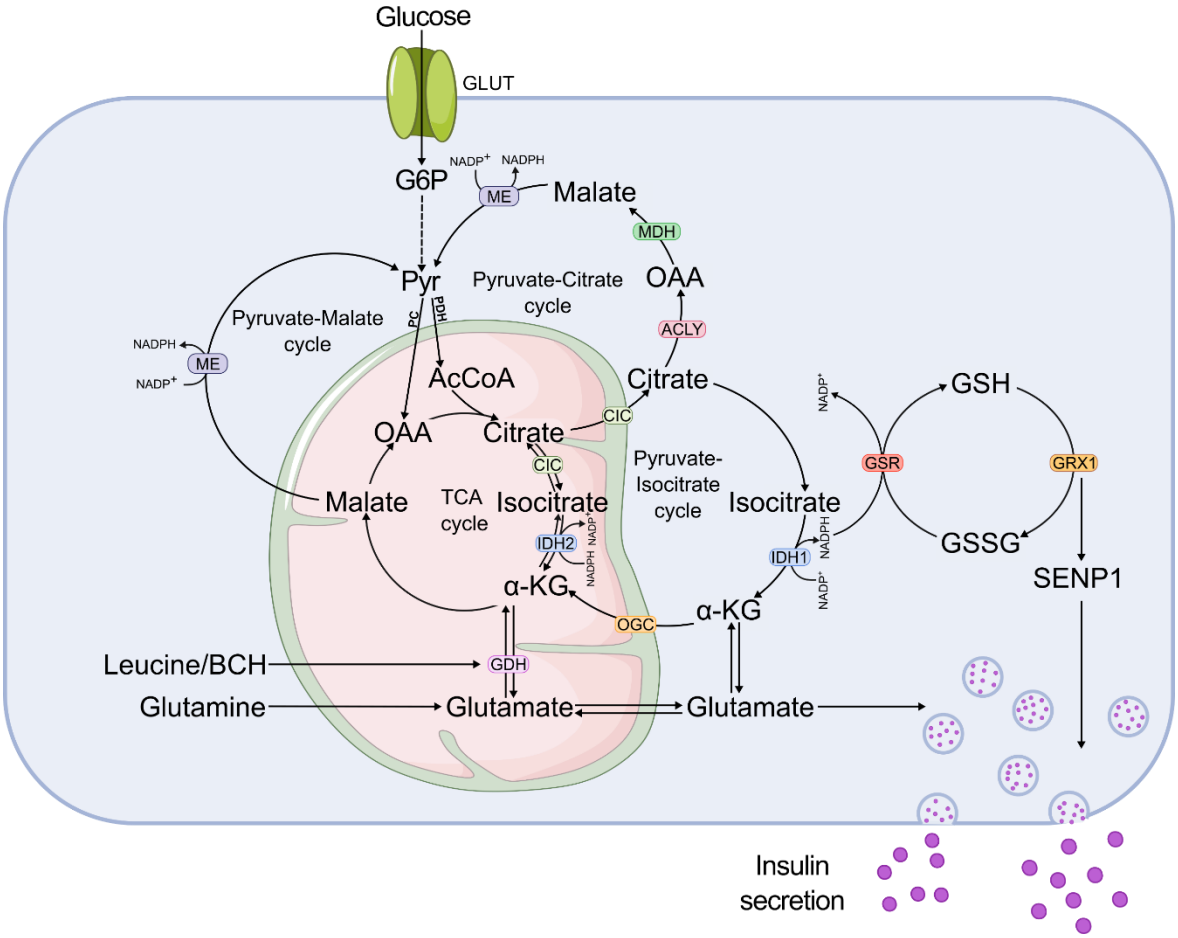

Figure 1.3 GSIS: amplifying pathways through anaplerotic metabolism: The increased anaplerotic metabolism of Pyr through the activity of PC leads to the accumulation of TCA cycle intermediates that are translocated into the cytosol to amplify GSIS. The transport of TCA cycle metabolites outside the mitochondrion is mediated by the activity of NADPH-producing organic acid carriers. The schematic shows three organic acid carriers: 1) the pyruvate-malate cycle, involving the activity of the malic enzyme (ME); 2) the pyruvate-citrate cycle regulated by the activity of the citrate/isocitrate carrier (CIC), ATP citrate lyase (ACLY), malate dehydrogenase (MDH) and ME; 3) the pyruvate-isocitrate cycle involving CIC, IDH1, IDH2 and the 2-oxoglutarate carrier (OGC). In particular, the increased amount of cytosolic NADPH deriving from the pyruvate-isocitrate cycle is employed by GSR to produce GSH from GSSG. This leads to the GRX1-mediated activation of SENP1, which results in increased insulin secretion. Insulin secretion is also sustained by glutamine-derived glutamate. In the presence of BCH and leucine, which regulate GDH, glutamate is converted into α-KG to supply the pyruvate-isocitrate cycle. Alternatively, glutamate can interact directly with the insulin granules to induce insulin secretion.

1.1.5.2 Free-fatty acids

Free-fatty acids (FFAs), particularly long-chain FFAs (LCFAs) can also amplify GSIS (Losada-Barragan, 2021). The first mechanism by which LCFAs potentiate GSIS is through interaction with the FFA receptor 1 (FFAR1, also known as G-protein coupled receptor 40 (GPR40)), on the plasma membrane. This is coupled to a $G\alpha_q$ protein and activates the metabolism of phosphoinositide bisphosphate (PIP2) to inositol triphosphate (IP3) and diacylglycerol (DAG). Although the function of IP3 remains under study, DAG can activate the protein kinase C (PKC) and protein kinase D (PKD1), the latter promoting insulin exocytosis (Ferdaoussi et al., 2012).

Another pathway involving LCFAs is their conversion to malonyl-CoA, following glucose stimulation and TCA cycle fueling. Malonyl-CoA can inhibit the key enzyme of β-oxidation, carnitine palmitoyltransferase 1 (CPT1), and divert the FFAs to the glycerolipid/FFA cycle. Within this cycle, the FFAs are esterified with glycerol-3-phosphate to form glycerolipids. These contribute to the production of DAG and monoacylglycerols (MAG), including 1-MAG. The latter is directly involved in insulin release by interacting with the trafficking protein Munc13-1 (Prentki, Corkey, & Madiraju, 2020).

1.1.5.3 Incretins

Incretins are gastrointestinal hormones, released in response to oral intake of glucose, fructose, proteins and FFAs, that stimulate insulin secretion in a glucose-dependent manner (Creutzfeldt, 1979; Roder et al., 2016). These are the glucagon-like peptide-1

(GLP-1) and the glucose-dependent insulinotropic polypeptide (GIP), secreted by the enteroendocrine cells (Campbell & Drucker, 2013).

GLP-1 is a 30 amino acid long peptide secreted by the intestinal L-cells, in response to carbohydrates, proteins and fats intake as well as to bile acids (Baggio & Drucker, 2007; Campbell & Drucker, 2013; Gribble & Reimann, 2021). The enteroendocrine L-cells are mainly found in the distal small intestine, hence the early phase of GLP-1 release is likely not only mediated by the direct action of the nutrients but also by the autonomic nervous system, gastrin-releasing peptide (GRP), acetylcholine and GIP (Baggio & Drucker, 2007). Once secreted, GLP-1 can bind to the GLP-1 receptors (GLP-1R) in the pancreas, nervous system, heart, kidney, gastrointestinal tract, Brunner's gland, stomach and lungs (McLean et al., 2021). However, the half-life of the human bioactive form GLP-1(7-36)NH_2 is less than two minutes, due to its fast inactivation by the ubiquitous proteolytic enzyme dipeptidyl peptidase-4 (DPP-4) (Deacon et al., 1995; Orskov, Rabenhoj, Wettergren, Kofod, & Holst, 1994). Therefore, about half of the GLP-1 secreted is inactivated before getting to its receptor (Hansen, Deacon, Orskov, & Holst, 1999). The GLP-1R is a G protein-coupled heterotrimeric receptor with an N-terminal region crucial for GLP-1 binding. GLP-1R can couple with $G\alpha_s$, $G\alpha_q$, $G\alpha_i$, and $G\alpha_o$ and activate several different pathways such as the cAMP/protein kinase A (PKA), the exchange protein directly activated by cAMP (Epac2) and the phosphatidylinositol-3 kinase (PI-3K) pathways (Hallbrink et al., 2001; Montrose-Rafizadeh et al., 1999).

However, the canonical GLP-1 pathway is mainly regulated by GLP-1R coupled with $G\alpha_s$. When GLP-1 binds to its receptor on the β-cells, the adenylate cyclase is activated by the $G\alpha_s$ subunit of the G protein and prompts the production of cAMP. The latter

can consequently induce insulin exocytosis in two different ways: PKA-dependently or PKA-independently. When PKA is activated, this can phosphorylate the K_{ATP} and Ca^{2+} channels and IP3 receptors inducing membrane depolarization and increased Ca^{2+} flux within β-cells. Moreover, PKA can act directly on the insulin granules, making them more sensitive to Ca^{2+} (Baggio & Drucker, 2007; Baukrowitz et al., 1998; Deriy et al., 2009; Holz, Kang, Harbeck, Roe, & Chepurny, 2006; Schmidt et al., 2001). Alternatively, cAMP can activate Epac2 and this can, in turn, induce insulin secretion in two different ways. The intracellular Ca^{2+} release channels can be opened via direct phosphorylation or through activation of the second messengers IP3, cyclic ADP-ribose, or nicotinic acid adenine dinucleotide (NAAD) phosphate by Epac2 (Holz et al., 2006). Epac2 can also interact with the SUR1 subunit of the K_{ATP} channels. If Epac2 is recruited by SUR1 in the plasma membrane, it leads to the activation of the phospholipase C-ε (PLC-ε) and consequent increase of IP3, which results in an enhanced sensitivity of the K_{ATP} channels to ATP (Baukrowitz et al., 1998; Schmidt et al., 2001). If Epac2 is recruited by SUR1 in the insulin granules membrane, it promotes acidification of the vesicle by activation of the voltage-gated chloride channel CLC-3 (Holz et al., 2006) **(Figure 1.4)**.

Following the GLP-1 binding to its receptor and the activation of the G proteins, GLP-1R is phosphorylated by the G protein receptor kinases (GRKs) and can interact with the β-arrestins. The β-arrestins are scaffold proteins that, upon binding with GLP-1R, reduce their sensitivity to the G proteins and induce the receptor endocytosis with consequent lysosomal degradation and signal termination. Additionally, β-arrestins can augment β-cell survival, by recruiting the non-receptor tyrosine kinase c-Src, which phosphorylates the extracellular signal-regulated kinases 1 and 2

(ERK1/2). This starts a series of anti-apoptotic events terminating with the inactivation of the pro-apoptotic protein Bcl-2-associated death promoter (BAD). (Jones, Bloom, Buenaventura, Tomas, & Rutter, 2018; Luttrell et al., 1999; Quoyer et al., 2010).

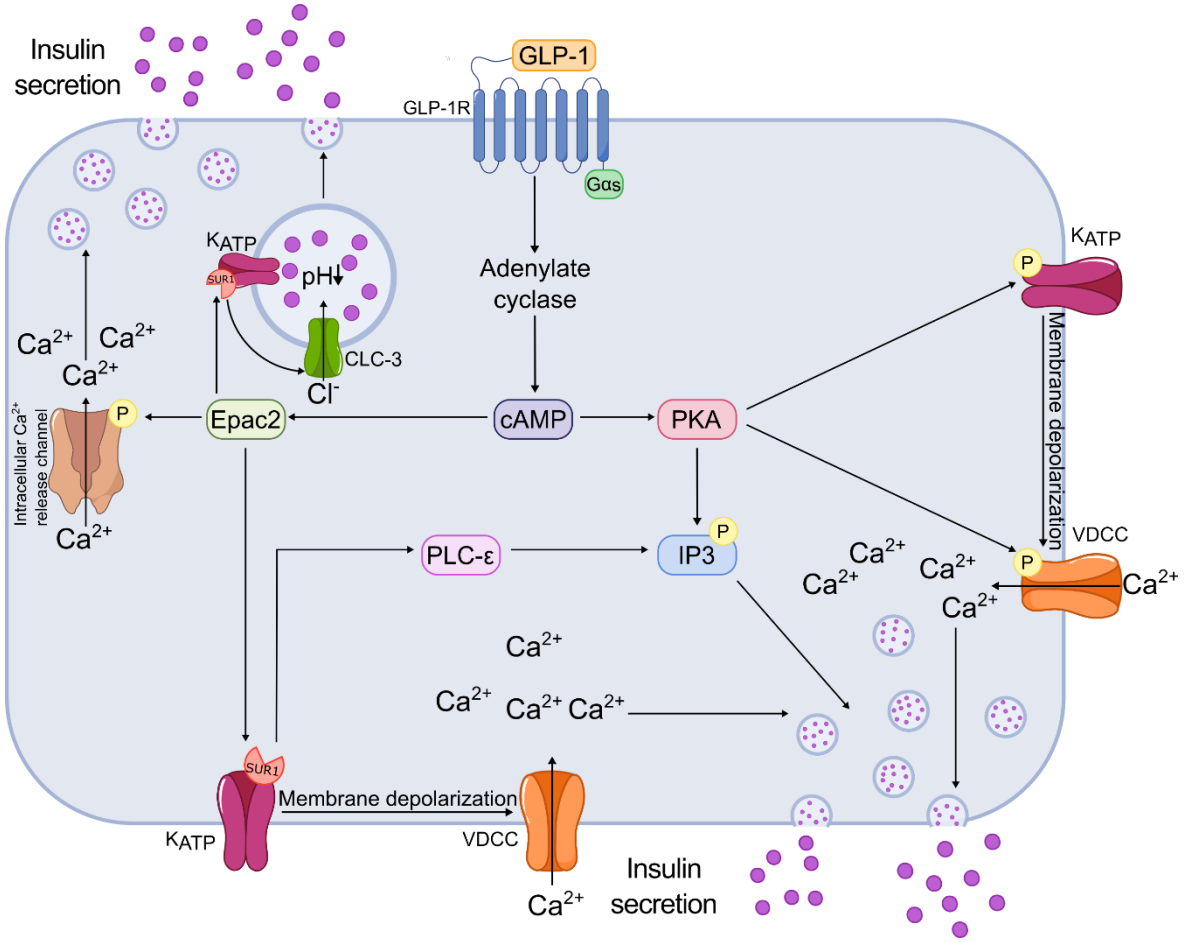

Figure 1.4 GLP1-R activity: GLP-1 binds to GLP-1R coupled to $G\alpha_s$, which activates the adenylate cyclase to produce cAMP. This can activate PKA, which phosphorylating KATP, VDCCs and IP3 can induce membrane depolarization and Ca^{2+} influx, leading to insulin secretion. Alternatively, cAMP can activate Epac2. This can phosphorylate the intracellular Ca^{2+} release channels, leading to Ca^{2+} accumulation and insulin exocytosis. Epac2 can also interact with the SUR1 subunit of K_{ATP} channels on the plasma membrane, causing membrane depolarization or activation of PLC-ε. The latter increases the levels of IP3 determining increased ATP sensitivity of the K_{ATP} channels. If Epac2 is recruited by SUR1 on the insulin granule membrane it stimulates the function of CLC-3 with consequent acidification and priming of the granule.

GIP is a 42 amino acid peptide, produced in the K-cells of the proximal small intestine (Baggio & Drucker, 2007). Its secretion is regulated by nutrients, neural stimuli and hormones. In particular, the ingestion of fat, glucose or proteins induces the dose-dependent secretion of GIP (Chia & Egan, 2020). Similar to GLP-1, it has a short half-life of two minutes in rodents and seven minutes in humans and it is inactivated by the action of DPP-4 (Deacon, Nauck, Meier, Hucking, & Holst, 2000; Kieffer, McIntosh, & Pederson, 1995). GIP exerts its action by binding to the GIP receptor (GIPR) on the pancreas, brain, bone and adipose tissue (Baggio & Drucker, 2007).

In the pancreatic β-cells, GIP binding to GIPR triggers a series of metabolic pathways increasing GSIS. As per GLP-1, GIP activates cAMP, which is linked to the activity of both PKA and Epac2, leading to K_{ATP} channel closure and increased Ca^{2+} influx (Baggio & Drucker, 2007; Ding & Gromada, 1997; Losada-Barragan, 2021). GIP is also responsible for the up-regulation of the transcription of the insulin gene (Wang et al., 1996).

Moreover, GIP is involved in increased β-cell proliferation and decreased apoptosis. These effects are mediated by the activity of PKA, the mitogen-activated protein kinase (MAPK), the cAMP response element binding protein (CREB) and the Akt-protein kinase B (PKB), that reduce the activity of pro-apoptotic factors such as caspase 3 and the Bcl-2-associated X protein (BAX) and increase that of the anti-apoptotic B-cell lymphoma 2 (Bcl-2) (Baggio & Drucker, 2007; Ehses et al., 2003; Kim et al., 2005; Trumper, Trumper, & Horsch, 2002).

Of note, GIPR has received much less interest than GLP-1R due to its downregulation, hence reduced insulinotropic effect during chronic high glucose. However, recent dual

GLP-1R/GIPR agonist approaches showed that GIPR is in fact therapeutically important (Bastin & Andreelli, 2019; Min & Bain, 2021).

1.1.5.4 Fructose

Although pancreatic β-cells do not possess the transporter for fructose, fructose can act as a potentiator of insulin secretion in combination with glucose (Curry, 1989). Fructose can either enter the β-cells through the glucose transporter GLUT2 or bind to the TIR2/3 receptors, activating PLC and inducing insulin secretion (Kyriazis, Soundarapandian, & Tyrberg, 2012; Tappy & Le, 2010). Alternatively, fructose was proven to be a secretagogue of GLP-1, which enables it to induce insulin exocytosis in an indirect way (Kong et al., 1999).

1.1.5.5 L-arginine

Several amino acids exert an insulinotropic action, in combination with glucose. In addition to the aforementioned glutamine and glutamate which can function through the activity of GDH, arginine can also stimulate insulin secretion in a glucose-dependent manner (Vetterli et al., 2012; Zhang et al., 2021). Arginine entrance into the β-cells, through the mCAT2A transporter, leads to the opening of the VDCCs, Ca^{2+} influx and consequent insulin exocytosis (Sener et al., 2000). Moreover, arginine can mediate an anti-apoptotic function decreasing the activation of caspase-3 within the islets (Ragy & Ahmed, 2019).

1.1.6 Disallowed genes

The pancreatic β-cell is a highly specialized insulin-secreting cell type, with a genetic profile that ensures the appropriate stimulus-secretion coupling. Mature β-cell identity is defined by the expression of a set of transcriptional factors, including *Pdx1*, *Nkx6.1* and *MafA* (Gao et al., 2014; Taylor, Benthuysen, & Sander, 2015; C. Zhang et al., 2005). In addition to this set of genes, there is also a pool of "disallowed" genes, whose repression guarantees the β-cells correct function (Quintens, Hendrickx, Lemaire, & Schuit, 2008). These are housekeeping genes that are specifically repressed or less abundant in β-cells or a few other cell types. The mechanisms by which their repression is achieved and maintained include histone methylation and microRNA (Martinez-Sanchez, Nguyen-Tu, & Rutter, 2015; Thorrez et al., 2011). Two of the best characterized disallowed genes are *Slc16a1* and *Ldha*, encoding for the monocarboxylate transporter 1 (MCT-1) and lactate dehydrogenase A (LDHA), respectively (Christensen & Gannon, 2019; Lemaire, Thorrez, & Schuit, 2016; Pullen & Rutter, 2013).

MCT-1 is responsible for transporting pyruvate and lactate across the plasma membrane, whereas LDHA converts pyruvate into lactate. Both these mechanisms are fundamental for anaerobic glycolysis, but their activity in β-cells would prevent the appropriate fueling of the TCA cycle and consequent insulin secretion (Pullen & Rutter, 2013; Schuit et al., 2012). Moreover, the repression of MCT-1 ensures that β-cells can discriminate intracellular pyruvate, produced in response to high glucose, and extracellular pyruvate likely derived from exercising (Otonkoski et al., 2007). This distinction is key for appropriate stimulus-secretion coupling (Otonkoski et al., 2007). Some disallowed genes such as hexokinases 1 and 3 (*HK1-HK3*) and the repressor

element 1 silencing transcription factor (*REST*) are not only repressed in β-cells but also in a few other cell types. The HKs catalyze the first and rate-limiting step of glycolysis, but HK1 and HK3 have a high affinity for glucose which would result in an overproduction of insulin by the β-cells. Pancreatic β-cells, as well as the liver and the pituitary gland, express GK, which has lower glucose affinity instead (Moukil, Veiga-da-Cunha, & Van Schaftingen, 2000; Quintens et al., 2008). Finally, REST is a transcriptional repressor, maintaining inactive chromatin during the maturation of neurons and embryonic stem cells. In most populations of neurons as well as in the pancreatic α and β-cells, *REST* is disallowed, as its expression would decrease the expression of SNAREs needed for synaptic transmission and insulin exocytosis (Cavadas et al., 2016; Lemaire et al., 2016; Martin & Grapin-Botton, 2017).

1.1.7 Amylin

Noticeably, the β-cells also secrete the islet amyloid polypeptide (IAPP) often called amylin, in a one-to-one ratio with insulin. Amylin plays a role in renal absorption, gastric mobility and metabolism, however, its overexpression can harm the β-cells leading to dysfunction and destruction (Leung, 2010b). This peptide induces the formation of cytotoxic amyloid fibrils as well as intracellular aggregates of proteins. These result in endoplasmic reticulum (ER) stress, a decrease of β-cell mass, reduced insulin secretion and increased apoptosis (Matveyenko & Butler, 2006; Montane, Klimek-Abercrombie, Potter, Westwell-Roper, & Verchere, 2012; Mukherjee, Morales-Scheihing, Butler, & Soto, 2015).

1.2 Hypoxia and prolyl hydroxylase domain proteins

1.2.1 Hypoxia

Hypoxia, or low oxygen tension, is a stimulus that has affected multicellular organisms since they evolved from their monocellular predecessors. Metazoans adapted to utilize oxygen to produce energy, which makes them susceptible to oxygen fluctuations. Depending on the intensity and duration, hypoxia can have both positive and negative effects on the tissues (Eales, Hollinshead, & Tennant, 2016). For instance, it is required during fetal development and liver zonation (Dunwoodie, 2009; Jungermann & Kietzmann, 2000). However, in most cases hypoxia is not compatible with normal, prolonged tissue functions, therefore, several biochemical pathways exist to sense hypoxia and induce acute cellular changes or long-term systemic alterations, to favor oxygen perfusion (Eales et al., 2016). The effects of hypoxia are often mediated by transcription factors that rapidly induce the expression of genes involved in proliferation, survival, metabolic adaptations, erythropoiesis and angiogenesis (Tirpe, Gulei, Ciortea, Crivii, & Berindan-Neagoe, 2019). The main regulators of cellular changes, in response to hypoxia, are the hypoxia-inducible factors (HIFs).

1.2.2 HIFs

The HIFs: HIF1, HIF2 and HIF3 are heteromeric complexes composed of one oxygen-sensing α subunit and a stable β subunit. During hypoxia, HIFα is stabilized and can dimerize, after translocation into the nucleus, with the HIFβ subunit. Moreover, in the nucleus HIFα interacts with the transcriptional co-activator cAMP response element-binding protein (CBP)/p300 to bind to the hypoxia-responsive elements (HREs) and

regulate the expression of its target genes (Tirpe et al., 2019; Yang, Su, Soga, Kranc, & Pollard, 2014) **(Figure 1.5)**. On the other hand, under normal oxygen tension, the expression of HIF target genes is prevented by the degradation of HIFα by the proteasome, primed by the activity of the prolyl hydroxylase domain proteins (PHDs), further described below. In addition to the latter, the HIFα function is regulated by the activity of the factor-inhibiting HIF (FIH). This is an α-KG-dependent dioxygenase that hydroxylates HIFα on an asparaginyl residue in its activation domain, preventing the CBP/p300 binding (Strowitzki, Cummins, & Taylor, 2019; Yang et al., 2014). Of note, there are three different isoforms of the α subunit, one for each heterodimer: HIF1α ubiquitously distributed, HIF2α to be found in endothelial, parenchymal and intestinal cells, and HIF3α that is less characterized (Yang et al., 2014). Not only do HIF1α and HIF2α have different expression profiles, but they also target different processes. Although their activities overlap sometimes, HIF1α acts mainly on energy production and metabolism, while HIF2α more often induces proliferation (Wiesener et al., 2003; Yang et al., 2014).

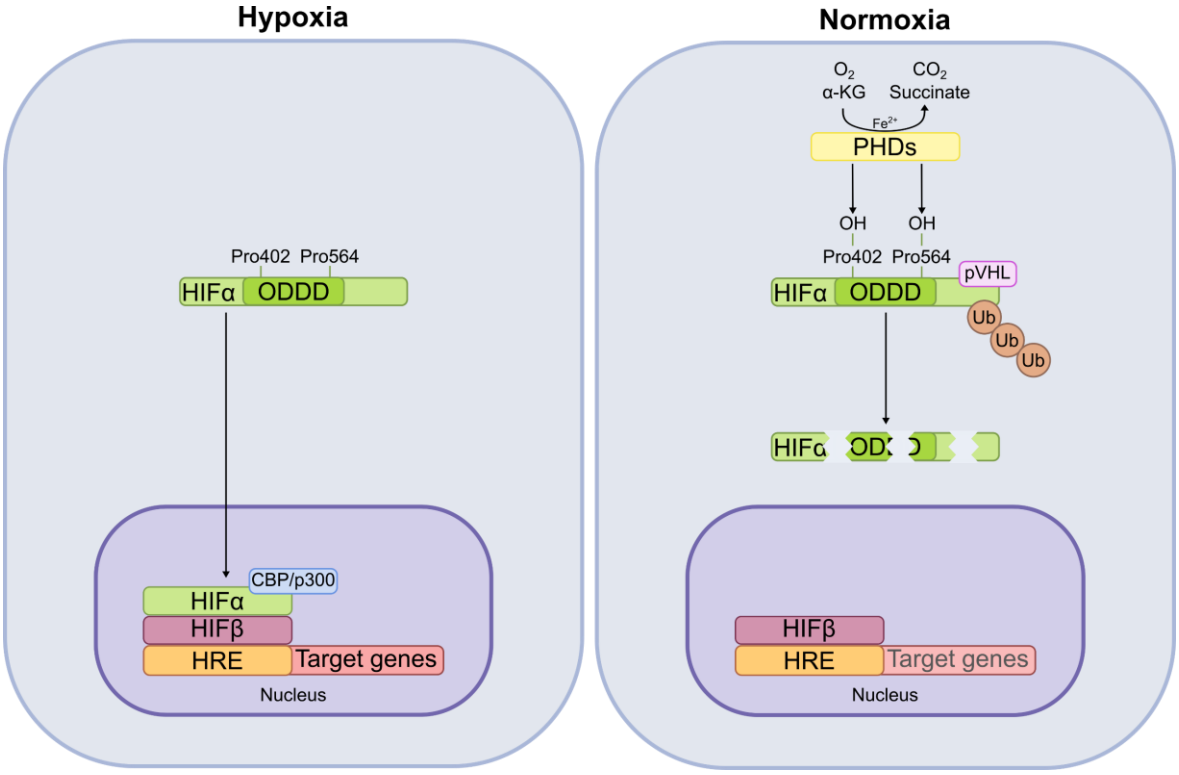

Figure 1.5 HIFs activity in hypoxia and normoxia: Under hypoxia, HIFα dimerizes with HIFβ into the nucleus. Here, through interaction with CBP/p300, the HIFα-HIFβ dimer can bind the HRE regulating the expression of target genes. During normoxia, the PHDs in presence of Fe^{2+} use α-KG to reduce O_2, to produce succinate, CO_2 and to hydroxylate HIFα on its Pro402 and Pro564 within the oxygen-dependent degradation domain (ODDD). Hydroxylated HIFα is recognized by the pVHL and polyubiquitinated for proteasomal degradation.

1.2.3 HIF-mediated processes

Both pathological and physiological events can induce hypoxia. This, through the activity of HIFs, leads to metabolic rewiring to sustain cell and tissue survival and function. However, these metabolic alterations can lead to malignant progression and poor prognosis of pathological conditions such as cancer. (Eales et al., 2016; Infantino, Santarsiero, Convertini, Todisco, & Iacobazzi, 2021). Amongst the most affected pathways, are glucose, mitochondrial, lipid and amino acid metabolism.

1.2.3.1 Glucose metabolism

During hypoxia, HIF1 can transcriptionally activate genes involved in glucose uptake and glycolysis. Thus, GLUTs, HKs, enolase 1, phosphoglycerate kinase 1, pyruvate kinase M2 (PKM2) and LDHA are overexpressed, increasing the glycolytic flux, the production of ATP and the accumulation of glycolytic intermediates (Nakazawa, Keith, & Simon, 2016; Xie & Simon, 2017). To meet the cell metabolic and energetic demand in spite of the reduce oxygen supply, the glycolytic intermediates can subsequently be used as substrates for biosynthetic pathways supporting cell growth, nucleotide and lipid synthesis (Infantino et al., 2021; Nakazawa et al., 2016; Yang et al., 2014). In addition to the anabolic function of PKM2, this can also act as a co-activator of HIF1α transcription (Luo et al., 2011).

Another target of HIF activity is pyruvate dehydrogenase kinase-1 (PDK1), which inhibits PDH leading to a decreased production of reduced nicotinamide adenine dinucleotide (NADH) and reduced flavin adenine dinucleotide ($FADH_2$), destined for the electron transport chain (ETC), hence for ATP production (Semenza, 2013).

Furthermore, through the induction of glycogen synthase 1 (GYS1), HIF stimulates the production and storage of glycogen (Pescador et al., 2010). This can be used to sustain the anaerobic glycolysis guaranteeing cell viability and proliferation, during prolonged hypoxic stress (Pescador et al., 2010). Finally, as mentioned above, LDHA is overexpressed in response to hypoxia, which leads to increased anaerobic metabolism of glucose and accumulation of lactate. As a consequence of the increased concentration of lactate, intracellular acidification occurs. This can inhibit the glycolytic flux, causing both lactate and hydrogen transport outside the cells, through MCT-1 and

carbonic anhydrase 9 (CA9). This, in turn, causes acidification of the extracellular space, a hallmark of cancer (Eales et al., 2016; Infantino et al., 2021).

1.2.3.2 Mitochondrial metabolism

Under oxygen-limiting conditions, the interplay between HIF and mitochondria is crucial to ensure cell survival. By increasing the expression of the gene encoding for PDK1, HIF limits pyruvate to acetyl-CoA conversion and reduces TCA cycle flux (Semenza, 2013). In addition to limiting the TCA cycle, HIF induces the transcription of genes encoding for succinate dehydrogenase, fumarate hydratase and isocitrate dehydrogenase, causing the accumulation of succinate, fumarate and L-2-hydroxyglutarate, which all contribute to HIF1α stabilization (King, Selak, & Gottlieb, 2006). Moreover, in hypoxia, the activities of Complex I and Complex II of the ETC are decreased while that of Complex IV is preserved to maintain membrane potential and to lower the accumulation of reactive oxygen species (ROS) (Infantino et al., 2021). In hypoxia, the COX4I2 subunit of Complex IV, also called cytochrome oxidase (COX), and the mitochondrial ATP-dependent LON protease are overexpressed (Fukuda et al., 2007; Hori et al., 2002; Semenza, 2007). Therefore, COX4I2 can substitute the COX4I1 subunit and lead to its degradation by LON. The COX4I2 subunit is more efficient as an electron transporter, resulting in the improved activity of Complex IV (Fukuda et al., 2007; Semenza, 2013). Finally, in the mitochondrion, HIF activates genes encoding for the BCL2 interacting protein 3 (BNIP3) and the BCL2 interacting protein 3 like (BNIP3L), triggering mitochondrial autophagy (mitophagy) (Bellot et al., 2009; Zhang et al., 2008). This mechanism is used by the cell to maintain oxygen homeostasis and to limit the accumulation of ROS

under hypoxia. Thus, mitophagy represents an adaptive response that keeps the cell surviving and reprogramming during hypoxic stress (Infantino et al., 2021; Zhang et al., 2008).

1.2.3.3 Lipid metabolism

Under hypoxia, HIF induces the expression of the fatty acid binding proteins 3 and 7 (FABP3 and FABP7), acylglycerol-3-phosphate acyltransferase 2 (AGPAT2) lipin-1 and the adipose differentiation-related protein (ADPR). These are all responsible for the accumulation and uptake of lipid droplets, which sustain cell survival and proliferation while protecting the cells from ROS (Bensaad et al., 2014; Mylonis et al., 2012; Triantafyllou, Georgatsou, Mylonis, Simos, & Paraskeva, 2018). The accumulation of lipid droplets is also induced by the HIF-mediated suppression of CPT1, which reduces the transport of fatty acids to the mitochondrion for β-oxidation (Du et al., 2017).

Moreover, HIF suppresses c-Myc, the transcriptional co-activator required for the activity of long- and medium-chain acetyl-CoA dehydrogenase, involved in the β-oxidation of fatty acids (Huang et al., 2014). Conversely, *de novo* lipid biosynthesis is promoted in hypoxia, where acetyl-CoA can accumulate from sources alternative to glucose (Xie & Simon, 2017).

Further, HIF induces the expression of the fatty acid synthase (FAS) and peroxisome proliferator-activated receptor-γ (PPAR-γ), stimulating fatty acids and glycerolipid synthesis, respectively (Infantino et al., 2021; Krishnan et al., 2009; Xie & Simon, 2017). Hypoxia also upregulates the ACLY that promotes lipid biosynthesis, acetyl-

CoA and NADPH production at the same time (Infantino, Iacobazzi, Palmieri, & Menga, 2013).

1.2.3.4 Amino acid metabolism

Both glutamine and serine play a central role in the hypoxic response. Given the reduced fueling of the TCA cycle by pyruvate, in hypoxia the glutamine transporters SLC1A5 and SLC38A2 are overexpressed and glutamine can enter the TCA cycle after being converted, by glutaminase (GLS), to glutamate and then α-KG (Morotti et al., 2019). The latter can either be turned into succinate following the oxidative TCA cycle or can go through reductive carboxylation to generate isocitrate (Metallo et al., 2011). This process can promote biosynthesis, energetics and homeostasis (Infantino et al., 2021). Serine is involved in the production of other amino acids and phospholipids and provides a carbon unit to the folate cycle. It is produced from glucose through the activity of three enzymes, including phosphoglycerate dehydrogenase (PHGDH), the latter being a target of HIF. In hypoxia, the hydroxymethyltransferase 2 of the folate cycle is overexpressed and catalyzes the degradation of serine with concurrent production of NADPH. The latter is then used for the GSSG to GSH conversion and antioxidant defense of the cells (Ye et al., 2014).

1.2.4 PHDs

PHDs are a superfamily of non-heme iron (Fe^{2+})-dependent dioxygenases that use electrons derived from α-KG to reduce molecular oxygen (O_2) producing succinate, carbon dioxide (CO_2) and *trans*-4-hydroxylated prolyl products (Schofield & Ratcliffe,

2004). Originally identified in *Caenorhabditis elegans* as HIF hydroxylases, PHDs are encoded by the *EGL-9* and its homologs *EGLNs* in mammalians (Epstein et al.). Humans and mice express three members of this family: *EGLN1, EGLN2* and *EGLN3* (*Egln1*, *Egln2* and *Egln3* in mice), encoding for PHD2, PHD1 and PHD3, respectively (Bruick, 2003; Bruick & McKnight, 2001; Schofield & Ratcliffe, 2004). Although sometimes overlapping, the three members have unique expression profiles, with PHD2 being expressed in all tissues, PHD1 highly expressed in testes, placenta, brain, kidney, heart and liver and PHD3 whose highest expression is in the heart (Lieb, Menzies, Moschella, Ni, & Taubman, 2002). Moreover, the isoforms have different localizations within the cells with PHD1 localized in the nucleus, PHD2 expressed in the cytosol and PHD3 being the only isoform expressed in both the nuclear and cytoplasmic compartments (Metzen et al., 2003).

1.2.5 Regulation of PHDs activity

Given their dependency on O_2 as substrate, PHDs play a crucial role as oxygen sensors. Under normoxia, PHDs bind α-KG, the HIFα subunit and O_2, leading to the hydroxylation of prolyl residues. These are Pro402 and Pro564, in two -Leu-X-X-Leu-Ala-Pro (X being any amino acid) sequences, within the highly conserved ODDD domain of HIFα (Boulahbel, Duran, & Gottlieb, 2009; Bruick & McKnight, 2001). This hydroxylation leads to the recognition of HIFα by the von Hippel-Lindau protein (pVHL) E3 ubiquitin ligase, for polyubiquitination and HIFα degradation by the proteasome (Kamura et al., 2000; Maxwell et al., 1999; Ohh et al., 2000; Schofield & Ratcliffe, 2004; Tanimoto, Makino, Pereira, & Poellinger, 2000) **(Figure 1.5)**. Conversely, a reduction

in the oxygen availability leads to PHD inhibition, stabilization of HIF and activation of the HIF-mediated pathways, as described above **(Figure 1.5)**.

Due to their dependency on several substrates and co-factors, in addition to oxygen, PHDs can also be regulated by the presence of succinate, fumarate, ascorbate, ROS and FK506 binding protein 38 (FKBP38). Succinate and fumarate are TCA cycle intermediates, structurally analogous to α-KG, that can compete with α-KG for its binding site, leading to inhibition of all PHDs (Kaelin & Ratcliffe, 2008; Koivunen et al., 2007). Antioxidants such as ascorbate can increase PHDs activity, by converting ferric iron (Fe^{3+}), derived from ROS production, to the PHDs co-factor Fe^{2+} (Fong & Takeda, 2008; Kaelin & Ratcliffe, 2008). Conversely, ROS accumulation leads to chelation and oxidation of Fe^{2+} to Fe^{3+}, reducing the activity of PHDs (Fong & Takeda, 2008). PHD2 availability is also limited by FKBP38, which leads to its degradation by the proteasome (Barth et al., 2009; Barth et al., 2007). Finally, a negative feedback role exists for HIF1α being able to induce the expression of PHD3 and, to a lesser extent, of PHD2 under hypoxia. Indeed, the increased activity of PHD2 and 3 under limiting oxygen conditions can guarantee fast HIF1α degradation after reoxygenation (del Peso et al., 2003; Schofield & Ratcliffe, 2004).

1.2.6 Non-HIF targets of PHDs

Although PHDs are historically known to target HIF leading to its degradation, it is becoming increasingly clear that these hydroxylases can also target other substrates, causing alterations in their stability, activity and interactions (Strowitzki et al., 2019). However, assigning the exact sites of hydroxylation remains difficult, even with high-

resolution techniques such as mass spectrometry (MS). In fact, for the identification of hydroxylation sites via MS, proteins of interest must be fragmented into shorter peptides. The gold standard for this procedure is the digestion with the serine-protease trypsin, leading to the formation of tryptic fragments (Laskay, Lobas, Srzentic, Gorshkov, & Tsybin, 2013). The non-enzymatic oxidation within the tryptic fragments results in their co-elution with the target prolyl-hydroxylated residues, confounding the identification of new hydroxylation sites (Cockman et al., 2019).

1.2.6.1 NF-κB

One substrate of particular interest is the nuclear factor kappa-light-chain-enhancer of activated B cells (NF-κB). This is a transcription factor involved in inflammation, immune and non-immune response, which is highly sensitive to hypoxia (Kennel, Burmeister, Schneider, & Taylor, 2018). Cummins *et al.* proved that the IKKβ, a kinase of the NF-κB pathway possesses a proline residue (Pro191) within a Leu-X-X-Leu-Ala-Pro motif that can be hydroxylated by PHD1. This negatively regulates the catalytic activity of the enzyme and the progression of the NF-κB pathway (Cummins et al., 2006).

1.2.6.2 CEP192

CEP192 is a centrosomal protein, involved in the correct formation of the centrosome during the cell cycle and in the production of cilia (Avidor-Reiss & Gopalakrishnan, 2013; Nigg & Stearns, 2011). CEP192 can be hydroxylated by PHD1 on its Pro1717, being ubiquitylated and targeted for proteasomal degradation. This ensures that the

levels of CEP192 are finely tuned during cell progression to guarantee centriole duplication, centrosome maturation, and spindle assembly (Moser et al., 2013).

1.2.6.3 RPB1

RPB1 is the biggest subunit of RNA polymerase II, which is regulated by phosphorylation and dephosphorylation of serine residues within its C-terminal domain. In human renal clear cell carcinoma, it was proven that PHD1 can hydroxylate the Pro1465 residue of RPB1. Thus, the hydroxylated RPB1 is recognized and ubiquitylated by the pVHL, however, this does not lead to proteasomal degradation. In fact, pVHL-dependent ubiquitylation is required to induce the phosphorylation of Ser5, the recruitment of RPB1 to the DNA and the control of the Pro1465 hydroxylation itself (Mikhaylova et al., 2008).

1.2.6.4 AKT

AKT is a serine-threonine kinase that promotes cell proliferation and survival. Its expression is often increased in cancer, favoring tumorigenesis and resistance to the therapies. It was shown that AKT is susceptible to oxygen level alteration, thus in hypoxia its degradation by pVHL is reduced, whereas in normoxia its stability is controlled by hydroxylation of its Pro125 and Pro313 by PHD2 (Guo et al., 2016).

1.2.6.5 mTOR

The serine/threonine kinase, mammalian target of rapamycin (mTOR), controls cellular metabolism in response to growth factors, oxygen, nutrients and amino acids.

However, the mechanisms by which mTOR detects the amino acids in the cells are yet to be elucidated. Several pathways were suggested, such as those involving the GTPase RHEB, the mitogen-activated protein kinase kinase kinase kinase 3 (MAP4K3), the human vacuolar protein sorting 34 (VPS34) and the RAS-related GTPase (RAG) (Findlay, Yan, Procter, Mieulet, & Lamb, 2007; Gulati et al., 2008; Kim, Goraksha-Hicks, Li, Neufeld, & Guan, 2008; Sancak et al., 2008). However, these do not explain how the amino acid availability is sensed to activate mTOR. As a consequence of amino acid catabolism, α-KG is produced and subsequently used by PHDs. These were inferred to be able to sense the amino acids and transduce the signal to mTOR (Boulahbel et al., 2009).

1.2.6.6 FOXO3a

Forkhead box O3 (FOXO3a) is a transcription factor involved in the suppression of cell proliferation and induction of autophagy, playing a central role in various cancer types (Greer & Brunet, 2005; H. Huang & Tindall, 2007). Within FOXO3a two prolyl residues, Pro426 and Pro437, can be hydroxylated by PHD1. This blocks FOXO3a interaction with USP9x deubiquitinase, leading to its degradation by the proteasome (Zheng et al., 2014).

1.2.6.7 TET

The ten-eleven translocation (TET) proteins are methylcytosine dioxygenases that play a crucial role in DNA methylation. This is a common hallmark of hypoxia and cancer progression, as it results in gene expression, cell proliferation and function, and

immune responses (Rasmussen & Helin, 2016). TET stability is controlled by pVHL-mediated ubiquitylation, which is primed by PHD2 and 3 hydroxylation of the TET proteins (S. Fan et al., 2020).

1.2.6.8 p53

P53 is a well-known tumor suppressor gene, commonly repressed in various cancer types, that is involved in the regulation of several cellular events such as DNA repair, apoptosis, arrest of cell cycle and senescence (Strowitzki et al., 2019). It was shown that PHD1 and PHD3 can hydroxylate Pro142 and Pro359 of p53, increasing its ubiquitination and proteasomal degradation (Rodriguez et al., 2018; Ullah et al., 2017). In addition to the alteration of p53 stability and localization exerted by both PHDs, PHD1 regulates its binding to p38α kinase, leading to chemoresistance, whereas PHD3 can modulate ubiquitination and have a greater impact on p53 stability (Deschoemaeker et al., 2015; Rodriguez et al., 2018).

1.2.6.9 Apoptotic pathways

Although some of the mechanisms have not been clarified yet, PHDs were found to interact with apoptotic pathways in several different backgrounds. PHD3 can regulate the activity of the kinesin family member 1B (KIF1B-β), involved in neuronal apoptosis. Although the hydroxylating function of PHD3 was confirmed in this pathway, KIF1B-β was not found to be the target, suggesting that the kinesin acts downstream from PHD3 (Schlisio et al., 2008). Another target of PHD3 was identified in the β2-adrenergic receptor (β2-AR). This is directly hydroxylated to be recognized by pVHL for

ubiquitylation and proteasomal degradation (Xie et al., 2009). In the embryonic rat heart-derived H9c2 cells, PHD3 was demonstrated to have a pro-apoptotic role by inhibition of the Bax-Bcl-2 pro-apoptotic complex formation (Liu et al., 2010). Finally, the expression of PHD1, and to a lesser extent, PHD2 in colonic epithelial cells was positively linked to the apoptotic marker caspase-3 (Van Welden, Laukens, Ferdinande, De Vos, & Hindryckx, 2013).

1.2.6.10 MAPK6

The mitogen-activated protein kinase 6 (MAPK6) is a pro-oncogenic gene that regulates cell differentiation, proliferation, migration and vascularization (Strowitzki et al., 2019). Its stability is affected by the hydroxylation, mediated by PHD3, of its Pro25. This leads to MAPK6 dissociation from the ubiquitin protein ligase E3A, preventing degradation by the proteasome (Rodriguez et al., 2016).

1.2.6.11 PAX2

Paired box 2 (PAX2) is a transcription factor, upregulated in several cancer types that controls cellular differentiation, proliferation, migration, survival and tissue development. Although the exact target prolyl residue is yet to be identified, it was shown that PHD3 can negatively control Pax2 by making it recognizable by pVHL, leading to its degradation by the proteasome (Yan et al., 2011).

1.2.6.12 ATF-4

The activating transcription factor 4 (ATF-4) is crucial during ER stress, regulates the amino acid metabolism and redox balance as well as autophagy and angiogenesis during tumor progression (Yang et al., 2014). It was found that PHD3 can hydroxylate ATF-4 on its Pro156, Pro162, Pro164, Pro167, and Pro174, negatively affecting its stability. However, ATF-4 degradation is not pVHL-dependent (Koditz et al., 2007). Although independently of its hydroxylation, a study by Hiwatashi Y *et al.*, indicated that the transcription activity of ATF-4 can be repressed by the co-expression of PHD1 and 3 (Hiwatashi et al., 2011).

1.2.6.13 CDKN1B

CDKN1B is a cyclin-dependent kinase inhibitor, playing a crucial role in the regulation of the cell cycle. Its increased expression during phase G1 blocks the transcription of the genes involved in the G1 to S transition. This is functional to cancer cells that are undergoing hypoxia as, being arrested before the S phase, they are less susceptible to cell death (Gardner et al., 2001). Although it is still unclear whether affecting its stability or inducing its expression, it was shown that PHD3, which is overexpressed in hypoxia, can control the activity of CDKN1B (Hogel, Rantanen, Jokilehto, Grenman, & Jaakkola, 2011).

1.2.6.14 PKM2

PKM2 is an isozyme of PK converting PEP to pyruvate. When oxygen levels are low, PHD3 can bind to PKM2, leading to dissociation or hindrance of the PKM2 tetramers

formation, therefore inhibiting its function (Chen et al., 2011). Moreover, PHD3 can facilitate PKM2 binding to HIF, making the kinase a co-factor for the expression of the HRE-dependent genes (Luo et al., 2011).

1.2.6.15 IRF7

During innate immunity, the interferon regulatory factor 7 (IRF7) is activated in response to viral infection to induce the expression of the interferon (IFN) (Tan, Sun, Chen, & Chen, 2018). In zebrafish, which conserves the IRF7 pathway similar to mammals, it was demonstrated that PHD3, although independent of its hydroxylating activity, suppresses the activity of IRF7, reducing the host protection from viral attack (Yu et al., 2020).

1.2.6.16 ACC2

The acetyl-CoA carboxylase (ACC) is the enzyme responsible for the conversion of acetyl-CoA to malonyl-CoA. There are two isoforms of ACC, namely ACC1 and ACC2 involved in the *de novo* lipogenesis and long-chain fatty acid oxidation (FAO), respectively. The malonyl-CoA produced by ACC2 inhibits the activity of the CPT1, the latter controlling the first step of mitochondrial FAO (Yoon et al., 2020). It was demonstrated, in acute myeloid leukemia (AML) and, more recently, in skeletal muscle, that PHD3 can hydroxylate ACC2 on its Pro450, in response to changes in nutrient abundance (German et al., 2016; Yoon et al., 2020). By hydroxylating this substrate, PHD3 inhibits FAO and prevents cells from using lipids. Conversely in AML and mouse skeletal muscle, the loss of PHD3 ensures the use of fatty acids to sustain cell

proliferation and exercise capacity respectively (German et al., 2016; Yoon et al., 2020).

1.3 PHD3 and the effect on glucose homeostasis

1.3.1 PHD3

As it appears from the alternative targets of PHDs, these hydroxylases are involved in a wide number of cellular events. They are closely connected to pathways related to cell cycle, proliferation, metabolism, immune response, cancer insurgence, progression and outcome, as well as to nutrient preference.

Amongst the three PHD isozymes, PHD3 is the only isoenzyme to be expressed in both the nuclear and cytoplasmic compartments, unlike PHD2 and PHD1 residing in the cytoplasm and nucleus, respectively (Metzen et al., 2003). In some cellular backgrounds, PHD3 preferentially hydroxylates HIF2α over HIF1α (Pugh, 2016). Notably, *EGLN3*, and to a lesser extent *EGLN2*, are also transcriptional targets of HIF, which induces their overexpression, providing a negative feedback mechanism in hypoxic conditions (Kaelin & Ratcliffe, 2008). Moreover, under chronic hypoxia PHD3 maintain its function and prevents cellular necrosis better than the other isoforms (Ginouves, Ilc, Macias, Pouyssegur, & Berra, 2008). In light of these differences, PHD3 can function adequately under both normoxia and hypoxia, in HIF-dependent and independent pathways (Jaakkola & Rantanen, 2013), accounting for its involvement in a wider range of mechanisms.

1.3.2 Regulation of glucose homeostasis

As discussed earlier, the activity of PHD3 is tightly linked to the availability of the reducing co-factor α-KG (Schofield & Ratcliffe, 2004). The latter is also one of the TCA cycle metabolites that accumulate in β-cells as a consequence of the anaplerotic

metabolism of pyruvate, working as a secretagogue for the second phase of GSIS (Rabaglia et al., 2005; Vetterli et al., 2012; Zhang et al., 2021). A study conducted by Huang, Paglialunga *et al.* identified PHDs, PHD3 in particular, as important mediators of insulin secretion (Huang et al., 2016). Using the PHD pan-inhibitor ethyl-3,4-dihydroxybenzoate (EDHB), they observed a significant decrease of glucose-stimulated production of TCA cycle metabolites and ATP/ADP ratio in the 832/13 cell line, derived from INS-1 rat insulinoma. Moreover, through siRNA-mediated knockdown of the three PHD isozymes, they could identify PHD3 as the isozyme with the highest impact on GSIS (Huang et al., 2016).

Despite previous studies excluding phenotypical and developmental alterations in response to whole-body PHD3 knockout (PHD3KO) (Minamishima et al., 2009; Takeda et al., 2006), the loss of PHD3 in hepatocytes influences insulin signaling, implying a more critical tissue-specific role (Taniguchi et al., 2013; Yano et al., 2018). *In vivo*, liver-specific PHD3KO was associated with the stabilization of HIF2α and the transcription of the insulin receptor substrate-2 (*Irs2*), central for insulin signaling and glucose tolerance (Taniguchi, Emanuelli, & Kahn, 2006; Taniguchi et al., 2013). Interestingly, another study from 2018 found that the effect of PHD3 abrogation in hepatocytes affects the stress signaling pathways independently of HIF2α and Irs2 (Yano et al., 2018). This divergence was probably due to the *in vitro* nature of the second study as opposed to the *in vivo* approach of the first. Although the difference likely resides in the activation of the stress pathways *in vivo* and *in vitro*, the exact mechanism by which PHD3KO eludes the activation of HIF2α *in vitro* is yet to be identified. Nevertheless, the *in vitro* setting unveiled a role for PHD3 in the suppression of stress signaling and consequent improvement of gluconeogenesis and insulin

signaling (Yano et al., 2018). These studies reported a central role for PHD3 in glucose sensing and insulin secretion. However, they focused on the use of immortalized cell lines or hepatocytes and did not investigate the effect of PHD3 directly in primary insulin-secreting pancreatic β-cells. Moreover, the recent findings about the ability of PHD3 to hydroxylate ACC2 in AML and skeletal muscle to inhibit fatty acid oxidation revealed an important function for PHD3 as gatekeeper of nutrient preferences, particularly the switch between glucose and fatty acid metabolism (German et al., 2016; Yoon et al., 2020).

Building upon this knowledge, the investigation of a potential role for PHD3 in β-cells metabolic rewiring and glucose homeostasis, with possible implications for diabetes risk is of the highest interest.

1.4 Metabolomics

The diverse functions of PHD3 and insulin secretion in the β-cells have a metabolic nature. Therefore, metabolomics represents a fundamental tool to understand how glucose homeostasis is regulated by PHD3. Metabolomics rose in the early 2000s, with the aim of providing a comprehensive identification of all the metabolites present in a biological sample at any given time (Newgard, 2017; Sussulini, 2017). This strategy can be employed for qualitative as well as quantitative analyses, through untargeted or targeted approaches, respectively. The former is used to profile hundreds of metabolites and it is often utilized to identify the differences between two experimental conditions (Newgard, 2017; Spegel & Mulder, 2020). This makes it the best technique for the generation of hypotheses. On the other hand, targeted metabolomics provides the actual metabolite concentrations, obtained by the ratio of its signal to that of an internal standard. Usually, stable isotope-labeled metabolites such as ^{13}C glucose or ^{2}H palmitate are used (Spegel & Mulder, 2020). This approach ensures the collection of data from a limited set of pre-selected metabolites, providing information about specific pathways or chemical classes (Sussulini, 2017).

Metabolomics is an analytical strategy comprising of three phases: sample preparation, separation and detection. The first step coincides with the extraction of the metabolites from the cells or tissues and it is commonly obtained by treatment with methanol, chloroform and water (Bligh & Dyer, 1959; Folch, Lees, & Sloane-Stanley, 1957). Following extraction, the samples are frequently separated via chromatography, to identify the different isomers. Most commonly they are separated by gas chromatography (GC) directly coupled to detection by MS (Fiehn, 2016). Alternatively,

data analysis can be performed via NMR, yielding more reproducible yet less sensitive data (Ren, 2018).

1.4.1 Radioactive isotopic tracing

It is worth noting that, although it was mostly overtaken by labeling with stable isotopes, radioactive isotopic tracing represented, for many years, the preferred tool for interpretation of metabolic pathways. Through scintillation spectrometry, the disappearance of radioactivity in the substrates and its appearance in the metabolic intermediates can be detected (Cantley et al., 2019; Lee, Wahjudi, Xu, & Go, 2010). However, this method measures activity with the assumption that the substrate and intermediate pools are homogeneous, whereas dilution with their non-labeled counterparts can confound the determination of specific pathways (Hellerstein & Neese, 1999). Although several techniques, including chemical degradation of the products are employed to overcome this, the use of stable isotopes proved advantageous as it does not require similar interventions; it is safer and has higher resolution (Lee et al., 2010).

1.4.2 Stable isotopic tracing

Each metabolite of an organism is simultaneously involved in several pathways, belonging to an intricate network of mechanisms occurring at the same time. This makes it extremely challenging to decipher the role of each metabolite into the pathway of interest, from its sole concentration (Fan et al., 2012). To facilitate this, cells or tissues that are under study can be labeled with non-radioactive stable isotopic tracers

(Metallo, Walther, & Stephanopoulos, 2009). The tracers are usually applied in a culture medium identical to that of non-treated cells or tissues, in which one or more nutrients are replaced with their labeled form containing, one or several heavier isotopes (Jang, Chen, & Rabinowitz, 2018). Understanding of metabolism is gained by tracking the fate of this nutrient and the incorporation of the isotopes into the various metabolites of the examined pathways. Both the number and the positions of the labeled atoms, within the metabolites deriving from the nutrient provided, are specific to the metabolic transformations occurring in a particular pathway. They are referred to as isotopologues and isotopomers, respectively, and are depicted by data acquisition through GC-MS and NMR (Fan et al., 2012).

1.4.3 GC-MS

GC-MS is currently the gold standard of metabolomics, providing high resolution, great sensitivity and ease of interpretation via comparison to universal spectral libraries (Lu, Liang, Dunn, Shen, & Kell, 2008; Ren, 2018). However, it is limited by technical variability and unsuitability for non-volatile analytes (Ren, 2018). To overcome these limitations GC-MS often requires a derivatization step, that through the addition of molecular groups containing carbon, oxygen, nitrogen, hydrogen and silicon, makes the metabolites volatile and more thermally stable (Hollinshead, 2016). Techniques usually employed include silylation, alkylation, acylation, methoximation and trimethylsilylation (Dunn et al., 2011; Fiehn, 2002; Ren, 2018).

Following GC-mediated separation, the samples are analyzed through MS which can detect and characterize ionized samples on the basis of their mass and charge (Murray

et al., 2013). MS is able to discern the mass shift of a metabolite containing one or more enriched isotopes, as compared to the same metabolite presenting all naturally abundant isotopes in its structure (Birkemeyer, Luedemann, Wagner, Erban, & Kopka, 2005). This analysis is referred to as mass isotopologues distribution (MID) and it is calculated as the ratio of each isotopologue abundance on the total amount of all possible isotopologues (Hollinshead, 2016). The information acquired by the MID analysis is representative of the incorporation of the labeled atoms from the nutrient provided into the deriving metabolites. Therefore, they describe the contribution of said nutrient to the pathways under study.

Although MID results can occasionally be sufficient to identify metabolic mechanisms occurring in a biological sample, greater accuracy can be gained by combining these data with NMR results.

1.4.4 NMR

Although hampered by lower sensitivity, NMR is a very useful tool for metabolomics studies, due to its high reproducibility, quantitative nature and simple preparation of the samples, which do not require derivatization or separation (Markley et al., 2017; Spegel & Mulder, 2020). Moreover, the use of more powerful NMR spectrometers operating at high frequencies is overcoming the sensitivity barrier, leading to quantitative and sensitive analyses (Ardenkjaer-Larsen et al., 2015).

NMR exploits the magnetic moment of the nuclei that possess an odd number of neutrons or protons, i.e. non-zero spin, to quantify or identify the metabolome within a biological sample (Heude, Nath, Carrigan, & Ludwig, 2017). Particularly effective for

NMR spectroscopy are those nuclei that have a spin number equal to ½, such as ^{1}H, ^{13}C, ^{31}P and ^{15}N. When subjected to a static magnetic field these nuclei are magnetized in its same direction. Following the application of a perpendicular magnetic field, induced by a short radiofrequency (RF) pulse, the magnetization of the nuclei is tilted. The precession of the magnetization back to the original static magnetic field produces the NMR signal, also known as free induction decay (FID) (Mlynarik, 2017).

Both one-dimensional (1D) and two-dimensional (2D) NMR methods are employed in metabolomics analyses. The most simple and common is the 1D-^{1}H NMR, which is ideal to quantify metabolite concentration, exploiting the ability of each proton within a molecule to produce a peak in a spectrum (Heude et al., 2017; Markley et al., 2017). However, equivocality can generate from the overlapping peaks and splitting of the signals occurring in 1D-^{1}H NMR (Heude et al., 2017). The signal of each ^{1}H on adjacent carbons causes J-coupling, thus splitting of their signal in several components, contributing to the ambiguity of the 1D-^{1}H NMR spectrum. 2D NMR spectroscopy can solve this by introducing a new dimension. A 2D method suitable for quantification is the 2D-^{1}H J-resolved NMR which separates the chemical shift from the J-coupling (Heude et al., 2017).

For identification purposes, 2D techniques such as proton-proton homonuclear correlated spectroscopy (^{1}H-^{1}H COSY), proton-proton homonuclear total correlation spectroscopy (^{1}H-^{1}H TOCSY) and proton-carbon heteronuclear single quantum coherence spectroscopy (^{1}H-^{13}C HSQC) are utilized (Markley et al., 2017). The latter, matching the peaks coming from ^{1}H and ^{13}C, is ideal for metabolic tracing and combination with GC-MS data. In ^{1}H-^{13}C HSQC NMR, in response to a sequence of RF pulses, the protons and the ^{13}C to which they are bonded are magnetized,

associating their resonance frequency. Therefore, the signal obtained is reflective of ^{1}H-^{13}C bonds and it is represented by the chemical shift of the protons, shown in the horizontal dimension, combined to the chemical shift of ^{13}C, in the vertical dimension (Heude et al., 2017; Hollinshead, 2016). The components of each metabolite spectrum, that is the multiplet, is specific to each ^{13}C binding to ^{1}H and neighboring carbons. Therefore, in tracing experiments, the evaluation of ^{13}C incorporation into the metabolites, detected in a biological sample, is achieved by multiplet analysis (Hollinshead, 2016). Finally, by combination with GC-MS isotopologues information, NMR can enable pathway determination by observation of isotopomer patterns (Fan et al., 2012).

1.5 Thesis aim

Pancreatic β-cells are exquisite sensors of glucose level in the body and the only source of circulating insulin in mammals. Thus, they possess mechanisms to finely regulate the stimulus-secretion coupling. The early response to high blood glucose is the activation of the triggering pathway of insulin secretion. This is mainly regulated by the presence of GLUTs and GK, whose low affinity for glucose ensures that the β-cells do not respond to inappropriately low glucose concentrations. In the post-prandial phase, the triggering pathway is complemented by the amplifying pathways, inducing sustained insulin secretion in response to other nutrients. Fructose, incretins, free-fatty acids and amino acids can all contribute to the second phase of GSIS, placing GLUTs and GK less centrally. Moreover, insulin secretion is supported by the anaplerotic metabolism of pyruvate and the consequent accumulation of citrate, malate, glutamine, glutamate and α-KG. The importance of α-KG as a co-factor for PHD3 provides the rationale for the investigation of the role of PHD3 in glucose metabolism.

PHD3 is a member of the PHD family of enzymes using O_2 and α-KG to obtain *trans*-4-hydroxylated prolyl products. The main and most characterized substrate of PHDs is the oxygen sensing HIFα, which is hydroxylated during normoxia to then undergo proteasomal degradation. In addition to their role as inhibitors of HIFα activity, PHDs have also been linked to several cellular events, dependent on alternative targets and often involved in cancer onset and progression. Of the three isoforms, PHD3 was found to be the one having the larger set of suggested targets. Interestingly, PHD3 was shown to be able to hydroxylate ACC2, controlling the nutrient preference for glucose over fatty acids, in AML and skeletal muscle. Additionally, studies on the effect of PHD3KO in a rat β-cell line and on the liver placed PHD3 on a central stage

for glucose metabolism and insulin secretion. However, these works did not investigate the role of PHD3 in primary pancreatic β-cells.

Building upon this knowledge, this thesis aims to investigate the effect of a β-cell specific PHD3KO on glucose metabolism in a mouse model. Based on the reported role of PHD3 as gatekeeper of nutrient preference, it was hypothesized that its loss could determine a shift towards fatty acid utilization to sustain insulin secretion. To investigate this, we subjected our model to phenotypical and functional characterization as well as to high-resolution isotope-resolved metabolic tracing. The effects of PHD3KO in β-cells were observed under three dietary conditions, namely standard chow, 4 weeks of high fat diet and 8 weeks of high fat diet (discussed in chapters 3, 4 and 5 respectively). Finally, high-resolution mapping of glucose fate in islets of wild-type mice and humans was performed. This allowed us to obtain even more detail on how glucose is handled, identifying potential mechanisms through which PHD3 may act. Importantly, we assessed where human and mouse glucose metabolic pathways converge and diverge and how our findings can translate to human β-cell function (chapter 6).

Chapter 2

MATERIALS AND METHODS

2.1 Animal generation and *in vivo* work

All animal studies were approved by the University of Birmingham's Animal Welfare and Ethical Review Body and regulated by the Animals (Scientific Procedures) Act 1986 of the U.K. (PPL P2ABC3A83 and PP1778740).

All *in vivo* experiments were performed together with Dr. Daniela Nasteska who is signed off for the animal procedures herein.

2.1.1 Mouse models

Mice with a β-cell specific deletion of *Egln3*, the gene encoding for PHD3, were generated with a Cre-LoxP system. Animals expressing the *Cre* recombinase within the *Ins1* gene (*Ins1Cre,* C57BL/6J background) (JAX stock no. 026801) and mice expressing floxed *Egln3* (*Egln3$^{fl/fl}$,* C57BL/6J background) (Takeda et al., 2006) were used for breeding. Of the resulting offspring, the *Ins1Cre;Egln3$^{wt/fl}$* mice were crossed with *Egln3* floxed ones (*Egln3$^{fl/fl}$)* to generate *Ins1$^{wt/wt}$;Egln3$^{wt/fl}$, Ins1$^{wt/wt}$;Egln3$^{fl/fl}$, Ins1Cre$^{+/-}$;Egln3$^{wt/fl}$* and *Ins1Cre$^{+/-}$;Egln3$^{fl/fl}$* mice. Animals with a β-cell specific PHD3KO (βPHD3KO) (*Ins1Cre$^{+/-}$;Egln3$^{fl/fl}$*) and controls (βPHD3CON) (*Ins1$^{wt/wt}$;Egln3$^{fl/fl}$*) were used from 8 to 20 weeks of age. Mice were either fed a standard chow (SC) or, starting at 7-8 weeks of age, a 60% high fat diet (HFD) (Research Diets) **(Appendix 1)** for 4 or 8 weeks.

For the investigation of the effect of *Cre* or floxed *Egln3 per se* a different breeding strategy was employed. Thus, the established control (*Ins1$^{wt/wt}$;Egln3$^{fl/fl}$)* was crossed to the wild-type (WT) C57BL/6J (JAX stock no. 000664) to obtain *Ins1$^{wt/wt}$;Egln3$^{wt/fl}$* and *Ins1Cre$^{+/-}$;Egln3$^{wt/fl}$*. These were further crossed, generating *Ins1$^{wt/wt}$;Egln3$^{fl/fl}$*,

Ins1$^{wt/wt}$*;Egln3*$^{wt/fl}$, *Ins1*$^{wt/wt}$*;Egln3*$^{wt/wt}$, *Ins1Cre*$^{+/-}$*;Egln3*$^{fl/fl}$, *Ins1Cre*$^{+/-}$*;Egln3*$^{wt/fl}$, *Ins1Cre*$^{+/-}$*;Egln3*$^{wt/wt}$. Of these, the *Ins1*$^{wt/wt}$ *Egln3*$^{fl/fl}$, *Ins1Cre*$^{+/-}$ *Egln3*$^{wt/wt}$, and *Ins1*$^{wt/wt}$ *Egln3*$^{wt/wt}$ animals were kept on a HFD for 4 weeks before being assessed for glucose tolerance as described below.

A R26-LSL-hM4Di/mCitrine (JAX stock no. 026219) DREADD reporter strain was used to confirm the recombination efficiency of the Ins1Cre allele. Furthermore, male 8 to 12 week-old WT CD1 mice (Charles River stock no. 022) were used for experiments under hypoxic (1% O_2) conditions as well as for the $^{13}C_6$ glucose tracing coupled GC-MS and NMR as indicated below

2.1.2 Mouse maintenance

All mice were housed in a specific pathogen-free facility, on a 12 h light/12 h dark cycle with lights being switched on at 6:00 a.m. All animals had free access to food and water.

2.1.3 Intraperitoneal and oral glucose tolerance test (IPGTT and OGTT)

Animals were fasted for 4 to 6 h before being challenged with glucose through intraperitoneal injection or oral gavage. Mice on SC were administered 2 g/kg body weight of glucose, whereas those fed an HFD received 1 g/kg body weight of glucose. After 0, 15, 30, 60, 90 and 120 min, blood samples were collected from the tail vein and measured for glucose concentration with a Contour XT glucometer (Bayer, Germany). Animals fed a SC underwent IPGTT every 2 weeks between 8 and 20 weeks of age, while HFD fed mice were only tested after 72 h, 4 and 8 weeks of HFD.

2.1.4 Insulin tolerance test (ITT)

Following 4 to 6 h (for SC and 4 weeks HFD) or overnight (for 8 weeks HFD) fasting the animals were challenged with an intraperitoneal dose of 0.75 U insulin (Humulin S, 100 U/mL, Lilly, UK) per kg of body weight and tested for blood glucose using a Contour XT glucometer (Bayer, Germany) after 0, 15, 30, 60, 90 and 120 min.

2.1.5 Serum insulin

Mice were challenged with 1 g of glucose per kg of body weight, injected via the intraperitoneal route and tested for serum insulin after 0, 15 and 30 min. Serum was obtained by centrifugation at 2500 rpm for 10 min at 4°C and measured using a Cisbio mouse serum insulin HTRF assay kit.

2.1.6 Body composition measurement

After 4 and 8 weeks of HFD, mice were weighed and culled by cervical dislocation. Epididymal fat pads, subcutaneous fat, brown adipose tissue, liver, and quadriceps femoris were harvested and immediately weighed. The body composition was expressed as a percentage of the body weight.

2.2 Tissue culture

2.2.1 Mouse islet isolation and dissociation

Animals were culled using a schedule-1 method followed by injection of the common bile duct with 1 mg/mL collagenase NB 8 (Serva) in RPMI 1640 (Gibco) and pancreas dissection. After dissection, the pancreas was incubated in a water bath at 37°C for 12 min. Subsequently, the tissues were shaken in 15 mL of RPMI 1640 and centrifuged for 1 min at 1500 rpm three times to induce mechanical digestion. Histopaque-1119 and 1083 (Sigma-Aldrich) or Ficoll (GE Healthcare) were used for gradient separation and islets isolation (Ficoll was occasionally used due to global shortages of Histopaque). Finally, the islets were hand-picked and placed in a 10 cm Petri dish for suspension culture. Unless otherwise stated, the islets obtained were kept in culture in RPMI 1640 supplemented with 10% fetal bovine serum (FBS, Gibco), 100 units/mL penicillin, and 100 µg/mL streptomycin (Sigma-Aldrich), at 37°C and 5% CO_2 for up to five days. In experiments that required treatments with exogenous fatty acids either 0.75% bovine serum albumin (BSA, Sigma-Aldrich), as control, or 150 µM sodium palmitate (Sigma-Aldrich) and 0.75% BSA, as treatment, were added to the medium for 48-72 h. Prior to the addition, sodium palmitate was reconstituted in methanol (Sigma-Aldrich), heated up to 65°C in a water bath and agitated for 15 min, to ensure dissolution. Hypoxic procedures were carried out in Don Whitely H35 Hypoxystations at oxygen tensions of either 21% O_2 or 1% O_2.

2.2.2 Human islets isolation and dissociation

Human islets were provided by the San Raffaele Diabetes Research Institute (DRI), Milan, Italy (ECIT Islet for Basic Research program). Further human islets were obtained under Dr. Ildem Akerman's material transfer agreement (MTA) from Prof. Julie Kerr-Conte/Pattou of the Translational Research for Diabetes at the University of Lille, Lille, France. Upon receipt, the islets were cleared of possible debris via filtration with a 40 µm cut-off filter, hand-picked and cultured in CMRL medium (Corning) supplemented with 5.5 mM glucose (Sigma-Aldrich), 10% FBS, 100 units/mL penicillin, 100 µg/mL streptomycin and 0.1% amphotericin B (Sigma-Aldrich) at 37°C and 5% CO_2. Donor characteristics are reported in **Appendix 2**.

2.2.3 Glucose- and Exendin4 (Ex4)-stimulated insulin secretion

Ten to fifteen size-matched islets were incubated in HEPES-bicarbonate buffer (120 mM NaCl, 4.8 mM KCl, 24 mM $NaHCO_3$, 0.5 mM Na_2HPO_4, 5 mM HEPES, 2.5 mM $CaCl_2$, 1.2 mM $MgCl_2$) supplemented with 0.1% BSA at 37°C. Following pre-incubation with 3 mM glucose for 30 min, the islets underwent stimulation with 3 mM glucose, 16.7 mM glucose and 16.7 mM glucose + 20 nM Exendin4 (Sigma-Aldrich), a GLP1R agonist, for 30 min at 37°C each. The supernatant fractions were collected after each incubation and used for insulin secretion analyses. Finally, total insulin was extracted, incubating the islets in acid ethanol (75% ethanol, 1.5% HCl) at 4°C, overnight. Insulin concentration (ng/mL) was measured, via an HTRF assay (PerkinElmer).

2.2.4 Homogenous Time-Resolved Fluorescence (HTRF) Assay

An HTRF insulin ultra-sensitive assay kit (PerkinElmer) was used to measure the concentration of the total and secreted insulin according to the manufacturer's instructions. This kit allows insulin to be detected through the use of an anti-insulin antibody labeled with Europium (Eu^{3+}) cryptate and an anti-insulin antibody labeled with XL665. When these two are in close proximity a light source can be used to excite the Eu^{3+} cryptate, triggering a Fluorescence Resonance Energy Transfer (FRET) towards XL665, which fluoresces at 665 nm. The intensity of the obtained signal is proportional to the amount of the antigen-antibody interaction, therefore, to the concentration of insulin. To measure the insulin concentration, the supernatant fractions of the total and secreted insulin samples were diluted. For experiments under SC, supernatant from islets stimulated with 3 mM glucose, 16.7 mM glucose and 16.7 mM glucose + 20 nM Exendin4 underwent 1:5, 1:30 and 1:60 dilutions, respectively. Total insulin samples were diluted 1:280. For the assay in islets from HFD-fed animals, the dilution ranges for insulin secretion samples were 1:4-1:5, 1:8-1:20 and 1:15-1:40 for stimulation with 3 mM glucose, 16.7 mM glucose and 16.7 mM glucose + 20 nM Exendin4, respectively, and 1:250-1:400 for total insulin content. Subsequently, 5 µL of the diluted supernatant fractions were incubated with 2.5 µL of anti-insulin-XL665 and 2.5 µL of anti-insulin- Eu^{3+} cryptate overnight and then analyzed at an HTRF compatible PHERAstar FS reader (BMG LABTECH). The obtained values were used to calculate insulin concentration against a standard curve (ranging from 0 to 8 ng/mL).

2.3 Molecular biology

2.3.1 RNA extraction and cDNA synthesis

RNA was extracted from mouse islets using 500 µL of TRIzol reagent (Sigma-Aldrich) and 100 µL of chloroform (Sigma-Aldrich). Following centrifugation at 12000 g for 15 min at 4°C, the aqueous phase was collected and the RNA was recovered through the addition of an equal volume of isopropanol (Sigma-Aldrich) and 2 µL of glycogen (Thermo Fisher). Upon further centrifugation, the pellet was washed with 70% ethanol, resuspended in nuclease-free water (Quiagen) and the RNA quantified at NanoDrop (ThermoFisher Scientific).

Subsequently, the genomic DNA was removed with DNase I treatment (ThermoFisher Scientific) in presence of magnesium chloride ($MgCl_2$) and ethylenediaminetetraacetic acid (EDTA). The cDNA was synthesized by reverse transcription of the extracted RNA, using a High-Capacity cDNA Reverse Transcription Kit (Applied Biosystems). A 10 µL mix of 10X RT Buffer, 10X RT Random Primers, 25X dNTP Mix and MultiScribe Reverse Transcriptase in water, was combined with 10 µL of RNA and incubated for 10 min at 25°C, 120 min at 37°C and finally for 5 min at 85°C.

2.3.2 Quantitative Real-Time PCR (qRT-PCR)

To assess gene expression through real-time qPCR, 5 µL of PowerUp SYBR Green solution (ThermoFisher Scientific) and 0.12 µL of 10 µM forward and reverse primer mixes, as per **Table 1**, were added to 1 µL cDNA. Amplification curves were obtained by detection of SYBR green fluorescence at the 7500 Real-Time PCR system or the QuantStudio™ 5 Real-Time PCR system. The relative quantification of the expression

of the genes was obtained by comparing the expression of each gene of interest in the treated samples, to the expression of the same gene in the untreated sample. This was calculated with the $2^{(-\Delta\Delta Ct)}$ method and expressed as fold-change of gene expression in βPHD3KO relative to βPHD3CON or βPHD3CON at 21%O_2 were appropriate. Housekeeping genes, namely *Ppia* and *Actb*, were used as a control for experimental variability.

Table 1: Primers used for qRT-PCR

Gene name	Forward sequence (5'-3')	Reverse sequence (5'-3')
Ppia	AAGACTGAGTGGTTGGATGG	ATGGTGATCTTCTTGCTGGT
Actb	CGAGTCGCGTCCACCC	CATCCATGGCGAACTGGTG
Egln3 (Exon 2)	GCTTGCTATCCAGGAAATGG	GCGTCCCAATTCTTATTCAG
Egn3 (Exon 1)	GGCTGGGCAAATACTATGTCAA	GGTTGTCCACATGGCGAACA
Egln1	TAAACGGCCGAACGAAAGC	GGGTTATCAACGTGACGGACA
Egln2	CATCAATGGGCGCACCA	GATTGTCAACATGCCTCACGTAC
Bnip3	CTGGGTAGAACTGCACTTCAG	CTGGGTAGAACTGCACTTCAG
Car9	GGAGCTACTTCGTCCAGATTCAT	CCGGAACTGAGCCTATCCAAC
Gls	TTCGCCCTCGGAGATCCTAC	CCAAGCTAGGTAACAGACCCT
Ldha	TTCAGCGCGGTTCCGTTAC	CCGGCAACATTCACACCAC
Cpt1a	CTCCGCCTGAGCCATGAAG	CACCAGTGATGATGCCATTCT
Acaca	CTTCCTGACAAACGAGTCTGG	CTGCCGAAACATCTCTGGGA
Acacb	CCTTTGGCAACAAGCAAGGTA	AGTCGTACACATAGGTGGTCC
Pdx1	CCAAAGCTCACGCGTGGA	TGTTTTCCTCGGGTTCCG
Nkx6-1	GCCTGTACCCCCCATCAAG	GTGGGTCTGGTGTGTTTTCTCTT
Mafa	CTTCAGCAAGGAGGAGGTCATC	CGTAGCCGCGGTTCTTGA
Ddit3	CTGGAAGCCTGGTATGAGGAT	CAGGGTCAAGAGTAGTGAAGGT
Xbp1	AGCAGCAAGTGGTGGATTTG	GAGTTTTCTCCCGTAAAAGCTGA
Hspa5	ACTTGGGGACCACCTATTCCT	GTTGCCCTGATCGTTGGCTA
Ccnd1	GCGTACCCTGACACCAATCTC	CTCCTCTTCGCACTTCTGCTC
Dll4	TTCCAGGCAACCTTCTCCGA	ACTGCCGCTATTCTTGTCCC

2.3.3 Transcriptomic data set visualization

All transcriptomic data sets used are freely available via EMBL-EBI and GEO databases and accessible through www.isletregulome.com. Human islets donor information and experimental procedures for RNA-Seq and ChIP-Seq were previously described (Akerman et al., 2021; Akerman et al., 2017; Moran et al., 2012; Pasquali et al., 2014). For their visualization, processed data files (EBI: E-MTAB-1919, E-MTAB-1294 and GEO: GSE151405) were downloaded and loaded onto the local open source University of California Santa Cruz Genome Browser (www.genome.ucsc.edu) (Kent et al., 2002).

2.4 Functional imaging

Ca^{2+}, ATP/ADP and cAMP imaging were all performed in 1 mL of HEPES-bicarbonate buffer with glucose and drugs being added at the indicated time points and concentrations, using a Crest X-Light spinning disk microscope coupled to a Nikon Ti-E base with 10 × 0.4 NA and 20 × 0.8 NA objectives.

2.4.1 Ca^{2+} imaging

For Ca^{2+} imaging either Fura2 or Fluo8 (both AAT Bioquest) were added to the 10 islets 40 min prior to imaging and used as sensors. The first probe was excited at λ = 340 nm and λ = 385 nm using FuraLEDs in widefield mode and emitting signals were collected at λ = 470-550 nm. Fura2 traces were normalized as the ratio of 340/385. For Fluo8, the excitation was delivered at λ = 458-482 nm using a Lumencor Spectra X light engine and the emitted signals were detected at λ = 500-550 nm through a highly sensitive Photometrics Delta Evolve EM-CCD. All Ca^{2+} imaging experiments were performed starting at 3 mM glucose, which was increased to 17 mM glucose after 3 min of imaging. After 20 min, 10 mM of the generic depolarizing stimulus, potassium chloride (KCl) were added, before concluding the experiment at minute 24. Analyses were performed on ImageJ (Schindelin et al., 2012; Schneider, Rasband, & Eliceiri, 2012) and data were presented as raw or F/Fmin where F = fluorescence at any time point and Fmin = minimum fluorescence.

2.4.2 ATP/ADP ratio

To evaluate the ATP/ADP ratios, the islets were transduced with the ATP/ADP sensor Perceval (gifted by Prof Gary Yellen, Harvard), using an adenoviral vector (Berg, Hung, & Yellen, 2009) and cultured at 37ºC and 5% CO_2 for 48 h. As for Ca^{2+} imaging with Fluo8, the probe was excited at λ = 458-482 nm using a Lumencor Spectra X light engine and the emission was detected at λ = 500-550 nm through a highly-sensitive Photometrics Delta Evolve EM-CCD. For ATP/ADP imaging an initial concentration of 3 mM glucose was employed and increased to 17 mM glucose after 5 min, before concluding the experiment at minute 29. When assessing the ATP/ADP responses to Etomoxir (ETX, Sigma-Aldrich), a CPT1 inhibitor, the initial concentration of glucose was 3 mM and was augmented to 11 mM after 3 min and kept constant until minute 23. To treat the islets, 100 µM of ETX were added at minute 13. ATP/ADP data were presented as R/R0 where R = fluorescence at any time point and R0 = fluorescence at 0 min.

2.4.3 cAMP imaging

For cAMP imaging, islets were transduced with an adenovirus containing Epac2-camps (gifted by Prof Dermot Cooper, Cambridge) (Everett & Cooper, 2013) and kept at 37ºC and 5% CO_2 for 48 h. Excitation was delivered at λ = 430-450 nm. The emitted signals were detected at λ = 460-500 nm and λ = 520-550 nm for Cerulean and Citrine, respectively. During cAMP imaging, the concentration of glucose was kept constant at 11 mM until min 29, and 10 nM of Exendin4 were added at minute 5. Epac2-camps traces were normalized as the ratio of Cerulean/Citrine using ImageJ (Schindelin et al., 2012; Schneider et al., 2012). Data were shown as F/Fmin.

2.4.4 Immunohistochemistry (IHC)

Isolated pancreata were fixed in 10% formalin, embedded in paraffin, cut in 1 µm-thick slices, at a distance of 50 µm from each other and deposited on Superfrost® Plus slides. Each slide was then deparaffinized and rehydrated through 3 incubations of 2 min each in Histoclear (National Diagnostic), 5 min in 100% ethanol, 5 min in 95% ethanol, 5 min in 70% ethanol and 2 incubations of 2 min each in water. Subsequently, the slides were exposed to citrate buffer at 95°C for 20 min for antigen retrieval and blocked with phosphate buffered saline (PBS) + 0.1% Triton-X-100 (Sigma-Aldrich) + 2% BSA for 60 min at room temperature (RT). The slices were incubated with primary antibodies at 4°C, overnight and with secondary antibodies for 1 h, at RT. Finally, coverslips were mounted using Vectashield HardSet with DAPI. Sections stained for PHD3 were incubated with guinea pig anti-insulin and rabbit anti-PHD3, followed by incubation with anti-guinea pig Alexa Fluor 568 and anti-rabbit Alexa Fluor 488 (See **Table 2** for antibody details). For PCNA staining a rabbit anti-insulin and mouse anti-PCNA were used as primary antibodies followed by anti-rabbit Alexa Fluor 568 and anti-mouse Alexa Fluor 488 **(Table 2)**. Images were acquired with a Zeiss LSM780 meta-confocal microscope equipped with highly-sensitive GaAsP detectors (See **Table 2** for excitation and emission wavelenghts). For β-cell mass (%) analysis, 425 images per section, stained with rabbit anti-insulin followed by anti-rabbit Alexa Fluor 647 and Vectashield HardSet with DAPI **(Table 2)**, were acquired with a Zeiss Axio Scan.Z1 automated slide scanner equipped with a 20× / 0.8 NA objective and the emitted signals were detected by an Orca Flash 4.0 camera **(Table 2)**. Calculations were performed on ImageJ (Schindelin et al., 2012; Schneider et al., 2012) dividing the area of the insulin-positive staining by the area of the whole pancreas section.

Isolated islets were fixed in 4% paraformaldehyde in PBS for 15 min at RT and, similarly to the sections, were incubated in citrate buffer at 95°C for 20 min to retrieve the antigens, prior to 1 h incubation with blocking buffer, primary antibody **(Table2)** at 4°C, overnight and with secondary antibodies **(Table 2)** for 1 h, at RT. To assess the α-cell/β-cell ratio the islets were stained with rabbit anti-insulin and mouse anti-glucagon followed by anti-rabbit Alexa Fluor 647 and anti-mouse Alexa Fluor 488 respectively **(Table 2)**. A Zeiss LSM780 meta-confocal microscope equipped with highly-sensitive GaAsP detectors was employed to image the islets **(Table 2)**, which were subsequently analyzed on ImageJ (Schindelin et al., 2012; Schneider et al., 2012). The area of the glucagon-positive staining was divided by that of the insulin-positive staining of each islet.

Table 2 Primary and secondary antibodies and counterstain used for IHC

	Target	Source	Working concentration	Supplier	Excitation wavelength	Emission wavelength
PHD3 staining						
Primary Ab	Insulin	Guinea pig	1:100	Abcam (ab7842)	n/a	n/a
	PHD3	Rabbit	1:100	Novus Bio (NB100-139)	n/a	n/a
Secondary Ab	Guinea pig-Alexa 568	Goat	1:300	ThermoFisher (A-11075)	561 nm†	570-694 nm†
	Rabbit-Alexa488	Donkey	1:1000	ThermoFisher (A-21206)	488 nm†	507-596 nm†
Counterstain	DAPI	n/a	n/a	Vector laboratories (H-1500)	405 nm†	410-472 nm†
PCNA staining						
Primary Ab	Insulin	Rabbit	1:500	Cell Signaling (3014S)	n/a	n/a
	PCNA	Mouse	1:500	Cell Signaling, (2586)	n/a	n/a
Secondary Ab	Rabbit-Alexa568	Donkey	1:500	ThermoFisher (A-10042)	561 nm†	579-641 nm†
	Mouse-Alexa488	Goat	1:500	Life Tech (A11001)	488 nm†	507-552 nm†
Counterstain	DAPI	n/a	n/a	Vector laboratories (H-1500)	405 nm†	418-507 nm†
β-cell mass						
Primary Ab	Insulin	Rabbit	1:500	Cell Signaling (3014S)	n/a	n/a
Secondary Ab	Rabbit-Alexa647	Goat	1:500	ThermoFisher (A-21244)	590-650 nm‡	633-738 nm‡
Counterstain	DAPI	n/a	n/a	Vector laboratories (H-1500)	330-375 nm‡	430-470 nm‡
α-cell/β-cell ratio						
Primary Ab	Insulin	Rabbit	1:500	Cell Signaling (3014S)	n/a	n/a
	Glucagon	Mouse	1:2000	Sigma-Aldrich (G 2654)	n/a	n/a
Secondary Ab	Rabbit-Alexa647	Donkey	1:500	ThermoFisher (A-10042)	633 nm†	643-715 nm†
	Mouse-Alexa488	Goat	1:500	Life Tech (A11001)	488 nm†	498-559 nm†
Counterstain	DAPI	n/a	n/a	Vector laboratories (H-1500)	405 nm†	428-551 nm†

† Relative to Zeiss LSM780 meta-confocal microscope
‡ Relative to Zeiss Axio Scan.Z1

2.4.5 TUNEL staining

The DeadEnd Fluorometric TUNEL System (Promega) was employed according to the manufacturer's instructions to assess apoptosis. The islets were fixed in 4% paraformaldehyde in PBS for 15 min at RT and upon two washes with PBS at RT they were permeabilized by immersion in 0.2% Triton-X-100 in PBS for 10 min and further washed with PBS for 5 min. 100 µL of equilibration buffer were added to the islets and after 10 min, 50 µL of TdT reaction mix (45 µL of equilibration buffer, 5 µL of nucleotide and 1 µL of rTdT) were added as well. Following 2h incubation at 37°C, the mix was removed and 500 µL of 2X SSC were applied to the islets for 15 min. Then, the islets were washed again with PBS for 5 min and co-stained with rabbit anti-insulin as described above. Finally, the islets were mounted on glass slides, using Vectashield HardSet mounting medium with DAPI. Images were acquired on a Zeiss LSM780 meta-confocal microscope equipped with highly-492 sensitive GaAsP PMT detectors. Excitation was delivered at λ = 405 nm, λ = 488 nm and λ = 633 nm and signals were detected at λ = 428-533 nm, λ = 498-559 nm and λ = 643-735 nm, for DAPI, TUNEL+ staining (fluorescein-12-dUTP) and Alexa647 respectively. ImageJ (Schindelin et al., 2012; Schneider et al., 2012) was used to calculate the apoptotic portion of β-cell dividing the area positive to TUNEL staining by the area positive to inulin staining.

2.5 Isotope-resolved metabolic tracing

2.5.1 ^{14}C Glucose oxidation assay (in collaboration with Dr. J. Cantley's laboratory)

For the glucose oxidation assay, βPHD3CON and βPHD3KO islets were isolated at our facilities as described above and sent to Dr. James Cantley's laboratory to perform radioactive isotopic tracing.

To evaluate ^{14}C glucose oxidation, 40 islets were cultured in Krebs-Ringer bicarbonate-HEPES buffer (30 mM HEPES, 10 mM $NaHCO_3$, 120 mM NaCl, 4 mM KH2PO4, 1 mM $MgSO_4$, 1 mM $CaCl_2$) supplemented with 0.1% BSA and 3 to 16.7 mM ^{14}C glucose, with 0.5×10^6 or 0.07×10^6 MBq/mol D-[U-^{14}C]glucose, respectively, at 37°C for 2 h. As previously described by Cantley *et al*. 2019 (Cantley et al., 2019), upon media acidification and $^{14}CO_2$ trapping with 0.1 mL of potassium hydroxide (KOH), the tracer was quantified via liquid scintillation spectrometry. For the quantification of ^{14}C incorporation into the cellular lipid phase, a chloroform-methanol (2:1 vol/vol) extraction was performed prior to scintillation spectrometry.

2.5.2 D31-palmitate incorporation and oxidation assays (in collaboration with Prof. L. Hodson's laboratory)

Batches of 140 islets were cultured in RPMI 1640 medium supplemented with 10% BSA, 10% FBS, 100 units/mL penicillin, 100 µg/mL streptomycin and 150 µM D31-palmitic acid (98%; Cambridge Isotope Laboratories). At 2 and 16 h post-incubation, 70 islets were moved to 250 µL of PBS, lysed via bath sonication for 5 min at 40 KHz and their DNA was quantified at NanoDrop. At the same time points, 200 µL

of tracing solution were collected. Samples were then shipped to Prof. Leanne Hodson's laboratory for lipid extraction and analysis.

Total lipids were extracted with a 2:1 choloroform-methanol mixture, followed by washing and analyzed by a 6890N Network GC System (Agilent Technologies; CA, USA) as previously described (Folch, Lees, & Sloane Stanley, 1957; Gunn, Green, Pramfalk, & Hodson, 2017). For the quantification of total fatty acids, internal standards of glyceryl triheptadecanoate (15:0) and 1,2-Diheptanoyl-sn-glycero-3-phosphocholine (17:0) at known concentrations were added. Fatty acid methyl esters were identified by comparison of their retention times with a standard containing 31 known fatty acids. GC-MS using a 5890 GC coupled to a 5973N MSD (Agilent Technologies; CA, USA) was used to detect intracellular D31 enrichment. A Finnigan GasBench-II (ThermoFisher Scientific, UK) measured the deuterated water (^2H_2O)/D31-palmitate ratio (Law et al., 2007).

2.5.3 $^{13}C_6$ glucose tracing

For $^{13}C_6$ glucose tracing, 50-100 (for GC-MS in βPHD3CON and βPHD3KO), 60 (for GC-MS in human and CD1) or 150-230 (for NMR in human and CD1) islets were used. Isolated islets were cultured in RPMI 1640, no glucose medium (Gibco), supplemented with 10% BSA, 10% FBS, 100 units/mL penicillin, and 100 µg/mL streptomycin plus 10 mM $^{13}C_6$ glucose (Sigma-Aldrich). After 24 h, the metabolites were extracted by adding HPLC-grade methanol, HPLC-grade distilled H_2O containing 1 µg/mL D6-glutaric acid and HPLC-grade chloroform (all from Sigma-Aldrich) in a 1:1:1 ratio, to the islets. Following centrifugation, the polar fractions were collected and vacuum

dried. Then, the $^{13}C_6$ glucose tracing samples were employed for either GC-MS or NMR analyses.

2.5.4 GC-MS

The dried polar extracts were prepared for GC-MS analysis through solubilization in 40 µL of 2% methoxyamine hydrochloric acid in pyridine (Fisher Scientific) at 60°C for 60 min and derivatization with 60 µL of N-tertbutyldimethylsilyl-N-methyltrifluoroacetamide (MTBSTFA) with 1% tertbutyldimethyl-chlorosilane (TBDMCS) (both from Sigma-Aldrich). The suspension was further incubated at 60°C for 60 min, before being centrifuged at 13300 rpm for 10 min at 4°C and transferred to chromatography vials with a glass insert (Restek) for GC-MS analysis. The samples were analyzed, by Dr. Alpesh Thakker, on an Agilent 7890B GC and 5977A MSD system on a DB-35MS column or an Agilent 8890 GC and 5977B MSD system by Dr. Jennie Roberts. In both cases, 1 µL of sample was injected in splitless mode with helium carrier gas at a rate of 1.0 mL/min. With the Agilent 7890B GC and 5977A MSD system, the compounds were detected in scan mode and the outcoming data were processed for MID analysis on MetaboliteDetector (Hiller et al., 2009). With the Agilent 8890 GC and 5977B MSD system, the compound detection was again carried out in scan mode and total ion counts of each metabolite were normalized to the internal standard D6-glutaric acid using an in-house MATLAB script.

2.5.5 NMR

Following the $^{13}C_6$ glucose tracing, the dried polar metabolites were resuspended in 60 µL of phosphate buffer: 57.8 mM disodium phosphate (Na_2HPO_4, Sigma-Aldrich), 42.2 mM monosodium phosphate (NaH_2PO_4, Sigma-Aldrich), 0.5 mM 3-(trimethylsilyl) propionic-2,2,3,3-d4 acid sodium salt (D4-TMSP, Sigma-Aldrich) in deuterium oxide (D_2O, Sigma-Aldrich). Subsequently, the samples were centrifuged for 10 min at 14800 rpm and sonicated in an ultrasonic bath for 5 min, before being loaded into NMR tubes (outer diameter: 1.7 mm, Bruker) for acquisition. With the collaboration of Dr. Christian Ludwig, a Bruker Neo 800 MHz NMR spectrometer equipped with a 1.7 mm z-PFG TCI Cryoprobe was used to acquire 2D $^{1}H,^{13}C$-HSQC NMR spectra. The HSQC spectra were acquired with echo/anti-echo gradient coherence selection with an additional pre-saturation for suppressing the water resonance. The spectral widths were 15.6298 ppm and 189.7832 ppm in the direct and indirect dimension, 512 complex data points were acquired for the ^{1}H dimension and 25% (512) out of 2048 complex data points were acquired for the ^{13}C indirect dimension using a non-uniform sampling scheme. The interscan relaxation delay was set to 1.5 s. 2D $^{1}H,^{13}C$-HSQC spectra were reconstructed via the compressed sensing algorithm using the MDDNMR (version 2.5) and NMRPipe (version 9.2) software.

2.6 Statistical analyses

Statistical significance of all the analyses was assessed with GraphPad Prism 9. All error bars represent mean ± S.E.M. and a p-value less than 0.05 was considered significant: *p< 0.05; **p< 0.01; ***p< 0.001. All experiments were discussed with a statistician as part of the ethical approval process to conduct studies involving protected species in the UK. In terms of defining the replicate as well as presenting data, we also referred to the *Journal of Cell Biology* and *Partnership for Assessment and Accreditation of Scientific Practice* statistical reporting guidelines. Both guidelines suggest that: 1) combining data from multiple independent experiments squanders useful information about variability; 2) averaging cell-level data before statistical analysis risks losing potentially important information; and 3) no measurement should be excluded from analysis unless the operator is confident that there will be no effect on analyses. In all experiments performed in islets, the isolation of islets from a single animal was considered the independent replicate. For these experiments, we used islets from at least three animals, taken from at least two or three separate islet isolation procedures, which is a nuisance variable, used as a blocking factor. The variation between individual islets or batch of islets is larger than that between animals; thus, islets or batches of islets were analyzed as separate data points rather than being averaged. Student's two-tailed unpaired or paired t-tests were used for comparison of pairs. Multiple comparisons were determined with one-way ANOVA or two-way ANOVA followed by Sidak's or Tukey's, pairwise *post-hoc* tests. However, the false discovery rate followed by the two-stage linear step-up method of Benjamini, Krieger and Yekutieli was employed when the two-way ANOVA showed highly significant interaction, despite the *post-hoc* testing being slightly above p = 0.05. Non-parametric

multiple comparisons were made using the Kruskal-Wallis test, followed by Dunn's *post-hoc* test.

Chapter 3

THE ROLE OF PHD3 IN β-CELL GLUCOSE METABOLISM UNDER STANDARD CHOW

Abstract

Background and aims

The α-KG-dependent dioxygenase PHD3 hydroxylates HIFα as well as a wide range of alternative targets. In the insulin-secreting β-cell, α-KG functions as a secretagogue for the second phase of insulin secretion. This posits PHD3 as a good candidate for the regulation of glucose homeostasis in β-cells. Other groups showed a central role for PHD3 in glucose metabolism and insulin secretion in a rat β-cells line and the liver. However, these works did not investigate the role of PHD3 in primary β-cells. Here we have produced a β-cell specific PHD3KO mouse model and characterized it under standard dietary conditions.

Materials and methods

PHD3 deletion in β-cells was achieved by cross-breeding *Ins1Cre* mice, with animals harboring a floxed *Egln3* (gene encoding for PHD3). SC-fed mice were phenotyped via IPGTT, OGTT, ITT, Ca^{2+}, ATP/ADP and cAMP imaging, glucose- and Ex4-stimulated insulin secretion assay as well as $^{13}C_6$ glucose tracing.

Results

The loss of PHD3 did not affect the hypoxic signaling, mice growth curves, glucose tolerance and insulin sensitivity. Similarly, β-cell mass, islet size distribution, β-cell maturity, stimulus-secretion coupling, glycolytic and TCA cycle progression were unaffected by the lack of PHD3. Although showing impairment after 3h of glucose starvation, glucose-stimulated and Ex4-potentiated insulin secretion did not change in βPHD3KO islets.

Discussion and Conclusion

No βPHD3KO-specific phenotype was identified under standard chow. Placing the animals on a high fat diet might unveil phenotypic alterations.

3.1 Introduction

β-cells are the pancreatic glucose sensors responsible for the secretion of insulin in response to high glucose levels in the blood. They are finely tuned to guarantee the correct stimulus-secretion coupling (Campbell & Newgard, 2021; Kaestner et al., 2021). During the first phase of insulin secretion, low-affinity GLUTs and phosphorylation by GK, rather than HK, make the β-cells less sensitive to glucose levels and ensure that insulin is only released at appropriate glucose levels (Losada-Barragan, 2021; Rutter et al., 2015). In the second phase, GSIS is amplified by a variety of other mechanisms relying on alternative stimuli, such as incretins, fatty acids, fructose and amino acids (Campbell & Drucker, 2013; Campbell & Newgard, 2021; Curry, 1989; Kyriazis et al., 2012; Losada-Barragan, 2021; Ragy & Ahmed, 2019; Sener et al., 2000; Tappy & Le, 2010; Vetterli et al., 2012; Zhang et al., 2021). The anaplerotic metabolism of glycolytically-derived pyruvate can also sustain the second phase of GSIS. Thus, the accumulation of intermediates such as malate, citrate, glutamine, glutamate and α-KG can boost the secretion of insulin (Vetterli et al., 2012; Zhang et al., 2021).

PHD3 is a member of the PHDs superfamily of Fe^{2+}- and α-KG-dependent dioxygenase, using O_2 to produce CO_2, succinate and *trans*-4-hydroxylated prolyl products (Schofield & Ratcliffe, 2004). Like other isoforms of the same family, it is historically known to be an oxygen sensor, able to hydroxylate HIFα, leading to its degradation under normoxia (Kamura et al., 2000; Maxwell et al., 1999; Ohh et al., 2000; Schofield & Ratcliffe, 2004; Tanimoto et al., 2000). However, it is becoming increasingly apparent that the PHDs can also hydroxylate targets alternative to HIFα. In particular, due to its ubiquitous localization, ability to work dependently and

independently of HIF, both under normoxia and hypoxia, PHD3 was found to have the widest range of alternative targets compared to PHD1 and PHD2 (Jaakkola & Rantanen, 2013).

The dependency of PHD3 on the presence of its co-factor α-KG, and the role played by the latter in the stimulation of the second phase of insulin secretion, suggest a potential role for PHD3 in the regulation of glucose metabolism. Works by Taniguchi *et al.* and Yano *et al.* identified a connection between PHD3 and glucose homeostasis in the liver, where it suppresses insulin sensitivity *in vivo*, while maintaining insulin signaling *in vitro*, through the limitation of stress-induced pathways (Taniguchi et al., 2013; Yano et al., 2018). Huang, Paglialunga *et al.* showed that glucose-stimulated insulin secretion is impaired by high doses of the PHD pan-inhibitor EDHB in 832/13 cell line, derived from INS-1 rat insulinoma. Moreover, through siRNA-driven silencing of the various PHD isoforms, they demonstrated that PHD3 has the greatest impact on insulin release (Huang et al., 2016). However, these works did not investigate the role of PHD3 in primary β-cells, in which metabolism and glucose sensitivity differ *versus* immortalized cell lines. This chapter aims to present the in-depth characterization of a mouse model lacking PHD3 specifically in the pancreatic β-cells. Through accurate *in vivo* and *in vitro* phenotyping of our model under standard chow-fed conditions, we sought to identify the role of PHD3 in the β-cell glucose metabolism.

3.2 Results

3.2.1 Animal generation and validation

To investigate the role of PHD3 in the β-cell glucose sensing machinery, β-cell specific *Egln3* knockout mice were generated. Within *Egln3*, the exon 2 encodes for the His135 and Asp137 residues implicated in the prolyl-hydroxylase function of PHD3 (Epstein et al.). Therefore the *Ins1Cre* strain of deleter mice (Thorens et al., 2015) was crossed with animals having the exon 2 of *Egln3* floxed (*Egln3*$^{fl/fl}$) (Takeda et al., 2006) **(Figure 3.1A)**. The obtained mice, termed βPHD3KO (*Ins1Cre*$^{+/-}$*;Egln3*$^{fl/fl}$), were compared to control littermates, named βPHD3CON (*Ins1*$^{wt/wt}$*;Egln3*$^{fl/fl}$). Confirming its loss, the expression of wild-type *Egln3* in βPHD3KO islets showed a 2-fold decrease compared to βPHD3CON **(Figure 3.1B),** as expected (Takeda et al., 2006). Notably, the deletion of *Egln3* was not accompanied by compensatory increases in the expression of other *Egln* family members **(Figure 3.1C, D)**. The loss of PHD3 was specifically displayed in the insulin-immunopositive β-cells of βPHD3KO islets but not by other cell types, as assessed by IHC **(Figure 3.1E)**. To exclude allele silencing in our *Ins1Cre* line as recently described by Mosleh, Ou *et al.* (Mosleh et al., 2020) and to confirm the recombination efficiency of our *Ins1Cre* allele, *R26-LSL-hM4Di/mCitrine* animals were employed. Using IHC, nearly all insulin-positive cells within *Ins1Cre*$^{+/-}$ *h4MDi*$^{fl/-}$ islets were found to successfully undergo *Ins1Cre*-mediated recombination, as observed through the mCitrine reporter fluorescence **(Figure 3.2A, B)**. Moreover, β-cell differentiation status was assessed in βPHD3KO islets by measuring the expression of the β-cell specific transcription factors, *Pdx1*, *Mafa* and *Nkx6-1*. The expression of these genes was unchanged in βPHD3KO *versus* βPHD3CON islets **(Figure 3.2C-E)**.

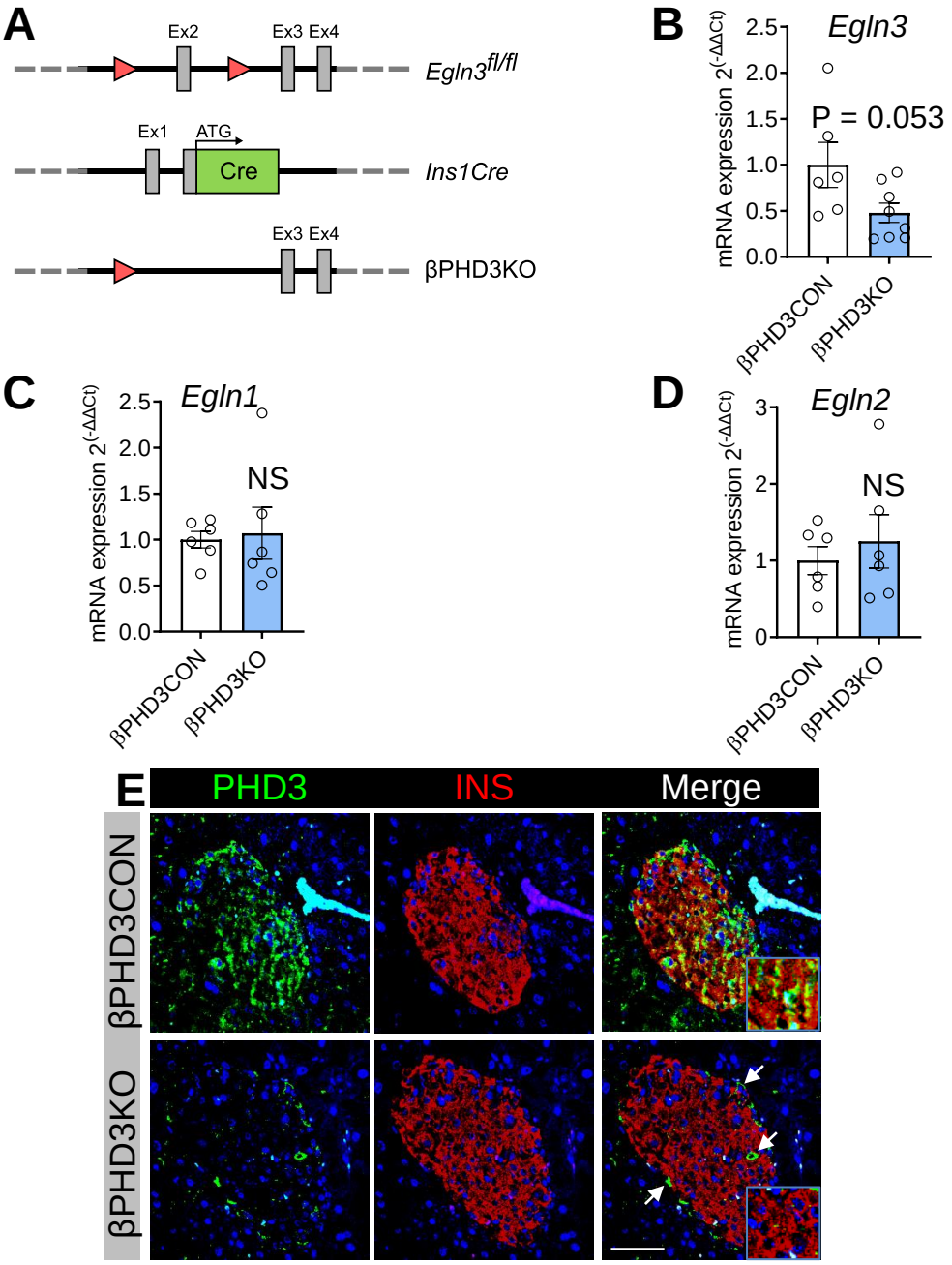

Figure 3.1 βPHD3KO generation and validation: (**A**) Schematic representation of the generation of βPHD3KO mice by crossbreeding of animals harboring the exon 2 of *Egln3* floxed with the *Ins1Cre* deleter strain (**B**) *Egln3* expression measured by qRT-PCR is reduced in βPHD3KO islets compared to βPHD3CON (n = 6-8 animals/genotype; unpaired *t*-test). (**C** and **D**) The mRNA expression of (**C**) *Egln1* and (**D**) *Egln2* is unchanged in βPHD3KO (n = 6 animals/genotype; unpaired *t*-test). (**E**) Representative images of PHD3 immunopositive (green) β-cells identified by insulin (red) staining in βPHD3CON but not in βPHD3KO islets of paraffin-embedded pancreas sections. Arrows indicate the presence of PHD3 in the other cell types (scale bar: 42.5 μm; inset is 1.75 × original magnification) (n = 3 animals/genotype). Bar graphs (scatter plot) show mean ± SEM.

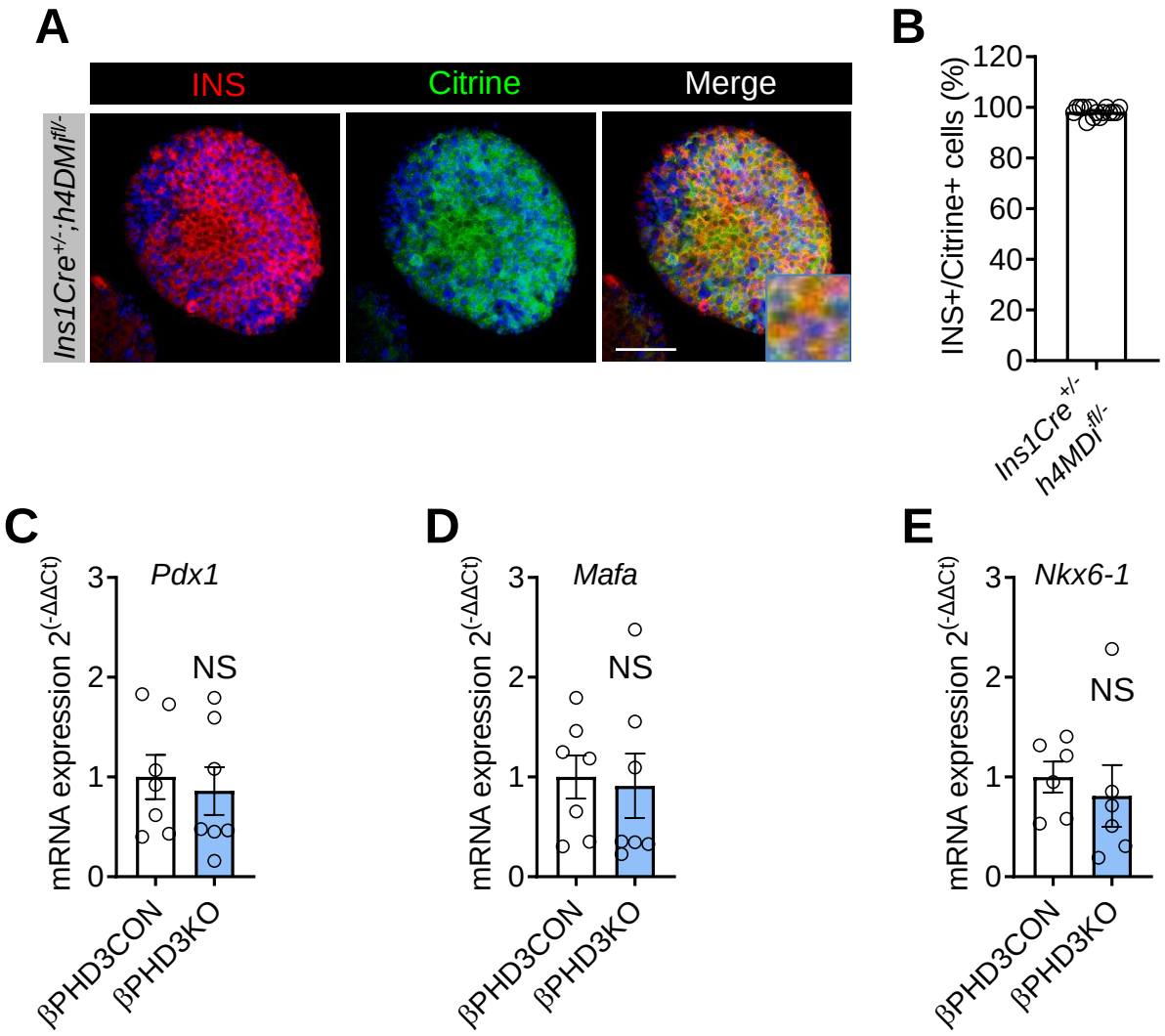

Figure 3.2 Recombination efficacy and β-cell identity: (**A**) Representative images of successful recombination in *Ins1Cre* islets of R26-LSL-hM4Di/mCitrine mice expressing the mCitrine reporter (green) in insulin-positive (red) β-cells of isolated and fixed islets (scale bar: 42.5 µm; inset is 3.5 × original magnification). (**B**) Percentage of insulin-positive (INS+) cells expressing mCitrine in *Ins1Cre* islets of R26-LSL-hM4Di/mCitrine mice (n = 15 islets). (**C** - **E**) The expression levels of (**C**) *Pdx1*, (**D**) *Mafa* and (**E**) *Nkx6-1* are similar in βPHD3CON and βPHD3KO islets (n = 6 animals/genotype; unpaired *t*-test). Bar graphs (scatter plot) show mean ± SEM.

3.2.2 Hypoxic signaling is intact in βPHD3KO

In line with previous literature (Kaelin & Ratcliffe, 2008), *Egln3* mRNA levels were found to be higher in islets cultured for 24 h at 1% oxygen tension (hypoxia) compared to those kept in 21% O_2 (normoxia) **(Figure 3.3A)**. It has previously been shown that PHD3 can destabilize HIFα and that HIF1α can regulate β-cell glucose metabolism (Cantley et al., 2009; Cheng et al., 2010; Kamura et al., 2000; Maxwell et al., 1999; Ohh et al., 2000; Puri, Cano, & Hebrok, 2009; Schofield & Ratcliffe, 2004; Tanimoto et al., 2000; Zehetner et al., 2008). Therefore, the expression of several HIF1α target genes were assessed by qRT-PCR to evaluate whether the hypoxic response was altered in islets lacking PHD3. The overall expression of *Bnip3*, *Car9* and *Gls* encoding for BCL2 interacting protein 3, carbonic anhydrase and glutaminase, respectively, were all increased under hypoxia, indicative of intact hypoxic signaling. Although showing a tendency to be higher, the expression of *Gls* was not significantly different in βPHD3CON compared to βPHD3KO islets under hypoxia, whereas the regulation of *Bnip3* and *Car9* was unchanged **(Figure 3.3B-D)**. Furthermore, glucose- and KCl-stimulated Ca^{2+} fluxes, which are HIF1α sensitive (Cantley et al., 2009), were similar in normoxic and hypoxic βPHD3KO and βPHD3CON islets **(Figure 3.3E-H)**, suggesting that HIF1α signaling remains intact despite the loss of PHD3.

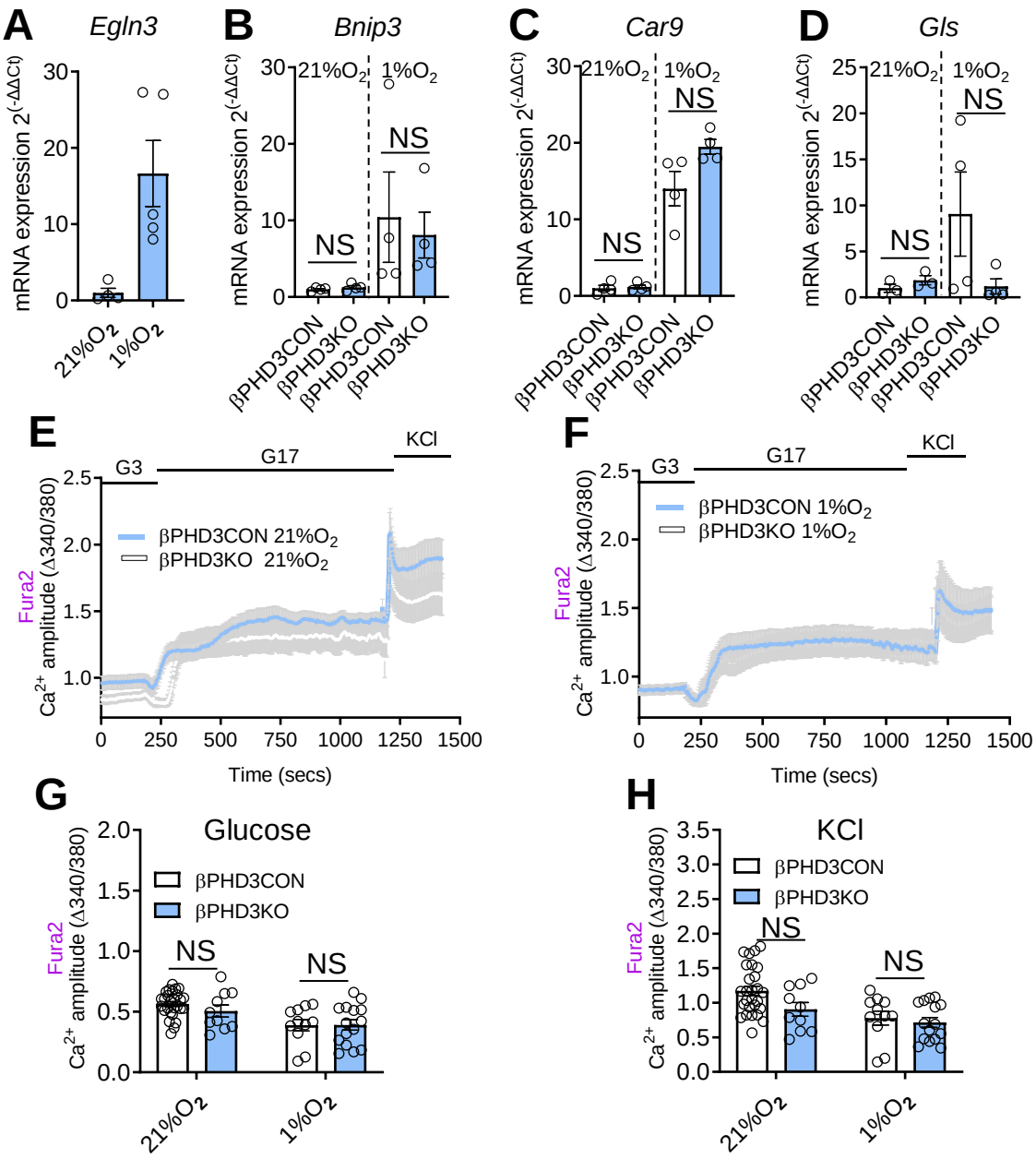

Figure 3.3 Effects of hypoxia on βPHD3KO under SC: (**A**) *Egln3* expression is increased in wild-type islets from CD1 mice, after 24 h of hypoxia 1% O_2 compared to 21% O_2 (n = 9-11 animals; unpaired *t*-test). (**B** - **D**) mRNA levels of (**B**) *Bnip3*, (**C**) *Car9* and (**D**) *Gls* are increased under 1% O_2 *versus* 21% O_2 but are not significantly altered in βPHD3KO *versus* βPHD3CON (n = 4 animals/genotype/condition; Kruskal-Wallis test, Dunn's multiple comparison test). (**E** and **F**) Following incubation with Fura2, 17mM glucose- and 10mM KCl-stimulated mean Ca^{2+} traces are similar in βPHD3CON and βPHD3KO islets exposed to (**E**) 21% O_2 or (**F**) 1% O_2 for 24 h. (**G** and **H**) Ca^{2+} fluxes in response to (**G**) glucose and (**H**) KCl are unchanged in βPHD3KO *versus* βPHD3CON islets exposed to 21% O_2 or 1% O_2 (n = 10-27 islets; 2 animals/genotype, two-way ANOVA; Sidak's multiple comparison test). Bar graphs (scatter plot) and line graphs show mean ± SEM.

3.2.3 The in vivo phenotype is unchanged in βPHD3KO

After confirming the validity of the model and its independence from HIF-mediated mechanisms, animals fed a SC diet were tested to identify a PHD3-associated phenotype. Male and female βPHD3KO mice between 8 and 18 weeks of age presented with similar body weight compared to βPHD3CON mice **(Figure 3.4A, B)** and no differences between female and male cohorts were identified **(Figure 3.4A, B)**. Glucose tolerance was also unaffected by the lack of PHD3, as assessed by IPGTT performed on 8 and 20 weeks old male and female mice **(Figure 3.4C-F)** and OGTT in animals at 8 weeks of age **(Figure 3.4G, H)**. Likewise, βPHD3KO and βPHD3CON male and female mice displayed comparable insulin sensitivity **(Figure 3.5A, B)**. Lastly, the analysis of the islet size distribution and β-cell mass revealed no significant differences in βPHD3KO *versus* βPHD3CON mice **(Figure 3.5C-E)**.

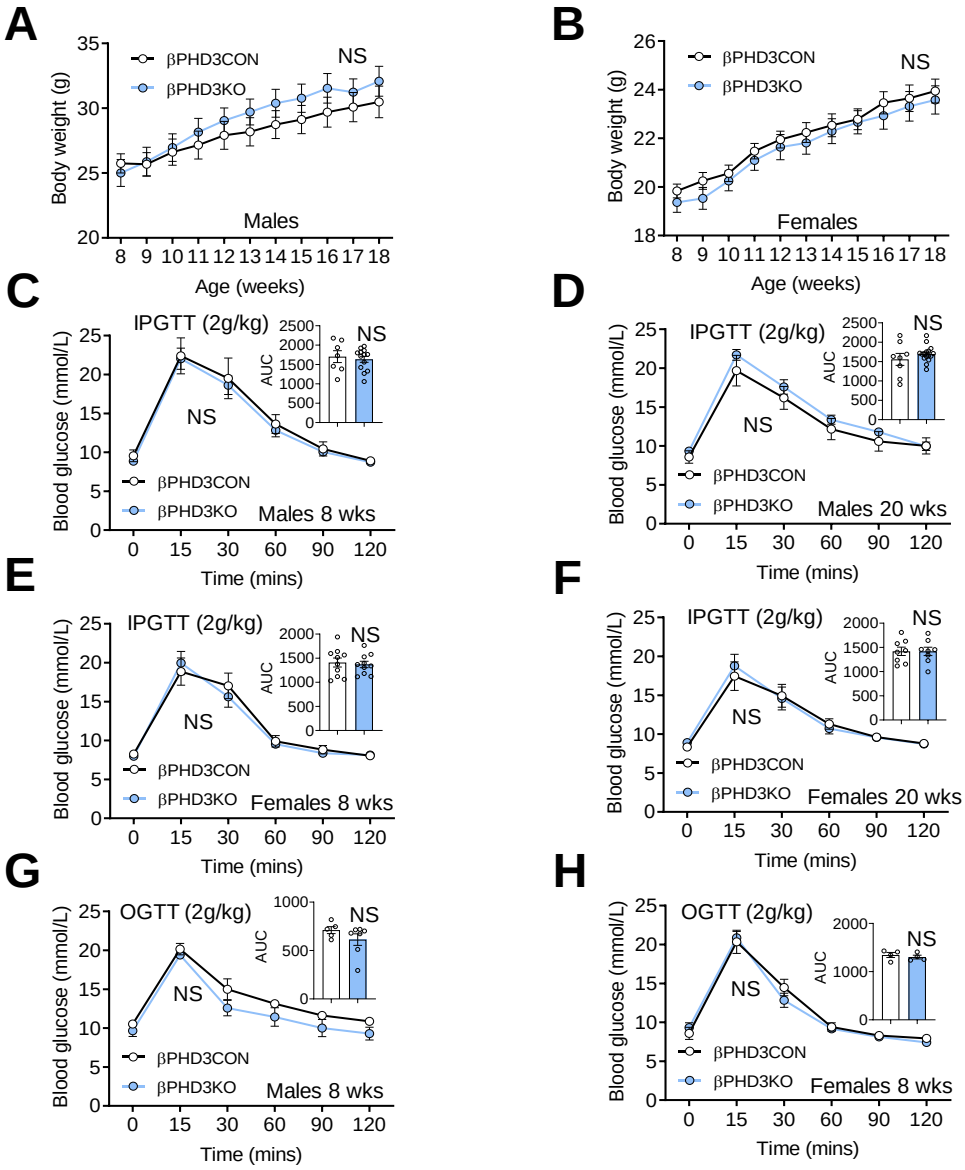

Figure 3.4 Growth and glucose tolerance of βPHD3KO under SC: (**A** and **B**) The body weight of (**A**) male and (**B**) female mice measured between 8 and 18 weeks of age is similar between βPHD3CON and βPHD3KO mice (n = 8-10 male and 15 female animals/genotype; 2-way RM ANOVA; Sidak's test). (**C** – **F**) Glucose tolerance and AUC at the IPGTT (2 g/kg glucose administered) are similar in (**C**) 8-weeks (n = 13 animals/genotype) or (**D**) 20-weeks old (n = 8–16 male animals/genotype), βPHD3CON and βPHD3KO male mice as well as in (**E**) 8-weeks (n = 10 animals/genotype) or (**F**) 20-weeks old (n = 8 animals/genotype), βPHD3CON and βPHD3KO female mice (IPGTT: 2-way RM ANOVA, Sidak's test; AUC: unpaired *t*-test). (**G** and **H**) Glucose tolerance and AUC at the OGTT (2 g/kg glucose administered) are unchanged in βPHD3KO (**G**) male (n = 5–8 male animals/genotype) and (**H**) female (n = 4 female animals/genotype), 8-weeks old mice, *versus* βPHD3CON (OGTT: 2-way RM ANOVA, Sidak's test; AUC: unpaired *t*-test). Bar graphs (scatter plot) and line graphs show mean ± SEM.

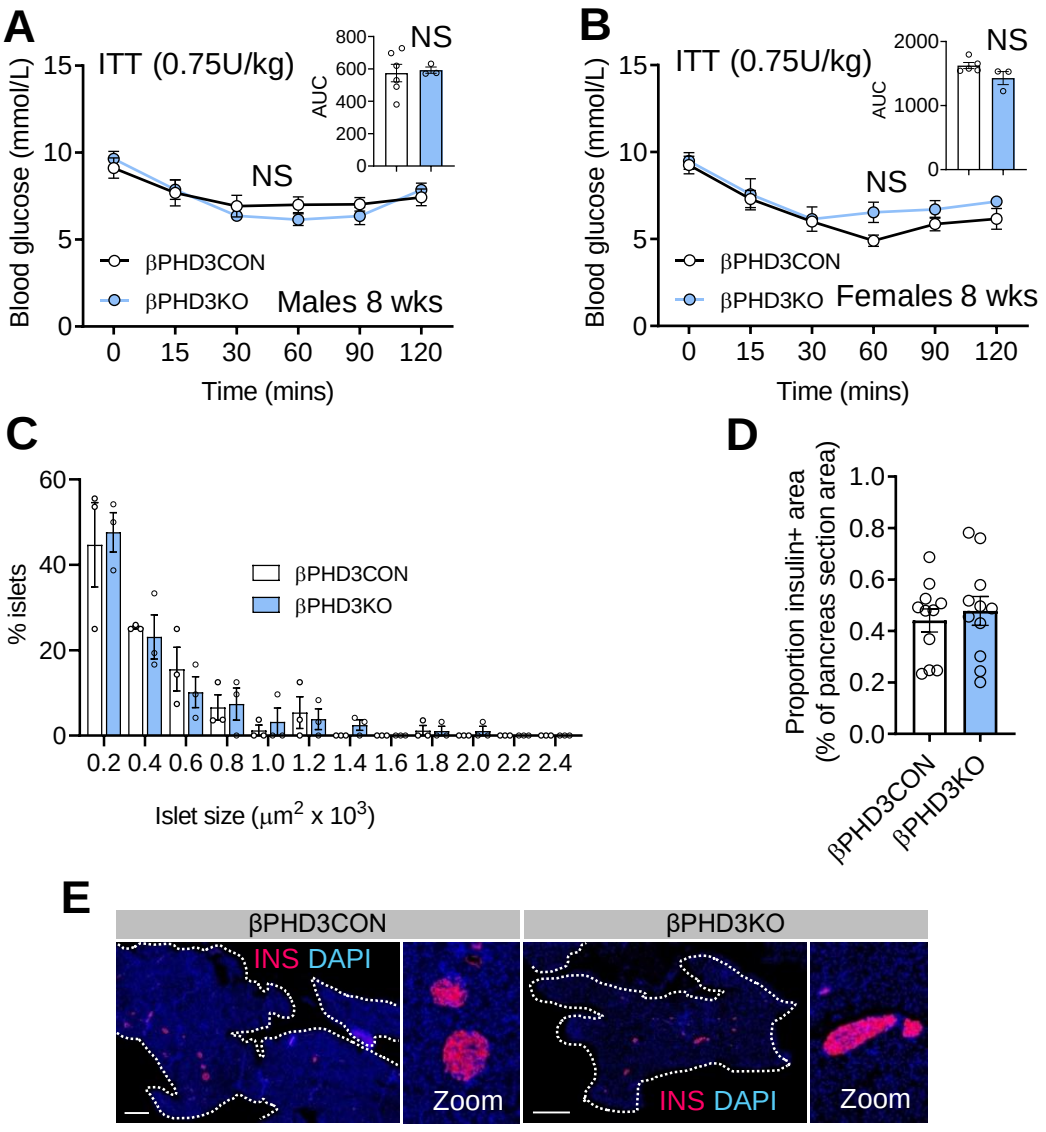

Figure 3.5 Insulin sensitivity and β-cell mass of βPHD3KO under SC: (**A** and **B**) Insulin sensitivity and AUC at the ITT (IP administration of 0.75U/kg insulin) are similar in 8-weeks old, βPHD3KO and βPHD3CON, (**A**) male (n = 6-7 animals/genotype) and (**B**) female (n = 4-7 animals/genotype) mice (ITT: 2-way RM ANOVA, Sidak's test; AUC: unpaired *t*-test). (**C** – **E**) βPHD3KO and βPHD3CON have similar (**C**) islet size distribution (n = 3 animals/genotype; 2-way ANOVA; Sidak's test) and (**D**) β-cell mass (n = 3 animals/genotype; unpaired *t*-test) as visible in the (**E**) representative images of entire pancreatic sections with β-cells stained with an anti-insulin antibody (red). (scale bar: 530 μm; 6.5 × zoom showing intact cell resolution). Bar graphs (scatter plot) and line graphs show mean ± SEM.

3.2.4 The in vitro phenotype is unchanged in βPHD3KO

Once a role for PHD3 in glucose homeostasis was excluded under SC, detailed *in vitro* functional workup of βPHD3KO was carried out in case *in vivo* assays were not sufficiently sensitive to detect any changes. To evaluate the impact of PHD3 on the triggering pathway for insulin secretion, Ca^{2+} fluxes and ATP/ADP ratio were measured in βPHD3KO and βPHD3CON islets. Ca^{2+} imaging showed that Ca^{2+} rises in response to high glucose and KCl were similar in βPHD3KO compared to βPHD3CON islets **(Figure 3.6A, B)**. Similarly, glucose-stimulated ATP/ADP ratios showed no differences between βPHD3KO and βPHD3CON islets **(Figure 3.6C, D)**. To investigate a potential role for PHD3 in the incretin signaling pathway, cAMP responses to the incretin-mimetic Ex4 as well as mRNA levels of *Glp1r*, the gene encoding for GLP-1R, were measured in βPHD3KO and βPHD3CON islets. Suggesting intact GLP-1R signaling, both Ex4-stimulated cAMP responses **(Figure 3.6E, F)** and *Glp1r* expression **(Figure 3.6G)** were found to be unchanged in βPHD3KO *versus* βPHD3CON islets. *In vitro* insulin secretion in response to basal and high concentrations of glucose, as well as to potentiation with Ex4 were similar in βPHD3KO and βPHD3CON islets **(Figure 3.6H)**. The total insulin content was unchanged by PHD3KO in β-cells **(Figure 3.6 I)**. However, it has been shown that in islets undergoing starvation, glucose oxidation, glycolytic enzymes and amino acids are less central for insulin secretion, while fatty acid utilization is predominant (Wortham & Sander, 2016). Therefore, to investigate the role of PHD3 in the β-cell nutrient preference, glucose fasting was induced in isolated islet. After 3 h with 3 mM glucose, GSIS was found to be significantly impaired in βPHD3KO islets challenged with 16.7 mM glucose **(Figure 3.6J)**.

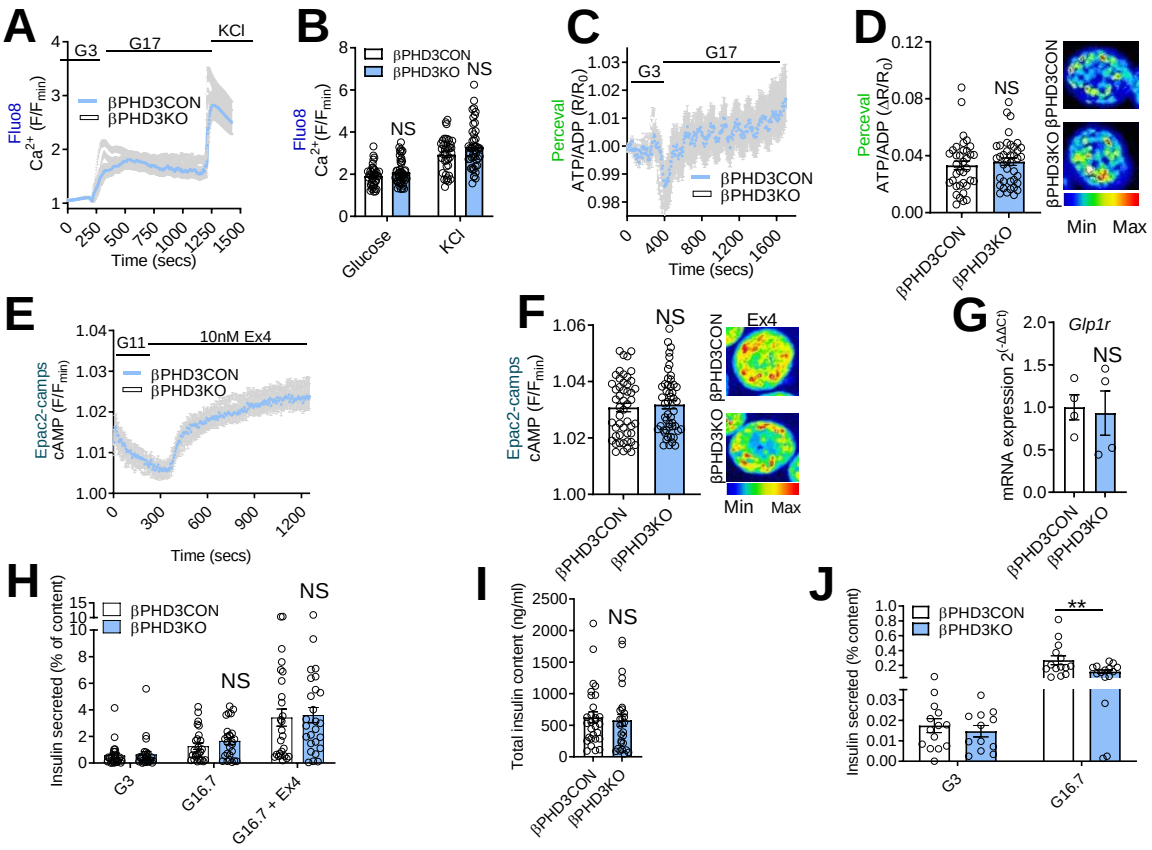

Figure 3.6 *In vitro* phenotype of βPHD3KO under SC: (**A** and **B**) 17mM glucose- and 10mM KCl-stimulated Ca^{2+} fluxes, detected with Fluo8, do not change in βPHD3KO compared to βPHD3CON islets as shown by (**A**) mean traces and (**B**) summary bar graph (n = 38-48 islets, 4-5 animals/genotype; 2-way ANOVA, Sidak's test). (**C** and **D**) The ATP/ADP ratio in response to 17mM glucose does not differ in βPHD3KO and βPHD3CON islets infected with a Perceval-expressing adenovirus as visible through (**C**) mean traces and (**D**) summary bar graph accompanied by representative images of single islets (n = 36-39 islets, 4-5 animals/genotype; unpaired *t*-test). (**E** and **F**) Following incubation with Epac2-camps, 10nM Ex4-stimulated cAMP response is similar in βPHD3KO and βPHD3CON islets as shown by (**E**) mean traces and (**F**) summary bar graph with representative images of single islets (n = 50 islets, 4-5 animals/genotype; unpaired *t*-test). (**G**) The expression of *Glp1r* is unchanged in βPHD3KO *versus* βPHD3CON islets (n = 4 animals/genotype; unpaired *t*-test). (**H**) Insulin secretion in response to 16.7 mM glucose (G 16.7) and Ex4 does not differ in βPHD3KO and βPHD3CON islets (n = 29 replicates, 6 animals/genotype; 2-way ANOVA; Sidak's test). (**I**)The total insulin content extracted from groups of 10-15 size-matched βPHD3KO and βPHD3CON islets is similar (n = 29 replicates, 6 animals/genotype; unpaired *t*-test). (**J**) G16.7-stimulated insulin secretion is decreased in βPHD3KO islets after 3 h preincubation with low glucose (n = 14-15 replicates, 6 animals/genotype; 2-way ANOVA, Sidak's test). Bar graphs (scatter plot) and line graphs show mean ± SEM. F/Fmin = fluorescence at any time point/minimum fluorescence and R/R0 = fluorescence at any time point/fluorescence at 0 min.

3.2.5 Glycolysis and TCA cycle progress normally in βPHD3KO

To decipher the fate of glucose within the βPHD3KO islets, stable isotopic tracing was performed in islets from mice fed a SC using $^{13}C_6$ glucose. Following GC-MS acquisition, the incorporation of each ^{13}C into various glycolytic and TCA cycle metabolites was assessed by MID analysis **(Figure 3.7)**. This revealed no significant differences in the contribution of glucose to the production of aspartate, glutamate, malate, fumarate, citrate and lactate between βPHD3KO and βPHD3CON **(Figure 3.8A-F)**.

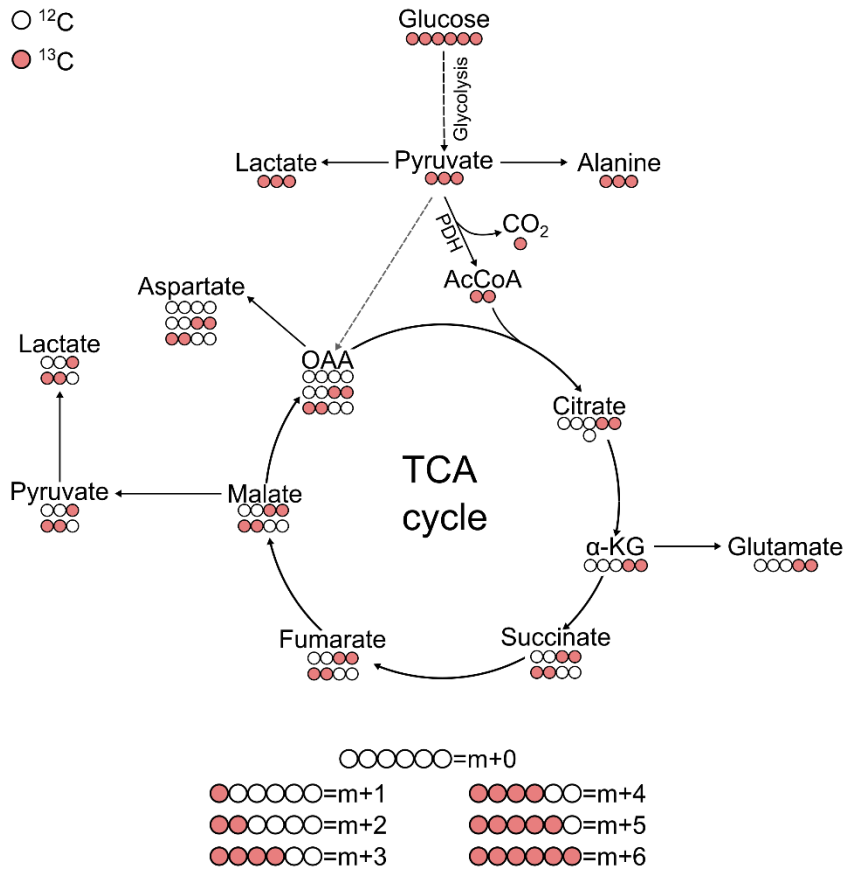

Figure 3.7 Schematic of the incorporation of ^{13}C from $^{13}C_6$ glucose into various metabolites: White and red circles represent the naturally abundant ^{12}C and the heavier ^{13}C isotopes, respectively. The schematic shows the metabolism of glucose from glycolysis into the TCA cycle, through the activity of PDH. The accumulation of ^{13}C from uniformly labeled glucose into each metabolite is depicted. Individual isotopologues are defined as m+n where n indicates the number of ^{13}C present in the metabolite structure.

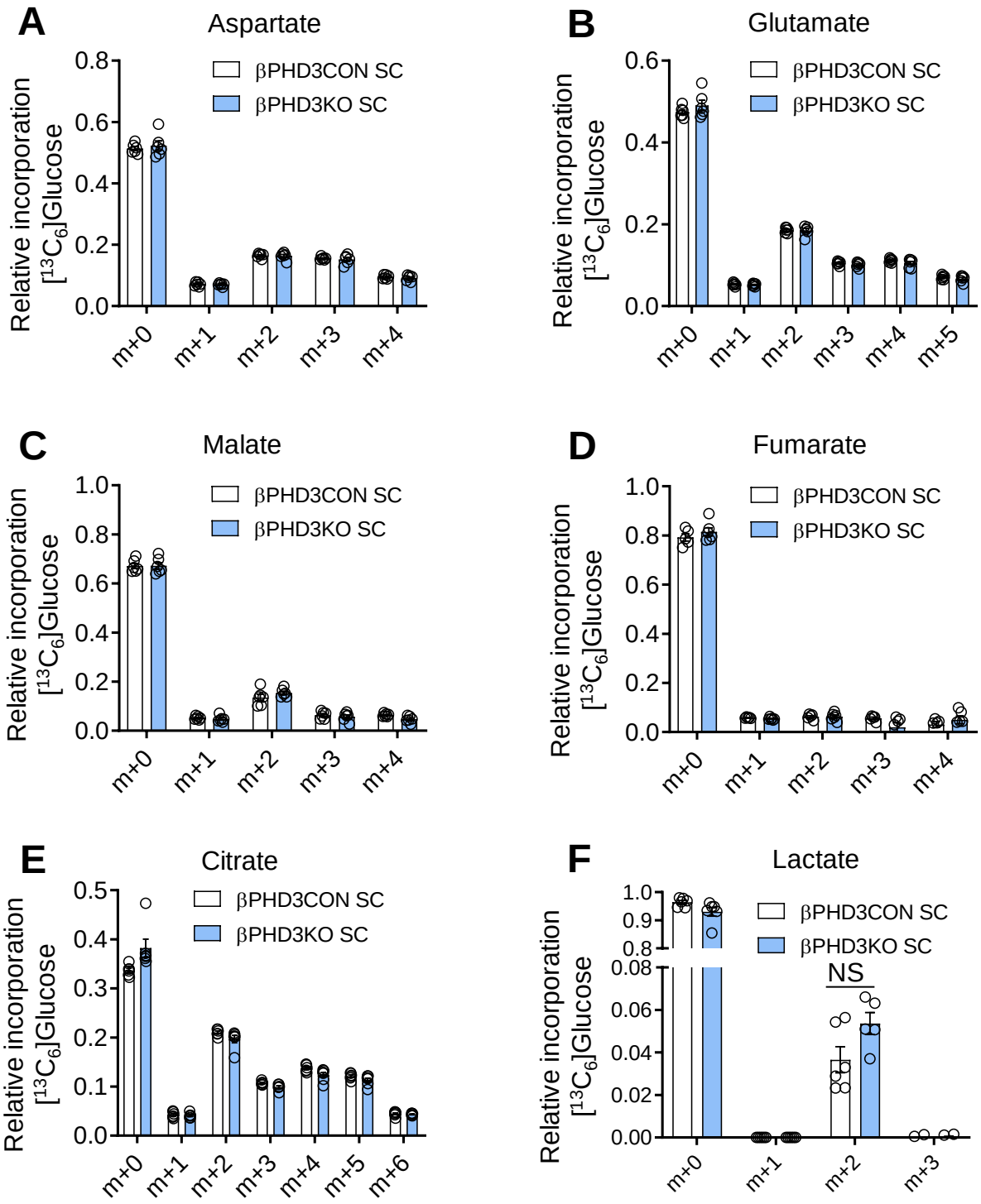

Figure 3.8 MID analysis of βPHD3KO under SC: Mass isotopologue distributions (MID) showing similar incorporation of ^{13}C from $^{13}C_6$ glucose into (**A**) aspartate, (**B**) glutamate, (**C**) malate, (**D**) fumarate, (**E**) citrate and (**F**) lactate of βPHD3KO and βPHD3CON islets (n = 6 islet preparations, 3 animals/genotype; 2-way ANOVA, Tukey's test). Bar graphs (scatter plot) show mean ± SEM.

3.3 Discussion

In the present chapter, the effect of the βPHD3KO is described, with the aim of investigating the role of PHD3 in pancreatic β-cells of mice kept under standard dietary conditions. In a previous study, the effect of PHD3 on insulin secretion of INS-1-832/13 clonal rat β-cells was observed through the use of EDHB or with siRNA (M. Huang et al., 2016). Here we used a Cre-LoxP system with the highly specific *Ins1Cre* deleter strain to induce *Egln3* silencing specifically in the β-cell compartment of the primary pancreatic islets (Takeda et al., 2006; Thorens et al., 2015). Thus, we fed this mouse model a standard diet and performed extensive phenotyping both *in vivo* and *in vitro* to establish whether the lack of PHD3 causes any alterations to β-cells functions and metabolism.

Although the *Ins1Cre* driver line is known to ensure efficient and selective recombination in the pancreatic β-cells, a recent work reported the risk of allele silencing in some *Cre* lines (Mosleh et al., 2020; Thorens et al., 2015). Therefore, the validity of our model was not only confirmed by the lower levels of *Egln3* mRNA and lack of PHD3 immunopositive β-cells but it was also corroborated by an *Ins1Cre*-mediated recombination efficiency of about 98.3%, in line with previous literature (Johnston et al., 2016; Nasteska, Fine, et al., 2021; Thorens et al., 2015). Notably, the mRNA levels of *Egln3* were only halved in the islets isolated from βPHD3KO mice, compared to βPHD3CON. In line with previously reported RNA sequencing data, the remainder is likely attributable to the higher expression of *Egln3* in α-cells than in β-cells (Benner et al., 2014; Blodgett et al., 2015).

Several studies showed a role for HIF1α in mediating β-cells glucose metabolism in a dose-dependent manner (Cantley et al., 2009; Cheng et al., 2010; Puri et al., 2009;

Zehetner et al., 2008). Based on these, and the known link between PHD3 and hypoxia, a first set of experiments was performed to assess whether hypoxia was responsible for any phenotypical changes. These experiments revealed no changes in β-cell expression of HIF1α targets, indicating that if there was a βPHD3KO phenotype, this was likely to be independent of HIF1α stability. This is in accordance with published studies, conducted in the liver and neurons, and consistent with PHD2 being the key hydroxylase regulating HIF1α stabilization (Berra et al., 2003; Bishop et al., 2008; Taniguchi et al., 2013; Tennant et al., 2009). Moreover, Glucose- and KCl-stimulated Ca^{2+} fluxes were measured as these were previously reported to be attenuated in absence of VHL, the key element of HIF degradation under normoxia (Cantley et al., 2009). Ca^{2+} dynamics were unchanged in βPHD3KO compared to controls, further supporting that the stabilization of HIF is unlikely to be determinant in the role of PHD3 in β-cells.

Upon detailed observation of the phenotypical characteristics of our model under SC, including analyses of growth curves, glycemia in response to intraperitoneal or oral administration of glucose, and insulin sensitivity, βPHD3KO mice were found to be identical to those expressing *Egln3*. These studies were performed in animals between 8 and 20 weeks of age, both males and females, excluding any age- or sex-dependent contribution of PHD3 to glucose homeostasis under SC. Furthermore, the loss of PHD3 did not affect the islet size distribution and β-cell mass, implying that the rate of proliferation, hypertrophy, neogenesis and apoptosis were unaltered by lack of PHD3.

From a functional point of view, islets isolated from βPHD3KO mice showed comparable responses to stimuli targeting the various components of the stimulus-secretion coupling pathway. Suggesting an intact function of the VDCCs, Ca^{2+} imaging

revealed identical responses to both glucose and the generic depolarizing stimulus KCl in βPHD3KO *versus* βPHD3CON mice. Similarly, the ATP/ADP ratio in response to glucose was unchanged, indicating that glycolysis and ATP generation are unaffected by the lack of PHD3 in animals fed a SC. Excluding an impact of PHD3 on the incretin-mediated amplification of GSIS the expression of *Glp1r* and the cAMP response to Ex4, mimicking the postprandial release of incretins, were unchanged in our model. Confirming the lack of PHD3-associated phenotype under SC, glucose stimulation and Ex4 potentiation did not result in altered *in vitro* insulin secretion in the absence of PHD3. This is unlike the previously reported effect of the PHD-inhibitor, EDHB, which increased GSIS when administered at low concentrations and impaired GSIS at high concentrations (Huang et al., 2016). The same study also identified PHD3 as the PHD isoform most involved in GSIS in the INS-1-832/13 cell line kept under normal culture conditions (Huang et al., 2016). However, this conflict can likely be explained by either the different glucose responsiveness of immortalized cells *versus* primary cultures (Hohmeier et al., 2000) or the use of siRNA as opposed to our Cre-LoxP approach for genetic ablation. Interestingly, suggestive of a dysregulated use of nutrients, βPHD3KO islets showed impaired insulin secretion when stimulated with a high concentration of glucose after acute glucose deprivation.

Finally, $^{13}C_6$ glucose tracing coupled to GC-MS was used to gain a higher understanding of glucose metabolism and its contribution to the production of glycolytic and TCA cycle intermediates. The data obtained were analyzed through observation of the MID. This permits the comparison of the accumulation of the various isotopologues of each metabolite. These are indicated as m+n, where m indicates the mass of the metabolite presenting all naturally abundant isotopes in its structure.

Therefore, m+0 is descriptive of the unlabeled portion of each metabolite present in a sample. Conversely, when n is different from 0, m+n indicates the isotopologue containing a number of heavier isotopes in its structure corresponding to n. For instance, the accumulation of m+2 lactate, refers to the portion of lactate, present in a sample, containing 2 heavier carbons in its structure **(Figure 3.7)**. Under SC, the MID analyses did not identify any significant differences between βPHD3KO and βPHD3CON, indicating that, consistent with the other findings, glycolysis and TCA cycle proceed without changes between the two conditions.

To summarize, we generated a mouse model bearing a conditional β-cell deletion of *Egln3*/PHD3 and subjected it to extensive workup, while feeding it a SC. The deletion of PHD3 was found not to be linked to the activity of HIF-mediated pathways and to hypoxic responses in the β-cells. Moreover, the loss of PHD3 was associated with an overall lack of specific phenotype, under SC, both at the macroscopic and functional level. Growth curves, glucose tolerance, insulin sensitivity, islet size distribution, β-cell mass, Ca^{2+}, ATP/ADP and cAMP imaging, *Glp1r* expression as well as glycolysis and TCA cycle progression were all unaltered in βPHD3KO. Despite a previous work indicating otherwise (M. Huang et al., 2016), PHD3 did not show any effect on the secretion of insulin when the β-cells were stimulated with glucose and Ex4. However, prolonged incubation with low concentration of glucose resulted in impaired GSIS.

3.4 Conclusion

The deletion of PHD3 in the pancreatic β-cells of animals under a SC does not result in the insurgence of a new phenotype. Therefore, no role was identified for PHD3 in the glucose homeostasis of the β-cells under SC. However, there are a few limitations to the study under SC that should be acknowledged. To validate our βPHD3KO model, the expression of *Egln3, Egln1 and Egln2* but not the PHDs protein level were assessed, since antibodies for western blot (WB) are not specific for PHD3. Although IHC was successfully used here to show the β-cell specific knockout of PHD3, cell sorting followed qRT-PCR and WB could be used to confirm *Egln3* silencing specifically in β-cells. Similarly, to investigate whether the hypoxic signaling of βPHD3KO mice was altered, the mRNA expression of HIF1α target genes was measured. Going forward, the protein level of HIF1α and its hydroxylation status could be tested through immunoblotting. Despite encouraging results showing impaired GSIS after 3h of glucose starvation, due to the limited time frame of this project no further functional assays, such as Ca^{2+} or ATP/ADP imaging, were conducted under this condition.

Nonetheless, to mimic the progression of metabolic diseases in humans and to unveil the interactions between the environment and the genotype, the induction of metabolic stress and obesity in mice, through HFD, can be an extremely useful tool (da Silva Xavier & Hodson, 2018). Moreover, PHD3 is known to act as a gatekeeper of nutrient preference in AML and skeletal muscle (German et al., 2016; Yoon et al., 2020). Thus, to further investigate the effects of PHD3 on glucose homeostasis and a possible shift towards the use of alternative fuel sources, the βPHD3KO mouse model was subjected

to HFD. In the following chapters the in-depth study of the role of PHD3 in β-cells after 4 and 8 weeks of HFD, is described.

Chapter 4

THE ROLE OF PHD3 IN β-CELL GLUCOSE METABOLISM AFTER 4 WEEKS OF HIGH FAT DIET

Abstract

Background and aims

Despite previous works reporting a role for PHD3 in glucose metabolism, βPHD3KO mice fed a SC did not display alterations in glucose homeostasis. Recent studies have described a role for PHD3 in limiting the switch towards fatty acid oxidation, via hydroxylation of ACC2, in AML and skeletal muscle. Following the induction of metabolic stress and fatty acid excess, here we sought to test the hypothesis that in β-cells PHD3 limits fatty acid oxidation under HFD conditions.

Materials and methods

βPHD3KO and βPHD3CON mice were fed a HFD for 4 weeks and assessed for glucose tolerance and insulin sensitivity *in vivo*, and for insulin secretion, Ca^{2+} dynamics and ATP/ADP ratio *in vitro*. Mapping of β-cell metabolism was obtained with radioactive and stable isotopic tracing. Treatments with palmitate and etomoxir were employed to assess the role of fatty acid oxidation. Gene expression data sets were interrogated to investigate the role of ACC in the PHD3-mediated phenotype.

Results

At 4 weeks of HFD, PHD3 maintained the appropriate coupling of glucose to insulin secretion. Conversely, βPHD3KO islets rewired their metabolism to utilize fatty acids as an alternative source to sustain the TCA cycle and insulin release.

Discussion and Conclusion

Mice lacking PHD3 in their β-cells rely more on β-oxidation than glycolysis to fuel insulin secretion at the onset of metabolic stress. The effects of longer exposure to metabolic stress are yet to be investigated.

4.1 Introduction

As discussed in chapter 3, the *in vivo* and *in vitro* characterization of the βPHD3KO model under SC did not reveal significant differences from control littermates. Thus, the loss of PHD3 in β-cells of mice fed a standard diet, is not associated with alterations in glucose homeostasis. These findings were surprising as previous works supported a central role for PHD3 in glucose metabolism. In INS-1-832/13 cells, GSIS was affected by the PHD pan-inhibitor EDHB and more strongly impaired by siRNA-mediated PHD3 knockdown (Huang et al., 2016). Moreover, studies employing liver-specific deletion of PHD3, found the enzyme to be central to insulin signaling, glucose tolerance and gluconeogenesis *in vivo* and *in vitro* (Taniguchi et al., 2013; Yano et al., 2018). Importantly, the induction of metabolic stress in the form of HFD may be necessary to reveal phenotypical alteration by altering nutrient abundance. Indeed, HFD represents a means by which the progression of type 2 diabetes and obesity are simulated in mice (da Silva Xavier & Hodson, 2018).

Also, as mentioned in the previous chapter, PHD3 was not found to have an influence on the stability of HIF1 in the β-cells. This suggests that a possible function of PHD3 in the β-cells could be mediated by PHD3 targeting substrates unrelated to hypoxia. In particular, in the studies by German *et al.* and Yoon *et al.*, it was shown that PHD3 can hydroxylate ACC2, influencing the activity of CPT1, thus regulating the β-oxidation of fatty acids in the skeletal muscle and AML (German et al., 2016; Yoon et al., 2020).

Building upon this knowledge, we hypothesized that 4 weeks of 60% HFD **(Appendix 1)**, would help to unveil a PHD3-associated phenotype in the β-cells. Indeed, 4 weeks of HFD is a useful model for the progression of diabetes and in particular the stage of pre-diabetes (da Silva Xavier & Hodson, 2018). Additionally, the high fat content of the

administered diet provides the exogenous fatty acids necessary to evaluate whether PHD3 might regulate the use of alternative fuel sources, particularly the β-oxidation of fatty acids, to sustain the TCA cycle and consequent production of energy necessary for insulin secretion.

In this chapter, the effects of 4 weeks of HFD on our βPHD3KO model are described. Mice and islets isolated from them were extensively studied both *in vivo* and *in vitro*, with a focus on their metabolic adaptation, as assayed by radioactive and stable isotopic tracing.

4.2 Results

4.2.1 Validation of mouse model and intact hypoxic signaling at 4 weeks of HFD

To examine whether metabolic stress can unmask a PHD3-associated phenotype in β-cells, male mice were fed a HFD for 4 weeks. Since PHD3 levels are highly regulated by hypoxia, which is associated with high fat feeding (Roat et al., 2014; Sato et al., 2011), the βPHD3KO model was re-validated after 4 weeks of HFD. Similar to SC conditions, *Egln3* mRNA levels remained significantly lower in βPHD3KO than in βPHD3CON islets **(Figure 4.1A)**. Although the expression of *Egln3* was found to be slightly higher in the islets isolated from control mice under HFD, this difference was not significant **(Figure 4.1A)**. Excluding a *Cre*- or *Egln3* floxed-mediated effect on the βPHD3KO phenotype at 4 weeks of HFD, glucose tolerance was identical in $Ins1^{wt/wt}$ $Egln3^{fl/fl}$, $Ins1Cre^{+/-}$ $Egln3^{wt/wt}$, and $Ins1^{wt/wt}$ $Egln3^{wt/wt}$ mice **(Figure 4.1B)**. To investigate if the stability of HIF1α is affected in βPHD3KO islets after 4 weeks of HFD, the expression of HIF1α targets were assessed. *Bnip3* and *Gls* remained unchanged, whereas *Car9* was significantly lower in the βPHD3KO **(Figure 4.1C-E)**. Overall, the mRNA levels suggested that at the onset of metabolic stress, hypoxia is unlikely to play a key role in the glucose homeostasis of βPHD3KO mice.

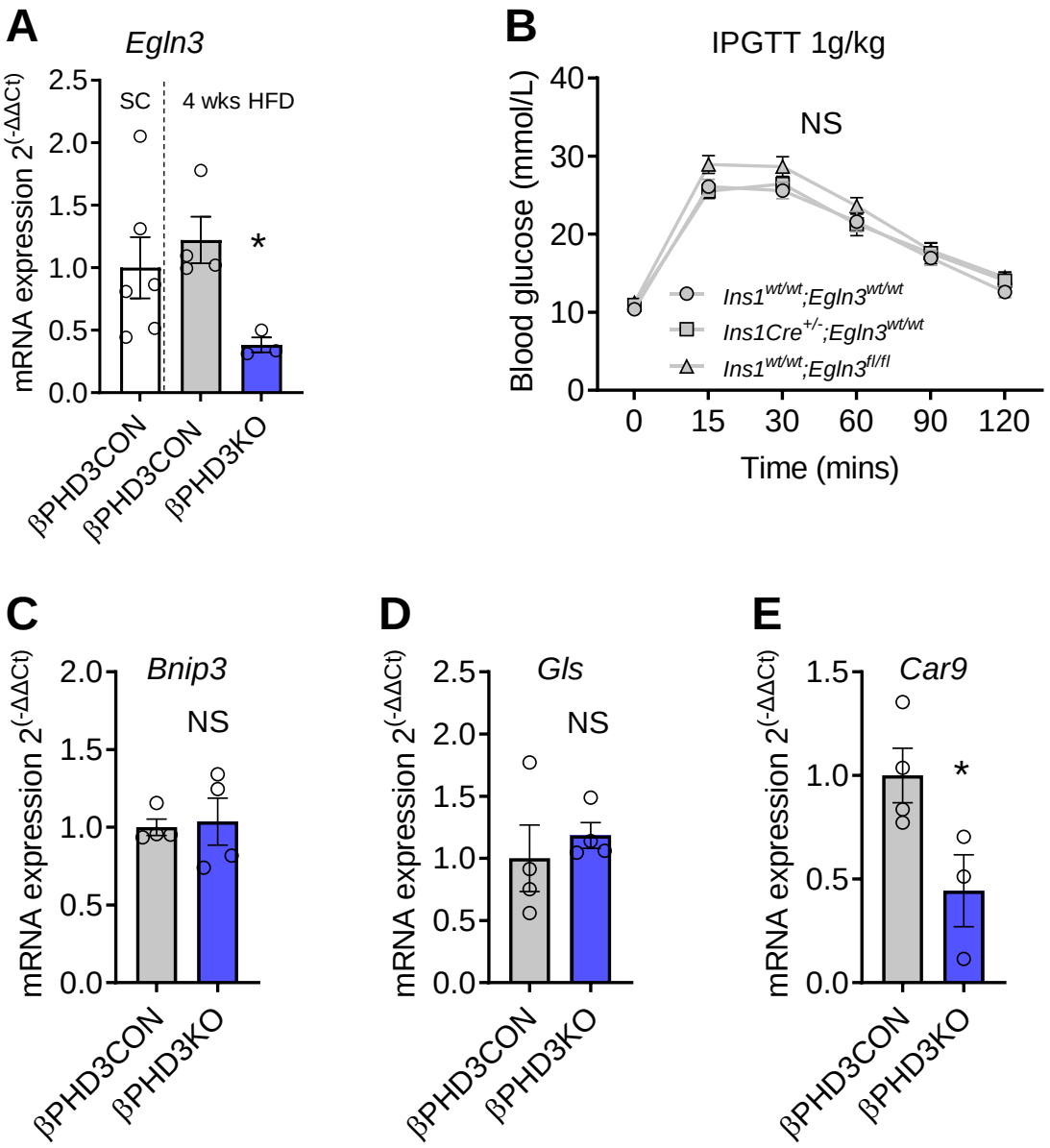

Figure 4.1 βPHD3KO validation and effects of hypoxia at 4 weeks HFD: (**A**) *Egln3* mRNA expression is downregulated in βPHD3KO 4 weeks HFD islets (n = 3-6 animals/genotype; unpaired *t*-test). (**B**) At 4 weeks of HFD, glucose tolerance during IPGTT (1 g/kg glucose administered) is unaffected in *Ins1*$^{wt/wt}$ *Egln3*$^{wt/wt}$, *Ins1Cre*$^{+/-}$ *Egln3*$^{wt/wt}$, and *Ins1*$^{wt/wt}$ *Egln3*$^{fl/fl}$ mice (n = 10-13 animals/genotype; 2-way RM ANOVA, Tukey's test). (**C**-**E**) The mRNA levels of (**C**) *Bnip3* and (**D**) *Gls* are similar, whereas those of (**E**) *Car9* are lower in βPHD3KO 4 weeks HFD islets compared to βPHD3CON (n = 3-4 animals/genotype, unpaired *t*-test). Bar graphs (scatter plot) and line graphs show mean ± SEM.

4.2.2 βPHD3KO mice are glucose intolerant but secrete more insulin at 4 weeks of HFD

Similar to SC-fed animals, mice on a HFD for 4 weeks featured no significant differences in body weight or body composition between βPHD3KO and controls littermates **(Figure 4.2A, B)**. The fasting blood glucose levels after 72 h or 4 weeks on HFD were used to pinpoint the shift in glucose tolerance and insulin secretion. Unsurprisingly, while the responses to IPGTT after 72 h on HFD were unchanged, after 4 weeks on HFD, the βPHD3KO animals started to display significant glucose intolerance, compared to βPHD3CON **(Figure 4.2C, D)**. Levels of serum insulin were similar in βPHD3KO and βPHD3CON mice undergoing IPGTT after 4 weeks of HFD **(Figure 4.2E)**. However, βPHD3KO mice showed higher magnitude of insulin responses than βPHD3CON, as shown by the *in vivo* stimulation index **(Figure 4.2F)**. On the other hand, oral glucose tolerance and insulin sensitivity were found to be similar in βPHD3KO *versus* controls **(Figure 4.3A, B)**. Finally, glucose-stimulated and Ex4-potentiated insulin secretion in isolated islets was increased in βPHD3KO compared to controls **(Figure 4.3C)**, while insulin content was unchanged after 4 weeks of HFD **(Figure 4.3D)**.

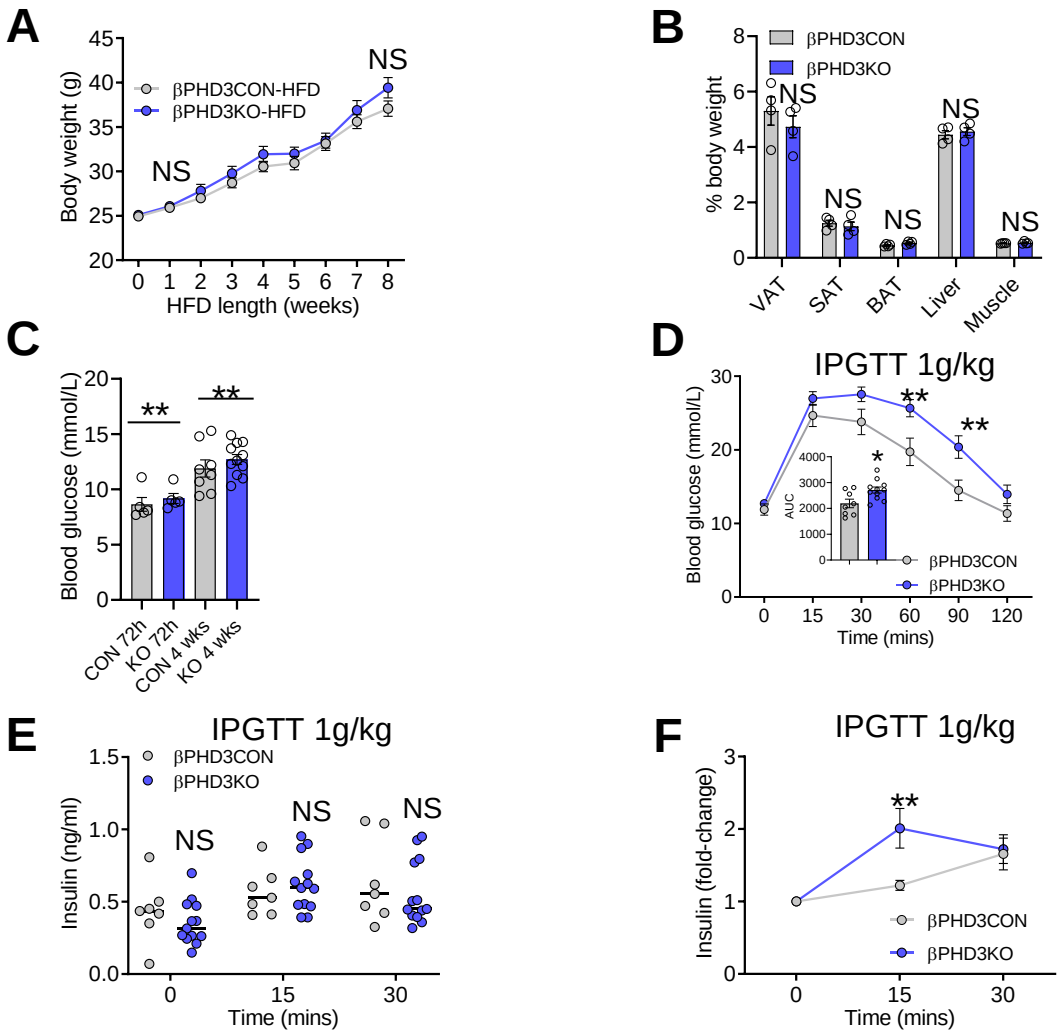

Figure 4.2 Mice growth and IPGTT of βPHD3KO on HFD: (**A**) Growth curves of βPHD3KO mice are similar to controls between 0 and 8 weeks of HFD (n = 11-12 animals/genotype; 2-way RM ANOVA, Sidak's test). (**B**) The percentage of body weight represented by visceral tissue (VAT), subcutaneous tissue (SAT), brown adipose tissue (BAT), liver and muscle is similar in βPHD3KO and βPHD3CON animals at 4 weeks of HFD (n = 4 animals/genotype; 2-way ANOVA, Sidak's test). (**C**) Fasting blood glucose levels do not differ in βPHD3KO mice after 72 h HFD but are increased after 4 weeks of HFD (n = 8-11 animals/genotype; 2-way RM ANOVA, Sidak's test). (**D**) Glucose tolerance and AUC at the IPGTT (1 g/kg glucose administered) are increased in βPHD3KO mice after 4 weeks of HFD (n = 8-11 animals/genotype; IPGTT: 2-way RM ANOVA, Sidak's test; AUC: unpaired *t*-test). (**E**) Serum insulin after IPGTT (1 g/kg glucose administered) is similar in βPHD3KO and βPHD3CON (n = 7-13 mice/genotype; 2-way RM ANOVA, Sidak's test). (**F**) Stimulation index, determined as the fold-change of serum insulin at any time point relative to that at minute 0, shows higher insulin secretion in response to IPGTT (1 g/kg glucose administered) in βPHD3KO 4 weeks HFD mice (n = 7-13 animals/genotype; 2-way RM ANOVA, Sidak's test). Bar graphs (scatter plot) and line graphs show mean ± SEM.

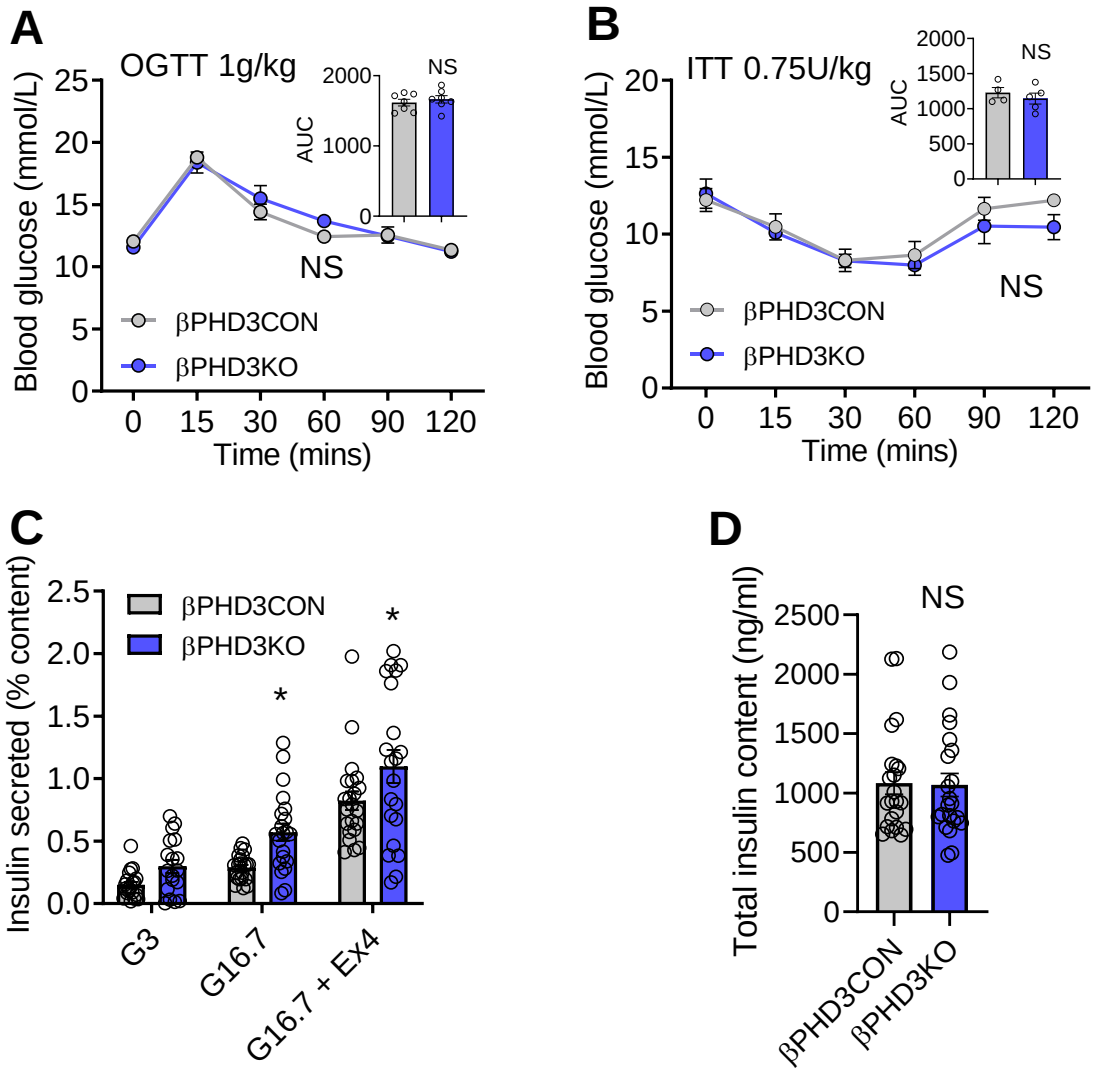

Figure 4.3 OGTT, ITT and GSIS of βPHD3KO at 4 weeks HFD: (**A**) Glucose tolerance and AUC at the OGTT (1 g/kg glucose administered) are unchanged in βPHD3KO 4 weeks HFD mice (n = 7 animals/genotype; OGTT: 2-way RM ANOVA, Sidak's test; AUC: unpaired *t*-test). (**B**) Insulin sensitivity and AUC at the ITT (IP administration of 0.75U/kg insulin) are unchanged in βPHD3KO 4 weeks HFD mice (n = 4-5 animals/genotype; ITT: 2-way RM ANOVA, Sidak's test; AUC: unpaired *t*-test). (**C**) G16.7-stimulated and Ex4-potentiated insulin secretion is increased in islets from βPHD3KO, 4 weeks HFD mice (n = 20 replicates, 4 animals/genotype; 2-way ANOVA, Sidak's test), while (**D**) the total insulin content extracted from βPHD3KO is unchanged compared to βPHD3CON islets (n = 20 replicates, 4 animals/genotype; unpaired *t*-test). Bar graphs (scatter plot) and line graphs show mean ± SEM.

4.2.3 Glucose fluxes into the TCA cycle and lipogenesis are decreased in βPHD3KO at 4 weeks of HFD

Given the reported roles of PHD3 in glucose metabolism (M. Huang et al., 2016; Taniguchi et al., 2013; Yano et al., 2018), we wondered whether the higher blood glucose levels and improved insulin secretion observed in the βPHD3KO model after 4 weeks on HFD might be associated with changes in glucose metabolism. Therefore, to decipher glucose metabolism, βPHD3KO and βPHD3CON islets were traced with ^{14}C glucose to look at its oxidation and incorporation into the aqueous and lipid phases. Glucose oxidation at low or high glucose was unchanged in βPHD3KO islets compared to βPHD3CON after 4 weeks of HFD **(Figure 4.4A)**. Nevertheless, in response to high glucose concentration, the incorporation of ^{14}C, in both the aqueous and the lipid pools, was significantly decreased in βPHD3KO 4 weeks HFD islets **(Figure 4.4B, C)**. This was suggestive of a decreased contribution of glycolysis to the TCA cycle and glucose-driven lipogenesis, respectively.

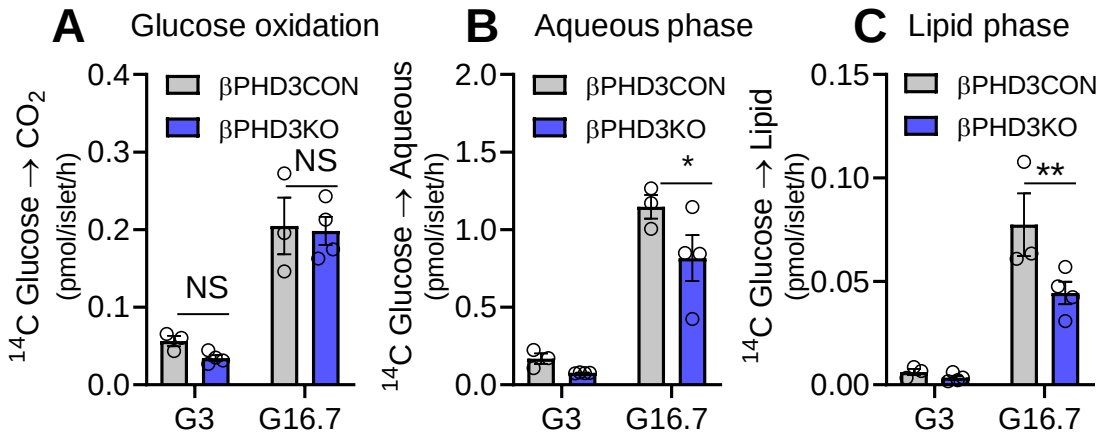

Figure 4.4 ^{14}C tracing analysis of βPHD3KO at 4 weeks HFD: At 4 weeks of HFD (**A**) ^{14}C glucose oxidation quantified by scintillation spectrometry is unchanged in βPHD3KO, but its incorporation in (**B**) the aqueous and (**C**) lipid phases are significantly impaired (n = 3 preparations from 3 animals/genotype; 2-way ANOVA, Benjamini-Krieger-Yekutieli 2-stage procedure). Bar graphs (scatter plot) show mean ± SEM.

4.2.4 βPHD3KO islets reduce more pyruvate to lactate at 4 weeks of HFD

To further investigate the changes in glucose metabolism and its contribution to the production of TCA cycle metabolites, $^{13}C_6$ glucose tracing coupled with GC-MS was performed. The MID analysis did not show any significant difference in the incorporation of ^{13}C from glucose into aspartate, glutamate, malate, fumarate, citrate and lactate in βPHD3KO compared to βPHD3CON islets from 4 weeks HFD mice **(Figure 4.5A-F)**. However, a significant difference was visible when comparing the MIDs for lactate under SC *versus* after 4 weeks of HFD. Indeed, both βPHD3KO and control islets from mice on SC showed accumulation of m+2 lactate, whereas after 4 weeks HFD a switch towards the production of m+3 lactate occurred in both genotypes **(Figure 4.6A)**. The accumulation of m+2 and m+3 lactate are respectively representatives of lactate produced as a result of the oxidative metabolism of glycolytically-derived pyruvate or direct conversion of pyruvate to lactate via LDHA. This m+2 to m+3 switch together with the overall higher amount of lactate found under HFD, and particularly in βPHD3KO islets **(Figure 4.6B)**, indicated a greater direct reduction of pyruvate to lactate occurring after 4 weeks of HFD. Although the mRNA level of the disallowed gene *Ldha* tended to be higher in βPHD3KO 4 weeks HFD islets, this was not significantly different from the βPHD3CON or the expression under SC **(Figure 4.6C)**. Taken together, the data from the ^{14}C and the $^{13}C_6$ tracing suggest that, despite progressing normally, after 4 weeks HFD, the TCA cycle occurs at a lower rate, with reduced input from glycolysis. Therefore, it was hypothesized that βPHD3KO islets might instead rely on the β-oxidation of fatty acids to maintain insulin secretion.

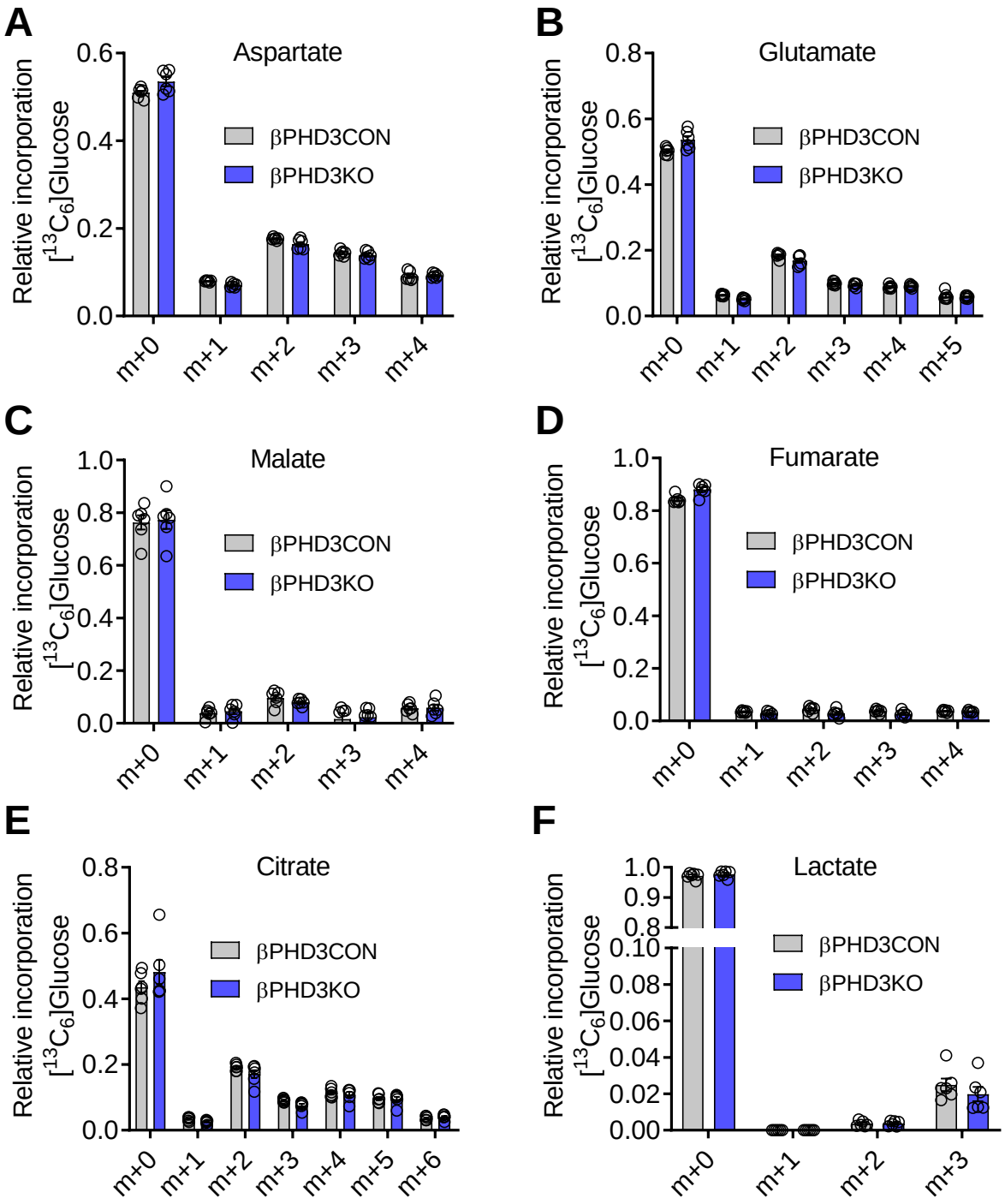

Figure 4.5 MID analysis of βPHD3KO at 4 weeks of HFD: MID showing that the incorporation of ^{13}C from $^{13}C_6$ glucose into (**A**) aspartate, (**B**) glutamate, (**C**) malate, (**D**) fumarate, (**E**) citrate and (**F**) lactate does not differ in βPHD3KO and βPHD3CON islets, after 4 weeks of HFD (n = 6 islet preparations, 3 animals/genotype; 2-way ANOVA, Tukey's test). Bar graphs (scatter plot) show mean ± SEM.

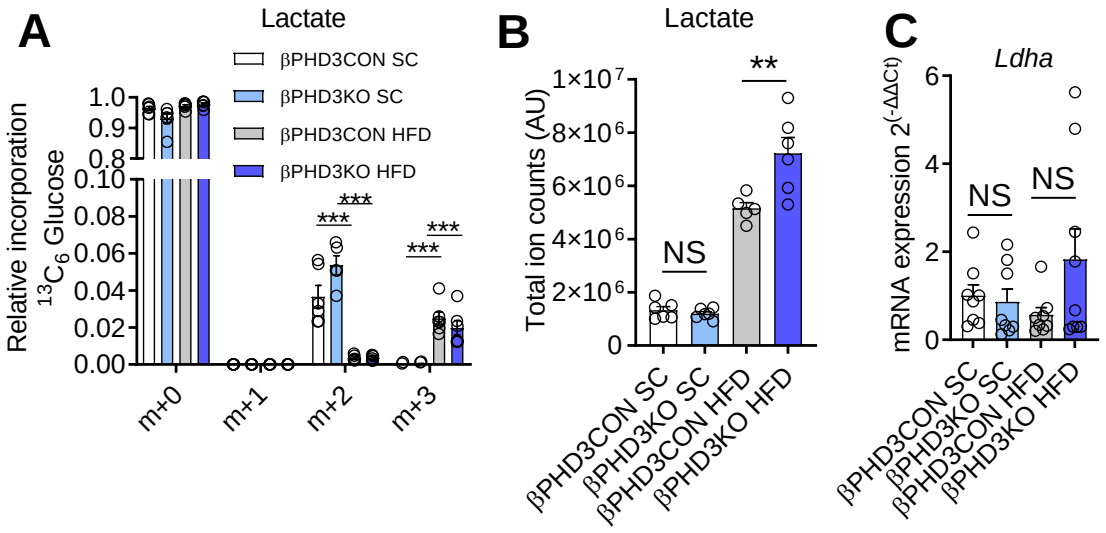

Figure 4.6 Lactate metabolism of βPHD3KO at 4 weeks of HFD: (**A**) MID data showing that ^{13}C incorporation from $^{13}C_6$ glucose into m+2 lactate is significantly higher under SC than after 4 weeks of HFD, while the incorporation into m+3 lactate is higher at 4 weeks of HFD than under SC (n = 6 islet preparations, 3 animals/genotype; 2-way ANOVA, Tukey's test). (**B**) Steady-state lactate expressed as total ion counts, is higher after 4 weeks HFD with a significant increase in βPHD3KO (n = 6 islet preparations, 3 animals/genotype; 1-way ANOVA, Sidak's test). (**C**) the mRNA levels of *Ldha* expressed as fold-change relative to βPHD3CON SC are similar in βPHD3CON islets at 4 weeks of HFD and βPHD3KO islets both under SC and at 4 weeks of HFD (n = 8-9 animals/genotype; Dunnett's test). Bar graphs (scatter plot) show mean ± SEM. AU = arbitrary unit.

4.2.5 βPHD3KO islets switch to β-oxidation of fatty acids at 4 weeks of HFD

To assess whether βPHD3KO islets could use β-oxidation of fatty acids as an alternative source to fuel the TCA cycle, GSIS and Ex4-potentiated insulin secretion were measured following 48-72 h culture with palmitate. Supporting the hypothesis of a shift toward fatty acid usage in βPHD3KO, the secretion assay showed increased insulin secretion in response to both high glucose and Ex4 **(Figure 4.7A)**. As expected, βPHD3CON islets did not show an increased response to high glucose but interestingly displayed a higher response to Ex4 **(Figure 4.7B)**. Moreover, the inhibition of the key enzyme for β-oxidation, CPT1, with etomoxir, augmented the glucose-stimulated

ATP/ADP ratio of βPHD3KO islets **(Figure 4.7C)**. However, mRNA levels of *Cpt1a* were similar in βPHD3KO and βPHD3CON islets **(Figure 4.7D)**. Consistent with this, under low palmitate culturing conditions (48-72 h), Ca^{2+} dynamics in response to high glucose were significantly reduced in 4 weeks HFD βPHD3KO islets **(Figure 4.7E, F)**. Additionally, glycolytically-derived Ca^{2+} fluxes were similar between βPHD3KO and βPHD3CON **(Figure 4.8A, B)**, with KCl responses being markedly elevated in βPHD3KO islets **(Figure 4.8A, B)**. Confirming a reduced dependency on glycolysis, βPHD3KO islets displayed decreased glucose-derived ATP/ADP **(Figure 4.8C, D)**, as well as steady-state pyruvate **(Figure 4.8E)**. Finally, to gain a higher resolution of fatty acid metabolism, a D31-palmitate tracing of 4 weeks HFD islets was carried out. The intracellular uptake of D31-palmitate was found to be unaltered in βPHD3KO islets **(Figure 4.9A)**. The $^{2}H_2O$/D31-palmitate ratio, representative of the accumulation in the medium of $^{2}H_2O$ deriving from the β-oxidation of D31-palmitate, was greatly increased following 16 h of incubation with D31-palmitate **(Figure 4.9B)**. Moreover, islets from βPHD3KO animals fed a HFD for 4 weeks had a significantly higher $^{2}H_2O$/D31-palmitate ratio than controls at the 16 h time point.

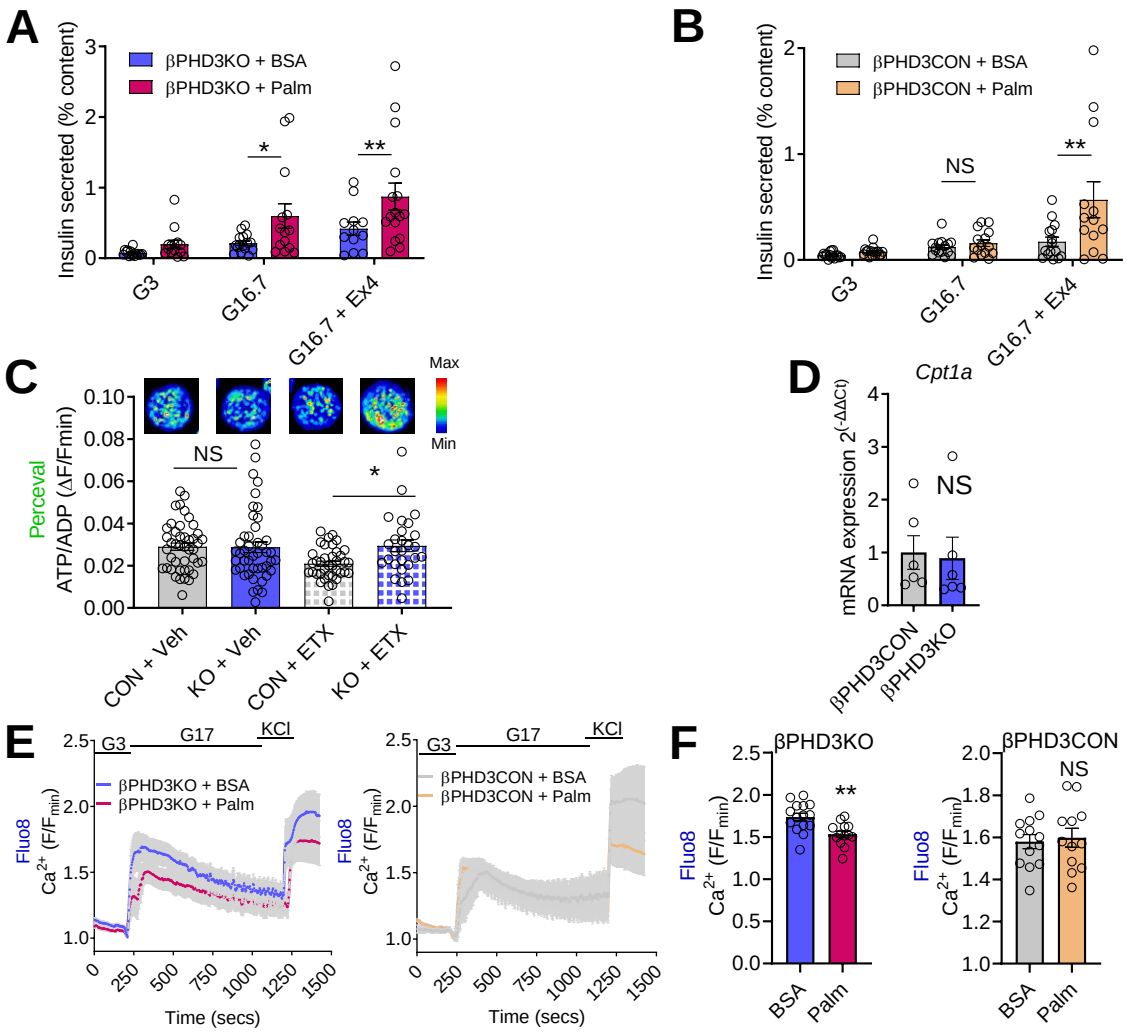

Figure 4.7 Effects of β-oxidation on the glucose homeostasis of βPHD3KO at 4 weeks of HFD: (**A** and **B**) 48-72 h incubation with 150 µM palmitate determines increased GSIS in (**A**) βPHD3KO (n = 12-17 replicates, 7-9 animals/genotype, 2-way ANOVA, Benjamini-Krieger-Yekutieli 2-stage procedure) but not in (**B**) βPHD3CON (n = 13–17 replicates, 7–9 animals/genotype; 2-way ANOVA, Benjamini-Krieger-Yekutieli 2-stage procedure) 4 weeks HFD islets. (**A**, **B**) Following chronic incubation with 150 µM palmitate, Ex4-stimulated insulin secretion is increased in both genotypes. (**C**) 11 mM glucose-stimulated ATP/ADP ratio, detected with Perceval, is rescued by treatment with 100 µM Etomoxir (ETX) in βPHD3KO after 4 weeks of HFD (representative image of individual islets included, n = 27-45 islets, 5-6 animals/genotype; 2-way ANOVA, Sidak's test). (**D**) *Cpt1a* mRNA levels are similar between βPHD3KO and βPHD3CON in 4 weeks of HFD islets (n = 6 animals/genotype; unpaired *t*-test). (**E** and **F**) Following treatment with 150 µM palmitate for 48-72 h, Ca^{2+} fluxes assessed with Fluo8 are reduced in βPHD3KO compared to βPHD3CON, 4 weeks HFD islets as shown by (**E**) mean traces and (**F**) summary bar graph (n = 13-15 islets, 2-3 animals/genotype; unpaired *t*-test). Bar graphs (scatter plot) and line graphs show mean ± SEM. F/Fmin = fluorescence at any time point/minimum fluorescence.

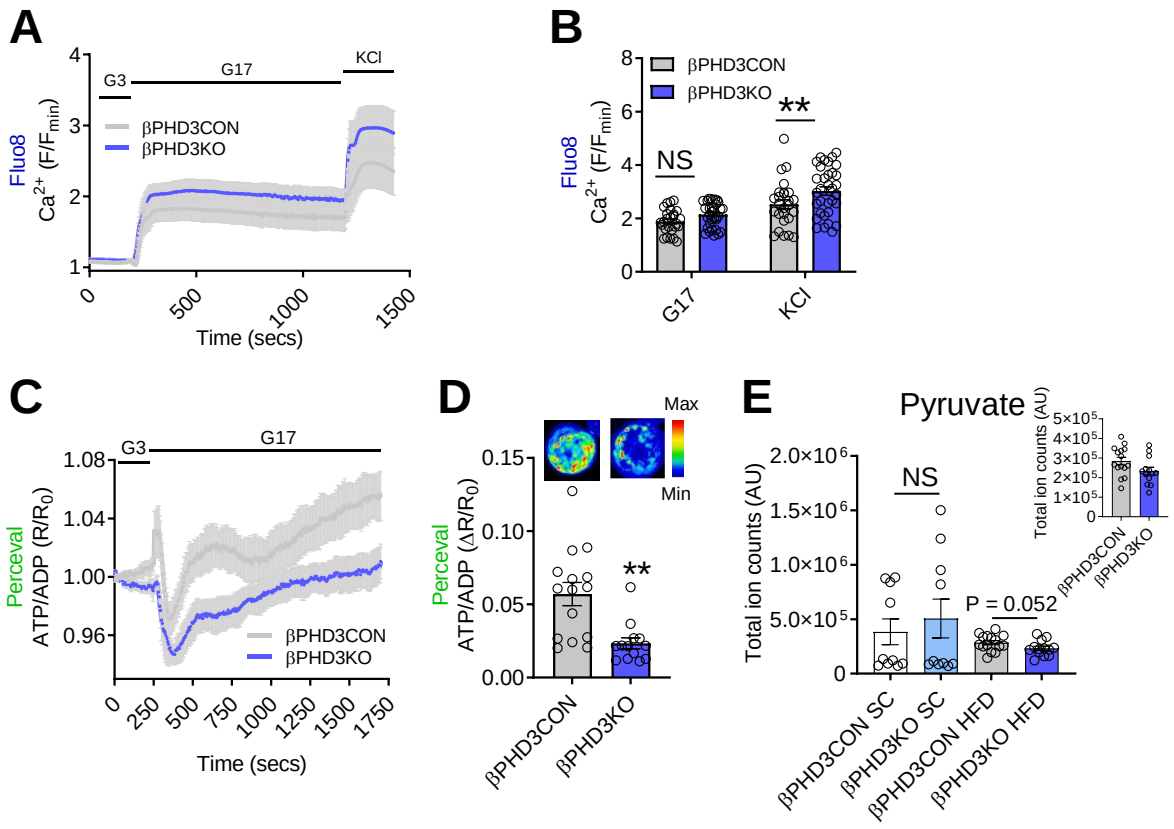

Figure 4.8 *In vitro* phenotype of βPHD3KO at 4 weeks HFD: (**A** and **B**) After 4 weeks of HFD, in βPHD3KO islets, Ca^{2+} fluxes detected with Fluo8 are unchanged or increased in response to 17 mM glucose and 10 mM KCl respectively, as shown by (**A**) mean traces and (**B**) summary bar graph (n = 26-33 islets, 6 animals/genotype; 2-way ANOVA, Sidak's test). (**C** and **D**) Following incubation with Perceval, the ATP/ADP ratio is significantly decreased in βPHD3KO after 4 weeks HFD stimulated with 17 mM glucose as shown by (**C**) mean traces and (**D**) summary bar graph with representative images of single islets (n = 13-15 islets, 4 animals/genotype; unpaired *t*-test. (**E**) Steady-state pyruvate is decreased in βPHD3KO 4 weeks HFD islets (n = 11-13 replicates, 5-8 animals/genotype; Mann-Whitney U test). Bar graphs (scatter plot) and line graphs show mean ± SEM. F/Fmin = fluorescence at any time point/minimum fluorescence; R/R0 = fluorescence at any time point/fluorescence at 0 min and AU = arbitrary unit.

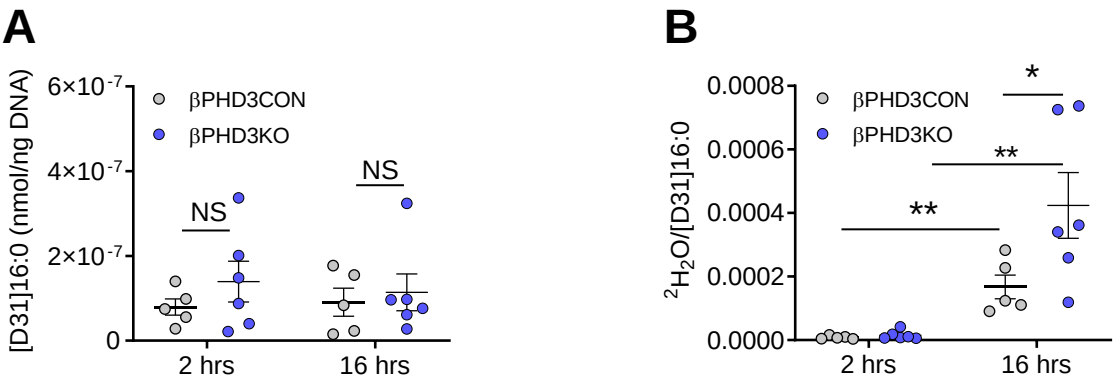

Figure 4.9 D31-palmitate tracing analysis in βPHD3KO at 4 weeks HFD: (**A**) D31-palmitate uptake, is similar in βPHD3CON and βPHD3KO, 4 weeks HFD islets after 2 and 16 h incubation with 150 µM D31-palmitate (n = 5-6 animals/genotype; 2-way ANOVA; Sidak's test). (**B**) $^{2}H_2O$/D31-palmitate, which is indicative of the β-oxidation rate, is increased in βPHD3KO 4 weeks HFD islets after 16h (n = 5-6 animals/genotype; unpaired *t*-test (within genotype); 2-way ANOVA, Sidak's test (between genotypes)). Bar graphs (scatter plot) and line graphs show mean ± SEM.

4.2.6 The expression of genes encoding acetyl-CoA carboxylase is unchanged in βPHD3KO at 4 weeks HFD

Previous works described a role for PHD3 in the hydroxylation of ACC2 in AML and skeletal muscle (German et al., 2016; Yoon et al., 2020). The hydroxylated ACC2 is responsible for the conversion of acetyl-CoA to mitochondrial malonyl-CoA, which prevents the β-oxidation of fatty acids by inhibiting CPT1 (German et al., 2016; Yoon et al., 2020). In β-cells, however, ACC2 expression is thought to be very low, with the ACC1 isoform being predominant (MacDonald, Dobrzyn, Ntambi, & Stoker, 2008; Ronnebaum et al., 2008). Consistent with this, the expression of *Acacb* (encoding for ACC2) was found to be about 1% of that of *Acaca* (encoding for ACC1) in control islets **(Figure 4.10A)**. Therefore, to investigate whether PHD3 could play a role in β-cells similar to that described in skeletal muscle and cancer, gene expression data sets from human islets and purified β-cells were examined (Blodgett et al., 2015; Hrvatin et al.,

2014; Moran et al., 2012). Although less expressed than *ACACA*, the mRNA levels of *ACACB* were comparable to those encoding for the β-cell transcription factor HNF1A **(Figure 4.10B)**. Moreover, the *ACACB* promoter was found to bind multiple β-cell specific transcription factors **(Figure 4.10C)**. Finally, the expression of the *Acaca* and *Acacb* genes was measured in βPHD3CON and βPHD3KO islets. Both were found to be similar in βPHD3KO as compared to control islets **(Figure 4.10D, E)**, suggesting the possibility of a mechanism by which PHD3 acts post-translationally by hydroxylation of ACC2.

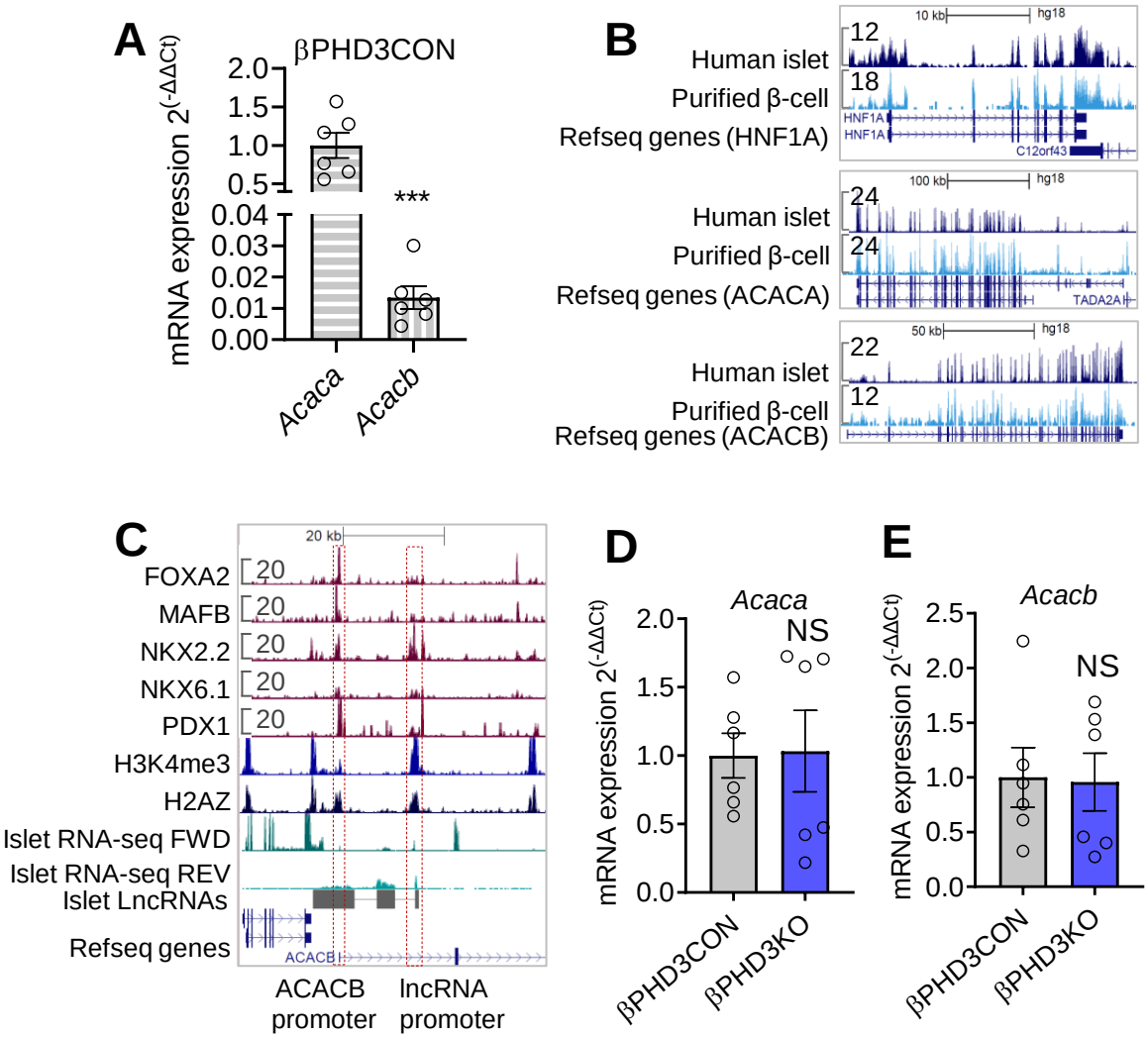

Figure 4.10 Acetyl-CoA carboxylase gene expression and gene regulation in βPHD3KO at 4 weeks HFD: (**A**) In βPHD3CON islets from mice at 4 weeks of HFD the mRNA levels of *Acacb* are significantly lower than those of *Acaca* (n = 6 animals; unpaired *t*-test). (**B** and **C**) The expression level of (**B**) *ACACB* is lower than *ACACA* in human islets and purified β-cells, but comparable to *HNF1A*. (**C**) *ACACB* is regulated by a number of β-cell transcription factors (data publicly available through EMBL-EBI and www.isletregulome.com, visualized with the open source University of California Santa Cruz (UCSC) Genome Browser). (**D** and **E**) The mRNA expression of (**D**) *Acaca* and (**E**) *Acacb* is unaltered in βPHD3KO compared to βPHD3CON (n = 6 animals/genotype; unpaired *t*-test). Bar graphs (scatter plot) show mean ± SEM.

4.3 Discussion

This chapter details the effect of 4 weeks of HFD on the βPHD3KO model, with an aim to identify the metabolic adaptation occurring in the β-cells lacking PHD3. Firstly, we confirmed that the Cre-LoxP system used to induce β-cell specific PHD3KO was still efficient after 4 weeks of HFD. Furthermore, since *Ins1Cre* itself was shown to exert a minor influence on glucose tolerance during HFD, we excluded a direct effect of the *Cre* or floxed alleles in our model. Similar to the study that used SC diet, the expression of the HIF1 targets were assessed after 4 weeks of HFD to evaluate whether the role of PHD3 could depend on HIF1 signaling. While the expression of *Bnip3* and *Gls* were found to be unchanged after 4 weeks of HFD, the mRNA levels of *Car9* were decreased in βPHD3KO islets. The overexpression of *Car9* is a common feature of hypoxia, where it determines extracellular acidification (Infantino et al., 2021). Therefore, the downregulation of *Car9* and the unaffected levels of *Bnip3* and *Gls* confirmed a lack of HIF1 transcriptional signature in βPHD3KO islets after 4 weeks of HFD.

The animals undergoing HFD for 72 h and 4 weeks were initially compared to evaluate whether the PHD3 loss would induce visible phenotypic changes at a very early stage of fat excess or if it required prolonged exposure. Mice lacking PHD3 did not display differences at 72 h of HFD, whereas longer exposure was needed to reveal a PHD3-associated phenotype. Indeed after 4 weeks of HFD, the βPHD3KO animals showed higher glucose levels when challenged with an intraperitoneal glucose load, i.e. they became glucose intolerant. Nevertheless, they were found to be more sensitized to exocytosis, releasing a bigger portion of insulin granules earlier than βPHD3CON. Based on previous studies indicating a crucial role for PHD3 in glucose metabolism

and insulin secretion (M. Huang et al., 2016; Taniguchi et al., 2013; Yano et al., 2018) we sought to test whether the discrepancy between improved insulin secretion and glucose intolerance observed in βPHD3KO animals after 4 weeks on HFD was due to altered glucose sensing and utilization. To investigate the usage of glucose within the β-cells, tracing with glucose labeled with the radioactive isotope ^{14}C was performed. While the oxidation of glucose did not change in βPHD3KO islets stimulated with low and high concentrations of glucose, the incorporation of ^{14}C glucose in the aqueous and lipid pool was reduced. The glucose to aqueous phase incorporation is representative of the glycolytic fueling of the TCA cycle. On the other hand, the incorporation into the lipid phase describes the contribution of glucose to *de novo* lipogenesis. Thus, the impaired incorporation of glucose in both pools is indicative of a reduced oxidative metabolism of pyruvate entering the TCA cycle and limited glucose-driven lipogenesis (Cantley et al., 2019).

We proceeded by gaining an even higher resolution of glucose metabolism through $^{13}C_6$ glucose tracing. In line with ^{14}C glucose oxidation data, the contribution of glucose to the various metabolites of the TCA cycle was found to be unchanged in βPHD3KO islets from animals on 4 weeks HFD, compared to controls. This, taken together with the reduced contribution of glycolysis to the aqueous phase of βPHD3KO islets, discussed previously, implies that regardless of the lesser glycolytic input to the TCA cycle, the net incorporation of glucose in each TCA cycle metabolite progresses normally. From the comparison of MIDs acquired under SC and after 4 weeks of HFD, a crucial switch in the production of lactate emerged. Consistent with the known mechanism of insulin secretion, where glucose sensing is crucially coupled to the

secretion of insulin (Campbell & Newgard, 2021; Kaestner et al., 2021), the accumulation of m+2 lactate was detected under SC.

The islets from animals fed a SC or HFD were cultured with glucose possessing all heavier carbons in its structure. From uniformly labeled glucose, through glycolysis, fully labeled pyruvate (m+3) is produced. In standard conditions, the glycolytic input to the oxidative TCA cycle is fundamental for the production of sufficient energy to sustain the TCA cycle. Therefore m+3 pyruvate metabolized by PDH is deprived of one of the labeled carbons, leading to all following metabolites, including lactate, to contain only 2 carbons labeled (m+2) **(Figure 3.7)**. However, the accumulation of m+3 lactate in islets from animals kept on HFD for 4 weeks suggested that lactate was produced from direct conversion of glycolytically-derived pyruvate. This was surprising, as the reduction of pyruvate to lactate is mediated by the activity of LDHA, encoded by the *Ldha* gene, known to be disallowed in the β-cells. Indeed, LDHA is key in the anaerobic metabolism of the cell and it would prevent the correct stimulus-secretion coupling in the β-cells (Pullen & Rutter, 2013; Schuit et al., 2012). Although the expression of *Ldha* in βPHD3KO tended to be increased at 4 weeks of HFD, the difference between the controls and the mRNA levels detected under SC was not statistically significant. Nonetheless, the conversion of pyruvate to lactate is associated with the generation of cytosolic nicotinamide adenine dinucleotide (NAD^+), a crucial co-factor of glycolysis, suggesting that the increased accumulation of m+3 lactate after 4 weeks of HFD, could support continued glycolysis. These results show that β-cells produce meaningful lactate during HFD, that LDHA is functional, and that the disallowed gene hypothesis likely does not apply during metabolic stress.

Taken together, these data pointed towards reduced fueling of the TCA cycle from glycolysis, accompanied by an altered usage of nutrients. This led us to hypothesize that βPHD3KO islets might use the β-oxidation of fatty acids, present in excess during HFD, as an alternative source to fuel the TCA cycle, providing sufficient energy to sustain insulin secretion.

Supporting a change in β-cell nutrient preference, prolonged exposure to low palmitate improved *in vitro* GSIS in βPHD3KO islets, but not in βPHD3CON islets. Intact GSIS in βPHD3CON islets treated with palmitate confirmed that the concentration of fatty acid employed was unlikely to cause lipotoxicity. Unexpectedly, 48-72 h of palmitate treatment led to an increase in Ex4-potentiated insulin secretion in both βPHD3KO and βPHD3CON islets.

Previous works showed that PHD3 can regulate nutrient preference by inhibiting fatty acid β-oxidation (German et al., 2016; Yoon et al., 2020). Thus, in AML and in skeletal muscle, PHD3 was found to hydroxylate ACC2, leading to the conversion of acetyl-CoA to malonyl-CoA, the latter inhibiting CPT1, which is the rate-limiting step of fatty acid oxidation (German et al., 2016; Yoon et al., 2020). To assess whether PHD3 could play a similar role in the pancreatic β-cells, a CPT1 inhibitor, namely etomoxir, was employed. In the presence of etomoxir, glucose-stimulated ATP/ADP ratios were rescued in βPHD3KO islets, implying that CPT1 might be regulated downstream of PHD3. However, the expression of *Cpt1a* was not altered by the loss of PHD3 in β-cells. Further supporting a switch to β-oxidation in βPHD3KO after 4 weeks of HFD, glucose-stimulated Ca^{2+} fluxes were lower in βPHD3KO that underwent palmitate treatment than untreated ones. Interestingly, glucose-stimulated Ca^{2+} dynamics of βPHD3KO islets were not different from controls. However, this is likely due to the

increased sensitivity of the VDCCs to membrane depolarization, displayed by the greater response of the βPHD3KO to KCl. Conversely, after 4 weeks of HFD, the glycolytically-derived ATP/ADP ratio was significantly decreased in βPHD3KO islets, supporting a reduced contribution of glycolysis to the triggering pathway of insulin secretion. Similarly, the steady-state for pyruvate, the final product of glycolysis, was found to be lower in βPHD3KO after 4 weeks of HFD. This, together with the aforementioned increased conversion of pyruvate to lactate, indicates that after 4 weeks of HFD in βPHD3KO, the handling of pyruvate is impaired. As a result, the production of pyruvate is altered and/or destined to the generation of lactate, accounting for a change in the NAD^+/NADH ratio. Indeed, the accumulation of lactate is associated with the production of NAD^+, which is consistent with higher rates of fatty acid oxidation producing NADH.

A higher understanding of fatty acid fate was obtained through tracing with D31-palmitate. The islets from βPHD3KO and βPHD3CON mice at 4 weeks of HFD were incubated with D31-palmitate for 2 h or 16 h, and after confirming that the tracer uptake was equal between βPHD3KO and controls, the ^2H_2O/D31-palmitate ratio was evaluated. Through isotope ratio mass spectrometry, the enrichment of the culture medium with ^2H_2O derived from D31-palmitate is monitored, providing a measure of β-oxidation flux (Law et al., 2007). The ^2H_2O/D31-palmitate ratio was found to be significantly increased after 16 h of incubation, particularly in the βPHD3KO. This implies that βPHD3KO does indeed determine a change in the use of fatty acids in islets, after 4 weeks of HFD.

Based on the increased β-oxidation rates found in βPHD3KO and the reported role of PHD3 in the hydroxylation of ACC2 (German et al., 2016; Yoon et al., 2020), we sought

to investigate the possibility of a mechanism by which PHD3 regulates β-oxidation in the β-cells, by hydroxylation and activation of ACC2. However, it is important to note that, consistent with our data, pancreatic β-cells are known to mainly express the other isoform of the acetyl-CoA carboxylase, ACC1, encoded by *Acaca* (MacDonald et al., 2008; Ronnebaum et al., 2008). This converts acetyl-CoA to malonyl-CoA, the latter being a substrate of FAS, involved in the *de novo* lipogenesis (Cantley et al., 2019). Therefore, to confirm whether PHD3 could regulate the nutrient preference in β-cells through ACC2, several data sets describing its gene expression were analyzed. From these, *ACACB*, the human gene encoding for ACC2, was found to be expressed in β-cells, at lower levels than *ACACA*, but comparable to the β-cell transcription factor HNF1A (Akerman et al., 2021; Akerman et al., 2017; Blodgett et al., 2015; Hrvatin et al., 2014; Moran et al., 2012; Pasquali et al., 2014). Thus, ACC2 is present in the β-cells at functional levels and falls under the regulation of several β-cell transcription factors, such as FOXA2, MAFB, NKX2.2, NKX6.1 and PDX1 (Akerman et al., 2021; Akerman et al., 2017; Moran et al., 2012; Pasquali et al., 2014). Finally, the expression of the mouse genes *Acaca* and *Acacb* was assessed to evaluate whether their expression was directly regulated by PHD3. They both displayed unchanged mRNA levels in βPHD3KO islets after 4 weeks of HFD. Taken together these data suggest that although not through direct regulation of its mRNA levels, there is the possibility of post-translational regulation of ACC2, via PHD3-mediated hydroxylation.

Interestingly, in a recent work from collaborators, some of the findings discussed here could be confirmed under SC (Hoang et al., 2022). Although presenting defective GSIS, βPHD3KO showed reduced glucose-stimulated ATP/ADP ratio and augmented production of NAD^+, consistent with increased β-oxidation. This was unlike our results

under SC, but probably due to the relatively older age of their mice and the higher fat content of their SC. Moreover, Hoang *et al.* identified decreased *Acacb* mRNA levels in βPHD3KO, further reinforcing the possibility of a mechanism by which PHD3 regulates nutrient preference in β-cells, through the activity of ACC2 (Hoang et al., 2022).

To summarize, 4 weeks of HFD were necessary to reveal a PHD3-associated phenotype in β-cells. Indeed, βPHD3KO animals displayed glucose intolerance accompanied by increased insulin secretion, which was suggestive of a change in the usage of nutrients. Further supporting this, the investigation of glucose metabolism via ^{14}C and $^{13}C_6$ glucose tracing allowed us to identify a reduced contribution of glucose to the TCA cycle and the *de novo* lipogenesis. Moreover, the m+2 to m+3 lactate switch observed in the islets from 4 weeks of HFD compared to those from SC, suggested an increased direct conversion of pyruvate to lactate. These data were suggestive of a switch away from glycolysis to sustain insulin secretion in the pancreatic β-cells, in favor of the β-oxidation of fatty acids. Consistent with this, prolonged exposure to low palmitate and treatment with etomoxir were found to respectively increase GSIS and rescue the glycolytically-derived ATP/ADP ratios. Finally, the increased rate of β-oxidation in the βPHD3KO islets after 4 weeks of HFD, was confirmed via D31-palmitate tracing. Thus, PHD3 plays an important role in maintaining the correct glucose homeostasis in mice in the early stages of dietary fat excess. Our data point towards a mechanism whereby PHD3 can inhibit fatty acid oxidation by hydroxylation of ACC2. Once hydroxylated, this enzyme is activated and can convert acetyl-CoA to malonyl-CoA. The latter can then prevent the activity of CPT1, limiting β-oxidation. Conversely, when PHD3 is lacking in the β-cells, fatty acid oxidation can provide an

alternative source of acetyl-CoA to sustain the activity of the TCA cycle, necessary for the production and release of insulin. At the same time, the glycolytic input is lost in the conversion of pyruvate to lactate to maintain the REDOX status **(Figure 4.11A, B)**.

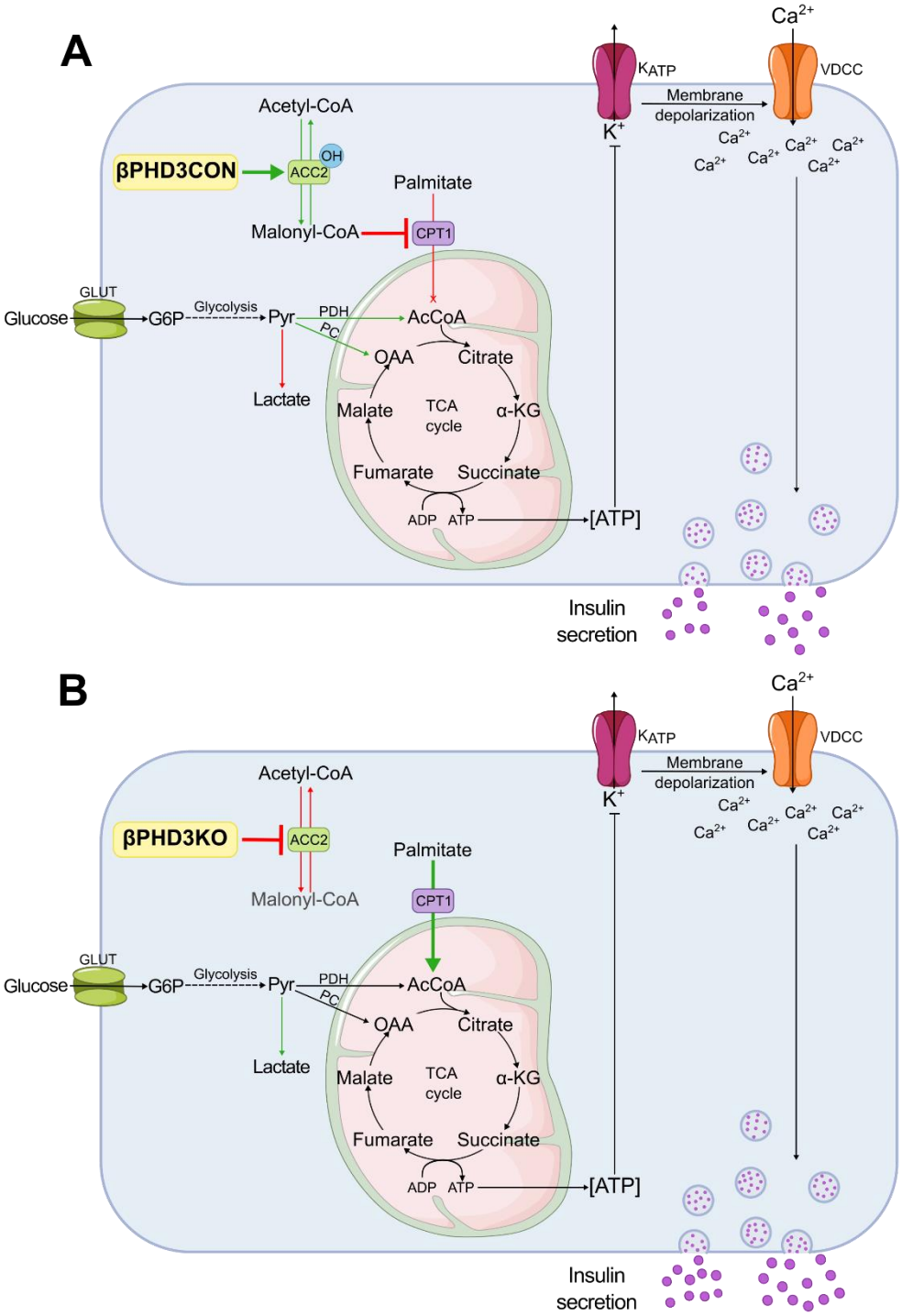

Figure 4.11 Schematic of the suggested pathway mediating PHD3 control of nutrient preference in the β-cells after 4 weeks of HFD: (**A**) When PHD3 is expressed (βPHD3CON) it can hydroxylate and activate ACC2, mediating the conversion of acetyl-CoA to malonyl-CoA. The latter inhibiting CPT1 prevents the use of fatty acids, ensuring glycolytic fueling of the TCA cycle. (**B**) When PHD3 is lacking (βPHD3KO), ACC2 remains inactivated, CPT1 is not inhibited and the β-oxidation of fatty acids can sustain the TCA cycle. At the same time, glycolytically-derived pyruvate is converted to lactate to maintain the REDOX balance.

4.4 Conclusion

The loss of PHD3 is associated with phenotypic alterations after 4 weeks of HFD. In line with previous work, PHD3 was able to function as a gatekeeper of nutrient preference. At the onset of metabolic stress, βPHD3KO animals were found to rely more heavily on the β-oxidation of fatty acids, perhaps as a way by which mice can compensate for their higher blood glucose levels, with higher insulin secretion.

Our data suggest that the βPHD3KO-specific phenotype at 4 weeks of HFD is likely independent of the stabilization of HIF1α. Indeed, the mRNA levels of *Bnip3* and *Gls* are unaffected and those of *Car9* are reduced in βPHD3KO. However, these are not sufficient to confidently exclude a role for hypoxia in the βPHD3KO mice glucose metabolism. In fact, the analysis of the protein levels of these and other targets of HIF1α as well as of HIF1α itself and its hydroxylation would have provided a more reliable method for the investigation of the hypoxic signaling. Moreover, through isotopic tracing we found that the conversion of pyruvate to lactate, catalyzed by LDHA, is increased in βPHD3KO islets at 4 weeks of HFD. The *Ldha* gene expression, which is normally disallowed in β-cells, tended to be higher in βPHD3KO islets, however, this was not significant and did not provide information on possible post-transcriptional modifications. Although not interrogated during the course of this PhD, the study of LDHA levels through immunoblotting could provide further insights into pyruvate handling and lactate production in βPHD3KO. Furthermore, after 4 weeks of HFD, βPHD3KO animals displayed glucose intolerance and improved insulin secretion *in vivo*, as well as increased glucose- and Ex4-stimulated insulin secretion *in vitro*. These results would have required further investigation of the β-cell mass, proliferation and of GLP-1R signaling at 4 weeks of HFD. However, due to time constraints, these could

not be addressed during the span of this project. Finally, based on the study of published gene expression data sets (Blodgett et al., 2015; Hrvatin et al., 2014; Moran et al., 2012) and previous works (German et al., 2016; Yoon et al., 2020) we suggest a mechanism by which, after 4 weeks of HFD, PHD3 maintains the appropriate glucose metabolism in β-cells through hydroxylation of ACC2. However, direct evidence of a post-translational modification of ACC2 by PHD3 is lacking at this stage and should be addressed via experiments of immunoprecipitation going forward.

Despite some drawbacks, it remains necessary to investigate the effects of the compensatory mechanism described for βPHD3KO after 4 weeks of HFD over more prolonged exposure to obesogenic diet. Therefore, the following chapter will focus on the effects of PHD3 and its loss in animals fed a HFD for 8 weeks.

Chapter 5

THE ROLE OF PHD3 IN β-CELL GLUCOSE METABOLISM AFTER 8 WEEKS OF HIGH FAT DIET

Abstract

Background and aims

After 4 weeks of HFD, mice lacking PHD3 in their β-cells were found to rewire their metabolism. The loss of PHD3 induced a shift towards the β-oxidation of fatty acids rather than glycolysis to fuel the TCA cycle. To understand how prolonged exposure to metabolic stress would impact the PHD3-associated phenotype, the effects of 8 weeks of HFD were also analyzed.

Materials and methods

After 8 weeks of HFD, mice underwent IPGTT, OGTT and ITT, whereas the isolated islets were tested for glucose-and Ex4-stimulated insulin secretion, and Ca^{2+} dynamics. Immunohistochemistry of isolated islets as well as of entire pancreas slices was used to assess proliferation, apoptosis, α-cell/β-cell ratio and β-cell mass.

Results

At 8 weeks of HFD, the βPHD3KO displayed glucose intolerance, impaired insulin secretion and increased apoptosis. However, this was not accompanied by changes in proliferation, α-cell/β-cell ratio and expression of ER stress marker. Finally, β-cell mass and the proportion of larger islets were increased in βPHD3KO.

Discussion and Conclusion

The prolonged exposure to fatty acid excess leads to a more generalized failure of the βPHD3KO mice and islets. However, glucose intolerance at this time point was less severe, suggesting that the loss of PHD3 might have a somehow protective role. Nonetheless, the imbalances highlighted after 8 weeks of HFD, pose the need for investigations over longer HFD feeding.

5.1 Introduction

In chapter 4, the characterization of the βPHD3KO model after 4 weeks of HFD was detailed. Under this dietary condition, the loss of PHD3 in β-cells determined metabolic rewiring towards the usage of fatty acids as an alternative energy source. PHD3 was suggested to act through hydroxylation of ACC2, to inhibit the central enzyme of β-oxidation and maintain the appropriate glycolytic stimulus for insulin secretion. However, the alterations displayed by the β-cells lacking PHD3, at 4 weeks of HFD, likely provide a compensatory mechanism to release insulin using fatty acids, which are abundant under HFD.

To investigate whether the nature of the adjustment observed after 4 weeks of HFD is protective or maladaptive, the duration of the obesogenic diet needed to be extended. Greater impairment is known to occur in animals undergoing HFD for longer periods, with β-cell failure appearing between 8 and 12 weeks of metabolic stress (da Silva Xavier & Hodson, 2018). Therefore, we decided to observe the effects of PHD3KO in the β-cells after prolonged metabolic stress in the form of HFD administered for 8 weeks.

In this chapter, the phenotype of the βPHD3KO model after 8 weeks of HFD is discussed. βPHD3KO mice were metabolically phenotyped, before examination of isolated islets, with particular emphasis on common hallmarks of β-cell failure, such as apoptosis, ER stress and altered α-cell/β-cell ratio.

5.2 Results

5.2.1 Changes in βPHD3KO metabolism are independent of HIF at 8 weeks of HFD

To establish whether, after 8 weeks of HFD, the hypoxic signaling has a more prominent role on glucose homeostasis of βPHD3KO islets, the expression of HIF targets was measured. *Ccnd1* and *Dll4* mRNA levels were unchanged or significantly decreased respectively in βPHD3KO compared to βPHD3CON islets **(Figure 5.1A, B)**. This suggested that after prolonged metabolic stress, the stabilization of HIF is still unlikely to be a major effector of the PHD3-related phenotype.

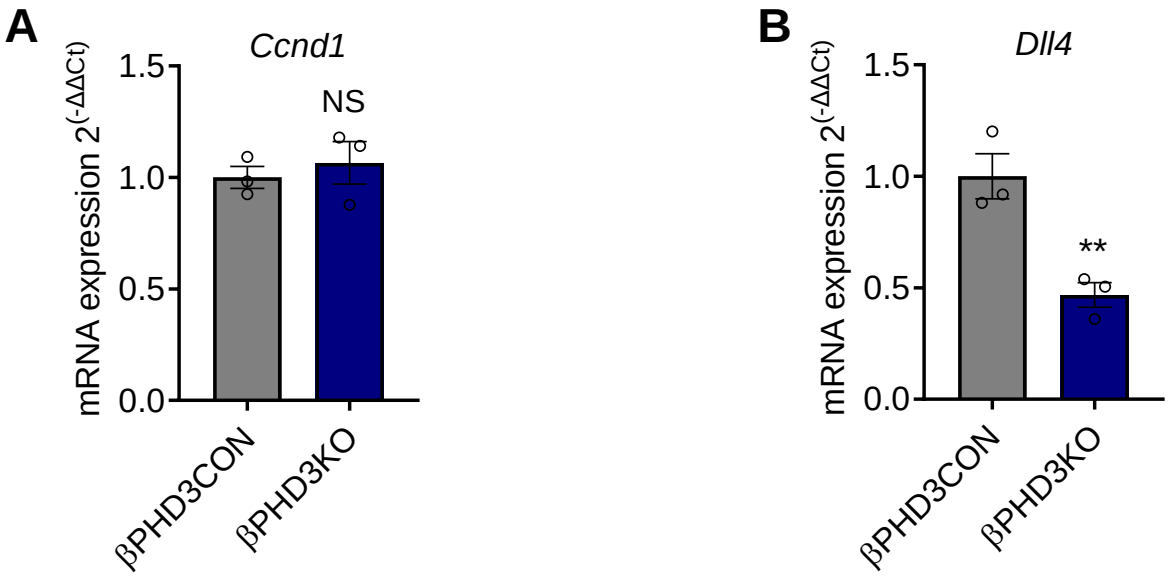

Figure 5.1 Effects of hypoxia on βPHD3KO at 8 weeks HFD: The expressions of (**A**) *Ccnd1* and (**B**) *Dll4* are respectively unchanged and decreased in βPHD3KO *versus* βPHD3CON after 8 weeks of HFD (n = 3 animals/genotype; unpaired *t*-test). Bar graphs (scatter plot) show mean ± SEM.

5.2.2 βPHD3KO mice are still glucose intolerant at 8 weeks of HFD

After 8 weeks of HFD, βPHD3KO mice had unchanged depots of visceral, subcutaneous and brown adipose tissue, as well as of liver and muscle, compared to controls **(Figure 5.2A)**. While βPHD3KO mice were glucose intolerant in response to intraperitoneal glucose **(Figure 5.2B)**, OGTT results were comparable to βPHD3CON mice **(Figure 5.2C)**. Mirroring the effects at 4 weeks, the loss of PHD3 did not lead to changes in insulin sensitivity after 8 weeks of HFD **(Figure 5.2D)**.

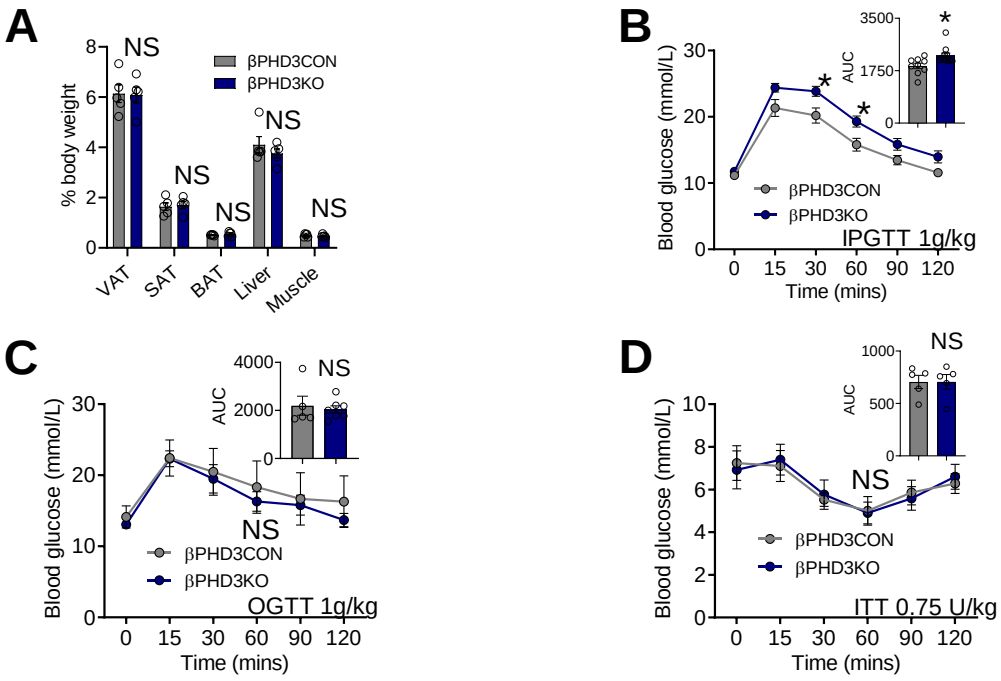

Figure 5.2 *In vivo* phenotype of βPHD3KO at 8 weeks HFD: (**A**) The percentage of VAT, SAT, BAT, live and muscle relative to total body weight of βPHD3KO does not differ from βPHD3CON animals at 8 weeks of HFD (n = 5 animals/genotype; 2-way ANOVA, Sidak's test). (**B**) Glucose tolerance and AUC during IPGTT (1 g/kg glucose administered) are augmented in βPHD3KO mice after 8 weeks of HFD (n = 9-11 animals/genotype; IPGTT: 2-way RM ANOVA, Sidak's test; AUC: unpaired *t*-test). (**C**) Glucose tolerance and AUC during OGTT (1 g/kg glucose administered) are unchanged in βPHD3KO 8 weeks HFD mice (n = 6-7 animals/genotype; OGTT: 2-way RM ANOVA, Sidak's test; AUC: unpaired *t*-test). (**D**) Insulin sensitivity and AUC during ITT (0.75U/kg insulin administered) are similar in βPHD3KO and βPHD3CON 8 weeks HFD mice (n = 5 animals/genotype, ITT: 2-way RM ANOVA; Sidak's test; AUC: unpaired *t*-test). Bar graphs (scatter plot) and line graphs show mean ± SEM.

5.2.3 In vitro functionality is impaired in βPHD3KO islets at 8 weeks of HFD

In contrast to the phenotype described at 4 weeks of HFD, islets from βPHD3KO mice fed a HFD for 8 weeks displayed impaired GSIS **(Figure 5.3A)**. However, potentiation with Ex4 was able to rescue this deficit in insulin secretion in βPHD3KO islets **(Figure 5.3A)**, while insulin content remained unchanged **(Figure 5.3B)**. Upstream of insulin secretion, Ca^{2+} fluxes in response to both glucose and KCl were blunted in βPHD3KO islets *versus* controls **(Figure 5.3C, D)**.

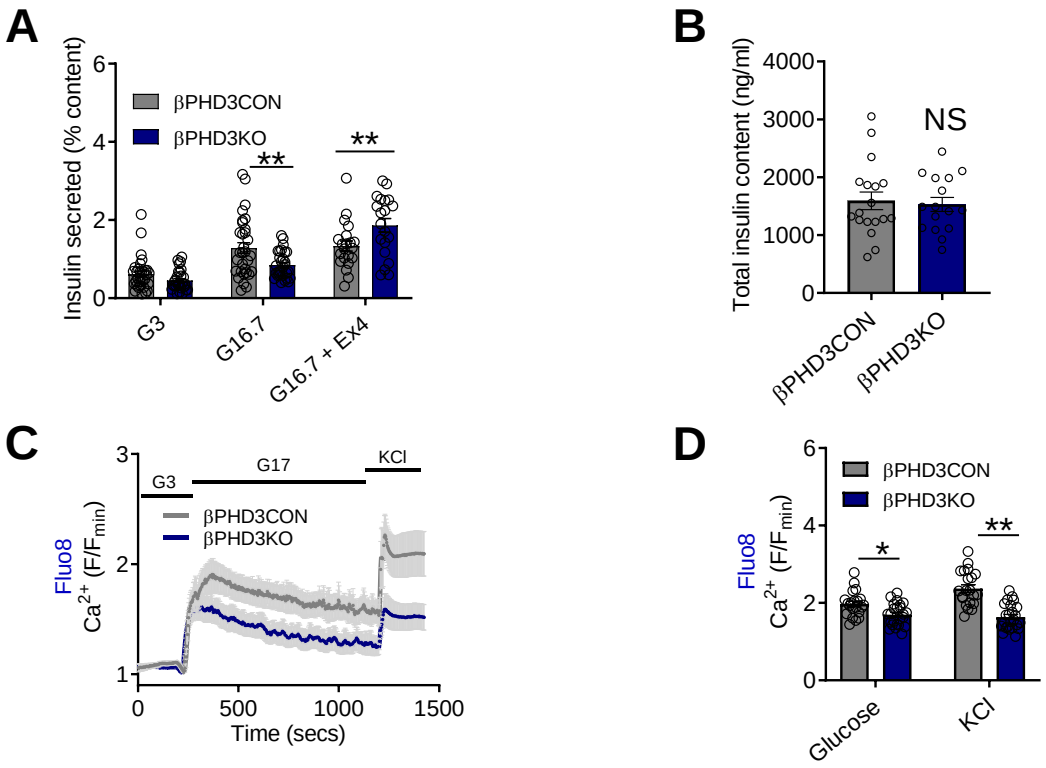

Figure 5.3 *In vitro* phenotype of βPHD3KO at 8 weeks HFD: (**A**) G16.7-stimulated insulin secretion is significantly lower in βPHD3KO after 8 weeks of HFD, but stimulation with 20 nM Ex4 can rescue insulin secretion to a level higher than βPHD3CON (n = 29-32 replicates, 4 animals/genotype; 2-way ANOVA, Sidak's test). (**B**) Total insulin content extracted from βPHD3KO and βPHD3CON islets is similar at 8 weeks HFD (16-18 replicates, 4 animals/genotype; unpaired *t*-test). (**C** and **D**) After 8 weeks of HFD, in βPHD3KO islets, Ca^{2+} rises measured with Fluo8 are decreased in response to 17 mM glucose and 10 mM KCl, as shown by (**C**) mean traces and (**D**) summary bar graph (n = 21-24 islets/genotype, 2 animals/genotype; 2-way ANOVA, Sidak's test). Bar graphs (scatter plot) and line graphs show mean ± SEM.

5.2.4 β-cells encounter failure in βPHD3KO mice at 8 weeks of HFD

In this context of generalized impairment, common hallmarks of β-cell failure such as proliferation, α-cell/β-cell ratio, apoptosis, ER stress and β-cell mass, were assessed. Thus, proliferating cell nuclear antigen (PCNA) staining of βPHD3KO was found to be similar to that of βPHD3CON **(Figure 5.4A)**. Likewise, the α-cell/β-cell ratio was not affected by the loss of PHD3 in the β-cell after 8 weeks of HFD **(Figure 5.4B)**. In line with the onset of β-cell failure, the rate of apoptosis, as assessed by TUNEL staining, was found to be significantly higher in βPHD3KO than in βPHD3CON **(Figure 5.4C)**. However, this was not accompanied by changes in the mRNA expression of the lipotoxic ER stress markers *Ddit3*, *Hspa5* and *Xbp1* **(Figure 5.4D)**. Despite proliferation not being increased relative to apoptosis, at 8 weeks of HFD, the β-cell mass of βPHD3KO islets was increased *versus* the controls **(Figure 5.4E)**. Moreover, βPHD3KO mice were found to have a significantly higher proportion of bigger islets, compared to βPHD3CON mice, after 8 weeks of HFD **(Figure 5.4F)**. Taken together these data suggest that either apoptosis at 8 weeks has not yet countered a previous increase of β-cell mass or apoptosis is limited to small and medium islets.

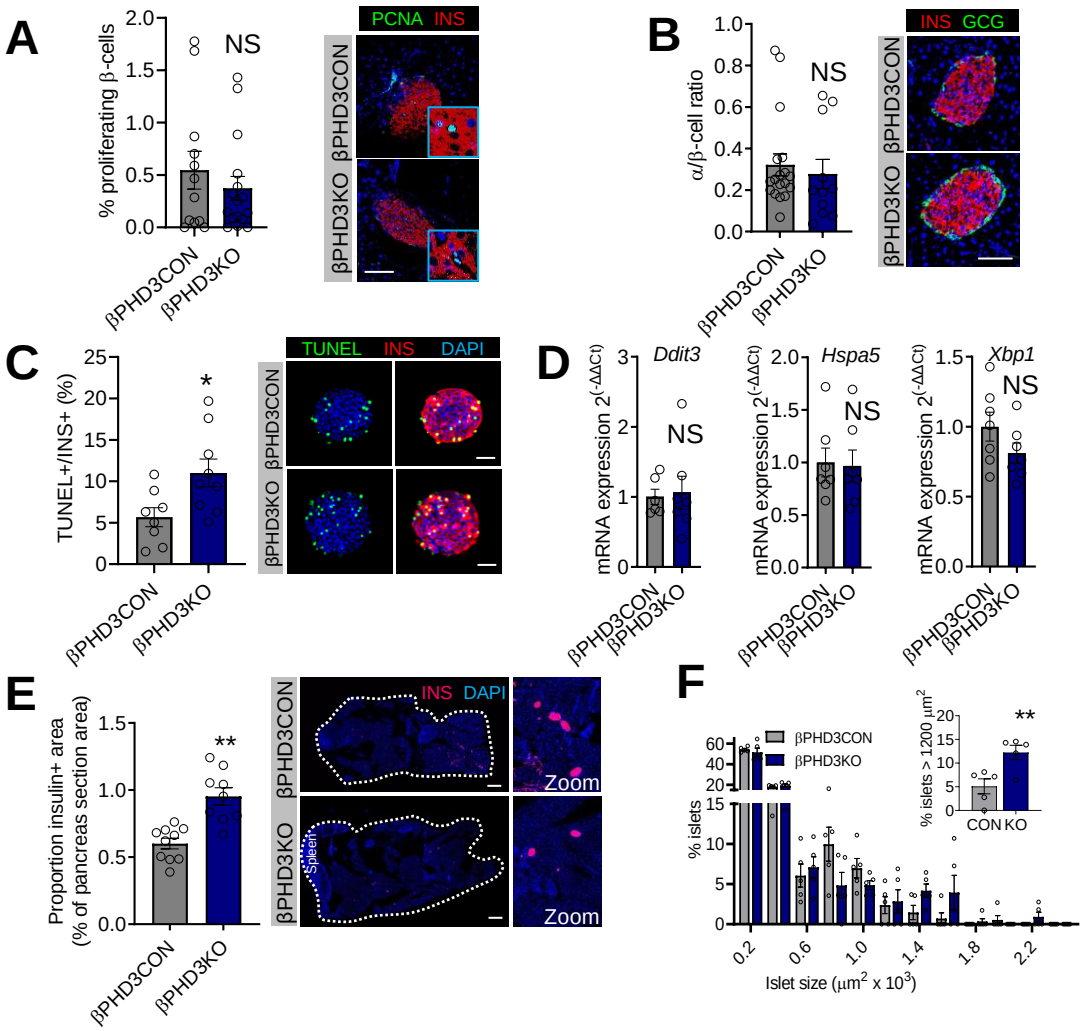

Figure 5.4 β-cell failure in βPHD3KO at 8 weeks HFD: (**A** and **B**) At 8 weeks of HFD (**A**) the percentage of proliferating (PCNA+) β-cells, stained with anti-insulin (red) and anti-PCNA (green) antibodies, is similar in βPHD3KO and βPHD3CON islets of paraffin-embedded pancreas sections (representative image of individual islets included, n = 12-17 islets, 3-4 animals/genotype; unpaired *t*-test). (**B**) Glucagon (green) and insulin (red) staining of islets of pancreatic slices reveals that the α-cell/β-cell ratio of βPHD3KO and βPHD3CON is similar (representative image of individual islets included, n = 11-18 islets, 3-4 animals/genotype; unpaired *t*-test). (**C**) TUNEL (green) and insulin (red) staining show a higher portion of apoptosis in βPHD3KO islets isolated and fixed after 8 weeks of HFD (representative image of individual islets included, n = 8-9 islets/genotype; unpaired *t*-test). (**D**) The mRNA levels of the ER stress markers *Ddit3*, *Hspa5* and *Xbp1* are unchanged in βPHD3KO 8 weeks HFD islets relative to βPHD3CON (n = 6-7 animals/genotype; unpaired *t*-test). (**E** and **F**) Bar graph and representative image (scale bar: 530 μm; inset is 5.25 × original magnification) show increased (**E**) β-cell mass, as assessed by insulin (red) staining in entire pancreatic sections, and (**F**) islet size distribution in βPHD3KO after 8 weeks of HFD (n = 3 animals/genotype, 2-way ANOVA; unpaired *t*-test). Bar graphs (scatter plot) and line graphs show mean ± SEM.

5.3 Discussion

In the present chapter, the effects of 8 weeks of HFD on the metabolic adaptations identified in βPHD3KO mice are presented. As for SC and 4 weeks of HFD the involvement of hypoxic signaling was evaluated. Since PHD3 is known to hydroxylate HIF2α in some backgrounds (Pugh, 2016), and HIF2α regulates the response to chronic hypoxia including during metabolic stress (Feng et al., 2018; Y. Xie et al., 2019), the expression of HIF1α and HIF2α target genes was measured. *Ccnd1*, commonly upregulated by HIF2α, is the gene encoding for cyclin D1, involved in cell proliferation. Cyclin D1, as well as the other cyclins, makes a complex with cyclin-dependent kinases (CDKs) to promote the progression from G1 to S phase of the cell cycle, in response to external stimuli (Qie & Diehl, 2016). *Dll4*, on the other hand, is a key element of the Notch signaling pathway regulating cell proliferation, apoptosis, differentiation and angiogenesis. Dll4 is one of five Notch ligands, which by binding Notch1-4 primes the translocation of the Notch intracellular domain to the nucleus (Patel et al., 2005). Here the Notch intracellular domain interacts with the DNA-binding protein CSL making it a transcriptional activator of genes regulating the processes mentioned above (Liu, Fan, Wang, Zheng, & Lu, 2014). Depending on the cellular background, the expression of *Dll4* can be increased by either HIF1α or HIF2α (Diez et al., 2007; Jubb et al., 2009; Patel et al., 2005; Skuli et al., 2009).

While the expression of *Ccnd1* remained unchanged in βPHD3KO after 8 weeks of HFD, the mRNA levels of *Dll4* were significantly lower. This confirmed that, even after prolonged obesogenic stress, the effects of the loss of PHD3 in the β-cells are probably independent of the stabilization of HIF.

The macroscopic characterization of βPHD3KO mice after 8 weeks of HFD presented with very similar characteristics to those observed after 4 weeks of HFD. Indeed, after 8 weeks of HFD mice lacking PHD3 displayed glucose intolerance compared to controls. Also in line with the results at 4 weeks of HFD, body composition, insulin sensitivity and oral glucose tolerance were normal in βPHD3KO at 8 weeks of HFD.

While glucose intolerance was counterbalanced by improved insulin secretion at the onset of metabolic stress, the *in vitro* GSIS of βPHD3KO islets was significantly impaired after 8 weeks of HFD. However, consistent with the intact oral glucose tolerance, the application of Ex4 could rescue the insulin secretion in the βPHD3KO islets.

Further differentiating from earlier stages of HFD, 8 weeks HFD βPHD3KO islets displayed reduced Ca^{2+} responses to glucose and the depolarizing agent KCl. These data suggest that at 8 weeks of HFD, the VDCCs, which had increased sensitivity at 4 weeks of HFD, are defective.

To further investigate the effects of glucose intolerance and the overall impairment described so far, we focused on some characteristic features of β-cell failure. Thus, apoptosis, proliferation, ER stress, α-cell/β-cell ratio and β-cell mass were assessed. Further corroborating the defects found at 8 weeks of HFD, the rate of apoptosis was found to be higher in βPHD3KO than βPHD3CON. However, the expression of ER stress markers was unaltered in βPHD3KO. Furthermore, glucose intolerance is generally associated to decreased β-cell mass, which is thought to result from imbalanced proliferation and apoptosis as well as from cell dedifferentiation or transdifferentiation (Fujita et al., 2018). However, the proliferation of PHD3KO β-cells,

as well as the α-cell/β-cell ratio, were normal suggesting that the β-cells are equally proliferative and are not transdifferentiating to α-cells. Moreover, the β-cell mass was increased and the βPHD3KO islets tended to be bigger in size than the βPHD3CON. These results were rather unexpected in islets undergoing apoptosis. However, they may be explained by a previous increase in the β-cell mass not being compensated yet by apoptotic rates at 8 weeks of HFD, or apoptosis being limited to islets of smaller dimensions.

In summary, animals and islets from 8 weeks of HFD were phenotyped. βPHD3KO displayed generalized failure, with glucose intolerance, impaired insulin secretion, defective Ca^{2+} signaling and increased apoptosis. The latter was not mirrored by increased expression of ER stress markers or decreased β-cell mass. Moreover, the proliferation rate and the α-cell/β-cell ratio were both unaltered after 8 weeks of HFD.

Noticeably, despite *in vitro* impairments, 8 weeks of HFD were associated with a milder *in vivo* phenotype, compared to 4 weeks of HFD. This might reflect a U-shaped response where β-cells might begin to rely on the use of fatty acid for improved responsiveness. However, it would be speculative to define whether the nature of the metabolic switch observed at 4 weeks of HFD has a protective function over the long term. Going forward, longer obesogenic feeding could help unveil this.

5.4 Conclusion

Although there are indications of a protective function mediated by metabolic adaptation caused by the lack of PHD3, animals and islets show numerous signs of impairment after 8 weeks of HFD. Therefore, the presence of PHD3 might be necessary to avoid β-cell decompensation and to ensure normal function after prolonged fatty acid excess. It is probable that the alternative mechanism, relying on β-oxidation, is overwhelmed at this time point. However, it is not possible to draw firm conclusions as to whether the nature of the metabolic switch is protective or maladaptive. To address this, the effects of glucose stimulation on insulin secretion *in vivo* and on the ATP/ADP ratio *in vitro*, as well as GLP1-R signaling should be studied. Furthermore, mapping of glucose metabolism after 8 weeks of HFD via isotopic tracing would be useful. Moreover, as for the other dietary conditions, the potential role of hypoxic signaling in the PHD3-mediated effect requires further investigation of HIF and HIF targets through WB. Most importantly, further extension of the HFD feeding to 12 or even 20 weeks would be necessary.

Nonetheless, the present study provides insights into the role of PHD3 in the glucose homeostasis of mice fed a HFD for 4 and 8 weeks, which are more reflective of pre-diabetes and early diabetes in humans (da Silva Xavier & Hodson, 2018). Therefore, it is important to investigate whether our results could translate to human islets. To do this, it is crucial to have a high-resolution representation of glucose handling within the human and mouse β-cells. Knowing where the similarities and differences stand, it will be possible to identify new potential mechanisms mediated by PHD3.

In the next chapter, the investigation of glucose fate through $^{13}C_6$ glucose tracing coupled to GC-MS and NMR in mouse *versus* human islets is described.

Chapter 6

GLUCOSE METABOLISM IN HUMAN ISLETS

Abstract

Background and aims

PHD3 was found to play a central role in mouse β-cells, where it maintains glucose metabolism during metabolic stress. To investigate whether our results could, in the future, extend to human islets, high-resolution mapping and comparison of glucose metabolism in wild-type CD1 mice and human islets were performed.

Materials and methods

$^{13}C_6$ glucose tracing coupled to GC-MS and high field 2D ^{1}H-^{13}C HSQC NMR was employed to investigate glucose handling in human and CD1 mouse islets.

Results

The contribution of glucose to the TCA cycle is similar in islets from wild-type CD1 mice and non-diabetic human donors. However, the production of m+3 lactate is significantly increased in human compared to mouse islets. The isotopomers distribution suggests that pyruvate fueling of the TCA cycle is mainly mediated by the activity of PDH rather than PC, in human and mouse islets.

Discussion and Conclusion

Islets from both species depend on pyruvate flux through PDH, more than PC, to sustain the TCA cycle. Additionally, the direct conversion of pyruvate to lactate was significantly increased in human islets. These findings suggest that human islets might have the means to maintain the REDOX balance in case of increased β-oxidation similar to that shown in βPHD3KO on HFD. Thus, our data support the possibility of a role for PHD3 in the glucose homeostasis of human β-cells. More widely, the results point to key differences in β-cell glucose handling between rodent and human islets.

6.1 Introduction

In previous chapters, the effects of PHD3KO in pancreatic β-cells were described. While no phenotypic alterations occurred in mice fed a SC, HFD feeding led to metabolic rewiring and increased use of FAO to sustain insulin secretion, in βPHD3KO mice. This compensatory mechanism was associated with improved insulin secretion at 4 weeks of HFD. However, it caused overall impairment after 8 weeks of HFD. Thus, it was shown that PHD3 is pivotal in maintaining the appropriate glucose metabolism in β-cells derived from mice subjected to metabolic stress.

Translation of these results to human β-cells however remains difficult since chemical inhibitors of PHD3 are still under investigation for specificity and shRNA against *EGLN3* does not work well in our hands. Moreover, while glucose fate is well detailed in mouse β-cells, relatively little is known about human β-cell metabolism. Therefore, to investigate whether the results detailed in the previous chapters could extend to human β-cells, it is important to have a clear depiction of glucose fate in human and mouse islets.

In this chapter, the contribution of glucose to glycolysis and the TCA cycle, through the activity of PDH and PC is described in human islets. Although literature exists describing the use of $^{13}C_6$ glucose tracing combined with NMR spectroscopy to understand the metabolism of INS-1 derived cell lines (Alves et al., 2015; Cline, Lepine, Papas, Kibbey, & Shulman, 2004; Cline, Pongratz, Zhao, & Papas, 2011; Lu et al., 2002; Simpson, Khokhlova, Oca-Cossio, & Constantinidis, 2006), its application to primary mouse and human islets is novel. Tracing of non-diabetic human and wild-type CD1 mouse islets with $^{13}C_6$ glucose, combined with GC-MS and 2D ^{1}H-^{13}C HSQC NMR enabled us to decipher the accumulation of isotopologues and isotopomers

representative of specific pathways. Importantly, we used CD1 outbred mice to maximize genetic diversity, which is more reflective of the natural variability of human islets. Through comparison of the results in human and mouse islets, we sought to identify similarities and differences to evaluate the possibility of a role for PHD3 on the glucose homeostasis of human β-cells. More broadly, a roadmap is provided for glucose fate in human β-cells.

6.2 Results

6.2.1 Glucose contribution to TCA cycle is similar in human and mouse islets

To investigate glucose handling, human and CD1 mouse islets were incubated with 10 mM $^{13}C_6$ glucose prior to metabolite extraction and GC-MS. The incorporation of ^{13}C from $^{13}C_6$ glucose into the TCA cycle metabolites was established via MID analysis **(Figure 3.7)**. Suggesting a similar progression of the glycolysis and TCA cycle, glucose incorporation did not show differences in aspartate, glutamate, malate and fumarate between human and mouse islets **(Figure 6.1A-D)**. To gain a higher understanding of pyruvate management, its contribution to the production of alanine and lactate was assessed. While the MID for alanine was unchanged in humans *versus* mice **(Figure 6.1E)**, the accumulation of m+3 lactate was significantly higher in human than in mouse islets **(Figure 6.1F)**. Surprisingly, the accumulation of m+2 and m+3 lactate were similar within each species **(Figure 6.1F)**. In line with the higher number of cells composing human islets, the total amount of lactate was higher in human than in CD1 islets **(Figure 6.1G)**.

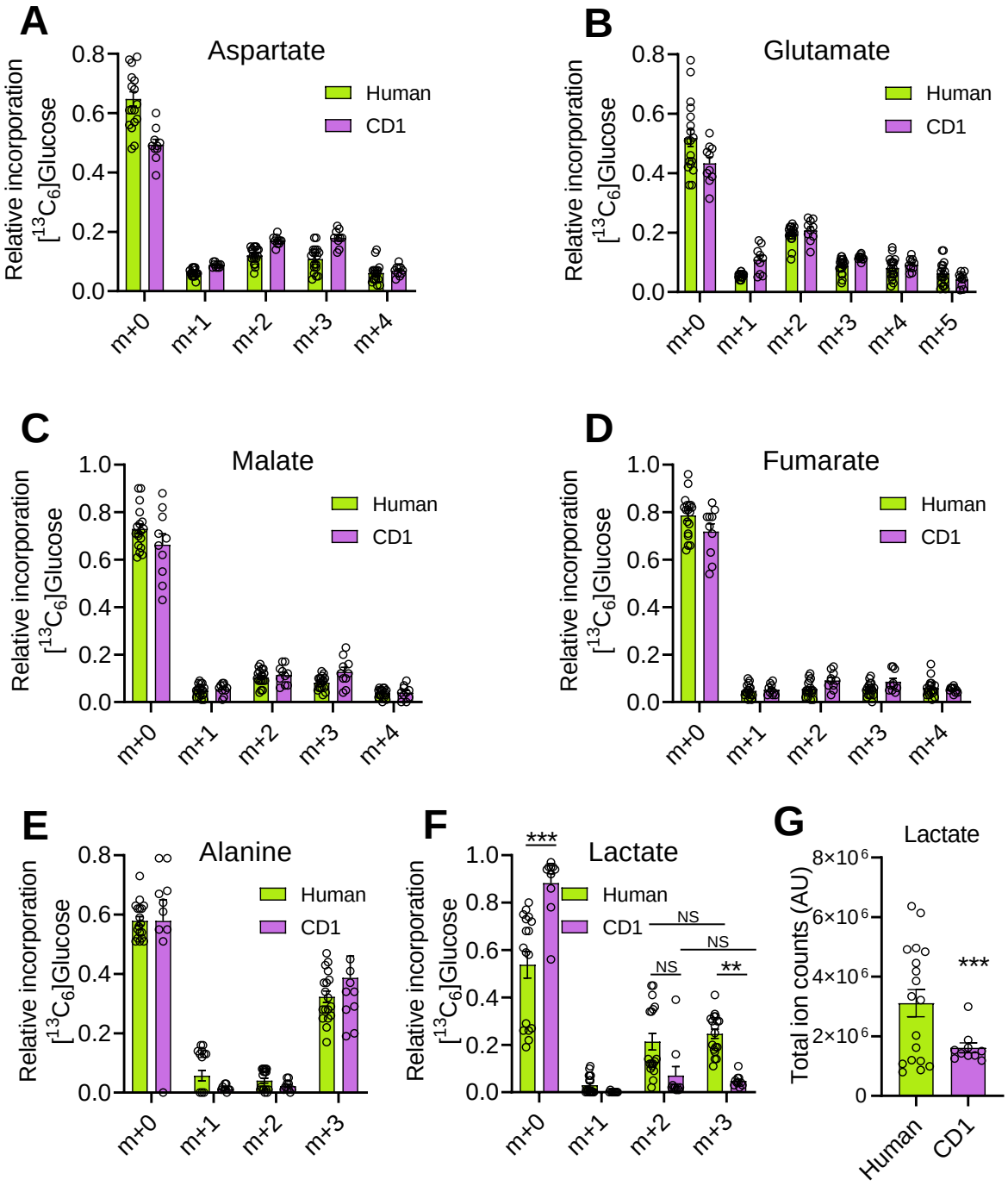

Figure 6.1 MID analysis of human and CD1 islets: MID showing similar incorporation of ^{13}C from $^{13}C_6$ glucose into (**A**) aspartate, (**B**) glutamate, (**C**) malate, (**D**) fumarate and (**E**) alanine of human and CD1 mouse islets. (**F**) The incorporation of ^{13}C into m+3 lactate is significantly decreased in CD1 compared to human islets. (**G**) The total amount of extracted lactate is significantly higher in human than in CD1 islets (n = 18 islet preparations, 9 human donors and n = 10 islet preparations, 15 animals; MID: 2-way ANOVA, Tukey's test; Total lactate: unpaired *t*-test). Bar graphs (scatter plot) show mean ± SEM. AU = arbitrary unit.

6.2.2 TCA cycle depends more on PDH than PC flux in human and mouse islets

Following $^{13}C_6$ glucose tracing, the combined analysis of the MID data from the GC-MS and the multiplet analysis from 2D ^{1}H-^{13}C HSQC NMR provides a useful tool to identify the isotopomer patterns. From uniformly labeled glucose, ^{13}C atoms are incorporated into the metabolites of the TCA cycle through the activity of PDH and PC. This leads to the formation of labeling patterns within the chemical structure of each metabolite that are specific to the pathway from which they are produced **(Figure 6.2A, B)**. Therefore, the positions of ^{13}C atoms within each metabolite can be utilized to elucidate the relative activities of PDH and PC.

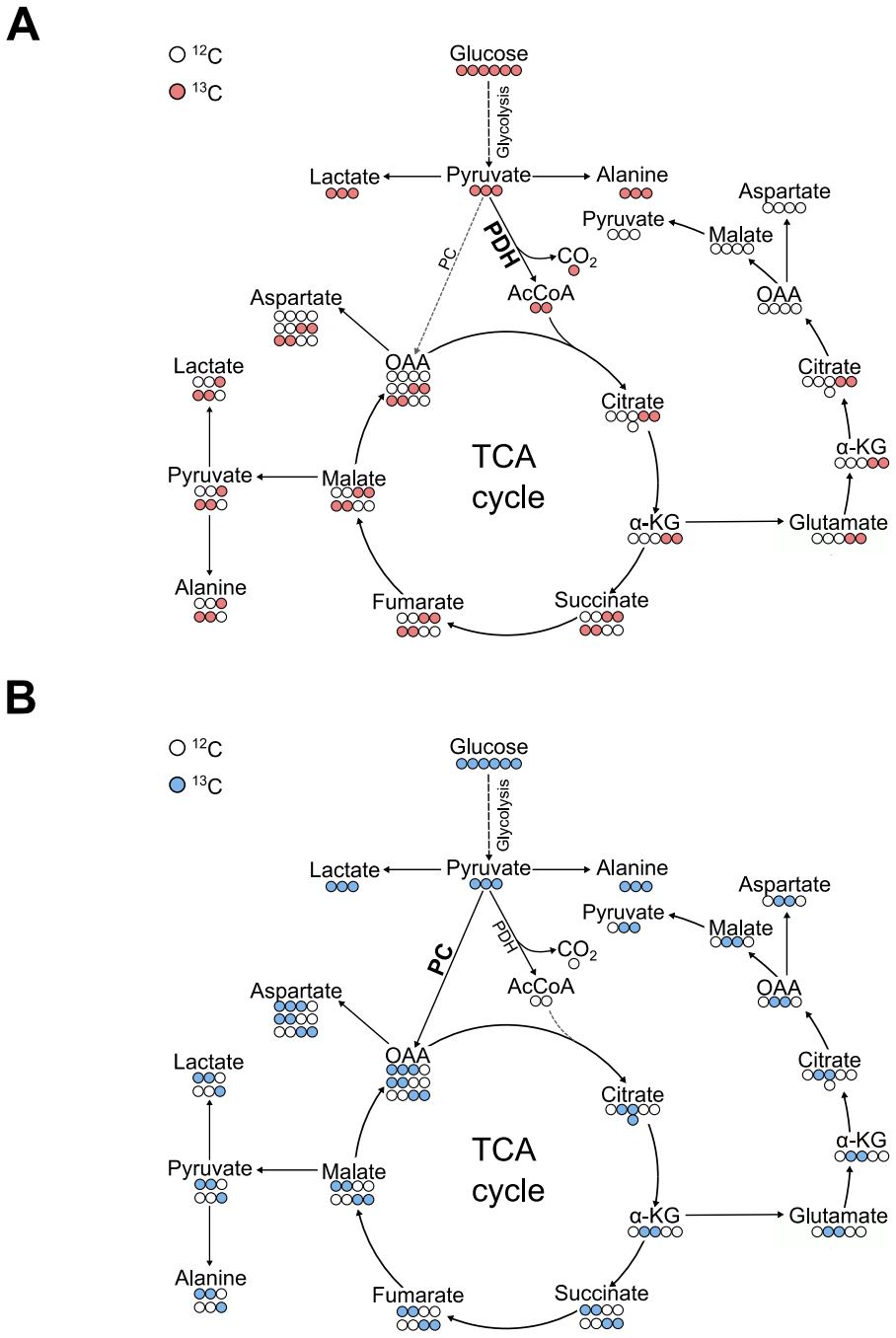

Figure 6.2 Schematics of the incorporation of ^{13}C from $^{13}C_6$ glucose into the TCA cycle metabolites through PDH and PC: The schematics show the contribution of $^{13}C_6$ glucose to the isotopomer patterns of the TCA cycle metabolites. (**A**) White and red circles respectively represent ^{12}C and ^{13}C atoms as incorporated from $^{13}C_6$ glucose into the TCA cycle through the activity of PDH converting pyruvate to acetyl-CoA. (**B**) White and blue circles are respectively used to show the incorporation of ^{12}C and ^{13}C into the TCA cycle metabolites arising from the PC-derived metabolization of pyruvate.

To define the different isotopomer patterns a numerical notation was used, where the numbers 0 and 1 indicate ^{12}C and ^{13}C atoms, respectively. Confirming the MID data, the accumulation of lactate$_{111}$ (i.e. fully labeled lactate) was significantly higher in human than in CD1 mouse islets **(Figure 6.3A)**. Moreover, both in human and mouse islets the greater contribution to the pool of m+2 isotopologues was found to derive from the accumulation of lactate$_{110}$ **(Figure 6.3A)**. This suggested that lactate is produced following the oxidative TCA cycle rather than the reductive metabolism of PC-derived glutamate, from which pyruvate$_{011}$ and then lactate$_{011}$ would arise **(Figure 6.2A, B)**. Interestingly, the majority of alanine was either 000 or 111, with only a very minor contribution to the other isotopomers **(Figure 6.3B)**. Thus, the labeled portion of alanine is produced from pyruvate upstream of the TCA cycle, suggesting that the accumulation of pyruvate$_{110}$ from malate$_{1100}$ is mostly employed in the regeneration of lactate$_{110}$ **(Figure 6.2A)**. Finally, the contribution of $^{13}C_6$ glucose to the labeling patterns of glutamate was similar in humans and mice **(Figure 6.3C)**. In the islets from both species, the most abundant labeled isotopomer was glutamate$_{00011}$ **(Figure 6.3C)**, deriving from TCA cycle flux through the activity of PDH **(Figure 6.2A)**.

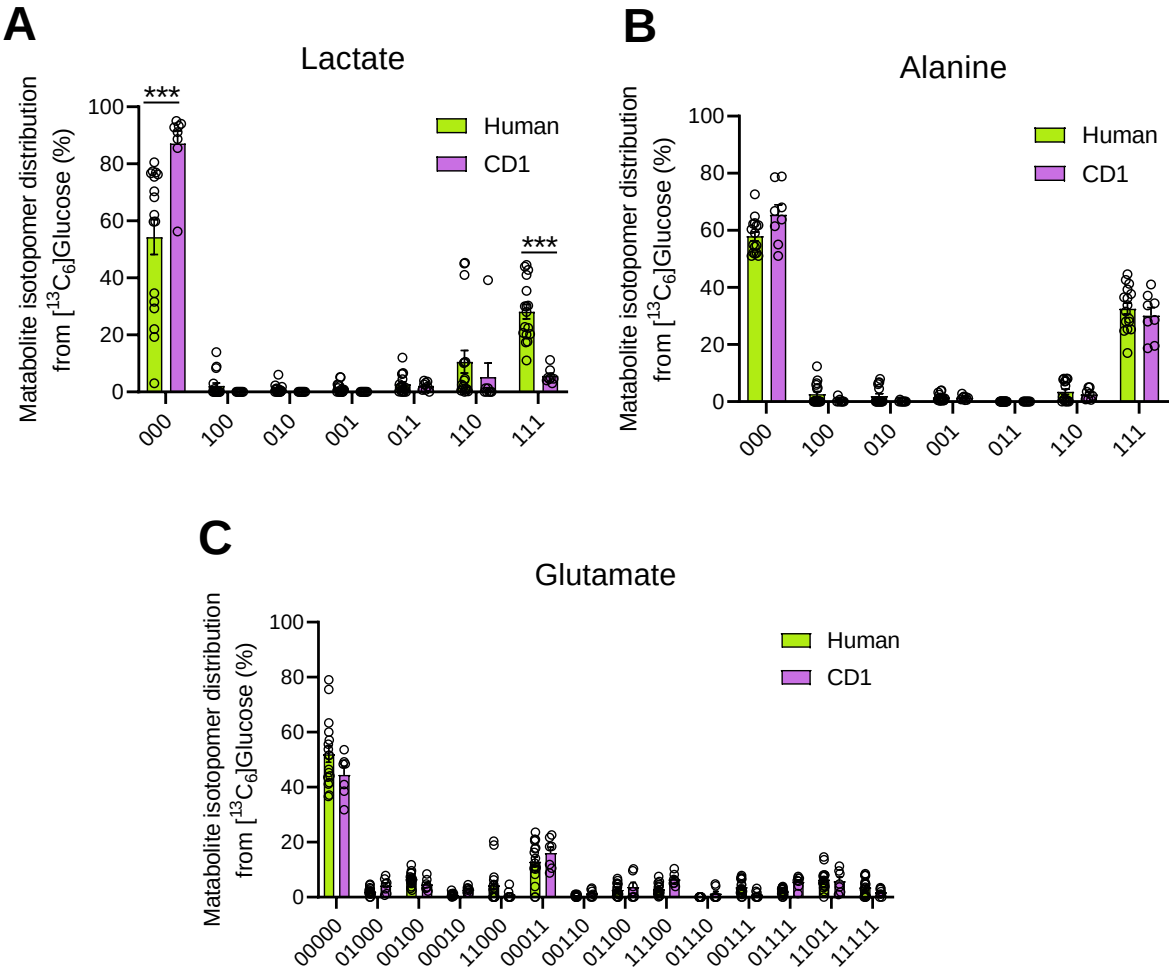

Figure 6.3 Metabolites isotopomer distribution in human and CD1 islets: (**A**) $Lactate_{000}$, $lactate_{111}$ and $lactate_{110}$ are the most abundant isotopomers in both humans and mice. The incorporation of ^{13}C from $^{13}C_6$ glucose into $lactate_{111}$ is significantly higher in human than CD1 islets. (**B**) ^{13}C incorporation into alanine isotopomers is similar in human and CD1 islets, with $alanine_{111}$ being the most represented labeled isotopomer. (**C**) The distribution of labeling patterns for glutamate are similar in human and CD1 islets, with $glutamate_{00011}$ being the most abundant labeled isotopomer in both species. (n = 16-17 islet preparations, 9 human donors and n = 7-8 islet preparations, 12-15 animals; 2-way ANOVA, Tukey's test). Bar graphs (scatter plot) show mean ± SEM.

6.3 Discussion

The overall aim of this chapter was to present the metabolic similarities and differences between non-diabetic human and wild-type CD1 mouse islets. Through $^{13}C_6$ glucose labeling coupled to GC-MS and NMR spectroscopy, we were able to gain a high-resolution map of glucose metabolism within human and mouse islets.

The MID analysis of the GC-MS data enabled us to evaluate the accumulation of different isotopologues formed by glucose contribution to the TCA cycle. Suggesting a similar rate of TCA cycle between human and mouse islet, the accumulation of the various isotopologues of aspartate, glutamate, malate, fumarate and alanine was comparable between the two species. However, the MID for lactate showed that humans, as well as mice, accumulate similar levels of m+3 and m+2 in their islets. As previously mentioned, m+2 lactate is produced downstream of the TCA cycle, whereas m+3 lactate is produced as a consequence of the direct conversion of pyruvate via LDHA. Therefore, the similar accumulation of m+2 and m+3 lactate suggested that the two pathways contributed to the same extent to the overall production of lactate. These findings were unexpected as they are in contrast with previous data showing that the expression of *Ldha* is disallowed in β-cells (Pullen & Rutter, 2013; Schuit et al., 2012). It is interesting to notice that glucotoxicity might induce the upregulation of disallowed genes in β-cells (Bensellam, Jonas, & Laybutt, 2018). This might partially explain the increased activity of LDHA in human islets, which were cultured at slightly supraphysiological glucose concentrations. However, it is unlikely that the accumulation of m+3 lactate in mouse islets was due to 24 h culture with 10 mM $^{13}C_6$ glucose. It is possible that other cell types within the islets, such as α-cells, are contributing to the accumulation of lactate. In particular, human α-cells account for

about 35% of the entire islet and express *LDHA* six times more than β-cells (Moin et al., 2020; Sanchez et al., 2021). However, lactate enters the α-cells through MCT, whereas the expression of MCT is disallowed in β-cells (Pullen & Rutter, 2013; Schuit et al., 2012; Zaborska et al., 2020). Since the culture medium used for $^{13}C_6$ tracing did not contain lactate in its formulation, it is unlikely that MCT, hence α-cells, made a large contribution to the overall lactate accumulation. Moreover, while the total amount of lactate was only doubled in humans compared to mice, the m+3 lactate accumulation was five-fold higher in human *versus* CD1 islets. Taken together these data suggest that although there might be a contribution from α-cells, this is unlikely to account for the whole m+3 lactate increase observed.

The end product of glycolysis, pyruvate, can enter the TCA cycle either being decarboxylated by PDH to form acetyl-CoA or being carboxylated to produce oxaloacetate. Therefore, to further investigate the glucose handling within human and mouse islets, the relative contribution of PDH and PC to the TCA cycle were assayed. To do this, the isotopomers patterns of lactate, alanine and glutamate derived from $^{13}C_6$ glucose, were observed. The incorporation of ^{13}C into specific positions within the molecules is assayed by multiplet analysis. Each ^{13}C binding to one or more ^{1}H within the chemical structure of a metabolite can provide labeling information about itself and the adjacent carbons. Indeed, the presence of functional groups on the neighboring carbons dictates the J-coupling, causing the splitting of the multiplet. The percentage of contribution of each multiplet is representative of the relative flux through PDH or PC. By integration of the multiplet analysis with the abundance of isotopologues obtained from MID, it is possible to determine the isotopomers distribution.

In accordance with the MID data, the multiplet analysis showed an increased direct conversion of pyruvate to lactate in human *versus* CD1 islets, as indicated by the significantly higher accumulation of lactate$_{111}$. Moreover, both humans and mice displayed a greater accumulation of lactate$_{110}$, rather than lactate$_{011}$. While the accumulation of lactate$_{110}$ is indistinguishable in PDH- and PC-mediated TCA cycle, the 011 isotopomer could only derive from the reductive metabolism of PC-derived glutamate **(Figure 6.2A, B)**. Thus, although indirectly, this provided a first indication of increased flux through PDH in islets from both species. Further corroborating this, in human and CD1 islets, the major glutamate isotopomer derived from exogenous $^{13}C_6$ glucose was glutamate$_{00011}$. Although glutamate is not a TCA cycle metabolite, it is in rapid exchange with α-KG and can be used as a read-out of TCA cycle flux through PDH or PC. Consequently, the accumulation of glutamate$_{00011}$ provided direct evidence of a higher reliance of the TCA cycle on the activity of PDH, rather than PC **(Figure 6.2A, B)**.

Although PC and PDH are thought to contribute equally to the TCA cycle in β-cells (Alves et al., 2015; Cline et al., 2004; Cline et al., 2011; Simpson et al., 2006), previous works, in several clones of INS-1 cells, showed that high glucose concentrations are associated with increased PDH activity (Lu et al., 2002). Therefore, it is likely that the greater contribution of PDH to the TCA cycle showed here is reflective of the relatively high concentration of glucose used in our studies.

While studies in INS-1 cells showed that increased rates of PDH flux do not have a direct effect on glucose responsiveness (Lu et al., 2002), the activity of PDH is linked to the accumulation of malate$_{1100}$. The latter contributing to the malate-pyruvate cycle leads to the production of pyruvate$_{110}$ which can be utilized to regenerate lactate$_{110}$.

Additionally, the alanine isotopomers distribution showed almost exclusively the accumulation of alanine$_{000}$ and alanine$_{111}$, suggesting that the pyruvate accumulated downstream of the TCA cycle is mostly employed in the production of lactate$_{110}$. The conversion of pyruvate to lactate is associated with the generation of cytosolic NAD^+. Thus, the higher levels of lactate$_{111}$ in humans, as well as the increased reliance on PDH in both humans and mice, might provide the oxidizing agents to balance the activity of NADH-producing pathways.

As discussed in previous chapters, in mice on HFD, the β-cell specific lack of PHD3 is associated with an increased rate of the β-oxidation of fatty acids. The latter leads to the production of NADH and it is likely counterbalanced by the NAD^+ deriving from the conversion of pyruvate to lactate. Based on the findings detailed in this chapter, the metabolism of glucose in human islets might have the potential to sustain a similar shift towards β-oxidation. It is, therefore, possible that our results in mice could translate to human islets. Going forward, experiments employing novel PHD3 inhibitors, such as salidroside or pyrithione Zn (Na, Woo, Kim, & Yang, 2016; Zhang et al., 2017), could help to identify a role for PHD3 on the glucose homeostasis of human β-cells.

To summarize, islets from human donors and wild-type CD1 mice were labeled with $^{13}C_6$ glucose and their metabolism was analyzed via GC-MS and 2D ^{1}H-^{13}C HSQC NMR. From the combination of the MID and multiplet analyses, an overall similar contribution to glycolysis and TCA cycle was found in humans and mice. Furthermore, the isotopomers distribution suggested that in islets from both humans and mice the relative activity of PDH is higher than that of PC. Importantly, the production of fully labeled lactate was found to be significantly higher in human than in mouse islets. These results suggested that in human islets the pyruvate to lactate direct conversion

is increased providing a means by which NAD^+ could be accumulated. Thus, it was inferred that future experiments to influence PHD3 expression levels might unveil a role for PHD3 on the glucose metabolism of human β-cells similar to that described in mice on HFD.

6.4 Conclusion

The comparison of glucose fate in human and mouse islets provided indications of an increased dependency on TCA cycle through PDH in both humans and mice. This was accompanied by a significantly increased accumulation of fully labeled lactate in human islets, which encourages future experiments to assess the role of PHD3 in human β-cells.

However, the results presented here are only preliminary and would require further optimization. Although previous works employed a similar approach to the investigation of glucose metabolism (Alves et al., 2015; Cline et al., 2004; Cline et al., 2011; Lu et al., 2002; Simpson et al., 2006), these were restricted to immortalized INS-1 cell lines. The innovative use of primary mouse and human islets proposed in this study can more closely represent the metabolism of β-cells and islets *in vivo*. On the other hand, purified β-cells cannot be used for tracing experiments. Thus, the investigation of glucose fate in β-cells is inevitably confounded by the contribution of other cell types within the islets.

Sample processing through GC-MS and NMR remains difficult as large amounts of isolated islets are required to guarantee proper signal detection. Further complications arise from the variable number of cells composing each islet.

Moreover, the islets utilized in this study were obtained from non-diabetic human donors. However, due to the limited availability of samples within the timeframe of this project we combined male and female patients of various ages, ranging from healthy to high BMI **(Appendix 2)**. In the future, sex-, age- and/or BMI-dependent grouping would be necessary.

Chapter 7

DISCUSSION AND CONCLUSION

7.1 Discussion

7.1.1 Background and aims

Crucial for maintaining glucose homeostasis, β-cells reside within the islets of Langerhans of the endocrine pancreas and are responsible for insulin secretion in response to increased blood glucose levels (Campbell & Newgard, 2021; Kaestner et al., 2021). GSIS is a biphasic event, comprising of an acute phase and a sustained phase, induced by the triggering and amplifying pathways, respectively (Campbell & Newgard, 2021; Henquin, 2000). In the early postprandial phase, glucose is metabolized within the β-cells to produce ATP, leading to the closure of the K_{ATP} channels, membrane depolarization, opening of the VDCCs and insulin exocytosis (Campbell & Newgard, 2021). Alternatively, a recent study proposed an ADP privation model where the closure of K_{ATP} channels and membrane depolarization are initiated by the activity of PK, rather than oxidative phosphorylation. In this 2-model state, PK induces the switch of the mitochondrion from the synthetic to the oxidative state, to sustain the PEP cycle and oxidative phosphorylation, respectively (Lewandowski et al., 2020). The amplifying pathways rely on a variety of stimuli regulating insulin secretion independently of K_{ATP} channels (Bratanova-Tochkova et al., 2002). One of the pathways sustaining the second phase of insulin secretion is the anaplerotic metabolism of glycolytically-derived pyruvate in β-cells. This leads together with other metabolites to the accumulation of α-KG, resulting in insulin secretion (Vetterli et al., 2012; Zhang et al., 2021).

Importantly, α-KG is also an essential reducing co-factor of the PHDs, a family of hydroxylases working as oxygen sensors (Schofield & Ratcliffe, 2004). In addition to their extensive characterization as HIFα hydroxylases, several other substrates were

identified for PHDs and especially for PHD3 (Jaakkola & Rantanen, 2013; Strowitzki et al., 2019). Of note, PHD3 was shown to hydroxylate ACC2, thus preventing the β-oxidation of fatty acids in AML and skeletal muscle (German et al., 2016; Yoon et al., 2020). Studies also showed that PHD3 is central for glucose homeostasis in studies conducted on hepatocytes and the rat 832/13 cell line (Huang et al., 2016; Taniguchi et al., 2013; Yano et al., 2018). However, these studies did not investigate the role of PHD3 in primary pancreatic β-cells. To address this lack of information, data from chapters 3, 4 and 5 of this thesis were included in our published article 'Prolyl-4-hydroxylase 3 maintains β cell glucose metabolism during fatty acid excess in mice' (Nasteska, Cuozzo, et al., 2021). Additionally, during the course of this PhD project, a paper from collaborators was published providing further insights into the role of PHDs in the function of primary β-cells (Hoang et al., 2022) (See **Appendix 3** for the entire list of Author's publications).

The overall aim of the present thesis was to investigate the role of PHD3 in the primary β-cell glucose metabolism. We found that the α-KG-dependent PHD3 is crucial to maintain the appropriate glucose sensing during early stages of metabolic stress induced by fatty acid abundance, in mice. Moreover, through high-resolution mapping of glucose metabolism in human islets we found that our results are likely to translate in human β-cells. More broadly, we identified differences in glucose metabolism of human and mouse islets, which might need to be addressed going forward.

For this project, we used a Cre-LoxP system to generate a mouse model lacking PHD3 specifically in β-cells and subjected this to *in vivo* and *in vitro* phenotyping under SC, 4 and 8 weeks of HFD. Finally, to gain a more detailed understanding of glucose handling in human β-cells, we compared the metabolism of wild-type CD1 mice and

human islets through $^{13}C_6$ glucose tracing coupled to GC-MS and 2D ^{1}H-^{13}C HSQC NMR.

7.1.2 Lack of phenotype under SC

The importance of PHD3 in the regulation of GSIS was previously demonstrated in a study employing the PHD pan-inhibitor EDHB and siRNA for PHD1, PHD2 and PHD3 in the INS1-832/13 clonal rat β-cell line. While EDHB affected GSIS in a dose-dependent manner, the siRNA-mediated knockdown of each isoform highlighted a stronger role for PHD3 in nutrient-stimulated insulin release (Huang et al., 2016).

Furthermore, several publications described a role for HIF1α in the regulation of β-cells, where mild increases lead to improved glucose tolerance and severe hypoxia impairs GSIS, attenuating Ca^{2+} dynamics (Cantley et al., 2009; Cheng et al., 2010; Puri et al., 2009; Zehetner et al., 2008). Based on this, we initially investigated whether the effects of PHD3 on the β-cell glucose homeostasis might be mediated by the stabilization of HIF1α. Our results showed that the expression of HIF1α target genes, such as *Bnip3*, *Car9* and *Gls*, as well as Ca^{2+} fluxes were similar in βPHD3KO and βPHD3CON, suggesting a hypoxia-independent phenotype. This is consistent with previous reports identifying PHD2 as being the primary HIF1α hydroxylase (Berra et al., 2003; Bishop et al., 2008; Taniguchi et al., 2013; Tennant et al., 2009; Zehetner et al., 2008).

Following extensive characterization, our βPHD3KO mouse model did not show any specific phenotype when fed a SC. Growth curves, glucose tolerance and insulin sensitivity were identical in βPHD3KO mice and control littermates. Similarly, islet size

distribution, β-cell mass, Ca^{2+} dynamics, ATP/ADP ratios, glucose metabolism, GSIS and Ex4-potentiated insulin secretion were unchanged in islets from βPHD3KO mice. This was unlike the reduced GSIS resulting from the knockdown of PHD3 in 832/13 cells, as described previously by Huang, Paglialunga *et al.*(Huang et al., 2016). However, this was probably due to the lower threshold for glucose response of the cells compared to isolated islets (Hohmeier et al., 2000).

Introducing the possibility of an altered use of nutrients for insulin secretion, βPHD3KO islets that were starved of glucose for 3 h before being challenged with high glucose concentration, showed decreased GSIS. Indeed, under nutrient-limiting conditions, islets are known to rely less on glucose metabolism and more on fatty acids (Wortham & Sander, 2016). Based on this and previous studies describing the PHD3-mediated inhibition of FAO in AML and skeletal muscle (German et al., 2016; Yoon et al., 2020), we hypothesized that PHD3 could play a similar role in β-cells.

Since a SC contains a low proportion of fatty acids **(Appendix 1)**, the induction of metabolic stress in the form of HFD was needed to evaluate whether PHD3 is a gatekeeper of nutrient preference in β-cells. Indeed, the HFD provides the exogenous fatty acids necessary to investigate the effects of PHD3 on the β-oxidation of fatty acids in β-cells. Moreover, mice on HFD present with hyperglycemia due to impaired GK and GLUT2 activity, hyperinsulinemia resulting from insulin resistance and high basal insulin levels and hypertension (Cerf, 2007; da Silva Xavier & Hodson, 2018). Thus, the HFD is a useful model to simulate the progression of obesity and type 2 diabetes in humans (da Silva Xavier & Hodson, 2018).

7.1.3 Metabolic rewiring at 4 weeks of HFD

After 4 weeks on HFD, the characterization of mice and isolated islets revealed a HIF1-independent, PHD3-specific phenotype in β-cells. In line with the hypothesis of a role for PHD3 in the control of nutrient usage, after 4 weeks of HFD, βPHD3KO mice displayed glucose intolerance but secreted more insulin than controls. Moreover, through ^{14}C and $^{13}C_6$ glucose tracing, it was shown that glucose contribution to the TCA cycle and the *de novo* lipogenesis are reduced in βPHD3KO at this stage. Additionally, the increased accumulation of m+3 lactate instead of the m+2 isotopologue at 4 weeks of HFD indicated an increased direct conversion of pyruvate to lactate. This was not accompanied by significant changes in the mRNA levels of *Ldha*, the gene encoding for LDHA mediating the pyruvate to lactate conversion. However, the production of lactate from pyruvate is associated with increased production of NAD^+, which is compatible with increased β-oxidation producing NADH. Taken together, these data pointed towards increased use of fatty acids as fuel source to sustain insulin secretion in PHD3KO β-cells.

To confirm this, we exposed the islets to low concentration of palmitate for 48-72 h, observed the effects of the CPT1 inhibitor etomoxir and performed D31-palmitate tracing. Following prolonged exposure to low palmitate, glucose- and Ex4-stimulated insulin secretion were increased in βPHD3KO from 4 weeks of HFD. Although the expression of the gene encoding for the key β-oxidation enzyme *Cpt1a* was unchanged in βPHD3KO, treatment with etomoxir was able to rescue the glucose-stimulated ATP/ADP ratio. It should be acknowledged that high concentrations (200 μM) of etomoxir are known to have an off-target effect on complex I of the ETC, which is *per se* responsible for an overall reduction of ATP/ADP ratio (Yao et al., 2018). Although

we used 100 μM etomoxir, it is possible that the slightly lower ATP/ADP ratio observed in the treated compared to the untreated βPHD3CON is due to a mild off-target effect. Finally, providing direct evidence of the increased β-oxidation rate, the accumulation of $^{2}H_2O$ upon islets incubation with D31-palmitate was significantly augmented in βPHD3KO at 4 weeks of HFD. Thus, our data suggest that βPHD3KO is associated with increased FAO, while PHD3 is necessary to maintain the appropriate glucose sensing at the onset of metabolic stress. Indeed, when PHD3 is expressed in β-cells, glucose is metabolized to fuel the TCA cycle, leading to the generation of ATP, opening of the VDCCs and insulin secretion. Alternatively, when PHD3 is lacking in the β-cells, they rewire their metabolism to rely more heavily on the β-oxidation of fatty acids. At the same time, in βPHD3KO the glycolytic contribution to the TCA cycle is reduced, being redirected to the increased conversion of pyruvate to lactate, to maintain the REDOX status.

As mentioned earlier, previous studies demonstrated the ability of PHD3 to inhibit the β-oxidation of fatty acids in skeletal muscle and AML. In these settings, PHD3 was shown to hydroxylate and activate ACC2. The latter mediates the conversion of acetyl-CoA to malonyl-CoA, leading to the inhibition of CPT1 and suppression of the β-oxidation (German et al., 2016; Yoon et al., 2020). Therefore, we investigated the possibility of a similar mechanism in β-cells. Noticeably, ACC1 is thought to be the predominant isoform of acetyl-CoA carboxylase in β-cells (MacDonald et al., 2008; Ronnebaum et al., 2008). Although the mechanism of action is still under investigation, several studies showed that ACC1 is necessary for normal insulin secretion (Cantley et al., 2019; MacDonald et al., 2008; Roche et al., 1998; Roduit et al., 2004; Ronnebaum et al., 2008; Zhang & Kim, 1998). This is consistent with the expression

levels of *Acaca* (encoding for ACC1) being significantly higher than *Acacb* (encoding for ACC2) in βPHD3CON. However, while βPHD3KO islets displayed an increased rate of FAO, a recent study showed that the β-cell specific deletion of *Acaca* does not alter the oxidation of palmitate in mice (Cantley et al., 2019). This is in line with the general consensus that ACC2 regulates the β-oxidation of fatty acids, whereas ACC1 provides malonyl-CoA as substrate for FAS (Abu-Elheiga et al., 2000; Brownsey, Boone, Elliott, Kulpa, & Lee, 2006). Therefore, we examined human islets and isolated β-cells gene expression data sets and found that ACC2 (*ACACB*) is expressed at functional levels, similar to the β-cell transcription factor HNF1A (Akerman et al., 2021; Akerman et al., 2017; Blodgett et al., 2015; Hrvatin et al., 2014; Moran et al., 2012; Pasquali et al., 2014). This, together with the unchanged expression of *Acaca* and *Acacb* in βPHD3KO, is consistent with the possibility of a mechanism by which PHD3 inhibits β-oxidation, via hydroxylation of ACC2. Alternatively, PHD3 could hydroxylate ACC1 and support lipid synthesis as suggested by the ^{14}C glucose tracing data.

Importantly, a recent publication by Hoang *et al.* partially confirmed the phenotype described here, under SC. In particular, the decreased ATP/ADP ratio, the increased NAD^+ and the downregulation of *Acacb* in βPHD3KO are consistent with increased β-oxidation rates achieved through PHD3-mediated regulation of ACC2. The metabolic adaptations described by them are different from the lack of phenotype described from us under SC. However, this is likely dependent on the older age of mice and the different nutrient composition of their SC containing 10% fat *versus* ours with about 7% of lipids (Banks, Burney, & Robinson, 2008; Hoang et al., 2022) **(Appendix 1)**.

In light of this, we propose a mechanism by which PHD3 controls the nutrient preference of β-cells during early development of obesity (4 weeks of HFD), through

the hydroxylation of ACC2. Thus, when PHD3 is expressed, it hydroxylates and activates ACC2 to convert acetyl-CoA to malonyl-CoA. The latter, inhibiting CPT1, suppresses the β-oxidation of fatty acids, ensuring the correct use of glucose as primary energy source in β-cells. Conversely, the loss of PHD3 leads to increased FAO, which provides an alternative source of acetyl-CoA to sustain the TCA cycle for the production of ATP and insulin secretion. As a consequence, the glycolytic input to the TCA cycle is reduced and the end product of glycolysis, pyruvate, is converted to lactate to ensure REDOX balance.

To investigate whether the metabolic rewiring described for βPHD3KO at 4 weeks of HFD has a protective or maladaptive nature, longer exposure to HFD was needed.

7.1.4 Islet failure at 8 weeks of HFD

Extension of the HFD to 8 weeks was associated with generalized β-cell failure. While still independent of the stabilization of HIF1α or HIF2α, the βPHD3KO mouse model presented with glucose intolerance, defective VDCCs, reduced insulin secretion and increased apoptosis. To investigate the extent of the impairment caused by prolonged metabolic stress, common traits of β-cells failure, such as proliferation, ER stress, α-cell/β-cell ratio and β-cell mass were also assessed. Despite the increased rate of apoptosis, no lipotoxic ER stress response was detected in βPHD3KO. The progression of glucose intolerance is known to be linked to a reduction of β-cell mass, due to altered proliferation, apoptosis, transdifferentiation and dedifferentiation (Fujita et al., 2018). However, suggesting a lack of transdifferentiation, α-cell/β-cell ratio and β-cell proliferation were unaffected in βPHD3KO after 8 weeks of HFD. In addition,

β-cell mass and islet size were increased in βPHD3KO *versus* βPHD3CON at 8 weeks of HFD. These findings imply that, at this time point, either apoptotic rates had not been able to compensate for previous β-cell mass increase, or that apoptosis is limited to small and medium-sized islets.

Interestingly, the *in vivo* phenotype at 8 weeks of HFD was still characterized by impaired glucose tolerance, although less severe than at 4 weeks. This suggests that the metabolic rewiring described for βPHD3KO at 4 weeks of HFD might, in fact, exert a protective function. Such a compensatory mechanism may reflect a U-shaped response where β-cells might be on the pathway to improved responsiveness. On the other hand, by 8 weeks of HFD, βPHD3KO show profound *in vitro* impairment, indicating that the expression of PHD3 might be necessary to prevent β-cell decompensation. Therefore, in the future, the investigation of the effects of even longer exposure to HFD will be necessary.

Despite the need for further studies in mice, the data presented in this thesis highlight a key function for PHD3 in glucose metabolism of mouse β-cells. To evaluate whether these findings could translate to glucose metabolism of human β-cells, a high-resolution depiction of glucose handling in human compared to mouse islets was needed.

7.1.5 Glucose metabolism in human islets

For the investigation of glucose metabolism in human β-cells, a metabolomics approach combining $^{13}C_6$ glucose tracing with GC-MS and NMR spectroscopy in primary islets was used. This allowed us to elucidate the similarities and differences in

glucose contribution to glycolysis and TCA cycle between human and mouse islets. Furthermore, providing a higher resolution of pyruvate management within the islets, the multiplet analysis of the NMR data, combined with the MID from GC-MS, helped to discriminate the relative activities of PDH and PC.

For our studies, islets from non-diabetic human donors and wild-type CD1 mice were cultured for 24 h with 10 mM $^{13}C_6$ glucose, prior to metabolite extraction. Subsequently, the MID data from GC-MS were either analyzed individually or combined with the multiplet analysis of the 2D ^{1}H-^{13}C HSQC NMR spectra. Suggesting that glucose contribution to glycolysis and TCA cycle is similar in human and CD1 islets, the MID analyses of aspartate, glutamate, malate, fumarate and alanine did not show significant differences between species. Interestingly, the MID for lactate displayed a comparable accumulation of the m+2 and m+3 isotopologues in islets from either species. This implies that the rates of lactate production downstream of the TCA cycle or through direct conversion of pyruvate via LDHA are similar. While this is in contrast with *Ldha* being disallowed in β-cells (Pullen & Rutter, 2013; Schuit et al., 2012), we cannot exclude that other cell types within the islets are contributing to the accumulation of these isotopologues. For instance, human α-cells, which account for a larger percentage of the islet than mouse α-cells (Dolensek et al., 2015), are known to have a much higher expression of *LDHA* than β-cells (Sanchez et al., 2021). However, while the expression of the lactate and pyruvate carrier, MCT, is disallowed in β-cells, MCT activity is required for lactate entry in α-cells (Pullen & Rutter, 2013; Schuit et al., 2012; Zaborska et al., 2020). Due to the absence of lactate in the $^{13}C_6$ tracing medium, it is implied that MCT does not provide a major contribution to the accumulation of lactate. Furthermore, the total amount of lactate extracted from the

human islets was only two-fold higher than that obtained from mice, whereas the magnitude of the m+3 lactate accumulation in humans was five-fold to that of mice. Thus, it is inferred that α-cells are unlikely to be the sole responsible for the increased accumulation of m+3 displayed by human islets.

Suggesting an increased flux through PDH in both human and mouse islets, the isotopomers distribution of lactate and glutamate showed a greater accumulation of $lactate_{110}$ and $glutamate_{00011}$ than PC-derived isotopomers. Noticeably, the most abundant labeling patterns for alanine were $alanine_{000}$ and $alanine_{111}$. From this, it is implied that the incorporation of ^{13}C into alanine is restricted to the transamination of pyruvate upstream of the TCA cycle fueling. Thus, given the increased rate of PDH flux, the majority of pyruvate produced from the conversion of malate is employed in the generation of lactate. This was accompanied by a significantly increased level of $lactate_{111}$ (corresponding to m+3 lactate) in human than in mouse islets. Taken together, these data suggest that the production of lactate from pyruvate in human islets is associated with the production of NAD^+. This was similar to the phenotype observed for βPHD3KO at 4 weeks of HFD, suggesting that a similar increase of β-oxidation might be sustainable in human β-cells.

7.1.6 Future perspectives

In the present thesis, the role of PHD3 in glucose metabolism of primary β-cells is described. At the onset of metabolic stress, βPHD3KO mice rewired their metabolism to exploit the excess of fatty acids as an alternative source to sustain insulin secretion. However, βPHD3KO animals presented with glucose intolerance at both 4 and 8

weeks of HFD and by 8 weeks the loss of PHD3 led to severe β-cell failure. Thus, PHD3 is crucial to maintain the appropriate glucose metabolism machinery, and its loss results in β-cell failure in mice undergoing metabolic stress. Furthermore, preliminary data in human islets indicated that PHD3 might play a similar role in human β-cells.

Since 4 and 8 weeks of HFD are used to mirror the progression of obesity and the stages of pre-diabetes and early diabetes in humans (da Silva Xavier & Hodson, 2018), it is possible to speculate that reduced expression of β-cell PHD3 might contribute to pre-diabetes to diabetes progression in overweight or obese patients. Diabetes is an irreversible metabolic disorder, which according to the International Diabetes Federation in 2021 affected 536.6 million people worldwide (Sun et al., 2022). It is characterized by high blood glucose and can be diagnosed for fasting plasma glucose values equal or above 126 mg/dL, for 2-h plasma glucose level during a 75-g OGTT of 200 mg/dL or above, or for glycated hemoglobin levels of 6.5% or more (American Diabetes Association Professional Practice, 2022). On the other hand, pre-diabetes is a reversible condition defined as the time preceding the onset of diabetes during which blood glucose levels are higher than normal but lower than those indicated for the diagnosis of diabetes (Khan et al., 2019). The development of diabetes from pre-diabetes is associated with a number of risk factors, such as a sedentary activity, ageing, smoking, cardiovascular diseases, genetic predisposition and obesity (Beulens et al., 2019; Khan et al., 2019). Importantly, life style changes, dietary interventions, as well as treatments with metformin, thiazolidinediones, α-glucosidase inhibitors, GLP1-R agonists, GLP-1R/GIPR co-agonists, sodium-glucose cotransporter (SGLT) 2 inhibitors and drugs reducing the absorption of fats might revert the

pre-diabetic phenotype to avoid the later insurgence of diabetes (Beulens et al., 2019; Khan et al., 2019). Thus, it would be interesting to investigate a possible correlation between the levels of PHD3 in human β-cells and the various stages of obesity and diabetes progression. This could potentially lead to the development of therapeutic approaches to modulate the expression of PHD3 and consequently to control the development of diabetes, although one should be careful in extrapolating therapeutic targets based upon early stage discovery science.

There are a number of limitations to the work presented in this thesis that should be addressed going forward. Our data show that the β-cell specific knockout of PHD3 is not associated with major alterations of the hypoxic signaling in SC, 4 or 8 weeks of HFD. Similar to previous publications describing the role of PHD3 in the liver and in neurons, and consistent with PHD2 being the main HIF1α hydroxylase (Berra et al., 2003; Bishop et al., 2008; Taniguchi et al., 2013; Tennant et al., 2009; Zehetner et al., 2008), the HIF1α transcriptional signature was not altered in βPHD3KO. However, further analyses are required to guarantee the independence of the PHD3-associated phenotype from the hypoxic metabolism. In the future, the use of specific HIF1 and HIF2 inhibitors or the observation of βPHD3KO metabolism in a HIF1-null and HIF2-null background would be necessary.

The suggested pathway described in this manuscript for PHD3 to control the use of nutrients under HFD relies on the ability of PHD3 to hydroxylate ACC2 or ACC1. Following the analysis of data sets describing the expression of *ACACB* (ACC2), we found that it is expressed at functional levels in human islets and β-cells. Moreover, ACC2 was already shown to be hydroxylated and activated by PHD3 in other tissues (German et al., 2016; Yoon et al., 2020), making it a more likely target for the

mechanism described here. To confirm whether PHD3 acts through interaction with ACC1 or ACC2, immunoprecipitation via ACC1- and ACC2-specific antibodies could be employed. Subsequently, the hydroxylation of either isoforms could be assessed through immunoblotting with hydroxyproline antibodies. Alternatively, ACC1 and ACC2 inhibitors or β-cell specific ACC1 and ACC2 knockouts could be employed. However, the identification of the hydroxylation sites for either ACC2 or ACC1 remains crucial. High-resolution techniques such as MS could do this, albeit hampered by the assignment of false positives due to artifactual oxidation of the tryptic fragments (Cockman et al., 2019).

The data presented here indicate that the increased conversion of lactate from pyruvate observed in βPHD3KO islets after 4 weeks of HFD could be necessary to keep the REDOX balance. Indeed, the production of lactate from pyruvate is associated with the generation of NAD^+, which could counter the NADH deriving from the increased rate of β-oxidation. To test this, the colorimetric quantification of the $NADH/NAD^+$ ratio and its change in response to palmitate treatment of βPHD3KO and βPHD3CON islets could provide a useful tool.

The nature of the compensatory mechanism described at 4 weeks of HFD was investigated prolonging the duration of the HFD feeding to 8 weeks. Importantly, the effects of the HFD resemble the progression of obesity and diabetes, with 4 and 8 weeks of HFD mimicking the stages of pre-diabetes and early diabetes (da Silva Xavier & Hodson, 2018). Although our data infer the possibility of a protective function for the βPHD3KO metabolic rewiring by 8 weeks of HFD, these are not sufficient to exclude a maladaptive profile. Further extension of the HFD to 12 or even 20 weeks would be necessary. Moreover, by 8 weeks of HFD, β-cell proliferation and α-cell/β-cell ratio

were unchanged in βPHD3KO compared to βPHD3CON islets. This is suggestive of a lack of β-cell dedifferentiation or transdifferentiation. However, further studies employing β-cell specific lineage tracing models, such as B6;129S4-*Gt(ROSA)26Sor*$^{tm9(EGFP/Rpl10a)Amc}$/J, would be needed to confirm β-cell fate in βPHD3KO.

Another drawback to the HFD studies presented here is that they were limited to male mice. Suggesting that the PHD3-associated phenotype is sex-independent, the experiments under SC did not reveal any differences between male and female animals. However, such differences cannot be excluded in HFD and going forward the effects of βPHD3KO in female mice undergoing metabolic stress should be investigated. Furthermore, it would be interesting to investigate the role of PHD3 in β-cell glucose metabolism in different models of metabolic stress, such as *ob/ob* or *db/db* mice.

The metabolomics approach to the study of glucose metabolism in islets from human donors and CD1 mice provided a powerful tool to investigate the possibility to translate the results observed in mice to humans. Although the data suggested that PHD3 might in fact have a role in glucose homeostasis of human β-cells, these were only preliminary. Therefore, further replicas and technical optimization would be needed for future experiments. Importantly, due to the need for a high concentration of metabolites for accurate signal acquisition, increased numbers of islet preparations and animals/donors would be required. Furthermore, the current human data refer to nine non-diabetic human donors of different sexes, ages and BMI. Going forward, a larger sample size would allow us to analyze the metabolism of more homogenous groups and to identify possible differences among them.

Finally, to effectively investigate the role of PHD3 in glucose metabolism of primary human β-cells, treatments with novel PHD3-specific inhibitors, such as salidroside or pyrithione Zn (Na et al., 2016; Zhang et al., 2017), will be necessary. Alternatively, models of human β-cells such as the EndoC-βH1 cell line or human pluripotent stem cells (hPSCs) treated to direct their differentiation towards a β-cell fate, could be employed to study the role of PHD3 in human β-cell glucose metabolism. It should be noted however that EndoC-βH1 cells are a fetal phenotype and do not express many of the mature β-cell traits seen in primary cultures (Tsonkova et al., 2018). Likewise, β-like cells do not function analogously to primary cells (Johnson, 2016; Kushner, MacDonald, & Atkinson, 2014). Nonetheless, using a combination of approaches, including EndoC-βH1 cells, β-like cells and primary cells should generate more knowledge concerning the role of PHD3 in β cell dfifferentiation, metabolism and function.

7.2 Conclusion

To conclude, in this thesis, the investigation of the role of PHD3 on glucose metabolism of mouse and human β-cells is described. Taken together, the data presented here establish an important role for PHD3 in gating the nutrient preference of β-cells, during metabolic stress in mice. Indeed, after 4 weeks of HFD, the loss of PHD3 in β-cells resulted in a metabolic shift towards the use of fatty acids to sustain increased insulin secretion. However, this compensatory mechanism led to overall β-cell failure by 8 weeks of HFD. Thus, PHD3 has a central function in ensuring appropriate glucose metabolism in mouse β-cells, during fatty acid excess. Furthermore, a novel metabolomics approach was used to compare glucose metabolism of human and mouse primary islets. Through this, key differences in the production of lactate were highlighted, opening the way for future research of the role of PHD3 and, more generally, glucose metabolism in human β-cells.

LIST OF REFERENCES

Abu-Elheiga, L., Brinkley, W. R., Zhong, L., Chirala, S. S., Woldegiorgis, G., & Wakil, S. J. (2000). The subcellular localization of acetyl-CoA carboxylase 2. *Proc Natl Acad Sci U S A, 97*(4), 1444-1449. doi:10.1073/pnas.97.4.1444

Affourtit, C., Alberts, B., Barlow, J., Carre, J. E., & Wynne, A. G. (2018). Control of pancreatic beta-cell bioenergetics. *Biochem Soc Trans, 46*(3), 555-564. doi:10.1042/BST20170505

Akerman, I., Maestro, M. A., De Franco, E., Grau, V., Flanagan, S., Garcia-Hurtado, J., . . . Ferrer, J. (2021). Neonatal diabetes mutations disrupt a chromatin pioneering function that activates the human insulin gene. *Cell Rep, 35*(2), 108981. doi:10.1016/j.celrep.2021.108981

Akerman, I., Tu, Z., Beucher, A., Rolando, D. M. Y., Sauty-Colace, C., Benazra, M., . . . Ferrer, J. (2017). Human Pancreatic beta Cell lncRNAs Control Cell-Specific Regulatory Networks. *Cell Metab, 25*(2), 400-411. doi:10.1016/j.cmet.2016.11.016

Alves, T. C., Pongratz, R. L., Zhao, X., Yarborough, O., Sereda, S., Shirihai, O., . . . Kibbey, R. G. (2015). Integrated, Step-Wise, Mass-Isotopomeric Flux Analysis of the TCA Cycle. *Cell Metab, 22*(5), 936-947. doi:10.1016/j.cmet.2015.08.021

American Diabetes Association Professional Practice, C. (2022). 2. Classification and Diagnosis of Diabetes: Standards of Medical Care in Diabetes-2022. *Diabetes Care, 45*(Suppl 1), S17-S38. doi:10.2337/dc22-S002

Ardenkjaer-Larsen, J. H., Boebinger, G. S., Comment, A., Duckett, S., Edison, A. S., Engelke, F., . . . Frydman, L. (2015). Facing and Overcoming Sensitivity Challenges in Biomolecular NMR Spectroscopy. *Angew Chem Int Ed Engl, 54*(32), 9162-9185. doi:10.1002/anie.201410653

Avidor-Reiss, T., & Gopalakrishnan, J. (2013). Building a centriole. *Curr Opin Cell Biol, 25*(1), 72-77. doi:10.1016/j.ceb.2012.10.016

Baggio, L. L., & Drucker, D. J. (2007). Biology of incretins: GLP-1 and GIP. *Gastroenterology, 132*(6), 2131-2157. doi:10.1053/j.gastro.2007.03.054

Banks, W. A., Burney, B. O., & Robinson, S. M. (2008). Effects of triglycerides, obesity, and starvation on ghrelin transport across the blood-brain barrier. *Peptides, 29*(11), 2061-2065. doi:10.1016/j.peptides.2008.07.001

Barth, S., Edlich, F., Berchner-Pfannschmidt, U., Gneuss, S., Jahreis, G., Hasgall, P. A., . . . Camenisch, G. (2009). Hypoxia-inducible factor prolyl-4-hydroxylase PHD2 protein abundance depends on integral membrane anchoring of FKBP38. *J Biol Chem, 284*(34), 23046-23058. doi:10.1074/jbc.M109.032631

Barth, S., Nesper, J., Hasgall, P. A., Wirthner, R., Nytko, K. J., Edlich, F., . . . Camenisch, G. (2007). The peptidyl prolyl cis/trans isomerase FKBP38 determines hypoxia-inducible transcription factor prolyl-4-hydroxylase PHD2 protein stability. *Mol Cell Biol, 27*(10), 3758-3768. doi:10.1128/MCB.01324-06

Bastin, M., & Andreelli, F. (2019). Dual GIP-GLP1-Receptor Agonists In The Treatment Of Type 2 Diabetes: A Short Review On Emerging Data And Therapeutic Potential. *Diabetes Metab Syndr Obes, 12*, 1973-1985. doi:10.2147/DMSO.S191438

Baukrowitz, T., Schulte, U., Oliver, D., Herlitze, S., Krauter, T., Tucker, S. J., . . . Fakler, B. (1998). PIP2 and PIP as determinants for ATP inhibition of KATP channels. *Science, 282*(5391), 1141-1144. doi:10.1126/science.282.5391.1141

Bellot, G., Garcia-Medina, R., Gounon, P., Chiche, J., Roux, D., Pouyssegur, J., & Mazure, N. M. (2009). Hypoxia-induced autophagy is mediated through hypoxia-inducible factor induction of BNIP3 and BNIP3L via their BH3 domains. *Mol Cell Biol, 29*(10), 2570-2581. doi:10.1128/MCB.00166-09

Benner, C., van der Meulen, T., Caceres, E., Tigyi, K., Donaldson, C. J., & Huising, M. O. (2014). The transcriptional landscape of mouse beta cells compared to human beta cells reveals notable species differences in long non-coding RNA and protein-coding gene expression. *BMC Genomics, 15*, 620. doi:10.1186/1471-2164-15-620

Bensaad, K., Favaro, E., Lewis, C. A., Peck, B., Lord, S., Collins, J. M., . . . Harris, A. L. (2014). Fatty acid uptake and lipid storage induced by HIF-1alpha contribute to cell growth and survival after hypoxia-reoxygenation. *Cell Rep, 9*(1), 349-365. doi:10.1016/j.celrep.2014.08.056

Bensellam, M., Jonas, J. C., & Laybutt, D. R. (2018). Mechanisms of beta-cell dedifferentiation in diabetes: recent findings and future research directions. *J Endocrinol, 236*(2), R109-R143. doi:10.1530/JOE-17-0516

Berg, J., Hung, Y. P., & Yellen, G. (2009). A genetically encoded fluorescent reporter of ATP:ADP ratio. *Nat Methods, 6*(2), 161-166. doi:10.1038/nmeth.1288

Berra, E., Benizri, E., Ginouves, A., Volmat, V., Roux, D., & Pouyssegur, J. (2003). HIF prolyl-hydroxylase 2 is the key oxygen sensor setting low steady-state levels of HIF-1alpha in normoxia. *EMBO J, 22*(16), 4082-4090. doi:10.1093/emboj/cdg392

Beulens, J., Rutters, F., Ryden, L., Schnell, O., Mellbin, L., Hart, H. E., & Vos, R. C. (2019). Risk and management of pre-diabetes. *Eur J Prev Cardiol, 26*(2_suppl), 47-54. doi:10.1177/2047487319880041

Birkemeyer, C., Luedemann, A., Wagner, C., Erban, A., & Kopka, J. (2005). Metabolome analysis: the potential of in vivo labeling with stable isotopes for metabolite profiling. *Trends Biotechnol, 23*(1), 28-33. doi:10.1016/j.tibtech.2004.12.001

Bishop, T., Gallagher, D., Pascual, A., Lygate, C. A., de Bono, J. P., Nicholls, L. G., . . . Ratcliffe, P. J. (2008). Abnormal sympathoadrenal development and systemic hypotension in PHD3-/- mice. *Mol Cell Biol, 28*(10), 3386-3400. doi:10.1128/MCB.02041-07

Bligh, E. G., & Dyer, W. J. (1959). A rapid method of total lipid extraction and purification. *Can J Biochem Physiol, 37*(8), 911-917. doi:10.1139/o59-099

Blodgett, D. M., Nowosielska, A., Afik, S., Pechhold, S., Cura, A. J., Kennedy, N. J., . . . diIorio, P. (2015). Novel Observations From Next-Generation RNA Sequencing of Highly Purified Human Adult and Fetal Islet Cell Subsets. *Diabetes, 64*(9), 3172-3181. doi:10.2337/db15-0039

Boulahbel, H., Duran, R. V., & Gottlieb, E. (2009). Prolyl hydroxylases as regulators of cell metabolism. *Biochem Soc Trans, 37*(Pt 1), 291-294. doi:10.1042/BST0370291

Bratanova-Tochkova, T. K., Cheng, H., Daniel, S., Gunawardana, S., Liu, Y. J., Mulvaney-Musa, J., . . . Sharp, G. W. (2002). Triggering and augmentation

mechanisms, granule pools, and biphasic insulin secretion. *Diabetes, 51 Suppl 1*, S83-90. doi:10.2337/diabetes.51.2007.s83

Brownsey, R. W., Boone, A. N., Elliott, J. E., Kulpa, J. E., & Lee, W. M. (2006). Regulation of acetyl-CoA carboxylase. *Biochem Soc Trans, 34*(Pt 2), 223-227. doi:10.1042/BST20060223

Bruick, R. K. (2003). Oxygen sensing in the hypoxic response pathway: regulation of the hypoxia-inducible transcription factor. *Genes Dev, 17*(21), 2614-2623. doi:10.1101/gad.1145503

Bruick, R. K., & McKnight, S. L. (2001). A conserved family of prolyl-4-hydroxylases that modify HIF. *Science, 294*(5545), 1337-1340. doi:10.1126/science.1066373

Campbell, J. E., & Drucker, D. J. (2013). Pharmacology, physiology, and mechanisms of incretin hormone action. *Cell Metab, 17*(6), 819-837. doi:10.1016/j.cmet.2013.04.008

Campbell, J. E., & Newgard, C. B. (2021). Mechanisms controlling pancreatic islet cell function in insulin secretion. *Nat Rev Mol Cell Biol, 22*(2), 142-158. doi:10.1038/s41580-020-00317-7

Cantley, J., Davenport, A., Vetterli, L., Nemes, N. J., Whitworth, P. T., Boslem, E., . . . Biden, T. J. (2019). Disruption of beta cell acetyl-CoA carboxylase-1 in mice impairs insulin secretion and beta cell mass. *Diabetologia, 62*(1), 99-111. doi:10.1007/s00125-018-4743-7

Cantley, J., Selman, C., Shukla, D., Abramov, A. Y., Forstreuter, F., Esteban, M. A., . . . Withers, D. J. (2009). Deletion of the von Hippel-Lindau gene in pancreatic beta cells impairs glucose homeostasis in mice. *J Clin Invest, 119*(1), 125-135. doi:10.1172/JCI26934

Cavadas, M. A., Mesnieres, M., Crifo, B., Manresa, M. C., Selfridge, A. C., Keogh, C. E., . . . Cheong, A. (2016). REST is a hypoxia-responsive transcriptional repressor. *Sci Rep, 6*, 31355. doi:10.1038/srep31355

Cerf, M. E. (2007). High fat diet modulation of glucose sensing in the beta-cell. *Med Sci Monit, 13*(1), Ra12-17.

Chen, N., Rinner, O., Czernik, D., Nytko, K. J., Zheng, D., Stiehl, D. P., . . . Frei, C. (2011). The oxygen sensor PHD3 limits glycolysis under hypoxia via direct binding to pyruvate kinase. *Cell Res, 21*(6), 983-986. doi:10.1038/cr.2011.66

Cheng, K., Ho, K., Stokes, R., Scott, C., Lau, S. M., Hawthorne, W. J., . . . Gunton, J. E. (2010). Hypoxia-inducible factor-1alpha regulates beta cell function in mouse and human islets. *J Clin Invest, 120*(6), 2171-2183. doi:10.1172/JCI35846

Chia, C. W., & Egan, J. M. (2020). Incretins in obesity and diabetes. *Ann N Y Acad Sci, 1461*(1), 104-126. doi:10.1111/nyas.14211

Christensen, A. A., & Gannon, M. (2019). The Beta Cell in Type 2 Diabetes. *Curr Diab Rep, 19*(9), 81. doi:10.1007/s11892-019-1196-4

Cline, G. W., Lepine, R. L., Papas, K. K., Kibbey, R. G., & Shulman, G. I. (2004). 13C NMR isotopomer analysis of anaplerotic pathways in INS-1 cells. *J Biol Chem, 279*(43), 44370-44375. doi:10.1074/jbc.M311842200

Cline, G. W., Pongratz, R. L., Zhao, X., & Papas, K. K. (2011). Rates of insulin secretion in INS-1 cells are enhanced by coupling to anaplerosis and Kreb's cycle flux independent of ATP synthesis. *Biochem Biophys Res Commun, 415*(1), 30-35. doi:10.1016/j.bbrc.2011.09.153

Cockman, M. E., Lippl, K., Tian, Y. M., Pegg, H. B., Figg, W. D. J., Abboud, M. I., . . . Ratcliffe, P. J. (2019). Lack of activity of recombinant HIF prolyl hydroxylases (PHDs) on reported non-HIF substrates. *Elife, 8*. doi:10.7554/eLife.46490

Creutzfeldt, W. (1979). The incretin concept today. *Diabetologia, 16*(2), 75-85. doi:10.1007/BF01225454

Cummins, E. P., Berra, E., Comerford, K. M., Ginouves, A., Fitzgerald, K. T., Seeballuck, F., . . . Taylor, C. T. (2006). Prolyl hydroxylase-1 negatively regulates IkappaB kinase-beta, giving insight into hypoxia-induced NFkappaB activity. *Proc Natl Acad Sci U S A, 103*(48), 18154-18159. doi:10.1073/pnas.0602235103

Curry, D. L. (1989). Effects of mannose and fructose on the synthesis and secretion of insulin. *Pancreas, 4*(1), 2-9. doi:10.1097/00006676-198902000-00002

da Silva Xavier, G., & Hodson, D. J. (2018). Mouse models of peripheral metabolic disease. *Best Pract Res Clin Endocrinol Metab, 32*(3), 299-315. doi:10.1016/j.beem.2018.03.009

De Vos, A., Heimberg, H., Quartier, E., Huypens, P., Bouwens, L., Pipeleers, D., & Schuit, F. (1995). Human and rat beta cells differ in glucose transporter but not

in glucokinase gene expression. *J Clin Invest, 96*(5), 2489-2495. doi:10.1172/JCI118308

Deacon, C. F., Nauck Ma Fau - Toft-Nielsen, M., Toft-Nielsen M Fau - Pridal, L., Pridal L Fau - Willms, B., Willms B Fau - Holst, J. J., & Holst, J. J. (1995). Both subcutaneously and intravenously administered glucagon-like peptide I are rapidly degraded from the NH2-terminus in type II diabetic patients and in healthy subjects. (0012-1797 (Print)).

Deacon, C. F., Nauck, M. A., Meier, J., Hucking, K., & Holst, J. J. (2000). Degradation of endogenous and exogenous gastric inhibitory polypeptide in healthy and in type 2 diabetic subjects as revealed using a new assay for the intact peptide. *J Clin Endocrinol Metab, 85*(10), 3575-3581. doi:10.1210/jcem.85.10.6855

del Peso, L., Castellanos, M. C., Temes, E., Martin-Puig, S., Cuevas, Y., Olmos, G., & Landazuri, M. O. (2003). The von Hippel Lindau/hypoxia-inducible factor (HIF) pathway regulates the transcription of the HIF-proline hydroxylase genes in response to low oxygen. *J Biol Chem, 278*(49), 48690-48695. doi:10.1074/jbc.M308862200

Deriy, L. V., Gomez, E. A., Jacobson, D. A., Wang, X., Hopson, J. A., Liu, X. Y., . . . Nelson, D. J. (2009). The granular chloride channel ClC-3 is permissive for insulin secretion. *Cell Metab, 10*(4), 316-323. doi:10.1016/j.cmet.2009.08.012

Deschoemaeker, S., Di Conza, G., Lilla, S., Martin-Perez, R., Mennerich, D., Boon, L., . . . Mazzone, M. (2015). PHD1 regulates p53-mediated colorectal cancer chemoresistance. *EMBO Mol Med, 7*(10), 1350-1365. doi:10.15252/emmm.201505492

Diez, H., Fischer, A., Winkler, A., Hu, C. J., Hatzopoulos, A. K., Breier, G., & Gessler, M. (2007). Hypoxia-mediated activation of Dll4-Notch-Hey2 signaling in endothelial progenitor cells and adoption of arterial cell fate. *Exp Cell Res, 313*(1), 1-9. doi:10.1016/j.yexcr.2006.09.009

Ding, W. G., & Gromada, J. (1997). Protein kinase A-dependent stimulation of exocytosis in mouse pancreatic beta-cells by glucose-dependent insulinotropic polypeptide. *Diabetes, 46*(4), 615-621. doi:10.2337/diab.46.4.615

Dolensek, J., Rupnik, M. S., & Stozer, A. (2015). Structural similarities and differences between the human and the mouse pancreas. *Islets, 7*(1), e1024405. doi:10.1080/19382014.2015.1024405

Du, W., Zhang, L., Brett-Morris, A., Aguila, B., Kerner, J., Hoppel, C. L., . . . Welford, S. M. (2017). HIF drives lipid deposition and cancer in ccRCC via repression of fatty acid metabolism. *Nat Commun, 8*(1), 1769. doi:10.1038/s41467-017-01965-8

Dunn, W. B., Broadhurst, D., Begley, P., Zelena, E., Francis-McIntyre, S., Anderson, N., . . . Human Serum Metabolome, C. (2011). Procedures for large-scale metabolic profiling of serum and plasma using gas chromatography and liquid chromatography coupled to mass spectrometry. *Nat Protoc, 6*(7), 1060-1083. doi:10.1038/nprot.2011.335

Dunwoodie, S. L. (2009). The role of hypoxia in development of the Mammalian embryo. *Dev Cell, 17*(6), 755-773. doi:10.1016/j.devcel.2009.11.008

Eales, K. L., Hollinshead, K. E., & Tennant, D. A. (2016). Hypoxia and metabolic adaptation of cancer cells. *Oncogenesis, 5*, e190. doi:10.1038/oncsis.2015.50

Ehses, J. A., Casilla, V. R., Doty, T., Pospisilik, J. A., Winter, K. D., Demuth, H. U., . . . McIntosh, C. H. (2003). Glucose-dependent insulinotropic polypeptide promotes beta-(INS-1) cell survival via cyclic adenosine monophosphate-mediated caspase-3 inhibition and regulation of p38 mitogen-activated protein kinase. *Endocrinology, 144*(10), 4433-4445. doi:10.1210/en.2002-0068

Epstein, A. C., Gleadle Jm Fau - McNeill, L. A., McNeill La Fau - Hewitson, K. S., Hewitson Ks Fau - O'Rourke, J., O'Rourke J Fau - Mole, D. R., Mole Dr Fau - Mukherji, M., . . . Ratcliffe, P. J. C. elegans EGL-9 and mammalian homologs define a family of dioxygenases that regulate HIF by prolyl hydroxylation. (0092-8674 (Print)).

Everett, K. L., & Cooper, D. M. (2013). An improved targeted cAMP sensor to study the regulation of adenylyl cyclase 8 by Ca2+ entry through voltage-gated channels. *PLoS One, 8*(9), e75942. doi:10.1371/journal.pone.0075942

Fan, Lorkiewicz, P. K., Sellers, K., Moseley, H. N., Higashi, R. M., & Lane, A. N. (2012). Stable isotope-resolved metabolomics and applications for drug development. *Pharmacol Ther, 133*(3), 366-391. doi:10.1016/j.pharmthera.2011.12.007

Fan, S., Wang, J., Yu, G., Rong, F., Zhang, D., Xu, C., . . . Xiao, W. (2020). TET is targeted for proteasomal degradation by the PHD-pVHL pathway to reduce DNA hydroxymethylation. *J Biol Chem, 295*(48), 16299-16313. doi:10.1074/jbc.RA120.014538

Feng, Z., Zou, X., Chen, Y., Wang, H., Duan, Y., & Bruick, R. K. (2018). Modulation of HIF-2alpha PAS-B domain contributes to physiological responses. *Proc Natl Acad Sci U S A, 115*(52), 13240-13245. doi:10.1073/pnas.1810897115

Ferdaoussi, M., Bergeron, V., Zarrouki, B., Kolic, J., Cantley, J., Fielitz, J., . . . Poitout, V. (2012). G protein-coupled receptor (GPR)40-dependent potentiation of insulin secretion in mouse islets is mediated by protein kinase D1. *Diabetologia, 55*(10), 2682-2692. doi:10.1007/s00125-012-2650-x

Ferdaoussi, M., Dai, X., Jensen, M. V., Wang, R., Peterson, B. S., Huang, C., . . . MacDonald, P. E. (2015). Isocitrate-to-SENP1 signaling amplifies insulin secretion and rescues dysfunctional beta cells. *J Clin Invest, 125*(10), 3847-3860. doi:10.1172/JCI82498

Fiehn, O. (2002). Metabolomics--the link between genotypes and phenotypes. (0167-4412 (Print)).

Fiehn, O. (2016). Metabolomics by Gas Chromatography-Mass Spectrometry: Combined Targeted and Untargeted Profiling. *Curr Protoc Mol Biol, 114*, 30 34 31-30 34 32. doi:10.1002/0471142727.mb3004s114

Findlay, G. M., Yan, L., Procter, J., Mieulet, V., & Lamb, R. F. (2007). A MAP4 kinase related to Ste20 is a nutrient-sensitive regulator of mTOR signalling. *Biochem J, 403*(1), 13-20. doi:10.1042/BJ20061881

Folch, J., Lees, M., & Sloane-Stanley, G. H. (1957). A simple method for the isolation and purification of total lipides from animal tissues. *J Biol Chem, 226*(1), 497-509. Retrieved from https://www.ncbi.nlm.nih.gov/pubmed/13428781

Folch, J., Lees, M., & Sloane Stanley, G. H. (1957). A simple method for the isolation and purification of total lipides from animal tissues. *J Biol Chem, 226*(1), 497-509. Retrieved from https://www.ncbi.nlm.nih.gov/pubmed/13428781

Fong, G. H., & Takeda, K. (2008). Role and regulation of prolyl hydroxylase domain proteins. *Cell Death Differ, 15*(4), 635-641. doi:10.1038/cdd.2008.10

Foster, H. R., Ho, T., Potapenko, E., Sdao, S. M., Huang, S. M., Lewandowski, S. L., . . . Merrins, M. J. (2022). beta-cell deletion of the PKm1 and PKm2 isoforms of pyruvate kinase in mice reveal their essential role as nutrient sensors for the KATP channel. *Elife, 11*. doi:10.7554/eLife.79422

Fujita, Y., Kozawa, J., Iwahashi, H., Yoneda, S., Uno, S., Eguchi, H., . . . Shimomura, I. (2018). Human pancreatic α- to β-cell area ratio increases after type 2 diabetes onset. *J Diabetes Investig, 9*(6), 1270-1282. doi:10.1111/jdi.12841

Fukuda, R., Zhang, H., Kim, J. W., Shimoda, L., Dang, C. V., & Semenza, G. L. (2007). HIF-1 regulates cytochrome oxidase subunits to optimize efficiency of respiration in hypoxic cells. *Cell, 129*(1), 111-122. doi:10.1016/j.cell.2007.01.047

Gaisano, H. Y. (2017). Recent new insights into the role of SNARE and associated proteins in insulin granule exocytosis. *Diabetes Obes Metab, 19 Suppl 1*, 115-123. doi:10.1111/dom.13001

Gao, T., McKenna, B., Li, C., Reichert, M., Nguyen, J., Singh, T., . . . Stanger, B. Z. (2014). Pdx1 maintains beta cell identity and function by repressing an alpha cell program. *Cell Metab, 19*(2), 259-271. doi:10.1016/j.cmet.2013.12.002

Gardner, L. B., Li, Q., Park, M. S., Flanagan, W. M., Semenza, G. L., & Dang, C. V. (2001). Hypoxia inhibits G1/S transition through regulation of p27 expression. *J Biol Chem, 276*(11), 7919-7926. doi:10.1074/jbc.M010189200

Gembal, M., Detimary, P., Gilon, P., Gao, Z. Y., & Henquin, J. C. (1993). Mechanisms by which glucose can control insulin release independently from its action on adenosine triphosphate-sensitive K+ channels in mouse B cells. *J Clin Invest, 91*(3), 871-880. doi:10.1172/JCI116308

German, N. J., Yoon, H., Yusuf, R. Z., Murphy, J. P., Finley, L. W., Laurent, G., . . . Haigis, M. C. (2016). PHD3 Loss in Cancer Enables Metabolic Reliance on Fatty Acid Oxidation via Deactivation of ACC2. *Mol Cell, 63*(6), 1006-1020. doi:10.1016/j.molcel.2016.08.014

Gheni, G., Ogura, M., Iwasaki, M., Yokoi, N., Minami, K., Nakayama, Y., . . . Seino, S. (2014). Glutamate acts as a key signal linking glucose metabolism to incretin/cAMP action to amplify insulin secretion. *Cell Rep, 9*(2), 661-673. doi:10.1016/j.celrep.2014.09.030

Ginouves, A., Ilc, K., Macias, N., Pouyssegur, J., & Berra, E. (2008). PHDs overactivation during chronic hypoxia "desensitizes" HIFalpha and protects cells from necrosis. *Proc Natl Acad Sci U S A, 105*(12), 4745-4750. doi:10.1073/pnas.0705680105

Greer, E. L., & Brunet, A. (2005). FOXO transcription factors at the interface between longevity and tumor suppression. *Oncogene, 24*(50), 7410-7425. doi:10.1038/sj.onc.1209086

Gribben, C., Lambert, C., Messal, H. A., Hubber, E. L., Rackham, C., Evans, I., . . . Behrens, A. (2021). Ductal Ngn3-expressing progenitors contribute to adult beta cell neogenesis in the pancreas. *Cell Stem Cell, 28*(11), 2000-2008 e2004. doi:10.1016/j.stem.2021.08.003

Gribble, F. M., & Reimann, F. (2021). Metabolic Messengers: glucagon-like peptide 1. *Nat Metab, 3*(2), 142-148. doi:10.1038/s42255-020-00327-x

Gulati, P., Gaspers, L. D., Dann, S. G., Joaquin, M., Nobukuni, T., Natt, F., . . . Thomas, G. (2008). Amino acids activate mTOR complex 1 via Ca2+/CaM signaling to hVps34. *Cell Metab, 7*(5), 456-465. doi:10.1016/j.cmet.2008.03.002

Gunn, P. J., Green, C. J., Pramfalk, C., & Hodson, L. (2017). In vitro cellular models of human hepatic fatty acid metabolism: differences between Huh7 and HepG2 cell lines in human and fetal bovine culturing serum. *Physiol Rep, 5*(24). doi:10.14814/phy2.13532

Guo, J., Chakraborty, A. A., Liu, P., Gan, W., Zheng, X., Inuzuka, H., . . . Wei, W. (2016). pVHL suppresses kinase activity of Akt in a proline-hydroxylation-dependent manner. *Science, 353*(6302), 929-932. doi:10.1126/science.aad5755

Hallbrink, M., Holmqvist, T., Olsson, M., Ostenson, C. G., Efendic, S., & Langel, U. (2001). Different domains in the third intracellular loop of the GLP-1 receptor are responsible for Galpha(s) and Galpha(i)/Galpha(o) activation. *Biochim Biophys Acta, 1546*(1), 79-86. doi:10.1016/s0167-4838(00)00270-3

Hansen, L., Deacon, C. F., Orskov, C., & Holst, J. J. (1999). Glucagon-like peptide-1-(7-36)amide is transformed to glucagon-like peptide-1-(9-36)amide by dipeptidyl peptidase IV in the capillaries supplying the L cells of the porcine intestine. *Endocrinology, 140*(11), 5356-5363. doi:10.1210/endo.140.11.7143

Hellerstein, M. K., & Neese, R. A. (1999). Mass isotopomer distribution analysis at eight years: theoretical, analytic, and experimental considerations. *Am J Physiol, 276*(6), E1146-1170. doi:10.1152/ajpendo.1999.276.6.E1146

Henquin, J. C. (2000). Triggering and amplifying pathways of regulation of insulin secretion by glucose. *Diabetes, 49*(11), 1751-1760. doi:10.2337/diabetes.49.11.1751

Heude, C., Nath, J., Carrigan, J. B., & Ludwig, C. (2017). Nuclear Magnetic Resonance Strategies for Metabolic Analysis. *Adv Exp Med Biol, 965*, 45-76. doi:10.1007/978-3-319-47656-8_3

Hiller, K., Hangebrauk, J., Jager, C., Spura, J., Schreiber, K., & Schomburg, D. (2009). MetaboliteDetector: comprehensive analysis tool for targeted and nontargeted GC/MS based metabolome analysis. *Anal Chem, 81*(9), 3429-3439. doi:10.1021/ac802689c

Hiwatashi, Y., Kanno, K., Takasaki, C., Goryo, K., Sato, T., Torii, S., . . . Yasumoto, K. (2011). PHD1 interacts with ATF4 and negatively regulates its transcriptional activity without prolyl hydroxylation. *Exp Cell Res, 317*(20), 2789-2799. doi:10.1016/j.yexcr.2011.09.005

Hoang, M., Jentz, E., Janssen, S. M., Nasteska, D., Cuozzo, F., Hodson, D. J., . . . Joseph, J. W. (2022). Isoform-specific Roles of Prolyl Hydroxylases in the Regulation of Pancreatic beta-Cell Function. *Endocrinology, 163*(1). doi:10.1210/endocr/bqab226

Hogel, H., Rantanen, K., Jokilehto, T., Grenman, R., & Jaakkola, P. M. (2011). Prolyl hydroxylase PHD3 enhances the hypoxic survival and G1 to S transition of carcinoma cells. *PLoS One, 6*(11), e27112. doi:10.1371/journal.pone.0027112

Hohmeier, H. E., Mulder, H., Chen, G., Henkel-Rieger, R., Prentki, M., & Newgard, C. B. (2000). Isolation of INS-1-derived cell lines with robust ATP-sensitive K+ channel-dependent and -independent glucose-stimulated insulin secretion. *Diabetes, 49*(3), 424-430. doi:10.2337/diabetes.49.3.424

Hollinshead, K. E. R. (2016). *Metabolic rewiring in response to genetic and environmental preturbations in cancer*: University of Birmingham.

Holz, G. G., Kang, G., Harbeck, M., Roe, M. W., & Chepurny, O. G. (2006). Cell physiology of cAMP sensor Epac. *J Physiol, 577*(Pt 1), 5-15. doi:10.1113/jphysiol.2006.119644

Hori, O., Ichinoda, F., Tamatani, T., Yamaguchi, A., Sato, N., Ozawa, K., . . . Ogawa, S. (2002). Transmission of cell stress from endoplasmic reticulum to mitochondria: enhanced expression of Lon protease. *J Cell Biol, 157*(7), 1151-1160. doi:10.1083/jcb.200108103

Hrvatin, S., O'Donnell, C. W., Deng, F., Millman, J. R., Pagliuca, F. W., DiIorio, P., . . . Melton, D. A. (2014). Differentiated human stem cells resemble fetal, not adult, beta cells. *Proc Natl Acad Sci U S A, 111*(8), 3038-3043. doi:10.1073/pnas.1400709111

Huang, Li, T., Li, X., Zhang, L., Sun, L., He, X., . . . Zhang, H. (2014). HIF-1-mediated suppression of acyl-CoA dehydrogenases and fatty acid oxidation is critical for cancer progression. *Cell Rep, 8*(6), 1930-1942. doi:10.1016/j.celrep.2014.08.028

Huang, Paglialunga, S., Wong, J. M., Hoang, M., Pillai, R., & Joseph, J. W. (2016). Role of prolyl hydroxylase domain proteins in the regulation of insulin secretion. *Physiol Rep, 4*(5). doi:10.14814/phy2.12722

Huang, H., & Tindall, D. J. (2007). Dynamic FoxO transcription factors. *J Cell Sci, 120*(Pt 15), 2479-2487. doi:10.1242/jcs.001222

Huang, M., Paglialunga, S., Wong, J. M., Hoang, M., Pillai, R., & Joseph, J. W. (2016). Role of prolyl hydroxylase domain proteins in the regulation of insulin secretion. *Physiol Rep, 4*(5). doi:10.14814/phy2.12722

Infantino, V., Iacobazzi, V., Palmieri, F., & Menga, A. (2013). ATP-citrate lyase is essential for macrophage inflammatory response. *Biochem Biophys Res Commun, 440*(1), 105-111. doi:10.1016/j.bbrc.2013.09.037

Infantino, V., Santarsiero, A., Convertini, P., Todisco, S., & Iacobazzi, V. (2021). Cancer Cell Metabolism in Hypoxia: Role of HIF-1 as Key Regulator and Therapeutic Target. *Int J Mol Sci, 22*(11). doi:10.3390/ijms22115703

Jaakkola, P. M., & Rantanen, K. (2013). The regulation, localization, and functions of oxygen-sensing prolyl hydroxylase PHD3. *Biol Chem, 394*(4), 449-457. doi:10.1515/hsz-2012-0330

Jang, C., Chen, L., & Rabinowitz, J. D. (2018). Metabolomics and Isotope Tracing. *Cell, 173*(4), 822-837. doi:10.1016/j.cell.2018.03.055

Jitrapakdee, S., Wutthisathapornchai, A., Wallace, J. C., & MacDonald, M. J. (2010). Regulation of insulin secretion: role of mitochondrial signalling. *Diabetologia, 53*(6), 1019-1032. doi:10.1007/s00125-010-1685-0

Johnson, J. D. (2016). The quest to make fully functional human pancreatic beta cells from embryonic stem cells: climbing a mountain in the clouds. *Diabetologia, 59*(10), 2047-2057. doi:10.1007/s00125-016-4059-4

Johnston, N. R., Mitchell, R. K., Haythorne, E., Pessoa, M. P., Semplici, F., Ferrer, J., . . . Hodson, D. J. (2016). Beta Cell Hubs Dictate Pancreatic Islet Responses to Glucose. *Cell Metab, 24*(3), 389-401. doi:10.1016/j.cmet.2016.06.020

Jones, B., Bloom, S. R., Buenaventura, T., Tomas, A., & Rutter, G. A. (2018). Control of insulin secretion by GLP-1. *Peptides, 100*, 75-84. doi:10.1016/j.peptides.2017.12.013

Jubb, A. M., Turley, H., Moeller, H. C., Steers, G., Han, C., Li, J. L., . . . Harris, A. L. (2009). Expression of delta-like ligand 4 (Dll4) and markers of hypoxia in colon cancer. *Br J Cancer, 101*(10), 1749-1757. doi:10.1038/sj.bjc.6605368

Jungermann, K., & Kietzmann, T. (2000). Oxygen: modulator of metabolic zonation and disease of the liver. *Hepatology, 31*(2), 255-260. doi:10.1002/hep.510310201

Kaelin, W. G., Jr., & Ratcliffe, P. J. (2008). Oxygen sensing by metazoans: the central role of the HIF hydroxylase pathway. *Mol Cell, 30*(4), 393-402. doi:10.1016/j.molcel.2008.04.009

Kaestner, K. H., Campbell–Thompson, M., Dor, Y., Gill, R. G., Glaser, B., Kim, S. K., . . . Powers, A. C. (2021). What is a β cell? – Chapter I in the Human Islet Research Network (HIRN) review series. *Molecular Metabolism, 53*, 101323. doi:https://doi.org/10.1016/j.molmet.2021.101323

Kamura, T., Sato, S., Iwai, K., Czyzyk-Krzeska, M., Conaway, R. C., & Conaway, J. W. (2000). Activation of HIF1alpha ubiquitination by a reconstituted von Hippel-Lindau (VHL) tumor suppressor complex. *Proc Natl Acad Sci U S A, 97*(19), 10430-10435. doi:10.1073/pnas.190332597

Kennel, K. B., Burmeister, J., Schneider, M., & Taylor, C. T. (2018). The PHD1 oxygen sensor in health and disease. *J Physiol, 596*(17), 3899-3913. doi:10.1113/JP275327

Kent, W. J., Sugnet, C. W., Furey, T. S., Roskin, K. M., Pringle, T. H., Zahler, A. M., & Haussler, D. (2002). The human genome browser at UCSC. *Genome Res, 12*(6), 996-1006. doi:10.1101/gr.229102

Khan, R. M. M., Chua, Z. J. Y., Tan, J. C., Yang, Y., Liao, Z., & Zhao, Y. (2019). From Pre-Diabetes to Diabetes: Diagnosis, Treatments and Translational Research. *Medicina (Kaunas), 55*(9). doi:10.3390/medicina55090546

Kieffer, T. J., McIntosh, C. H., & Pederson, R. A. (1995). Degradation of glucose-dependent insulinotropic polypeptide and truncated glucagon-like peptide 1 in vitro and in vivo by dipeptidyl peptidase IV. *Endocrinology, 136*(8), 3585-3596. doi:10.1210/endo.136.8.7628397

Kim, Goraksha-Hicks, P., Li, L., Neufeld, T. P., & Guan, K. L. (2008). Regulation of TORC1 by Rag GTPases in nutrient response. *Nat Cell Biol, 10*(8), 935-945. doi:10.1038/ncb1753

Kim, Winter, K., Nian, C., Tsuneoka, M., Koda, Y., & McIntosh, C. H. (2005). Glucose-dependent insulinotropic polypeptide (GIP) stimulation of pancreatic beta-cell survival is dependent upon phosphatidylinositol 3-kinase (PI3K)/protein kinase B (PKB) signaling, inactivation of the forkhead transcription factor Foxo1, and down-regulation of bax expression. *J Biol Chem, 280*(23), 22297-22307. doi:10.1074/jbc.M500540200

King, A., Selak, M. A., & Gottlieb, E. (2006). Succinate dehydrogenase and fumarate hydratase: linking mitochondrial dysfunction and cancer. *Oncogene, 25*(34), 4675-4682. doi:10.1038/sj.onc.1209594

Koditz, J., Nesper, J., Wottawa, M., Stiehl, D. P., Camenisch, G., Franke, C., . . . Katschinski, D. M. (2007). Oxygen-dependent ATF-4 stability is mediated by the PHD3 oxygen sensor. *Blood, 110*(10), 3610-3617. doi:10.1182/blood-2007-06-094441

Koivunen, P., Hirsila, M., Remes, A. M., Hassinen, I. E., Kivirikko, K. I., & Myllyharju, J. (2007). Inhibition of hypoxia-inducible factor (HIF) hydroxylases by citric acid

cycle intermediates: possible links between cell metabolism and stabilization of HIF. *J Biol Chem, 282*(7), 4524-4532. doi:10.1074/jbc.M610415200

Komatsu, M., Takei, M., Ishii, H., & Sato, Y. (2013). Glucose-stimulated insulin secretion: A newer perspective. *J Diabetes Investig, 4*(6), 511-516. doi:10.1111/jdi.12094

Kong, M. F., Chapman, I., Goble, E., Wishart, J., Wittert, G., Morris, H., & Horowitz, M. (1999). Effects of oral fructose and glucose on plasma GLP-1 and appetite in normal subjects. *Peptides, 20*(5), 545-551. doi:10.1016/s0196-9781(99)00006-6

Krishnan, J., Suter, M., Windak, R., Krebs, T., Felley, A., Montessuit, C., . . . Krek, W. (2009). Activation of a HIF1alpha-PPARgamma axis underlies the integration of glycolytic and lipid anabolic pathways in pathologic cardiac hypertrophy. *Cell Metab, 9*(6), 512-524. doi:10.1016/j.cmet.2009.05.005

Kushner, J. A., MacDonald, P. E., & Atkinson, M. A. (2014). Stem cells to insulin secreting cells: two steps forward and now a time to pause? *Cell Stem Cell, 15*(5), 535-536. doi:10.1016/j.stem.2014.10.012

Kyriazis, G. A., Soundarapandian, M. M., & Tyrberg, B. (2012). Sweet taste receptor signaling in beta cells mediates fructose-induced potentiation of glucose-stimulated insulin secretion. *Proc Natl Acad Sci U S A, 109*(8), E524-532. doi:10.1073/pnas.1115183109

Laskay, U. A., Lobas, A. A., Srzentic, K., Gorshkov, M. V., & Tsybin, Y. O. (2013). Proteome digestion specificity analysis for rational design of extended bottom-up and middle-down proteomics experiments. *J Proteome Res, 12*(12), 5558-5569. doi:10.1021/pr400522h

Law, L. K., Tang, N. L., Hui, J., Ho, C. S., Ruiter, J., Fok, T. F., . . . Lam, C. W. (2007). A novel functional assay for simultaneous determination of total fatty acid beta-oxidation flux and acylcarnitine profiling in human skin fibroblasts using (2)H(31)-palmitate by isotope ratio mass spectrometry and electrospray tandem mass spectrometry. *Clin Chim Acta, 382*(1-2), 25-30. doi:10.1016/j.cca.2007.03.011

Lee, W. N., Wahjudi, P. N., Xu, J., & Go, V. L. (2010). Tracer-based metabolomics: concepts and practices. *Clin Biochem, 43*(16-17), 1269-1277. doi:10.1016/j.clinbiochem.2010.07.027

Lemaire, K., Thorrez, L., & Schuit, F. (2016). Disallowed and Allowed Gene Expression: Two Faces of Mature Islet Beta Cells. *Annu Rev Nutr, 36*, 45-71. doi:10.1146/annurev-nutr-071715-050808

Leung, P. S. (2010a). Overview of the pancreas. *Adv Exp Med Biol, 690*, 3-12. doi:10.1007/978-90-481-9060-7_1

Leung, P. S. (2010b). Physiology of the pancreas. *Adv Exp Med Biol, 690*, 13-27. doi:10.1007/978-90-481-9060-7_2

Lewandowski, S. L., Cardone, R. L., Foster, H. R., Ho, T., Potapenko, E., Poudel, C., . . . Merrins, M. J. (2020). Pyruvate Kinase Controls Signal Strength in the Insulin Secretory Pathway. *Cell Metab, 32*(5), 736-750 e735. doi:10.1016/j.cmet.2020.10.007

Lieb, M. E., Menzies, K., Moschella, M. C., Ni, R., & Taubman, M. B. (2002). Mammalian EGLN genes have distinct patterns of mRNA expression and regulation. *Biochemistry and Cell Biology, 80*(4), 421-426. doi:10.1139/o02-115

Liu, Fan, F., Wang, A., Zheng, S., & Lu, Y. (2014). Dll4-Notch signaling in regulation of tumor angiogenesis. *J Cancer Res Clin Oncol, 140*(4), 525-536. doi:10.1007/s00432-013-1534-x

Liu, Huo, Z., Yan, B., Lin, X., Zhou, Z. N., Liang, X., . . . Chen, Y. H. (2010). Prolyl hydroxylase 3 interacts with Bcl-2 to regulate doxorubicin-induced apoptosis in H9c2 cells. *Biochem Biophys Res Commun, 401*(2), 231-237. doi:10.1016/j.bbrc.2010.09.037

Losada-Barragan, M. (2021). Physiological effects of nutrients on insulin release by pancreatic beta cells. *Mol Cell Biochem, 476*(8), 3127-3139. doi:10.1007/s11010-021-04146-w

Lu, Liang, Y., Dunn, W. B., Shen, H., & Kell, D. B. (2008). Comparative evaluation of software for deconvolution of metabolomics data based on GC-TOF-MS. *TrAC Trends in Analytical Chemistry, 27*(3), 215-227. doi:https://doi.org/10.1016/j.trac.2007.11.004

Lu, Mulder, H., Zhao, P., Burgess, S. C., Jensen, M. V., Kamzolova, S., . . . Sherry, A. D. (2002). 13C NMR isotopomer analysis reveals a connection between pyruvate cycling and glucose-stimulated insulin secretion (GSIS). *Proc Natl Acad Sci U S A, 99*(5), 2708-2713. doi:10.1073/pnas.052005699

Luo, W., Hu, H., Chang, R., Zhong, J., Knabel, M., O'Meally, R., . . . Semenza, G. L. (2011). Pyruvate kinase M2 is a PHD3-stimulated coactivator for hypoxia-inducible factor 1. *Cell, 145*(5), 732-744. doi:10.1016/j.cell.2011.03.054

Luttrell, L. M., Ferguson, S. S., Daaka, Y., Miller, W. E., Maudsley, S., Della Rocca, G. J., . . . Lefkowitz, R. J. (1999). Beta-arrestin-dependent formation of beta2 adrenergic receptor-Src protein kinase complexes. *Science, 283*(5402), 655-661. doi:10.1126/science.283.5402.655

MacDonald, M. J., Dobrzyn, A., Ntambi, J., & Stoker, S. W. (2008). The role of rapid lipogenesis in insulin secretion: Insulin secretagogues acutely alter lipid composition of INS-1 832/13 cells. *Arch Biochem Biophys, 470*(2), 153-162. doi:10.1016/j.abb.2007.11.017

Maechler, P., & Wollheim, C. B. (1999). Mitochondrial glutamate acts as a messenger in glucose-induced insulin exocytosis. *Nature, 402*(6762), 685-689. doi:10.1038/45280

Markley, J. L., Bruschweiler, R., Edison, A. S., Eghbalnia, H. R., Powers, R., Raftery, D., & Wishart, D. S. (2017). The future of NMR-based metabolomics. *Curr Opin Biotechnol, 43*, 34-40. doi:10.1016/j.copbio.2016.08.001

Martin, D., & Grapin-Botton, A. (2017). The Importance of REST for Development and Function of Beta Cells. *Front Cell Dev Biol, 5*, 12. doi:10.3389/fcell.2017.00012

Martinez-Sanchez, A., Nguyen-Tu, M. S., & Rutter, G. A. (2015). DICER Inactivation Identifies Pancreatic beta-Cell "Disallowed" Genes Targeted by MicroRNAs. *Mol Endocrinol, 29*(7), 1067-1079. doi:10.1210/me.2015-1059

Matveyenko, A. V., & Butler, P. C. (2006). Beta-cell deficit due to increased apoptosis in the human islet amyloid polypeptide transgenic (HIP) rat recapitulates the metabolic defects present in type 2 diabetes. *Diabetes, 55*(7), 2106-2114. doi:10.2337/db05-1672

Maxwell, P. H., Wiesener, M. S., Chang, G. W., Clifford, S. C., Vaux, E. C., Cockman, M. E., . . . Ratcliffe, P. J. (1999). The tumour suppressor protein VHL targets

hypoxia-inducible factors for oxygen-dependent proteolysis. *Nature, 399*(6733), 271-275. doi:10.1038/20459

McLean, B. A., Wong, C. K., Campbell, J. E., Hodson, D. J., Trapp, S., & Drucker, D. J. (2021). Revisiting the Complexity of GLP-1 Action from Sites of Synthesis to Receptor Activation. *Endocr Rev, 42*(2), 101-132. doi:10.1210/endrev/bnaa032

Metallo, C. M., Gameiro, P. A., Bell, E. L., Mattaini, K. R., Yang, J., Hiller, K., . . . Stephanopoulos, G. (2011). Reductive glutamine metabolism by IDH1 mediates lipogenesis under hypoxia. *Nature, 481*(7381), 380-384. doi:10.1038/nature10602

Metallo, C. M., Walther, J. L., & Stephanopoulos, G. (2009). Evaluation of 13C isotopic tracers for metabolic flux analysis in mammalian cells. *J Biotechnol, 144*(3), 167-174. doi:10.1016/j.jbiotec.2009.07.010

Metzen, E., Berchner-Pfannschmidt, U., Stengel, P., Marxsen, J. H., Stolze, I., Klinger, M., . . . Fandrey, J. (2003). Intracellular localisation of human HIF-1 alpha hydroxylases: implications for oxygen sensing. *J Cell Sci, 116*(Pt 7), 1319-1326. doi:10.1242/jcs.00318

Mikhaylova, O., Ignacak, M. L., Barankiewicz, T. J., Harbaugh, S. V., Yi, Y., Maxwell, P. H., . . . Czyzyk-Krzeska, M. F. (2008). The von Hippel-Lindau tumor suppressor protein and Egl-9-Type proline hydroxylases regulate the large subunit of RNA polymerase II in response to oxidative stress. *Mol Cell Biol, 28*(8), 2701-2717. doi:10.1128/MCB.01231-07

Min, T., & Bain, S. C. (2021). The Role of Tirzepatide, Dual GIP and GLP-1 Receptor Agonist, in the Management of Type 2 Diabetes: The SURPASS Clinical Trials. *Diabetes Ther, 12*(1), 143-157. doi:10.1007/s13300-020-00981-0

Minamishima, Y. A., Moslehi, J., Padera, R. F., Bronson, R. T., Liao, R., & Kaelin, W. G., Jr. (2009). A feedback loop involving the Phd3 prolyl hydroxylase tunes the mammalian hypoxic response in vivo. *Mol Cell Biol, 29*(21), 5729-5741. doi:10.1128/MCB.00331-09

Mlynarik, V. (2017). Introduction to nuclear magnetic resonance. *Anal Biochem, 529*, 4-9. doi:10.1016/j.ab.2016.05.006

Moin, A. S. M., Cory, M., Gurlo, T., Saisho, Y., Rizza, R. A., Butler, P. C., & Butler, A. E. (2020). Pancreatic alpha-cell mass across adult human lifespan. *Eur J Endocrinol, 182*(2), 219-231. doi:10.1530/EJE-19-0844

Montane, J., Klimek-Abercrombie, A., Potter, K. J., Westwell-Roper, C., & Verchere, B. C. (2012). Metabolic stress, IAPP and islet amyloid. *Diabetes Obes Metab, 14 Suppl 3*, 68-77. doi:10.1111/j.1463-1326.2012.01657.x

Montrose-Rafizadeh, C., Avdonin, P., Garant, M. J., Rodgers, B. D., Kole, S., Yang, H., . . . Bernier, M. (1999). Pancreatic glucagon-like peptide-1 receptor couples to multiple G proteins and activates mitogen-activated protein kinase pathways in Chinese hamster ovary cells. *Endocrinology, 140*(3), 1132-1140. doi:10.1210/endo.140.3.6550

Moran, I., Akerman, I., van de Bunt, M., Xie, R., Benazra, M., Nammo, T., . . . Ferrer, J. (2012). Human beta cell transcriptome analysis uncovers lncRNAs that are tissue-specific, dynamically regulated, and abnormally expressed in type 2 diabetes. *Cell Metab, 16*(4), 435-448. doi:10.1016/j.cmet.2012.08.010

Morotti, M., Bridges, E., Valli, A., Choudhry, H., Sheldon, H., Wigfield, S., . . . Harris, A. L. (2019). Hypoxia-induced switch in SNAT2/SLC38A2 regulation generates endocrine resistance in breast cancer. *Proc Natl Acad Sci U S A, 116*(25), 12452-12461. doi:10.1073/pnas.1818521116

Moser, S. C., Bensaddek, D., Ortmann, B., Maure, J. F., Mudie, S., Blow, J. J., . . . Rocha, S. (2013). PHD1 links cell-cycle progression to oxygen sensing through hydroxylation of the centrosomal protein Cep192. *Dev Cell, 26*(4), 381-392. doi:10.1016/j.devcel.2013.06.014

Mosleh, E., Ou, K., Haemmerle, M. W., Tembo, T., Yuhas, A., Carboneau, B. A., . . . Golson, M. L. (2020). Ins1-Cre and Ins1-CreER Gene Replacement Alleles Are Susceptible To Silencing By DNA Hypermethylation. *Endocrinology, 161*(8). doi:10.1210/endocr/bqaa054

Moukil, M. A., Veiga-da-Cunha, M., & Van Schaftingen, E. (2000). Study of the regulatory properties of glucokinase by site-directed mutagenesis: conversion of glucokinase to an enzyme with high affinity for glucose. *Diabetes, 49*(2), 195-201. doi:10.2337/diabetes.49.2.195

Mukherjee, A., Morales-Scheihing, D., Butler, P. C., & Soto, C. (2015). Type 2 diabetes as a protein misfolding disease. *Trends Mol Med, 21*(7), 439-449. doi:10.1016/j.molmed.2015.04.005

Murray, K. K., Boyd, R. K., Eberlin, M. N., Langley, G. J., Li, L., & Naito, Y. (2013). Definitions of terms relating to mass spectrometry (IUPAC Recommendations 2013). *Pure and Applied Chemistry, 85*(7), 1515-1609. doi:doi:10.1351/PAC-REC-06-04-06

Mylonis, I., Sembongi, H., Befani, C., Liakos, P., Siniossoglou, S., & Simos, G. (2012). Hypoxia causes triglyceride accumulation by HIF-1-mediated stimulation of lipin 1 expression. *J Cell Sci, 125*(Pt 14), 3485-3493. doi:10.1242/jcs.106682

Na, Y. R., Woo, D. J., Kim, S. Y., & Yang, E. G. (2016). Pyrithione Zn selectively inhibits hypoxia-inducible factor prolyl hydroxylase PHD3. *Biochem Biophys Res Commun, 472*(2), 313-318. doi:10.1016/j.bbrc.2016.02.115

Nakazawa, M. S., Keith, B., & Simon, M. C. (2016). Oxygen availability and metabolic adaptations. *Nat Rev Cancer, 16*(10), 663-673. doi:10.1038/nrc.2016.84

Nasteska, D., Cuozzo, F., Viloria, K., Johnson, E. M., Thakker, A., Bany Bakar, R., . . . Hodson, D. J. (2021). Prolyl-4-hydroxylase 3 maintains beta cell glucose metabolism during fatty acid excess in mice. *JCI Insight, 6*(16). doi:10.1172/jci.insight.140288

Nasteska, D., Fine, N. H. F., Ashford, F. B., Cuozzo, F., Viloria, K., Smith, G., . . . Hodson, D. J. (2021). PDX1(LOW) MAFA(LOW) beta-cells contribute to islet function and insulin release. *Nat Commun, 12*(1), 674. doi:10.1038/s41467-020-20632-z

Newgard, C. B. (2017). Metabolomics and Metabolic Diseases: Where Do We Stand? *Cell Metab, 25*(1), 43-56. doi:10.1016/j.cmet.2016.09.018

Nigg, E. A., & Stearns, T. (2011). The centrosome cycle: Centriole biogenesis, duplication and inherent asymmetries. *Nat Cell Biol, 13*(10), 1154-1160. doi:10.1038/ncb2345

Ohh, M., Park, C. W., Ivan, M., Hoffman, M. A., Kim, T. Y., Huang, L. E., . . . Kaelin, W. G. (2000). Ubiquitination of hypoxia-inducible factor requires direct binding to the beta-domain of the von Hippel-Lindau protein. *Nat Cell Biol, 2*(7), 423-427. doi:10.1038/35017054

Orskov, C., Rabenhoj, L., Wettergren, A., Kofod, H., & Holst, J. J. (1994). Tissue and plasma concentrations of amidated and glycine-extended glucagon-like peptide I in humans. *Diabetes, 43*(4), 535-539. doi:10.2337/diab.43.4.535

Otonkoski, T., Jiao, H., Kaminen-Ahola, N., Tapia-Paez, I., Ullah, M. S., Parton, L. E., . . . Kere, J. (2007). Physical exercise-induced hypoglycemia caused by failed silencing of monocarboxylate transporter 1 in pancreatic beta cells. *Am J Hum Genet, 81*(3), 467-474. doi:10.1086/520960

Pasquali, L., Gaulton, K. J., Rodriguez-Segui, S. A., Mularoni, L., Miguel-Escalada, I., Akerman, I., . . . Ferrer, J. (2014). Pancreatic islet enhancer clusters enriched in type 2 diabetes risk-associated variants. *Nat Genet, 46*(2), 136-143. doi:10.1038/ng.2870

Patel, N. S., Li, J. L., Generali, D., Poulsom, R., Cranston, D. W., & Harris, A. L. (2005). Up-regulation of delta-like 4 ligand in human tumor vasculature and the role of basal expression in endothelial cell function. *Cancer Res, 65*(19), 8690-8697. doi:10.1158/0008-5472.CAN-05-1208

Pescador, N., Villar, D., Cifuentes, D., Garcia-Rocha, M., Ortiz-Barahona, A., Vazquez, S., . . . del Peso, L. (2010). Hypoxia promotes glycogen accumulation through hypoxia inducible factor (HIF)-mediated induction of glycogen synthase 1. *PLoS One, 5*(3), e9644. doi:10.1371/journal.pone.0009644

Pipatpolkai, T., Usher, S., Stansfeld, P. J., & Ashcroft, F. M. (2020). New insights into KATP channel gene mutations and neonatal diabetes mellitus. *Nat Rev Endocrinol, 16*(7), 378-393. doi:10.1038/s41574-020-0351-y

Prentki, M., Corkey, B. E., & Madiraju, S. R. M. (2020). Lipid-associated metabolic signalling networks in pancreatic beta cell function. *Diabetologia, 63*(1), 10-20. doi:10.1007/s00125-019-04976-w

Pugh, C. W. (2016). Modulation of the Hypoxic Response. *Adv Exp Med Biol, 903*, 259-271. doi:10.1007/978-1-4899-7678-9_18

Pullen, T. J., & Rutter, G. A. (2013). When less is more: the forbidden fruits of gene repression in the adult beta-cell. *Diabetes Obes Metab, 15*(6), 503-512. doi:10.1111/dom.12029

Puri, S., Cano, D. A., & Hebrok, M. (2009). A role for von Hippel-Lindau protein in pancreatic beta-cell function. *Diabetes, 58*(2), 433-441. doi:10.2337/db08-0749

Qie, S., & Diehl, J. A. (2016). Cyclin D1, cancer progression, and opportunities in cancer treatment. *J Mol Med (Berl), 94*(12), 1313-1326. doi:10.1007/s00109-016-1475-3

Quintens, R., Hendrickx, N., Lemaire, K., & Schuit, F. (2008). Why expression of some genes is disallowed in beta-cells. *Biochem Soc Trans, 36*(Pt 3), 300-305. doi:10.1042/BST0360300

Quoyer, J., Longuet, C., Broca, C., Linck, N., Costes, S., Varin, E., . . . Dalle, S. (2010). GLP-1 mediates antiapoptotic effect by phosphorylating Bad through a beta-arrestin 1-mediated ERK1/2 activation in pancreatic beta-cells. *J Biol Chem, 285*(3), 1989-2002. doi:10.1074/jbc.M109.067207

Rabaglia, M. E., Gray-Keller, M. P., Frey, B. L., Shortreed, M. R., Smith, L. M., & Attie, A. D. (2005). Alpha-Ketoisocaproate-induced hypersecretion of insulin by islets from diabetes-susceptible mice. *Am J Physiol Endocrinol Metab, 289*(2), E218-224. doi:10.1152/ajpendo.00573.2004

Ragy, M. M., & Ahmed, S. M. (2019). Protective effects of either C-peptide or l-arginine on pancreatic beta-cell function, proliferation, and oxidative stress in streptozotocin-induced diabetic rats. *J Cell Physiol, 234*(7), 11500-11510. doi:10.1002/jcp.27808

Rasmussen, K. D., & Helin, K. (2016). Role of TET enzymes in DNA methylation, development, and cancer. *Genes Dev, 30*(7), 733-750. doi:10.1101/gad.276568.115

Ren, J. Z., A; Konga, L; Wang X. (2018). Advances in mass spectrometry-based metabolomics for investigation of metabolites. *RSC Advances, 8*(40). doi:10.1039/c8ra01574k

Roat, R., Rao, V., Doliba, N. M., Matschinsky, F. M., Tobias, J. W., Garcia, E., . . . Imai, Y. (2014). Alterations of pancreatic islet structure, metabolism and gene expression in diet-induced obese C57BL/6J mice. *PLoS One, 9*(2), e86815. doi:10.1371/journal.pone.0086815

Roche, E., Farfari, S., Witters, L. A., Assimacopoulos-Jeannet, F., Thumelin, S., Brun, T., . . . Prentki, M. (1998). Long-term exposure of beta-INS cells to high glucose concentrations increases anaplerosis, lipogenesis, and lipogenic gene expression. *Diabetes, 47*(7), 1086-1094. doi:10.2337/diabetes.47.7.1086

Roder, P. V., Wu, B., Liu, Y., & Han, W. (2016). Pancreatic regulation of glucose homeostasis. *Exp Mol Med, 48*, e219. doi:10.1038/emm.2016.6

Rodriguez, J., Herrero, A., Li, S., Rauch, N., Quintanilla, A., Wynne, K., . . . von Kriegsheim, A. (2018). PHD3 Regulates p53 Protein Stability by Hydroxylating Proline 359. *Cell Rep, 24*(5), 1316-1329. doi:10.1016/j.celrep.2018.06.108

Rodriguez, J., Pilkington, R., Garcia Munoz, A., Nguyen, L. K., Rauch, N., Kennedy, S., . . . von Kriegsheim, A. (2016). Substrate-Trapped Interactors of PHD3 and FIH Cluster in Distinct Signaling Pathways. *Cell Rep, 14*(11), 2745-2760. doi:10.1016/j.celrep.2016.02.043

Roduit, R., Nolan, C., Alarcon, C., Moore, P., Barbeau, A., Delghingaro-Augusto, V., . . . Prentki, M. (2004). A role for the malonyl-CoA/long-chain acyl-CoA pathway of lipid signaling in the regulation of insulin secretion in response to both fuel and nonfuel stimuli. *Diabetes, 53*(4), 1007-1019. doi:10.2337/diabetes.53.4.1007

Ronnebaum, S. M., Joseph, J. W., Ilkayeva, O., Burgess, S. C., Lu, D., Becker, T. C., . . . Newgard, C. B. (2008). Chronic suppression of acetyl-CoA carboxylase 1 in beta-cells impairs insulin secretion via inhibition of glucose rather than lipid metabolism. *J Biol Chem, 283*(21), 14248-14256. doi:10.1074/jbc.M800119200

Rorsman, P., & Ashcroft, F. M. (2018). Pancreatic beta-Cell Electrical Activity and Insulin Secretion: Of Mice and Men. *Physiol Rev, 98*(1), 117-214. doi:10.1152/physrev.00008.2017

Rorsman, P., & Huising, M. O. (2018). The somatostatin-secreting pancreatic delta-cell in health and disease. *Nat Rev Endocrinol, 14*(7), 404-414. doi:10.1038/s41574-018-0020-6

Rutter, G. A., Pullen, T. J., Hodson, D. J., & Martinez-Sanchez, A. (2015). Pancreatic beta-cell identity, glucose sensing and the control of insulin secretion. *Biochem J, 466*(2), 203-218. doi:10.1042/BJ20141384

Sancak, Y., Peterson, T. R., Shaul, Y. D., Lindquist, R. A., Thoreen, C. C., Bar-Peled, L., & Sabatini, D. M. (2008). The Rag GTPases bind raptor and mediate amino acid signaling to mTORC1. *Science, 320*(5882), 1496-1501. doi:10.1126/science.1157535

Sanchez, P. K. M., Khazaei, M., Gatineau, E., Geravandi, S., Lupse, B., Liu, H., . . . Ardestani, A. (2021). LDHA is enriched in human islet alpha cells and upregulated in type 2 diabetes. *Biochem Biophys Res Commun, 568*, 158-166. doi:10.1016/j.bbrc.2021.06.065

Sato, Y., Endo, H., Okuyama, H., Takeda, T., Iwahashi, H., Imagawa, A., . . . Inoue, M. (2011). Cellular hypoxia of pancreatic beta-cells due to high levels of oxygen consumption for insulin secretion in vitro. *J Biol Chem, 286*(14), 12524-12532. doi:10.1074/jbc.M110.194738

Schindelin, J., Arganda-Carreras, I., Frise, E., Kaynig, V., Longair, M., Pietzsch, T., . . . Cardona, A. (2012). Fiji: an open-source platform for biological-image analysis. *Nat Methods, 9*(7), 676-682. doi:10.1038/nmeth.2019

Schlisio, S., Kenchappa, R. S., Vredeveld, L. C., George, R. E., Stewart, R., Greulich, H., . . . Kaelin, W. G., Jr. (2008). The kinesin KIF1Bbeta acts downstream from EglN3 to induce apoptosis and is a potential 1p36 tumor suppressor. *Genes Dev, 22*(7), 884-893. doi:10.1101/gad.1648608

Schmidt, M., Evellin, S., Weernink, P. A., von Dorp, F., Rehmann, H., Lomasney, J. W., & Jakobs, K. H. (2001). A new phospholipase-C-calcium signalling pathway mediated by cyclic AMP and a Rap GTPase. *Nat Cell Biol, 3*(11), 1020-1024. doi:10.1038/ncb1101-1020

Schneider, C. A., Rasband, W. S., & Eliceiri, K. W. (2012). NIH Image to ImageJ: 25 years of image analysis. *Nat Methods, 9*(7), 671-675. doi:10.1038/nmeth.2089

Schofield, C. J., & Ratcliffe, P. J. (2004). Oxygen sensing by HIF hydroxylases. *Nat Rev Mol Cell Biol, 5*(5), 343-354. doi:10.1038/nrm1366

Schuit, F., Van Lommel, L., Granvik, M., Goyvaerts, L., de Faudeur, G., Schraenen, A., & Lemaire, K. (2012). beta-cell-specific gene repression: a mechanism to protect against inappropriate or maladjusted insulin secretion? *Diabetes, 61*(5), 969-975. doi:10.2337/db11-1564

Semenza, G. L. (2007). Oxygen-dependent regulation of mitochondrial respiration by hypoxia-inducible factor 1. *Biochem J, 405*(1), 1-9. doi:10.1042/BJ20070389

Semenza, G. L. (2013). HIF-1 mediates metabolic responses to intratumoral hypoxia and oncogenic mutations. *J Clin Invest, 123*(9), 3664-3671. doi:10.1172/JCI67230

Sener, A., Best, L. C., Yates, A. P., Kadiata, M. M., Olivares, E., Louchami, K., . . . Malaisse, W. J. (2000). Stimulus-secretion coupling of arginine-induced insulin release: comparison between the cationic amino acid and its methyl ester. *Endocrine, 13*(3), 329-340. doi:10.1385/ENDO:13:3:329

Simpson, N. E., Khokhlova, N., Oca-Cossio, J. A., & Constantinidis, I. (2006). Insights into the role of anaplerosis in insulin secretion: A 13C NMR study. *Diabetologia, 49*(6), 1338-1348. doi:10.1007/s00125-006-0216-5

Skelin Klemen, M., Dolensek, J., Slak Rupnik, M., & Stozer, A. (2017). The triggering pathway to insulin secretion: Functional similarities and differences between the human and the mouse beta cells and their translational relevance. *Islets, 9*(6), 109-139. doi:10.1080/19382014.2017.1342022

Skuli, N., Liu, L., Runge, A., Wang, T., Yuan, L., Patel, S., . . . Keith, B. (2009). Endothelial deletion of hypoxia-inducible factor-2alpha (HIF-2alpha) alters vascular function and tumor angiogenesis. *Blood, 114*(2), 469-477. doi:10.1182/blood-2008-12-193581

Spegel, P., & Mulder, H. (2020). Metabolomics Analysis of Nutrient Metabolism in beta-Cells. *J Mol Biol, 432*(5), 1429-1445. doi:10.1016/j.jmb.2019.07.020

Strowitzki, M. J., Cummins, E. P., & Taylor, C. T. (2019). Protein Hydroxylation by Hypoxia-Inducible Factor (HIF) Hydroxylases: Unique or Ubiquitous? *Cells, 8*(5). doi:10.3390/cells8050384

Sudhof, T. C. (2013). Neurotransmitter release: the last millisecond in the life of a synaptic vesicle. *Neuron, 80*(3), 675-690. doi:10.1016/j.neuron.2013.10.022

Sun, H., Saeedi, P., Karuranga, S., Pinkepank, M., Ogurtsova, K., Duncan, B. B., . . . Magliano, D. J. (2022). IDF Diabetes Atlas: Global, regional and country-level diabetes prevalence estimates for 2021 and projections for 2045. *Diabetes Res Clin Pract, 183*, 109119. doi:10.1016/j.diabres.2021.109119

Sussulini, A. (2017). Erratum to: Chapters 1 and 11 of Metabolomics: From Fundamentals to Clinical Applications. *Adv Exp Med Biol, 965*, E1-E2. doi:10.1007/978-3-319-47656-8_14

Takeda, K., Ho, V. C., Takeda, H., Duan, L. J., Nagy, A., & Fong, G. H. (2006). Placental but not heart defects are associated with elevated hypoxia-inducible

factor alpha levels in mice lacking prolyl hydroxylase domain protein 2. *Mol Cell Biol, 26*(22), 8336-8346. doi:10.1128/MCB.00425-06

Tan, X., Sun, L., Chen, J., & Chen, Z. J. (2018). Detection of Microbial Infections Through Innate Immune Sensing of Nucleic Acids. *Annu Rev Microbiol, 72*, 447-478. doi:10.1146/annurev-micro-102215-095605

Taniguchi, C. M., Emanuelli, B., & Kahn, C. R. (2006). Critical nodes in signalling pathways: insights into insulin action. *Nat Rev Mol Cell Biol, 7*(2), 85-96. doi:10.1038/nrm1837

Taniguchi, C. M., Finger, E. C., Krieg, A. J., Wu, C., Diep, A. N., LaGory, E. L., . . . Giaccia, A. J. (2013). Cross-talk between hypoxia and insulin signaling through Phd3 regulates hepatic glucose and lipid metabolism and ameliorates diabetes. *Nat Med, 19*(10), 1325-1330. doi:10.1038/nm.3294

Tanimoto, K., Makino, Y., Pereira, T., & Poellinger, L. (2000). Mechanism of regulation of the hypoxia-inducible factor-1 alpha by the von Hippel-Lindau tumor suppressor protein. *EMBO J, 19*(16), 4298-4309. doi:10.1093/emboj/19.16.4298

Tappy, L., & Le, K. A. (2010). Metabolic effects of fructose and the worldwide increase in obesity. *Physiol Rev, 90*(1), 23-46. doi:10.1152/physrev.00019.2009

Taylor, B. L., Benthuysen, J., & Sander, M. (2015). Postnatal beta-cell proliferation and mass expansion is dependent on the transcription factor Nkx6.1. *Diabetes, 64*(3), 897-903. doi:10.2337/db14-0684

Tennant, D. A., Frezza, C., MacKenzie, E. D., Nguyen, Q. D., Zheng, L., Selak, M. A., . . . Gottlieb, E. (2009). Reactivating HIF prolyl hydroxylases under hypoxia results in metabolic catastrophe and cell death. *Oncogene, 28*(45), 4009-4021. doi:10.1038/onc.2009.250

Thorens, B., Tarussio, D., Maestro, M. A., Rovira, M., Heikkila, E., & Ferrer, J. (2015). Ins1(Cre) knock-in mice for beta cell-specific gene recombination. *Diabetologia, 58*(3), 558-565. doi:10.1007/s00125-014-3468-5

Thorrez, L., Laudadio, I., Van Deun, K., Quintens, R., Hendrickx, N., Granvik, M., . . . Schuit, F. (2011). Tissue-specific disallowance of housekeeping genes: the other face of cell differentiation. *Genome Res, 21*(1), 95-105. doi:10.1101/gr.109173.110

Thurmond, D. C. (2007). Regulation of Insulin Action and Insulin Secretion by SNARE-Mediated Vesicle Exocytosis. In: Mechanisms of Insulin Action. In: Springer, New York, NY.

Tirpe, A. A., Gulei, D., Ciortea, S. M., Crivii, C., & Berindan-Neagoe, I. (2019). Hypoxia: Overview on Hypoxia-Mediated Mechanisms with a Focus on the Role of HIF Genes. *Int J Mol Sci, 20*(24). doi:10.3390/ijms20246140

Triantafyllou, E. A., Georgatsou, E., Mylonis, I., Simos, G., & Paraskeva, E. (2018). Expression of AGPAT2, an enzyme involved in the glycerophospholipid/triacylglycerol biosynthesis pathway, is directly regulated by HIF-1 and promotes survival and etoposide resistance of cancer cells under hypoxia. *Biochim Biophys Acta Mol Cell Biol Lipids, 1863*(9), 1142-1152. doi:10.1016/j.bbalip.2018.06.015

Trumper, A., Trumper, K., & Horsch, D. (2002). Mechanisms of mitogenic and anti-apoptotic signaling by glucose-dependent insulinotropic polypeptide in beta(INS-1)-cells. *J Endocrinol, 174*(2), 233-246. doi:10.1677/joe.0.1740233

Tsonkova, V. G., Sand, F. W., Wolf, X. A., Grunnet, L. G., Kirstine Ringgaard, A., Ingvorsen, C., . . . Frogne, T. (2018). The EndoC-betaH1 cell line is a valid model of human beta cells and applicable for screenings to identify novel drug target candidates. *Mol Metab, 8*, 144-157. doi:10.1016/j.molmet.2017.12.007

Ullah, K., Rosendahl, A. H., Izzi, V., Bergmann, U., Pihlajaniemi, T., Maki, J. M., & Myllyharju, J. (2017). Hypoxia-inducible factor prolyl-4-hydroxylase-1 is a convergent point in the reciprocal negative regulation of NF-kappaB and p53 signaling pathways. *Sci Rep, 7*(1), 17220. doi:10.1038/s41598-017-17376-0

Vakilian, M., Tahamtani, Y., & Ghaedi, K. (2019). A review on insulin trafficking and exocytosis. *Gene, 706*, 52-61. doi:10.1016/j.gene.2019.04.063

Van Welden, S., Laukens, D., Ferdinande, L., De Vos, M., & Hindryckx, P. (2013). Differential expression of prolyl hydroxylase 1 in patients with ulcerative colitis versus patients with Crohn's disease/infectious colitis and healthy controls. *J Inflamm (Lond), 10*(1), 36. doi:10.1186/1476-9255-10-36

Vetterli, L., Carobbio, S., Pournourmohammadi, S., Martin-Del-Rio, R., Skytt, D. M., Waagepetersen, H. S., . . . Maechler, P. (2012). Delineation of glutamate pathways and secretory responses in pancreatic islets with beta-cell-specific

abrogation of the glutamate dehydrogenase. *Mol Biol Cell, 23*(19), 3851-3862. doi:10.1091/mbc.E11-08-0676

Wang, Y., Montrose-Rafizadeh, C., Adams, L., Raygada, M., Nadiv, O., & Egan, J. M. (1996). GIP regulates glucose transporters, hexokinases, and glucose-induced insulin secretion in RIN 1046-38 cells. *Mol Cell Endocrinol, 116*(1), 81-87. doi:10.1016/0303-7207(95)03701-2

Wiesener, M. S., Jurgensen, J. S., Rosenberger, C., Scholze, C. K., Horstrup, J. H., Warnecke, C., . . . Eckardt, K. U. (2003). Widespread hypoxia-inducible expression of HIF-2alpha in distinct cell populations of different organs. *FASEB J, 17*(2), 271-273. doi:10.1096/fj.02-0445fje

Wilson, J. E. (2003). Isozymes of mammalian hexokinase: structure, subcellular localization and metabolic function. *J Exp Biol, 206*(Pt 12), 2049-2057. doi:10.1242/jeb.00241

Wortham, M., & Sander, M. (2016). Mechanisms of beta-cell functional adaptation to changes in workload. *Diabetes Obes Metab, 18 Suppl 1*, 78-86. doi:10.1111/dom.12729

Xie, & Simon, M. C. (2017). Oxygen availability and metabolic reprogramming in cancer. *J Biol Chem, 292*(41), 16825-16832. doi:10.1074/jbc.R117.799973

Xie, Xiao, K., Whalen, E. J., Forrester, M. T., Freeman, R. S., Fong, G., . . . Stamler, J. S. (2009). Oxygen-regulated beta(2)-adrenergic receptor hydroxylation by EGLN3 and ubiquitylation by pVHL. *Sci Signal, 2*(78), ra33. doi:10.1126/scisignal.2000444

Xie, Y., Shi, X., Sheng, K., Han, G., Li, W., Zhao, Q., . . . Gu, Y. (2019). PI3K/Akt signaling transduction pathway, erythropoiesis and glycolysis in hypoxia (Review). *Mol Med Rep, 19*(2), 783-791. doi:10.3892/mmr.2018.9713

Yan, B., Jiao, S., Zhang, H. S., Lv, D. D., Xue, J., Fan, L., . . . Fang, J. (2011). Prolyl hydroxylase domain protein 3 targets Pax2 for destruction. *Biochem Biophys Res Commun, 409*(2), 315-320. doi:10.1016/j.bbrc.2011.05.012

Yang, M., Su, H., Soga, T., Kranc, K. R., & Pollard, P. J. (2014). Prolyl hydroxylase domain enzymes: important regulators of cancer metabolism. *Hypoxia (Auckl), 2*, 127-142. doi:10.2147/HP.S47968

Yano, H., Sakai, M., Matsukawa, T., Yagi, T., Naganuma, T., Mitsushima, M., . . . Matsumoto, M. (2018). PHD3 regulates glucose metabolism by suppressing stress-induced signalling and optimising gluconeogenesis and insulin signalling in hepatocytes. *Sci Rep, 8*(1), 14290. doi:10.1038/s41598-018-32575-z

Yao, C. H., Liu, G. Y., Wang, R., Moon, S. H., Gross, R. W., & Patti, G. J. (2018). Identifying off-target effects of etomoxir reveals that carnitine palmitoyltransferase I is essential for cancer cell proliferation independent of beta-oxidation. *PLoS Biol, 16*(3), e2003782. doi:10.1371/journal.pbio.2003782

Ye, J., Fan, J., Venneti, S., Wan, Y. W., Pawel, B. R., Zhang, J., . . . Thompson, C. B. (2014). Serine catabolism regulates mitochondrial redox control during hypoxia. *Cancer Discov, 4*(12), 1406-1417. doi:10.1158/2159-8290.CD-14-0250

Yoon, H., Spinelli, J. B., Zaganjor, E., Wong, S. J., German, N. J., Randall, E. C., . . . Haigis, M. C. (2020). PHD3 Loss Promotes Exercise Capacity and Fat Oxidation in Skeletal Muscle. *Cell Metab, 32*(2), 215-228 e217. doi:10.1016/j.cmet.2020.06.017

Yu, G., Li, X., Zhou, Z., Tang, J., Wang, J., Liu, X., . . . Xiao, W. (2020). Zebrafish phd3 Negatively Regulates Antiviral Responses via Suppression of Irf7 Transactivity Independent of Its Prolyl Hydroxylase Activity. *J Immunol, 205*(4), 1135-1146. doi:10.4049/jimmunol.1900902

Zaborska, K. E., Dadi, P. K., Dickerson, M. T., Nakhe, A. Y., Thorson, A. S., Schaub, C. M., . . . Jacobson, D. A. (2020). Lactate activation of alpha-cell KATP channels inhibits glucagon secretion by hyperpolarizing the membrane potential and reducing Ca(2+) entry. *Mol Metab, 42*, 101056. doi:10.1016/j.molmet.2020.101056

Zehetner, J., Danzer, C., Collins, S., Eckhardt, K., Gerber, P. A., Ballschmieter, P., . . . Krek, W. (2008). PVHL is a regulator of glucose metabolism and insulin secretion in pancreatic beta cells. *Genes Dev, 22*(22), 3135-3146. doi:10.1101/gad.496908

Zhang, Bosch-Marce, M., Shimoda, L. A., Tan, Y. S., Baek, J. H., Wesley, J. B., . . . Semenza, G. L. (2008). Mitochondrial autophagy is an HIF-1-dependent adaptive metabolic response to hypoxia. *J Biol Chem, 283*(16), 10892-10903. doi:10.1074/jbc.M800102200

Zhang, Jensen, M. V., Gray, S. M., El, K., Wang, Y., Lu, D., . . . Newgard, C. B. (2021). Reductive TCA cycle metabolism fuels glutamine- and glucose-stimulated insulin secretion. *Cell Metab, 33*(4), 804-817 e805. doi:10.1016/j.cmet.2020.11.020

Zhang, Kasim, V., Xie, Y. D., Huang, C., Sisjayawan, J., Dwi Ariyanti, A., . . . Wu, S. R. (2017). Inhibition of PHD3 by salidroside promotes neovascularization through cell-cell communications mediated by muscle-secreted angiogenic factors. *Sci Rep, 7*, 43935. doi:10.1038/srep43935

Zhang, & Kim, K.-H. (1998). Essential Role of Acetyl-CoA Carboxylase in the Glucose-Induced Insulin Secretion in a Pancreatic β-Cell Line. *Cellular Signalling, 10*(1), 35-42. doi:https://doi.org/10.1016/S0898-6568(97)00070-3

Zhang, C., Moriguchi, T., Kajihara, M., Esaki, R., Harada, A., Shimohata, H., . . . Takahashi, S. (2005). MafA is a key regulator of glucose-stimulated insulin secretion. *Mol Cell Biol, 25*(12), 4969-4976. doi:10.1128/MCB.25.12.4969-4976.2005

Zheng, X., Zhai, B., Koivunen, P., Shin, S. J., Lu, G., Liu, J., . . . Zhang, Q. (2014). Prolyl hydroxylation by EglN2 destabilizes FOXO3a by blocking its interaction with the USP9x deubiquitinase. *Genes Dev, 28*(13), 1429-1444. doi:10.1101/gad.242131.114

APPENDICES

Appendix 1

Diet composition

Nutrients	Standard chow (SC) (% Kcal)	High fat diet (HFD) (% Kcal)
Protein	~17	20
Carbohydrate	~76	20
Fat	~7	60
Total	100	100

Appendix 2

Human donors

Unique identifier	Age group (years)	Gender	BMI (Kg/m^2)	Glycemia (mmol/L)* HbA1C (%)	History of diabetes**	Islet purity (%)	Islet culture duration (h)	Country of origin
HP1404	50-55	♂	29.4	7.8 mmol/L	No	80	18	Italy
HP1406	60-65	♂	26.1	N/A	No	90	96	Italy
HP1408	55-60	♀	19.0	N/A	No	90	18	Italy
HP1416	60-65	♂	31.1	N/A	No but IFG	75	20	Italy
HP1419	55-60	♂	22.8	7.3 mmol/L	No	90	18	Italy
HP1431	60-65	♀	26.9	8.0 mmol/L	No	90	18	Italy
HI1117	45-50	♂	24.0	5.4%	No	80	N/A	France
HI1120	50-55	♂	29.5	5.7%	No	90	N/A	France
HI1121	60-65	♂	32	5.5%	No	90	N/A	France

Appendix 3

Author's publications

1. Westbrook RL, Bridges E, Roberts J, Escribano-Gonzalez C, Eales KL, Vettore LA, Walker PD, Vera-Siguenza E, Rana H, **Cuozzo F**, Eskla KL, Vellama H, Shaaban A, Nixon C, Luuk H, Lavery GG, Hodson DJ, Harris AL, Tennant DA. *Proline synthesis through PYCR1 is required to support cancer cell proliferation and survival in oxygen-limiting conditions*. Cell Rep. 2022 Feb 1;38(5):110320. doi: 10.1016/j.celrep.2022.110320.

2. Karsai M, Zuellig RA, Lehmann R, **Cuozzo F**, Nasteska D, Luca E, Hantel C, Hodson DJ, Spinas GA, Rutter GA, Gerber PA. *Lack of ZnT8 protects pancreatic islets from hypoxia- and cytokine-induced cell death*. J Endocrinol. 2022 Feb 11;253(1):1-11. doi: 10.1530/JOE-21-0271.

3. Hoang M, Jentz E, Janssen SM, Nasteska D, **Cuozzo F**, Hodson DJ, Tupling AR, Fong GH, Joseph JW. *Isoform-specific Roles of Prolyl Hydroxylases in the Regulation of Pancreatic β-Cell Function*. Endocrinology. 2022 Jan 1;163(1):bqab226. doi: 10.1210/endocr/bqab226.

4. Nasteska D, **Cuozzo F**, Viloria K, Johnson EM, Thakker A, Bany Bakar R, Westbrook RL, Barlow JP, Hoang M, Joseph JW, Lavery GG, Akerman I, Cantley J, Hodson L, Tennant DA, Hodson DJ. *Prolyl-4-hydroxylase 3 maintains β cell glucose metabolism during fatty acid excess in mice*. JCI Insight. 2021 Aug 23;6(16):e140288. doi: 10.1172/jci.insight.140288.

5. Nasteska D, Fine NHF, Ashford FB, **Cuozzo F**, Viloria K, Smith G, Dahir A, Dawson PWJ, Lai YC, Bastidas-Ponce A, Bakhti M, Rutter GA, Fiancette R, Nano R, Piemonti L, Lickert H, Zhou Q, Akerman I, Hodson DJ. Author Correction: *PDX1LOW MAFALOW β-cells contribute to islet function and insulin release*. Nat Commun. 2021 Jul 20;12(1):4521. doi: 10.1038/s41467-021-24848-5. Erratum for: Nat Commun. 2021 Jan 29;12(1):674.

6. Viloria K, Nasteska D, Briant LJB, Heising S, Larner DP, Fine NHF, Ashford FB, da Silva Xavier G, Ramos MJ, Hasib A, **Cuozzo F**, Manning Fox JE, MacDonald PE, Akerman I, Lavery GG, Flaxman C, Morgan NG, Richardson SJ, Hewison M, Hodson DJ. *Vitamin-D-Binding Protein Contributes to the Maintenance of α Cell Function and Glucagon Secretion*. Cell Rep. 2020 Jun 16;31(11):107761. doi: 10.1016/j.celrep.2020.107761.

7. Hollinshead, K., Munford, H., Eales, K. L., Bardella, C., Li, C., Escribano-Gonzalez, C., Thakker, A., Nonnenmacher, Y., Kluckova, K., Jeeves, M., Murren, R., **Cuozzo, F**., Ye, D., Laurenti, G., Zhu, W., Hiller, K., Hodson, D. J., Hua, W., Tomlinson, I. P., Ludwig, C., Ying Mao Tennant, D. A. (2018). *Oncogenic IDH1 Mutations Promote Enhanced Proline Synthesis through PYCR1 to Support the Maintenance of Mitochondrial Redox Homeostasis*. Cell reports, 22(12), 3107–3114. doi:10.1016/j.celrep.2018.02.084